NASA Conference Publication 2456

Closed-Cycle, Frequency-Stable CO_2 Laser Technology

Proceedings of a workshop held at
Langley Research Center
Hampton, Virginia
June 10-12, 1986

RSRE
Royal Signals and
Radar Establishment

NASA

NASA Conference Publication 2456

Closed-Cycle, Frequency-Stable CO_2 Laser Technology

Edited by
Carmen E. Batten
Irvin M. Miller
and George M. Wood, Jr.
Langley Research Center
Hampton, Virginia

David V. Willetts
Royal Signals and Radar Establishment
Malvern, Worcester
United Kingdom

Proceedings of a workshop
sponsored by the National Aeronautics
and Space Administration and held at
Langley Research Center
Hampton, Virginia
June 10–12, 1986

NASA
National Aeronautics
and Space Administration

Scientific and Technical
Information Branch

1987

PREFACE

These proceedings contain a collection of papers and comments presented at a workshop on technology associated with long-duration closed-cycle operation of frequency-stable, pulsed carbon dioxide lasers. This workshop was held at the NASA Langley Research Center June 10 to 12, 1986. The workshop, jointly sponsored by the National Aeronautics and Space Administration (NASA) and the Royal Signals and Radar Establishment (RSRE), was attended by 63 engineers and scientists from the United States and the United Kingdom. During the 2 1/2 days of the workshop, a number of issues relating to obtaining frequency-stable operation and to the catalytic control of laser gas chemistry were discussed, and specific recommendations concerning future activities were drafted. Of particular importance was the recognition of an inability to quantitatively compare catalytic efficiencies when measured in different laboratories due to the lack of a standardized testing procedure, and the necessity to undertake careful studies of the catalytic surface in order to design catalysts capable of providing gigapulse operational lifetimes using rare oxygen isotope carbon dioxide. Several areas of research to alleviate chirp and to obtain high-energy pulses of uniform quality were also cited. The recommendations of the panel chairmen concerning these and other issues are included in these proceedings.

The considerable efforts of the panel chairmen and other members of the program committee and the sponsorship of Dr. John Theon and Dr. Robert Curran, Atmospheric Dynamics and Radiation Branch, NASA Headquarters, were crucial to the success of this workshop. A special note of appreciation is also extended to all those who helped make this workshop a success.

George M. Wood, Jr.
Workshop Chairman

CONTENTS

Session IV. Catalytic Oxidation of CO

Session V(a). Catalytic Oxidation of CO

Session V(b). Frequency Stability and Chirp

III. PANEL CHAIRMEN REPORTS

IV. CLOSING REMARKS

WORKSHOP COMMITTEE

Sponsors

Dr. John S. Theon, Chief
Atmos. Dynamics and Radiation Branch
NASA Headquarters
Washington, DC

Dr. Robert J. Curran
Atmos. Dynamics and Radiation Branch
NASA Headquarters
Washington, DC

Chairman

Dr. George M. Wood, Jr.
General Research Instrumentation Branch
NASA Langley Research Center
Hampton, Virginia

Co-Chairmen

Mr. Robert V. Hess, Head
Laser Technology and Applications Branch
NASA Langley Research Center
Hampton, Virginia

Dr. David V. Willets
Royal Signals and Radar Establishment
Malvern
Worcester, United Kingdom

Panel Chairmen

Prof. Richard D. Gonzalez
Dept. of Chemical Engineering
University of Illinois
Chicago, Illinois

Dr. Harry T. Price
GEC Avionics, Ltd.
Borehamwood, Herts.
United Kingdom

Program Chairmen

Mr. David R. Schryer
Laser Technology and
Applications Branch
NASA Langley Research Center
Hampton, Virginia

Dr. Richard K. Herz
Dept. of Chemical Engineering
University of California/
San Diego
La Jolla, California

Publicity and Publications Chairman

Ms. Carmen E. Batten
General Research Instrumentation Branch
NASA Langley Research Center
Hampton, Virginia

Arrangements Chairman

Mr. Irvin M. Miller
General Research Instrumentation Branch
NASA Langley Research Center
Hampton, Virginia

Arrangements Committee

Patricia A. Paulin
General Research Instrumentation Branch
NASA Langley Research Center
Hampton, Virginia

Jacqueline Schryer
Department of Chemical Sciences
Old Dominion University
Norfolk, Virginia

ATTENDEES

NASA Attendees

Dr. Frank Allario
NASA Langley Research Center
Mail Stop 476
Hampton, VA 23665-5225

Clayton H. Bair
NASA Langley Research Center
Mail Stop 468
Hampton, VA 23665-5225

Carmen E. Batten
NASA Langley Research Center
Mail Stop 234
Hampton, VA 23665-5225

Dr. James W. Bilbro
NASA George C. Marshall
Space Flight Center
Mail Stop EB-23
Marshall Space Flight Center, AL 35812

Philip Brockman
NASA Langley Research Center
Mail Stop 468
Hampton, VA 23665-5225

Dr. Robert J. Curran
Code EET
NASA Headquarters
Washington, DC 20546

Dr. Russell J. Deyoung
NASA Langley Research Center
Mail Stop 160
Hampton, VA 23665-5225

Robert V. Hess
NASA Langley Research Center
Mail Stop 468
Hampton, VA 23665-5225

Dr. John C. Hoppe
NASA Langley Research Center
Mail Stop 236
Hampton, VA 23665-5225

David R. Johnson
NASA Langley Research Center
Mail Stop 235
Hampton, VA 23665-5225

Beverley W. Lewis
NASA Langley Research Center
Mail Stop 234
Hampton, VA 23665-5225

Dr. Robert Menzies
Jet Propulsion Laboratory
Mail Stop 183-401
4800 Oak Grove Drive
Pasadena, CA 91109

Irvin M. Miller
NASA Langley Research Center
Mail Stop 234
Hampton, VA 23665-5225

Dr. Robert S. Rogowski
NASA Langley Research Center
Mail Stop 231
Hampton, VA 23665-5225

David R. Schryer
NASA Langley Research Center
Mail Stop 468
Hampton, VA 23665-5225

Barry D. Sidney
NASA Langley Research Center
Mail Stop 468
Hampton, VA 23665-5225

Dr. Jag J. Singh
NASA Langley Research Center
Mail Stop 235
Hampton, VA 23665-5225

Martin E. Smithers
Marshall Space Flight Center
Code EG-23
Huntsville, AL 35812

Dr. Martin M. Sokoloski
Code RC
NASA Headquarters
Washington, DC 20546

Dr. George M. Wood, Jr.
NASA Langley Research Center
Mail Stop 234
Hampton, VA 23665-5225

Paul R. Yeager
NASA Langley Research Center
Mail Stop 234
Hampton, VA 23665-5225

Non-NASA Attendees

Dr. Jeffry L. Ahl
Army Night Vision Directorate
AMSEL-NV-L
Fort Belvoir, VA 22060

Dr. Kenneth G. Brown
Old Dominion University
Mail Stop 234
NASA Langley Research Center
Hampton, VA 23665-5225

Dr. Nee-Yin Chou
Science and Technology Corporation
Mail Stop 910
NASA LaRC
Hampton, VA 23665-5225

David L. Clark
Barr and Stroud, Ltd.
Caxton Street
Anniesland, Glasgow
SCOTLAND

Dr. David B. Cohn
Hughes Aircraft Company
Building E1, M. S. B131
P. O. Box 902
El Segundo, CA 90245

Marcia Collins
Teledyne Water Pik
1730 E. Prospect Street
Ft. Collins, CO 80525

Alan Crocker
RSRE/UOP
"Grithacre" Marlbank Road, Welland
Malvern, Worcs., WR13 6NE
United Kingdom

Dr. James M. Cruickshank
Defense Research Establishment
Valcartier
2459 Boulevard Pie XI North
P. O. Box 8800
Courcelette, Quebec GOA IRD
Canada

Dr. Victor R. Deitz
Naval Research Laboratory
Surface Chemistry Branch
Code 6170
Washington, DC 20375

Prof. John Dillard
Department of Chemistry
Davidson Hall, 402
Virginia Polytechnic Institute
and State University
Blacksburg, VA 24061

Dr. Charles H. Fisher
Spectra Technolgoy
2755 Northup Way
Bellevue, WA 98004-1495

Dr. Farley Fisher
National Science Foundation
1800 G. St., NW
Room 1126
Washington, DC 20550

Dr. Jay Fox
Army Night Vision Directorate
AMSEL-NV-L
Fort Belvoir, VA 22060

Dr. Charles Freed
MIT Lincoln Laboratory, Room 201
244 Wood Street
P. O. Box 73
Lexington, MA 02173-0073

Dr. Haren Gandhi
Ford Motor Company
P. O. Box 2053, Room S-3085
Scientific Research Laboratory
Dearborn, MI 48121

Prof. Richard D. Gonzalez
Department of Chemical Engineering
P. O. Box 4348
University of Illinois
Chicago, IL 60680

Michael R. Harris
RSRE
St. Andrews Road
Malvern, Worcs., WR14 3PS
United Kingdom

Dr. Richard K. Herz
Mail Code B-010, UCSD
Chemical Engineering
University of California/San Diego
La Jolla, CA 92093

Lin Higley
Hughes Aircraft Company
E01E1-5150
P. O. Box 902
El Segundo, CA 90245

Dr. Gar B. Hoflund
Department of Chemical Engineering
University of Florida
Gainesville, FL 32611

Dr. John H. Kolts
368A PL, R and D
Phillips Petroleum Company
Bartlesville, OK 74004

Dr. Frank Ludwig
Hughes Aircraft Company
E01E1-5150
P. O. Box 902
El Segundo, CA 90245

Dr. Robert W. McCabe
General Motors Research Laboratory
Physical Chemistry Department
Warren, MI 48090

J. W. Mohlman
Northrop
32542 Coastsite Drive
Rancho Palos Verdes, CA 90274

Dr. Harry T. Price
GEC Avionics, Ltd.
Elstree Way
Borehamwood, Herts., WDI 6RX
United Kingdom

Dr. John R. Richmond
UMP Limited
Jeffreys Road
Brimsdown Enfield Middlesex, EN3 7PN
United Kingdom

Chris F. Sampson
UK Atomic Energy Authority
Harwell Laboratory AERE
Harwell, Oxon OX11 ORA
ENGLAND

Mark Samuels
GEC Avionics
P. O. Box 81999
Atlanta, GA 30366

Dr. Richard C. Sharpe
Raytheon Company
Research Division
131 Spring Street
Lexington, MA 02173

Steve R. Shaw
GEC Avionics Ltd.
Elstree Way
Borehamwood, Herts., WD1 6RX
United Kingdom

Don S. Stark
c/o Dr. David V. Willetts
RSRE
St. Andrews Blvd.
Malvern, Worcs., WR14 3PS
United Kingdom

Don Stewart
768 N. First St.
Hampton, VA 23664

Dr. Samuel J. Tauster
Exxon Research and Engineering Company
Corporate Res. Advance. and Transf.
Route 22 East, Clinton Township
Annandale, NJ 08801

Richard Tilton
Hughes Aircraft Company
6155 El Camino Real
Mail Stop 138
Carlsbad, CA 92008

Prof. Thedore T. Tsotsis
Dept. of Chemical Engineering
Univ. of Southern California
HEDCO 210
University Park, CA 90089

Dr. Billy T. Upchurch
Mail Stop 234
NASA Langley Research Center
Hampton, VA 23665-5225

Prof. Albert M. Vannice
Department of Chemical Engineering
Fensky Laboratory
Pennsylvania State University
University Park, PA 16802

Dr. Tom Watson
Hughes Aircraft Company
6155 El Camino Real
Mail Stop 138
Carlsbad, CA 92008

Edwin L. Wildner
Mail Stop 234
NASA Langley Research Center
Hampton, VA 23665-5225

Dr. David V. Willetts
RSRE
St. Andrews Road
Malvern, Worcs., WR14 3PS
United Kingdom

Dr. Leonard Winchester
Science and Technology Corp.
Mail Stop 910
NASA Langley Research Center
Hampton, VA 23665-5225

W. F. Woods
Ferranti Ltd.
Rupertson Avenue
Edinburgh, Scotland
United Kingdom

CALL TO ORDER

George M. Wood, Jr.
NASA Langley Research Center
Hampton, Virginia

I would like to welcome you to the NASA Langley Research Center and to the workshop on closed-cycle pulsed CO_2 laser technology. I would particularly like to extend a welcome to our colleagues from the United Kingdom, who have made every effort to come so far to meet with us, and to point out that the success of this workshop, based on the attendance, is due largely to the efforts of the Chairman for the United Kingdom, David Willetts, from the RSRE. Also, I would like to thank John Theon, Robert Curran, and Marty Sokoloski of NASA Headquarters, for supporting the research program and for sponsoring this workshop.

We are at this workshop because of a common interest in the development and application of pulsed CO_2 lasers. There are a number of projected applications for these lasers, and it is my personal opinion that it is a technology that is waiting in the wings to be developed, primarily because of the lack of a means of reliable, long-term, closed-cycle operation. Our interest at NASA has to do with improving our measurement capability in various areas related to aerospace research, and the NASA Langley people who are involved in this program are in fact measurement scientists. Our most immediate application is the Marshall Space Flight Center's Windstat program that you will be hearing more about later. This particular application will require a lifetime of at least 10^9 pulses using rare isotope CO_2 in order to minimize transmission losses, so that in addition to providing long lifetimes, the isotopic integrity of the operating gas must be maintained. At Langley, the requirement is for miniaturized lasers to be used for measurements related to aerodynamic and aerothermodynamic research in our high enthalpy test facilities, on research aircraft, and on advanced hypersonic research vehicles. In these applications, the power of the pulsed laser will be exploited to solve measurement difficulties associated with thick boundary layers, and the sharp, well-defined pulse shapes will be combined with advanced signal processing techniques to improve signal-to-noise ratios and resolution.

Although our interest lies in measurements with the CO_2 laser, the potential for technology transfer to industrial, medical, defense, and other research applications is significant. In some of these, the use of rare isotopes is also important. For example, one medical application currently being considered is the removal of plaque from clogged arteries with a pulsed CO_2 laser and appropriate fiber optics. However, the blood contains a large amount of adsorbed CO_2, which could result in large transmission losses with concurrent excess heating if the common isotope CO_2 is used. In others, such as industrial process control, laser ranging, or perhaps communications, frequency stability and reliable long-term unattended operation are most important.

In either case, we are beyond the point where it is simply sufficient to "shovel on a little more coal" whenever needed. At pulse rates of 10-20 pps, 10^9 pulses still require about 10^8 seconds--and that is about 3 years. It is clearly impractical, therefore, to take a sample from each batch of catalyst produced and to run a full lifetime test on it. But if it is to be used in a satellite or in any other application where reliability is of prime importance, then the ability to predict catalyst performance and to control frequency stability is critical. It is,

therefore, absolutely necessary that the mechanisms involved be understood on the scientific as well as the engineering level or if these mechanisms cannot be measured both qualitatively and quantitatively, we will not be able to predict the operational lifetime with any degree of certainty. This will require some highly innovative studies of the catalyst, including measurements of: surface properties; oxidation, reduction, adsorption and diffusion mechanism; and, the catalytic process itself.

This workshop therefore has the following goals: first, to provide a forum for the exchange of ideas and information between those people working this field--whatever your application for the CO_2 laser--and to foster a continuing collaboration between us as a group, thus minimizing duplication of effort; second, to discuss the current status and problems related to obtaining the necessary frequency stability and lifetime; and third, to identify and discuss methods to solve these problems.

It is with pleasure that I introduce Mr. William D. Mace, the Director for Electronics at Langley, who will extend some welcoming remarks. The Center is divided into several research Directorates. One of these is the Electronics Directorate, which includes the two divisions that are involved in research in the measurement sciences: the Instrument Research Division directed by David R. Johnson and the Flight Electronics Division directed by Frank Allario. Bill Mace's philosophy has always been that if you can't measure something with confidence, you can't understand or model the process, and consequently, good measurements are the foundations of good research. In this directorate and these divisions, therefore, innovation in measurement methods is not only encouraged--it is expected.

WELCOMING REMARKS

William D. Mace
Director for Electronics
NASA Langley Research Center
Hampton, Virginia

It has been of interest to me over the years to look at the people who assemble for workshops and conferences of this type and to get an idea of the different perspectives that are represented amongst the attendees. I have found an interesting and surprising scope to their interests. I would like to share with you the perspective that I bring to this type of workshop and to illustrate the interests that we have here at Langley. As George Wood has suggested, the soapbox that I'm standing on has the term "Measurement Science" plastered across the base of it. For some years now at Langley, we have maintained a respectable research capability in atmospheric sciences, controls, aerodynamics, materials, and structures, and in the course of doing this, we have learned (perhaps I'm showing my prejudice here a bit) that through the research process the scientific process both begins and ends with data. Data are used initially to provide a window through which the phenomenon which is being investigated might be viewed, and on the basis of these data, scientists then express observations mathematically or quantitatively. Having done so, it is then necessary to gain additional data in order to validate those quantitative expressions. In the past, up until the 1960's or 1970's, the emphasis here at Langley has been on hardware simulation as a means for gathering the data which provided this window. In more recent times, however, with the advent of microelectronics and computer science, and also due to the success of mathematicians in devising better mathematical tools and methods for describing the phenomena which are observed, there has been a growing dependence upon analytical simulation.

So the source of and requirements for data are evolving, evolving from a climate characterized by hardware simulation and parametric experiments toward highly focused, carefully controlled experimental conditions. This trend toward increasing dependence upon analytical simulation is having a significant impact upon our measurements technology research programs at Langley. In the past, hardware-based simulations have been, relatively speaking, at a large scale, and we have been able to successfully use various probes, thermocouples, and devices that are inserted into the test environment. In analytical simulations, however, we can use analytical methods that present studies at a scale which is very small. We can, as an example, track a molecule as it goes over the wing, past the fuselage, engine, and tail assembly, and merges back with prestream conditions. If one does consider the need for data to support analytical simulation at this level, it becomes apparent that the measurement technologies we have employed in the past won't be suitable anymore. We can't, for example, use thermocouples and pitot tubes because of the size of the transducer. It interferes with the very parameters you are trying to measure. We have to turn to nonintrusive measurement techniques which can get data at the molecular level without disturbing the measurement. Again, I say, therein is our charter, our goal, and in it we need your help!

Now, I'm sure there are a lot of you in the workshop that have a different motivation. I don't know the extent that we can help you, but we are sure going to try. I think that through the open exchange of the data, information, and insights that you have gained through your research efforts, there will be definite gains to us, and I hope that in our sharing with you what we have learned, you will find some benefit.

OPENING REMARKS

Robert J. Curran
NASA Headquarters
Washington, DC

It is always a pleasure to attend a workshop at Langley Research Center. I came to Langley almost monthly in the mid-1970's when we were jointly trying to get the Earth Radiation Budget Experiment started.

Dr. John Theon had wished to attend this workshop and indicate NASA's interest both in the meeting and in this report. Unfortunately, because of an unscheduled meeting requiring his attendance, John was not able to attend and asked that I represent him. In addition to the workshop, Dr. Theon asked me to indicate our interest in working closely with the British in the development of the techniques needed for a future satellite-borne wind profiler. I would also like to mention that I have my own interests in the subject matter, and I'll discuss those later in this paper.

John Theon had prepared some opening comments and I would like to present those comments from his prepared statement because I think they set the tone for the meeting:

> I had planned to be here to welcome you personally to this workshop on closed-cycle frequency-stable CO_2 laser technology, but a last-moment assignment has prevented me from following through. Nevertheless, I believe this will be an important workshop not only for the technical information that will be disseminated but also because it marks the first time that we have entered into joint sponsorship of such a workshop on CO_2 laser technology by both RSRE and NASA.
>
> As one who represents the users of lidar technology, my colleagues and I believe that lidar has the potential for significant advances in our ability to observe the atmosphere remotely. The combination of excellent remote sensing techniques and the perspective of space is very powerful indeed. It could revolutionize the way we look at the atmosphere and improve not only our understanding of atmosphere behavior but also vastly improve our ability to predict that behavior. I would like to thank the organizers of this workshop, both at RSRE and at NASA Langley Research Center. Their diligence and hard work are already apparent. I know you will have a successful meeting, and I look forward to hearing first-hand reports of your accomplishments and to reading the proceedings of the workshop.

I manage the NASA Global Scale Atmospheric Processes Research Program. One of the objectives of that program is to use space technology to better understand the large-scale dynamics of the Earth's atmosphere. The procedures that the satellite meteorological community has developed in the past decade for global weather prediction and study start by using atmospheric density fields produced by combining in situ temperature soundings with satellite remotely sensed temperature retrievals. These observations are then assimilated into global models of the atmosphere. Finally, the global model is used to determine the large-scale motions in the atmosphere by making horizontal

differences in the input density field. As you can readily understand from this procedure, errors in the input density field, or even small-scale irregularities in this field, are amplified through this differencing process. The forces which produce the calculated large-scale motions are proportional to the density gradients. The large-scale motions calculated by these models are used to predict what tomorrow's or next week's weather will be. In some cases we have been very successful in these predictions. However, in many notable cases large errors in prediction have been made. Because weather affects our everyday lives, I'm sure each of you can attest to the lack of precision in forecasting. A basic problem in this prediction calculation is that the input parameter which is remotely sensed, temperature, is one step removed from the calculation of the atmospheric dynamics. The key measurement requested by the atmospheric scientists is the direct observation of the motion of the atmosphere, that is, to measure the wind motions globally. In the past we have not had that opportunity. The Doppler lidar technology is very appealing in terms of being able to make precisely that observation. We at NASA, because of our relationship with space technology and the use of satellites, are encouraged to see the development of these coherent CO_2 laser systems in the hope that we will be able to apply these systems in space. It has been demonstrated that once we are able to observe winds, we certainly will improve our ability to predict the longer term weather. That is my personal and programmatic interest in this workshop. Last summer we had a workshop in Columbia, Maryland, in which we assembled the scientific requirements for a wind observing instrument. We also tried to assess the status of technology in this area. You may know that there are a number of remote sensing techniques which are possible for measuring wind from a satellite platform. Of those techniques, it is agreed that the coherent CO_2 Doppler lidar is the most mature. All of the workshop recommendations and the review of the techniques for measuring wind are contained in the workshop proceedings.*

*Proceedings of a NASA Symposium on Global Wind Measurements, Columbia, Md., Wayman E. Baker and Robert J. Curran, eds., A. Deepak Publishing, Hampton, Va., 1985.

OPENING REMARKS

David V. Willetts
Royal Signals and Radar Establishment
Malvern, Worcester, United Kingdom

Dr. Viv Roper, who is the Superintendent of the Laser Devices and Techniques Division at RSRE, was originally scheduled to present his opening remarks to this workshop; unfortunately he had to attend another meeting in the US, and I was asked to give the presentation on his behalf. I welcome the opportunity to address the workshop and make some introductory comments particularly on behalf of the UK visitors and RSRE as one of the organizations co-sponsoring this workshop. For those of you unfamiliar with UK organization, RSRE is a Research and Development Establishment within the UK Ministry of Defence. It is the foremost UK electronics research Establishment and serves the needs of all three armed services. For historic reasons RSRE is located in Worcestershire, and the largest site is at Great Malvern, nestling beneath the Malvern Hills. There are roughly two thousand employees at this site and about one-half of them are graduate staff. For administrative purposes, the Establishment is divided into two departments, each of which has three groups. There is a bias towards electronics with heavy commitments to research and development in various areas such as microwave radar, communications, and computing. The team at RSRE concerned with CO_2 laser systems is in the Microwave and Electro-optics structure, while by contrast, the staff from RSRE present today represents the Laser Devices and Techniques Division.

I will attempt to give you some perspective on RSRE involvements in carbon-dioxide laser device work. The Establishment has been active in both pulsed and CW lasers. On the pulsed side, work early in the 1970s by Peter Pearson led to the trigger wire preionization scheme, and the sealed trigger wire preionization laser was demonstrated by Don Stark and Alan Crocker (both present at the workshop) as early as 1974. Work on improved preionization techniques has continued until quite recently. Considerable effort beginning eight years ago has been expended on CO oxidation catalysts for long lifetime operation, and this is one of the areas of particular interest to this workshop. These various techniques have been brought together in the development of high-performance sealed repetition rate devices. Work is continuing on the physical mechanisms which give rise to frequency variations during the output pulse, and obviously this is the other main topic that needs to be addressed at this workshop.

We also have ongoing programs in such areas as target effects and signal statistics and a considerable commitment on CW laser technology and research. I won't go into that in any detail, although of course it is an area which is of interest to any pulse heterodyne system to provide the local oscillator. In several areas we believe that we now possess knowledge unsurpassed elsewhere. We have a policy of technology transfer to industry, a good example of which is basic transversely excited laser technology. This area we believe is quite mature, and our programs have been completed and the technology transferred into UK industry. However, work continues on the two topics of immediate interest to this workshop.

Turning now to our interaction with NASA, initial discussions on setting up this meeting took place with John Theon and Bob Curran during December 1985 but we have had close links with the organization for some time before that. Since RSRE is an organization primarily addressing military needs, we also have quite close links with

various DOD agencies in the United States through the Technical Cooperation Programme (TTCP) and numerous bi-lateral agreements. There has been extensive planning which we hope will allow these NASA and RSRE interactions to be as useful as our other contacts in the USA, and I want to thank George Wood, Bob Hess, and their colleagues at NASA Langley for all of the hard work that they have done to make this event possible.

Workshop objectives as seen from a UK standpoint are to promote a better scientific exchange in the areas of CO oxidation catalysts and the physics of frequency stabilization. We look forward over the next few days to a greater awareness of NASA activities and requirements, and hope and expect that NASA will get a clearer view enhancing their perspective of UK capabilities. A word on UK attendance: in addition to staff from the Laser Physics Division at RSRE, we have representatives from a number of other UK industrial organizations who are contributing to this workshop and I would like to thank them for their efforts in this respect.

Finally, in addition to the staff at Langley who have put in so much work to make this meeting possible, I would like to thank the people from NASA Headquarters who have so generously sponsored this activity. We hope that this workshop will be fully interactive and productive and will promote a long and fruitful association between our two countries.

OPENING REMARKS

Robert V. Hess
NASA Langley Research Center
Hampton, Virginia

In my brief introductory remarks, I would like to note that although separate sessions were chosen for frequency chirp, CO_2 laser configurations, and catalysts, there are important interconnections. The comparatively large laser cross sections for reducing the frequency chirp will affect the discharge preionization/sustaining techniques. The nature of the laser discharge will help to determine the recombination efficiency requirements of the catalyst used in closed-cycle laser operation. Of course each discharge preionization/sustaining technique has its own lifetime characteristics, which may have to be improved. The laser configuration, through its far-field pattern, will affect the heterodyne detection efficiency of the Doppler or Differential Absorption Lidar measurement. The far-field pattern of unstable resonators, which have the comparatively large laser cross sections for frequency chirp reduction, can be improved for increased heterodyne detection efficiency through use of Gaussian or super-Gaussian mirrors. These mirrors further permit unstable resonator operation with lower magnification, which in turn, offers a compromise between the laser cross section for frequency chirp reduction and for improved discharge preionization/sustaining techniques; lifetime of mirrors must also be considered. The possibility of using unstable resonators with lower magnification also enables their use as lower pulse energy master oscillators in combination with higher power amplifiers. The ultimate choice of the compromise between minimizing the frequency chirp and highly efficient long lifetime closed-cycle CO_2 laser operation represents an important technological challenge.

REVIEW OF THE FREQUENCY STABILIZATION OF TEA CO_2 LASER OSCILLATORS

D. V. Willetts
Royal Signals and Radar Establishment
Malvern, Worcestershire
United Kingdom

SUMMARY

Most applications of TEA CO_2 lasers in heterodyne radar systems require that the transmitter has a high degree of frequency stability. This ensures good Doppler resolution and maximizes receiver sensitivity. However the environment within the device is far from benign with fast acoustic and electrical transients being present. Consequently the phenomena which govern the frequency stability of pulsed lasers are quite different from those operative in their cw counterparts. This review concentrates on the mechanisms of chirping within the output pulse; pulse to pulse frequency drift may be eliminated by frequency measurement and correction on successive pulses. It emerges that good stability hinges on correct cavity design. The energy-dependent laser-induced frequency sweep falls dramatically as mode diameter is increased. Thus it is necessary to construct resonators with good selectivity for single mode operation while having a large spot size.

INTRODUCTION

This review will attempt to explore the gradual development of the understanding of frequency chirp mechanisms in TEA CO_2 lasers from a largely historical perspective. The format of this submission will briefly review the need for frequency constancy and pertinent TEA laser technology, and then go on to examine methods of mode selection, experimental techniques and chirp mechanisms. Finally some general methods of overcoming the chirp will be described, leading on to the following paper by Harris (ref. 1) in which our favored route to alleviation of these effects so as to produce a frequency stable laser will be described.

FREQUENCY STABILITY REQUIREMENTS

Heterodyne detection results in superior sensitivity to direct detection and is in addition a fundamental requirement in Doppler velocimetry systems such as those of interest to this workshop. However, stringent frequency control is required of the transmitter laser. The theory of the required frequency characteristics of such pulsed radars has been developed by Woodward (ref. 2). He proved that range accuracy was proportional to the pulse bandwidth and Doppler accuracy to the pulse length, provided that the pulses are reproducible and that a suitable matched filter can be constructed. It should be noted that for good Doppler resolution, reproducible pulses of the required length, irrespective of frequency modulation, are adequate provided that the signal processing complexity can be tolerated. It turns out that making reproducible pulses is very difficult. There is a pulse-to-pulse energy variation in TEA laser outputs and during the course of this review it will emerge

that the frequency behavior is intimately related to output energy. Thus constructing a matched filter, not necessarily easy for nonlinear chirps, is made more complex by non-reproducibility; an active option would have to be pursued. An alternative approach is to attempt to obtain chirp-free pulses, which imposes a constraint on the laser performance while relaxing the processing requirements. In both cases an understanding of the mechanism of self frequency modulation is desired in order that the appropriate degree of frequency control may be exercised.

The accuracy of frequency measurement depends on the pulse length alone, as described above. This may be visualized as follows. N cycles of a sine wave of frequency f occupy a time T where

$$N = fT$$

The fractional frequency accuracy $\Delta f/f$ is inversely proportional to the number of cycles, the proportionality constant being about unity for SNRs of about one. Hence the frequency precision is inversely proportional to pulse length. This is a special case of the Fourier Transform limit, which states that the accuracy with which the frequency can be measured is given by the Fourier Transform of the pulse envelope. Estimates vary of the Doppler needs of a global wind sensor but the Transform-limited pulse length estimate has remained at four microseconds within a factor of two.

TEA LASERS

Discharge Technology

Figure 1 illustrates the construction of a typical small TEA laser. Two profiled electrodes of length tens of centimeters are separated by a few centimeters. The envelope contains a gas mixture of N_2, CO_2 and helium and a pulsed discharge is initiated between the electrodes by a fast switch such as a spark gap or thyratron. Discharge durations are limited to a few hundred nanoseconds by onset of the glow-arc transition; indeed, it is normally necessary to 'seed' the gas with electrons before the voltage is applied in order to obtain any glow discharge at all. For repetition rate operation of TEA lasers it is necessary to change the gas from pulse to pulse to prevent build-up of dissociation products in the active region and to replace heated gas with cool. Gas flow is usually arranged to be transverse to the optical axis but longitudinal flow devices have also been constructed. The flow duct also may contain a heat exchanger to control the gas temperature and CO oxidation catalyst.

Output Characteristics

Typical short TEA lasers emit a pulse of duration about 50 ns followed by a tail of length several microseconds as shown in figure 2. This pulse is called a gain switched spike (GSS) and is a manifestation of the significant depletion in gain that occurs when the exponentially increasing photon flux saturates the inverted medium. The tail arises from the slower energy transfer from molecular nitrogen to CO_2. Alternatively, if a standing wave of laser radiation is present within the cavity when the discharge is pulsed, the output is as shown in figure 3. Since photons do not now have to build up from noise, the threshold is crossed sooner and the optical pulse follows more quickly on the electrical discharge. The gain switching process is suppressed and the tail is enhanced, so that a longer pulse, of duration about one microsecond, results.

Finally, it must be pointed out that transverse discharges such as these may be operated in a non-self-sustained fashion by injecting electrons into the discharge from a gun. This is normally done through a very thin foil because the gun operates at much lower pressures than the laser. The field between the electrodes is then just a drift field, too low to allow the glow-arc transition to occur. Consequently the discharge can be run for very long periods and give long output pulses, such as shown in figure 4. Such discharges are also scalable to large volumes and result in particularly efficient excitation of CO_2. They are thus attractive from several points of view.

Mode Selection

Clearly, in order to assign an unambiguous value to Doppler shifts, the laser must oscillate on a single frequency, ie a single mode.

Single longitundinal mode (SLM) operation can be obtained by a variety of means. The laser can be made very short so that only one of its longitudinal modes will fit under the molecular transition bandwidth, or etalons may be incoporated within the cavity, or multiple mirror cavities can be constructed. The other means of longitudinal mode selection is to ensure that when the rapid discharge circuit is pulsed there is already within the cavity a standing field of the appropriate frequency so that one particular mode is favored over all others. One method of doing this, called hybridization, has already been alluded to, in which a CW gain section is incorporated within the pulsed cavity. The other method is to inject or seed the cavity with radiation from an external source, and this is usually called injection mode selection. It is also necessary to ensure that a single transverse mode oscillates and frequently this is done by incorporation of apertures in the cavity so as to favor the fundamental mode over higher order modes due to loss considerations. It will emerge that one means of frequency stabilization requires very large diameter modes and restrictive apertures are not suitable to the task in hand. Reference 1 discusses ways of proceeding under these circumstances.

EXPERIMENTAL METHODS

An obvious method of very high resolution spectroscopy suitable for studying small frequency changes is the use of an interferometer. Early studies (3) using a Fabry-Perot etalon met with little success since chirps of the order of a Megahertz in a source at 30 THz are being sought. This implies a resolution of about 10^8 which is asking a lot even of an interferometer. A much better route utilizes the heterodyne method and was done for the first time by Stiehl and Hoff (ref. 4). An example of this technique is illustrated in figure 5. The pulsed laser output is mixed with a cw local oscillator on a square law detector, which will respond at the difference between the two laser frequencies. The difference in frequency occurs in the RF and so standard RF analytic procedures can be used.

RESULTS

A typical beat signal arising from such a heterodyne experiment is shown in figure 6. The frequency actually increases from a value less than that of the local oscillator (LO), through a zero beat frequency, and through increasingly positive

values relative to the LO as time goes on. The envelope of the difference signal is a function of the pulse shape of the pulsed laser. The temporal dependence of frequency may be abstracted from such data by for instance measuring the positions of peaks or zero crossings in the waveform. Such a plot is shown in figure 7, where it is seen that a frequency change of about 20 MHz takes place in around two microseconds. The transform limit of such a pulse would be less than a Megahertz so such an output would be useless for accurate velocimetry.

Since the laser cavity is a Fabry-Perot etalon, frequency changes arise from changes in its optical length. On a timescale of a few microseconds, the cavity is mechanically rigid and so optical length changes arise from refractive index variations alone. Examination of figure 7 suggests that two processes are taking place, one giving rise to the early fall in frequency, and another to the rise during the remainder of the pulse. We will deal with these two phenomena in turn, dealing for convenience firstly with the effect in the tail of the pulse.

LASER-INDUCED MEDIUM PERTURBATION (LIMP)

One suggestion which was extant at the time of these experiments was that the upchirp in the tail, known to fit accurately to the square of time (ref. 5) might be due to non-uniform gas heating. The hydrodynamics of a non-uniformly heated gas have been treated by Longaker and Litvak (ref. 6), who showed that the density ρ was related to the rate of energy deposition/unit volume $\dot{E}$ by the equation

$$\frac{\partial^3 \rho}{\partial t^3} = (\gamma-1)\ \nabla^2\ \dot{E}$$

for short times t satisfying $\nu t/a \ll 1$. Here a is the characteristic size of the non-uniformity, and γ is the ratio of specific heats at constant pressure and constant volume respectively.

The density perturbation may be related to the change in refractive index by the Gladstone-Dale law

$$\frac{\partial n}{\partial t} = K \frac{\partial \rho}{\partial t}$$

where K is the Gladstone-Dale constant $(dn/d\rho)$.

Refractive index n and resonant frequency of a Fabry-Perot resonator are related by

$$\frac{dn}{n} = -\frac{d\nu}{\nu}$$

so that combining these equations we find

$$\Delta\nu(t) = \frac{K}{2}\ \nu(\gamma-1)\ \nabla^2 E\ t^2\ f(t)$$

with $f(t) = 1$ for a very short pulse (eg, a gain-switched spike (GSS)) and $f(t) = t/3\tau$ for a square pulse of length τ.

Thus the good fit of the pulse frequency to a parabolic time dependence which is observed for a GSS is immediately explained provided that $\nabla^2 E$ is constant during the pulse, ie all the energy is deposited at the beginning of the pulse. The question still arises as to whether such a non-zero $\nabla^2 E$ is produced by the electric discharge. By alteration of the discharge circuitry so as to deliberately destabilize the TEA discharge, or by the addition of low ionization potential seeds such as xylene and ferrocene, the discharge homogeneity was altered (ref. 7). No significant alteration in chirp rate resulted at constant output energy, implying that discharge non-uniformities are not the major contribution to $\nabla^2 E$. However, it was observed that the magnitude of the chirp depended on the laser energy, suggestive of a laser-induced medium perturbation (LIMP) (ref. 8). In regions of high laser intensity there is a rapid depopulation of the upper laser level by stimulated emission to the lower laser level, which rapidly undergoes V-T relaxation to the ground state. Thus the rate of deposition of translational energy E is a function of intensity, which in turn is a function of radial position, so that $\nabla^2 E$ is non-zero. A good fit to a parabolic time dependence of frequency requires that most of the translational energy is deposited at the beginning of the pulse, in other words that E should closely approximate a δ-function near the start of the pulse.

We proceed to calculate $\nabla^2 E$ as follows. Since, neglecting loss, each photon emitted by the laser results in the appearance of one CO_2 (10°0) molecule, which rapidly relaxes to CO_2 (00°0) by a V-T process, E will be equal to

$$\frac{E_L}{V}\left(\frac{\nu_o}{\nu}\right)$$

where E_L is the laser output energy, V is the mode volume, and $h\nu_o$ is the energy of the CO_2 (10°0) level above the ground state. We assume that the laser output is entirely TEM_{00} mode, whose Gaussian radial dependence may be expressed in cylindrical polar co-ordinates (r,θ,z) as

$$E_L = A \exp[-(r^2/\sigma^2)] \quad .$$

Thus

$$\nabla^2 E = \frac{4E_L}{\pi\sigma^4 \ell}\left(\frac{\nu_o}{\nu}\right)\left(\frac{r^2}{\sigma^2} - 1\right) \exp\left[-\left(\frac{r^2}{\sigma^2}\right)\right]$$

where ℓ is the active length of the TEA section. Since the refractive index follows $\nabla^2 E$, it would be desirable to find the resonant frequencies of a cavity partially filled with the appropriate non-uniform index. This difficult problem was avoided by adopting the major approximation of the analysis, namely that the index is constant at the axial value. This recognizes that most of the light is concentrated near the optical axis. The final chirp formula then becomes

$$\Delta\nu(t) = \frac{2K\nu_o(\gamma-1)\ E_L}{\pi\sigma^4\ nL}\ t^2\ f(t)$$

for a total cavity length L.

This equation summarizes the LIMP chirp completely. A linear dependence on laser output energy (power for long pulses) arises together with an inverse cavity length factor. It is noteworthy that cavity filling factor ℓ/L does not appear in

the final equation. Most importantly, however, the σ^{-4} term is the key to low chirp operation of high energy compact lasers. Accordingly experiments were carried out to test this prediction of the σ dependence (ref. 9). A plane-plane resonator configuration was chosen since σ could then readily be controlled by alteration of an intracavity aperture diameter; values between 4.2 and 8.5 mm were used. In figure 8 the normalized chirp rate is plotted against spot size σ on a log-log scale (to test a power-law dependence). It is clear that the experimental points lie close to the predicted slope of -4. However, the intercept is about one order of magnitude lower than the theoretical prediction, presumably due to the approximate modal analysis. It would appear therefore confirmed that large mode radius resonators would alleviate LIMP effects and this technique will be explored in more detail in reference 1.

Finally, the temporal dependence of chirp for long pulses was explored (ref. 10) using an e-beam sustained system whose output pulse is shown in Figure 4. Figure 9 reveals that the time dependence fits very well to the t^3 prediction rather than t^2, and figure 10 illustrates for two pulse lengths the linear dependence of chirp rate on output power. It would thus seem that a reasonable understanding of the LIMP chirp has been built up with all the parametric dependencies investigated. We now return to examine the effect at the beginning of the pulse.

PLASMA

It is clear from Figure 7 that there is a small downsweep in frequency at the start of the optical emission. The phenomenon was investigated by omission of CO_2 from the TEA laser mixture to avoid lasing and LIMP, but otherwise the arrangement of figure 5 was used. The resulting chirp on short timescales is shown in figure 11; it mirrors the shape of the current pulse very closely implying that something present during the discharge is responsible. This species must be free electrons since the contribution to the index change is <u>negative</u>. The magnitude of the process is given by the plasma dispersion function

$$\Delta n = -\omega_p^2/2\omega^2$$

where the plasma frequency ω_p is given by

$$\omega_p^2 = \frac{4\pi N e^2}{m}$$

where N is the electron density. Then it is found that

$$\Delta\nu = \frac{e^2 \ell}{2\pi m \nu L n} N$$

that is, the initial chirp should depend linearly on the electron density N. The electron density is related to the current density J by the relation

$$J = Ne\nu'$$

where ν' is the drift velocity of electrons in the gas mixture under the applied field. Thus the plasma-induced chirp should linearly follow the discharge current pulse, as observed. The measured and calculated frequency changes are in very good agreement. The process exhibited by the TEA laser pulse in figure 7 is the decay of

free electrons in the discharge tail taking place as the optical output begins. By operating the cw section of the hybrid laser below threshold, the pulse advance described earlier is reduced and optical output occurs after the electron density has decayed substantially to zero. This is shown in figure 12.

An excellent means of elimination of the plasma effect is to maintain the discharge current constant throughout the optical output pulse. This can be achieved with an e-beam sustained laser as described previously, which also possesses other desirable features for long pulse operation. However methods do exist (albeit having some drawbacks) for correcting any chirping phenomena that may be taking place, and these will now be described.

GENERAL CORRECTION TECHNIQUES

Electro-Optic Index Compensation

An obvious method to correct chirps consists of incorporating an electro-optic crystal within the laser cavity and applying a voltage to exactly compensate for any chirp process going on (ref. 11). This technique requires that the index perturbation is reproducible and is expected to be severely limited in power handling capability by optical damage to the modulator or its antireflection coatings.

Phase Conjugation

Phase conjugate mirrors have the property of reversing the wavefront incident upon them, so that a distortion caused by traverse of an index perturbed medium is removed on phase conjugate reflection through that medium. Thus a laser containing a one phase conjugate mirror can remove index perturbations within the cavity, and since frequency is simply the time derivative of phase, frequency distortions will also be removed. Figure 13 shows the apparatus used by Ouhayoun (ref. 12) to obtain phase conjugation by degenerate four-wave mixing (DFWM) in saturated CO_2. Pump radiation is provided by a loosely focused cw laser and its reflection in the cavity hard mirror; the pulsed laser output should lock in frequency to the cw laser. Current experiments have not established unambiguously that frequency locking is taking place due to the finite pulse length and the use of a Fourier Transform method of frequency examination. Assuming that frequency locking does occur, these systems do suffer from the inefficiency consequent upon using the phase conjugate approach.

Slow Vibration-to-translation* Transfer

It was stated earlier that translational heating of the ground state from the lower laser level is very fast; in fact the process typically takes a few hundred nanoseconds at atmospheric pressure. If this V-T transfer can be forced to occur on a timescale larger than the optical pulse, insignificant chirping due to LIMP will occur. The transfer can be slowed by manipulation of the gas composition or reduction of the gas pressure. Figure 14 compares the frequency sweeping for infinitely fast V-T transfer with a finite transfer rate of T^{-1}. For long times the two curves are displaced by T in time and T^2 in frequency. For short times, the region of main

*Vibration-to-translation (V-T).

interest, as much as an order of magnitude chirp reduction can result, but at the cost of reduced pressure and thus an output energy reduction.

CONCLUSIONS

The foregoing review attempts to show that the chirping mechanisms in pulse CO_2 lasers are now well understood. In particular it should be noted that these mechanisms are independent of details such as method of longitudinal mode selection and apply to all TEA CO_2 lasers. Two phenomena are of importance: a plasma effect at the beginning of the pulse and a laser induced effect during the remainder of the pulse. The latter is dependent on the laser output energy and especially on the intracavity beam size. Since these phenomena are well understood it is possible to alleviate the chirping effects by appropriate measures, of which the most practical is correct resonator design. This subject will be examined in detail in the next paper.

REFERENCES

1 Harris, M. R.: Large Mode Radius Resonators. NASA/RSRE Workshop on Closed-Cycle, Frequency-Stable CO_2 Laser Technology. NASA CP-2456, 1987.

2 Woodward, P. M.: Probability and Information Theory with Applications to Radar. Pergamon Press, 1953.

3 Nurmikko, A., Detemple, T., and Schwarz, S.: Appl. Phys. Letts. 18, 130 (1971).

4 Stiehl, W. A. and Hoff, P. W.: Appl. Phys. Letts. 22, 680 (1973).

5 Pace, P. and Lacombe, M.: Can. J. Phys. 57, 1350 (1979).

6 Longaker, P. R. and Litvak, M. M.: J. Appl. Phys. 40, 4033 (1969).

7 Willetts, D. V. and Harris, M. R.: J. Phys. D15, 51 (1982).

8 Roper, V. G., Lamberton, H., Parcell, E., and Manley, A., Opt. Commun. 25, 235 (1978).

9 Willetts, D. V. and Harris, M. R.: IEEE J. Quant. Electron. QE-19, 810 (1983).

10 Willetts, D. V. and Harris, M. R.: Opt. Commun. 49, 151 (1984).

11 Willetts, D. V. and Harris, M. R.: J. Phys. D18, 185 (1985).

12 Ouhayoun, M.: Proc. CLEO 85. Baltimore, M. A. (1985).

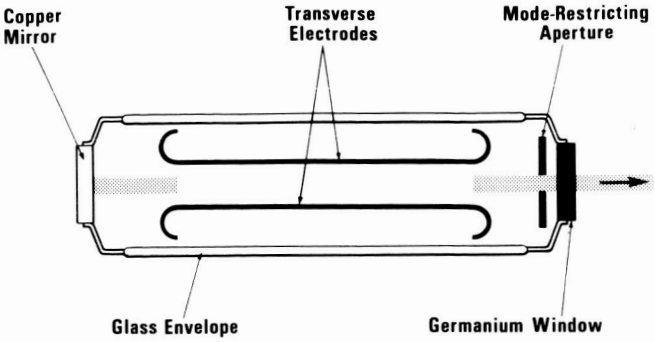

Figure 1. Longitudinal section of typical TEA CO_2 laser.

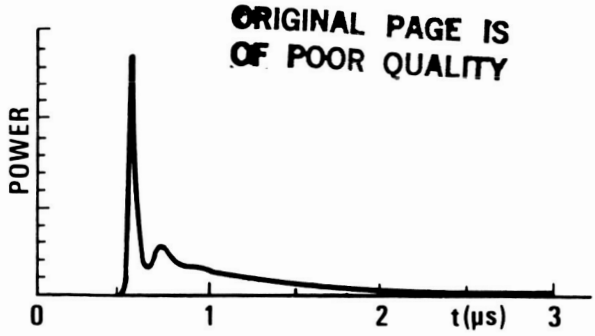

Figure 2. Output pulse shape of a simple self-sustained CO_2 TEA laser. Output energy 80 mJ.

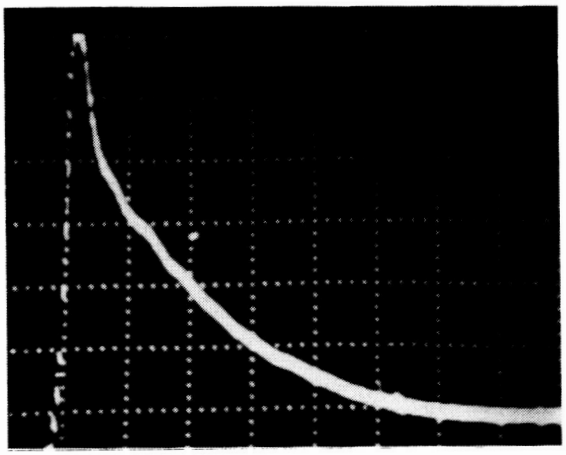

Figure 3. Output pulse shape of a hybrid self-sustained CO_2 TEA laser. Output energy 80 mJ, timescale 0.5 μs/division.

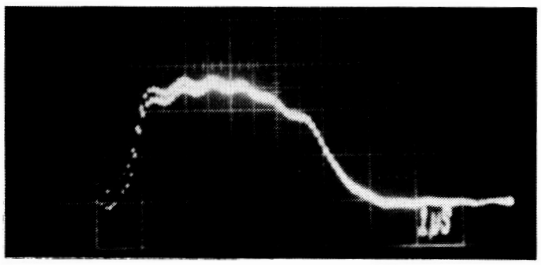

Figure 4. Output pulse shape of a hybrid electron-beam sustained CO_2 TEA laser. Output energy 80 mJ, timescale 1 μs/division.

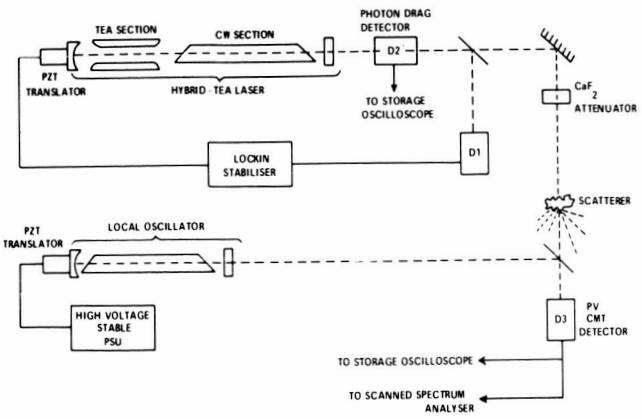

Figure 5. Typical heterodyne equipment for the determination of the frequency characteristics of a CO_2 TEA laser.

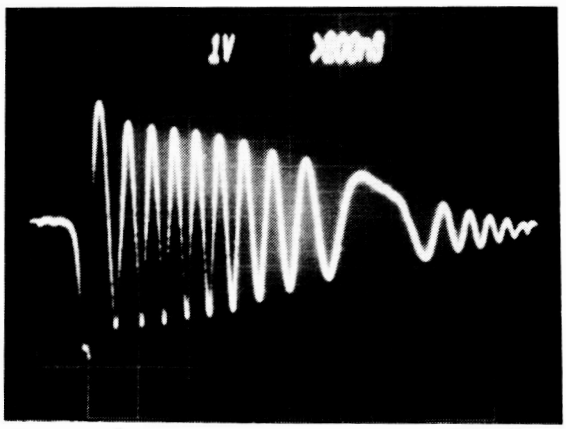

Figure 6. Example of beat signal between LO and TEA CO_2 laser. Timescale 300 ns/division.

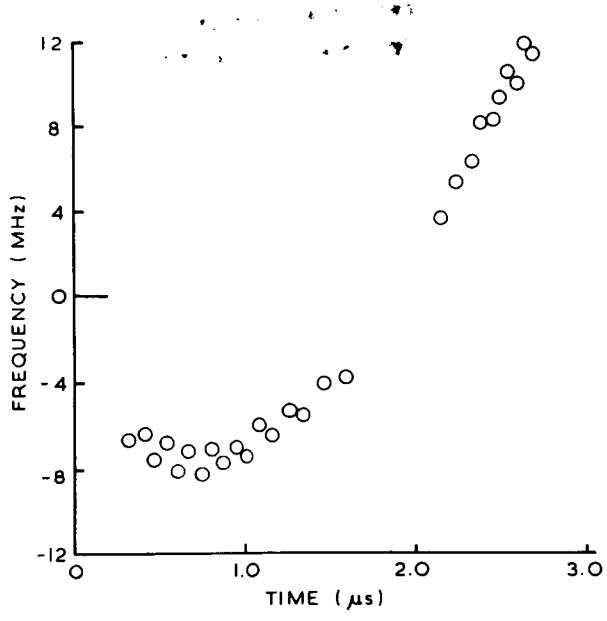

Figure 7. Frequency behavior derived from Figure 6. Frequency increases in the tail of the pulse at 3.0 MHz/μsec.

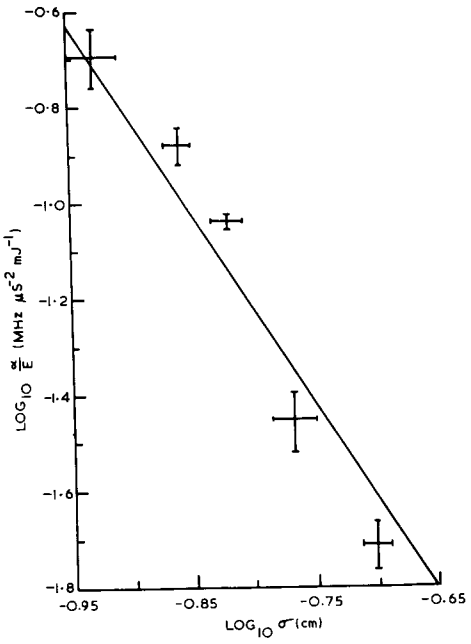

Figure 8. Chirp coefficient versus spot size for injection mode selected CO_2 laser. Line of predicted slope (-4) is shown for comparison.

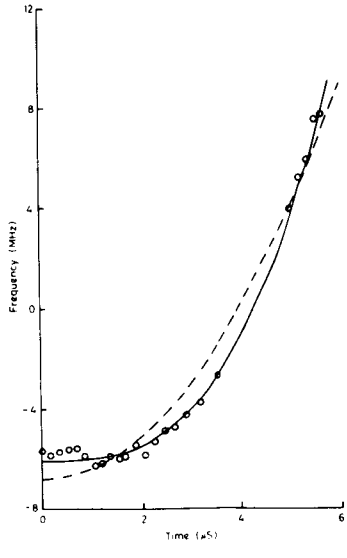

Figure 9. Frequency behavior of hybrid e-beam sustained CO_2 laser (circles). Best fit parabolic and cubic curves shown by dashed and solid lines, respectively.

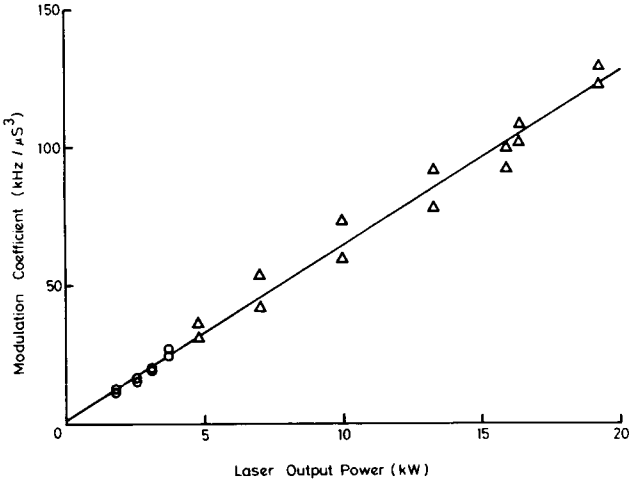

Figure 10. Graph illustrating linear dependence of modulation coefficient on output power for two different pulse lengths of an e-beam sustained TEA laser.

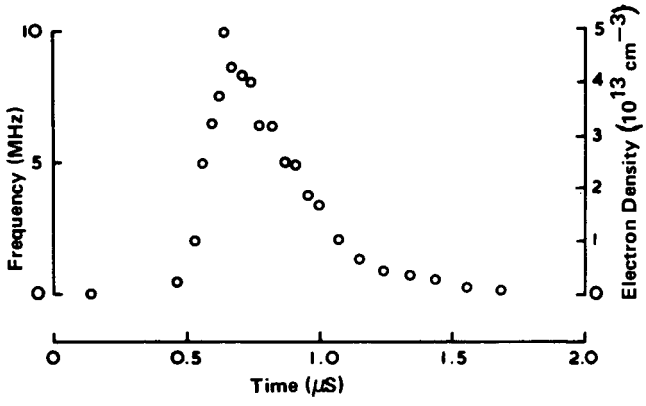

Figure 11. Plasma effect on cavity frequency during a transverse discharge.

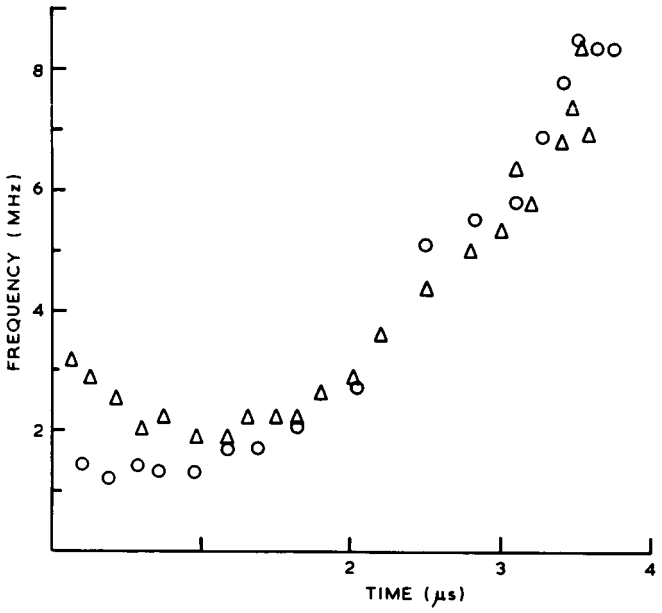

Figure 12. Frequency behavior at beginning of a hybrid laser pulse showing effect of time delay. Δ CW section above threshold, 0 CW section off.

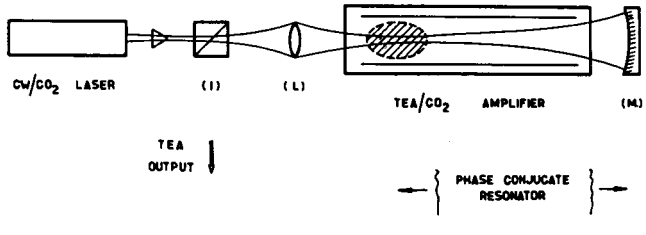

Figure 13. Frequency stabilization by phase conjugation in saturated CO_2.

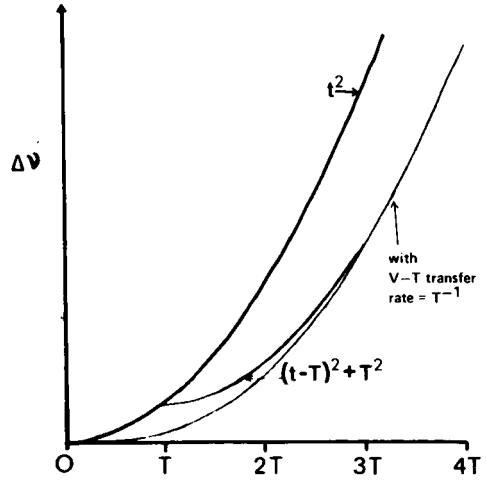

Figure 14. Effect of LIMP chirp of a finite V→T transfer rate T^{-1}.

LARGE MODE RADIUS RESONATORS

Michael R Harris
Royal Signals and Radar Establishment
Malvern, Worcestershire
United Kingdom

SUMMARY

Resonator configurations permitting operation with large mode radius while maintaining good transverse mode discrimination are considered. Stable resonators incorporating an intracavity telescope and unstable resonator geometries utilizing an output coupler with a Gaussian reflectivity profile are shown to enable large radius single mode laser operation. Results of heterodyne studies of pulsed CO_2 lasers with large (11mm e^{-2} radius) fundamental mode sizes are presented demonstrating minimal frequency sweeping in accordance with the theory of laser-induced medium perturbations.

INTRODUCTION

In pulsed CO_2 lasers both plasma effects and a laser-induced effect (LIMP) lead to frequency sweeping (1), of these, particularly for longer pulse operation, LIMP is the major offender. This chirp process exhibits an inverse 4th power dependence on beam spot size, hence a laser which has a large intracavity beam diameter can be expected to show a minimal laser-induced frequency sweep. Further advantages accrue from such a geometry; large mode volumes are obtainable from short resonators thus allowing high energy operation from compact structures, furthermore since the energy is dispersed over a large area of the mirror surface, good resistance to mirror damage should ensue. Unfortunately single mode operation from large mode radius resonators is not readily achievable; therefore, it is intended in this paper to consider possibilities for large single mode operation.

STABLE RESONATORS

Smooth Gaussian intracavity mode profiles coupled with relative insensitivity to mirror misalignment are desirable features associated with lasers employing stable resonators.

Figure 1 shows a plot derived from the analysis of Kogelnik and Li (2) of beam spot size versus $g_1\ g_2$ where $g_1 = 1 - L/R_1$ and $g_2 = 1 - L/R_2$, L is cavity length and R_1 and R_2 are the radii of curvature of the two laser mirrors. The resonator is stable when $0 < g_1\ g_2 < 1$, and within this regime the cavity rays are confined. The form of this plot is typical of stable resonators although this is calculated for the particular case of a 40cm long cavity having one mirror with a 5m convex radius of curvature. The beam size shown is that at the concave mirror.

Spot Size Limitations

Over the majority of the stable region spot sizes are typically less than 2mm; it is only at the two extremes where the threshold of stability is approached that the beam blows up in size. The left hand extreme, $g_1 g_2 = 0$, represents the hemispherical cavity configuration and although the beam tends to become infinitely large at the concave mirror at the other mirror the tendency is towards an infinitely small spot. Since any ray is reflected back on itself to the focus there is no mode selectivity. Of course mirror damage problems associated with the small spot will be severe.

The right hand extreme, $g_1 g_2 = 1$, represents the equivalent plane-plane resonator configuration in which beam size is only limited by mirror dimensions. But in order to ensure fundamental mode operation a small iris needs to be inserted into the cavity to aperture the beam and introduce loss to higher order modes.

So stable resonators with large spots have little or no mode selectivity, but this only applies to simple cavities - if we are allowed to introduce other optical elements then this gives a further degree of freedom.

Telescopic Stable Resonator

Hanna et al (3) have demonstrated a Nd:YAG laser employing a stable resonator with a x4 intracavity telescope. This laser exhibits good fundamental mode operation yet produces a large beam over a portion of the cavity.

Figure 2 shows this resonator configuration applied to the CO_2 wavelength (4). An electron beam sustained discharge (5) is used to pump the pulsed gain module; this technique is a convenient and reliable way to operate larger cross section discharges and has the advantage that long pulse (several microseconds) operation can be assured. Since one leg of the resonator comprises a small diameter beam it is possible to hybridize the laser by the insertion of a low pressure cw gain cell, thus ensuring SLM operation as well as achieving a degree of gain switched spike suppression. The telescope is x4 and of Galilean configuration in order to avoid air breakdown problems associated with an intracavity focus. Overall cavity length is 1.75m and is invar spaced. Both the 100%R mirror and the 70%R output coupler are plane and to ensure that the cavity is an equivalent confocal resonator the telescope is slightly defocussed.

Figure 3 shows the near field beam profile of the output which has a Gaussian-like appearance, a best fit Gaussian to this profile has an e^{-2} intensity radius of 11.2mm which agrees well with the theoretical prediction of 10.9mm.

Single mode operation was confirmed by examination of the cw output on a CMT detector; no beats were detected over the 0-100MHz bandwidth of the detector. The mode purity is further confirmed by the lack of beats on the power vs time waveform shown in figure 4. The gain switched spike is only partially suppressed here, presumably due to the low intracavity intensity of the cw radiation in the expanded portion of the beam within the pulsed gain region.

Shown in figure 5 is a typical beat signal between the pulsed output and a local oscillator. The output energy is 1.1J, the heterodyne signal being obtained from the scattered radiation off the joule meter surface. Measurement of peak positions

enables a frequency versus time plot to be generated and figure 6 represents on overlay of several such measurements of pulses ranging in energy between 0.64J and 1.1J. No trend in energy is observable and the plots are essentially flat indicating that LIMP is negligible. Any residual shape is most probably attributable to plasma effect.

A plot of normalized chirp coefficient against beam spot size showing the inverse 4th power dependence is depicted in figure 7. Plotted in the figure is the result with the 11.2mm beam radius shown falling close to the theoretical line of slope -4 demonstrating that the extrapolation to large spots is valid. This confirms that the technique of operating with a large intracavity mode is successful in overcoming the laser-induced chirp.

Larger magnifications than the x4 telescope used here are feasible, unfortunately the power density in the small beam leg of the resonator becomes extremely high as the mode volume and hence pulse energy is increased and ultimately mirror damage becomes a limiting factor. Clearly a configuration producing large spot sizes throughout the resonator is a necessary requirement.

UNSTABLE RESONATORS

Hard Mirror Unstable Resonators

In unstable resonators (6) the rays are divergent and are allowed to spread off the mirror surfaces with characteristically high losses. The leakage of radiation around the periphery of one mirror often forms the useful laser output. Unstable resonators offer a solution to the problem of filling large mode volumes but must be viewed with some reservation. Unlike stable resonators the mode properties are not well understood, the modes are not smoothly varying in intensity but are characteristically rippled, a feature which cannot be conducive to minimizing the laser-induced frequency sweep. A further problem pertinent to the realization of a fieldable laser is the tendency of these resonators to be highly alignment sensitive.

Gaussian Mirror Resonators

Operation of a laser with an unstable resonator incorporating an output coupler with a Gaussian reflectivity profile has been demonstrated (7). This technique largely overcomes the problems associated with unstable resonators; the intracavity mode is constrained to be Gaussian and the system shows relative insensitivity to mirror misalignment.

A feature of these cavities is that although the geometric configuration is that of an unstable resonator the rays are in fact confined so that the resonators are arguably stable. This arises because the spot reflected from the Gaussian mirror is reduced in size relative to the spot incident upon it. The Gaussian beam incident upon the mirror can be expressed as

$$I_i(r) = I_{io} \exp - (2r^2/\overleftarrow{w}_1^2)$$

the mirror intensity reflectivity profile as

$$R(r) = R_o \exp - (r^2/w_{int}^2)$$

The reflected beam is the product of these two Gaussians:

$$I_i(r) = I_i(r)R(r)$$

$$= I_{io}R_o \exp - \left[(2r^2/\overleftarrow{w}_1^2) + (r^2/w_{int}^2)\right]$$

$$= I_{ro} \exp - (2r^2/\overrightarrow{w}_1^2)$$

Thus

$$\frac{1}{\overrightarrow{w}_1^2} = \frac{1}{\overleftarrow{w}_1^2} + \frac{1}{2w_{int}^2}$$

where r is radial distance; $\overrightarrow{w}_1$ and $\overleftarrow{w}_1$ are the e^{-2} intensity radii of the right and left travelling beams respectively when the Gaussian mirror is at the left; and w_{int} is the e^{-1} reflectivity intensity radius of the Gaussian mirror (GM).

The graph shown in figure 8 plots the ratio of spot size reflected from the Gaussian mirror to the mirror Gaussian profile size as a function of g_1g_2. Although calculated for a 5m convex GM the plot, with only minor deviations, is general to GM resonators. In the stable region the beam radius is essentially the same as a conventional hard mirror resonator, an interpretation is that since the spot is small only the central portion of the GM is addressed over which the variation in reflectivity is small, ie the GM looks much like a conventional hard mirror. But, as the incident beam blows up in size the GM asserts itself and ultimately as the incident spot size tends to infinity the reflected spot tends to $\sqrt{2}\ w_{int}$.

In recent work at RSRE a Gaussian mirror has been incorporated in a short resonator 40cm long, this cavity length has been chosen not only for compactness but also to try to ensure SLM* operation. The e-beam sustained discharge module mentioned earlier was used again in this arrangement. The results of a scan across the GM in order to measure its reflectivity profile are shown in figure 9. Fitted to the experimental points is the best fit Gaussian which for this particular section has an e^{-1} intensity radius of 9.33mm, but the profile is not perfectly circular and varies depending on scan direction between 9.1mm and 10.0mm.

Figure 10 is a plot of beam spot sizes calculated for such a 40cm long cavity having a convex 5m radius of curvature GM with an e^{-1} intensity reflectivity radius (w_{int}) of 10mm. Along the top is indicated the radius of curvature of the hard mirror for which the specific value used was 8m concave giving beam radii in the vicinity of 10-11mm.

Reproduced in figure 11 is the near-field beam profile of the output from the laser utilizing this cavity configuration. Taking into account the uncertainty in w_{int} the beam dimensions are in agreement with theory. The central dip arises from the relatively high on-axis reflectivity of the Gaussian reflectivity output coupler. Lavigne (7) have demonstrated that the propagation characteristics of a beam with such a near field profile are good, the far field profile being nearly Gaussian and free of side lobes.

---

*Single Longitudinal Mode (SLM).

A power-time waveform of the laser output is shown in Figure 12; the lack of mode beating confirms the good mode selectivity of this GM resonator. The good transverse mode discrimination is unsurprising when the weighted mean reflectivity of 40% for the fundamental (on axis) mode is compared with the TEM_{01} mode value of only 20%. On faster timescales longitudinal mode beating is just discernible but again - although perhaps more surprisingly - rejection is very good the mode ratio being greater than 10^4 for the 40cm cavity length used here.

Figure 13 shows the beat signal between the GM resonator laser output and a local oscillator. The output pulse energy is just over 1J. The beat frequency is remaining essentially constant throughout the pulse at 3.85 ± 0.25 MHz.

CONCLUSIONS

Large mode radius resonators offer potential for high output energies from compact laser structures with good resistance to mirror damage as well as for minimizing LIMP. The effectiveness of such resonators in minimizing the laser-induced-frequency sweep has been demonstrated at output energies of 1J for pulses several microseconds long. The GM resonator shows much promise for large single mode operation, the intracavity mode has a Gaussian profile, transverse mode discrimination is high and the cavities are reasonably insensitive to mirror misalignment.

REFERENCES

1. D V Willetts: Review of the Frequency Stabilization of TEA CO_2 Laser Oscillators, NASA/RSRE Workshop on Closed-Cycle, Frequency-Stable CO_2 Laser Technology, NASA CP-2456, 1987.

2. H Kogelnik and T Li: Laser Beams and Resonators Appl Opt 5 (1966) pp 1550-67.

3. D C Hanna, C G Sawyers, M A Yuratich: Telescopic Resonators for Large-Volume TEM_{oo}-mode Operation, Optical and Quantum Electronics 13 (1981) pp 493-507.

4. D V Willetts and M R Harris: Attainment of Frequency Stable High-Energy Operation of a CO_2 TEA Laser by Use of a Telescopic Resonator, IEEE J Q.E. 21 No 3 (1985) pp 188-191.

5. A Crocker, H Foster, H M Lamberton and J H Holliday: Pulsed Atmospheric Pressure Carbon Dioxide Laser Initiated by a Cold Cathode Glow-Discharge Electron Gun, Electron Lett 8 No 18 (1972) PP 460-461.

6. A E Siegmann: Unstable Optical Resonators, Applied Optics 13 No 2 (1974) pp 353-367.

7. N McCarthy and P Lavigne: Large Size Gaussian Mode in Unstable Resonators Using Gaussian mirrors, Optics Letters 10 No 11 (1985) pp 553-555.

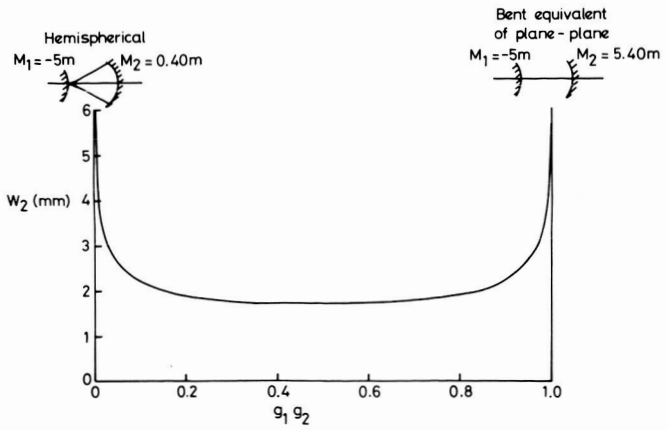

STABLE RESONATOR MODE RADIUS VS $g_1 g_2$ ($\lambda = 10.6\mu$, $R_1 = -5.0m$, $L = 0.40m$)

Figure 1.

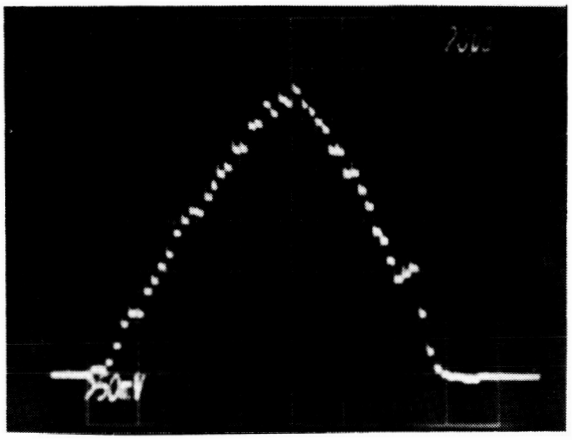

Near-field section of telescopic resonator laser output; pitch of elements = 0.5mm

Figure 3.

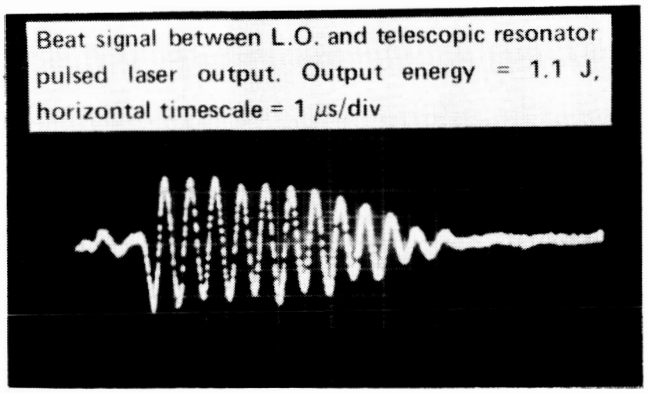

Figure 5.

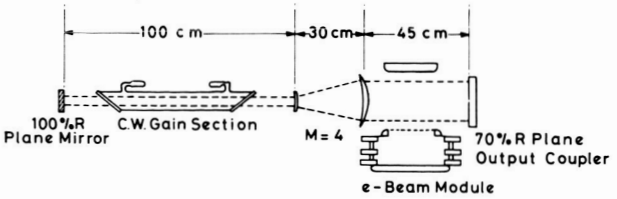

Hybrid e-beam sustained CO_2 laser with telescopic resonator

Figure 2.

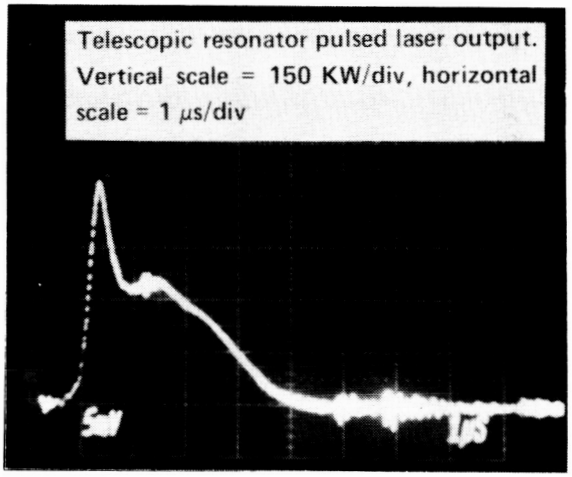

Figure 4.

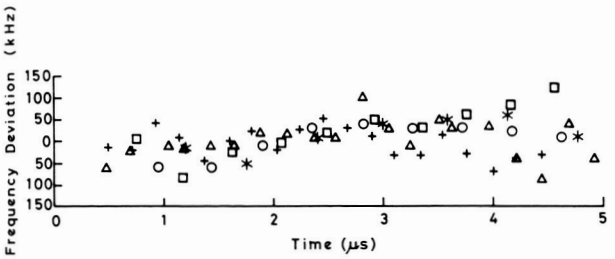

Telescopic resonator laser; temporal variation from mean of beat frequency for the following output energies
□ = 0.64 J; + = 0.70 J; * = 0.85 J;
0 = 1.00 J; Δ = 1.07 J.

Figure 6.

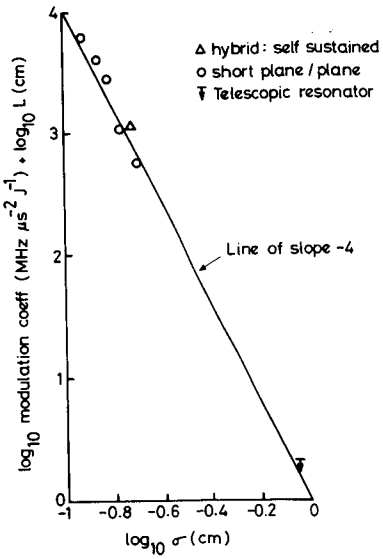

NORMALISED MODULATION COEFFICIENT VERSUS BEAM RADIUS SHOWING PREDICTED INVERSE 4th POWER DEPENDENCE

Figure 7.

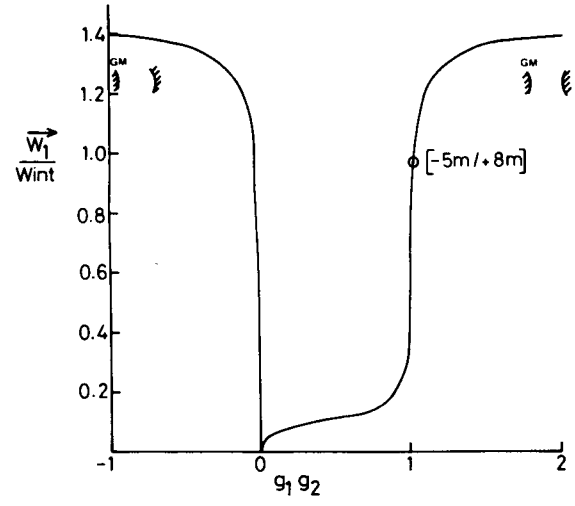

GAUSSIAN RESONATORS: NORMALISED SPOTSIZE REFLECTED FROM GAUSSIAN MIRROR

Figure 8.

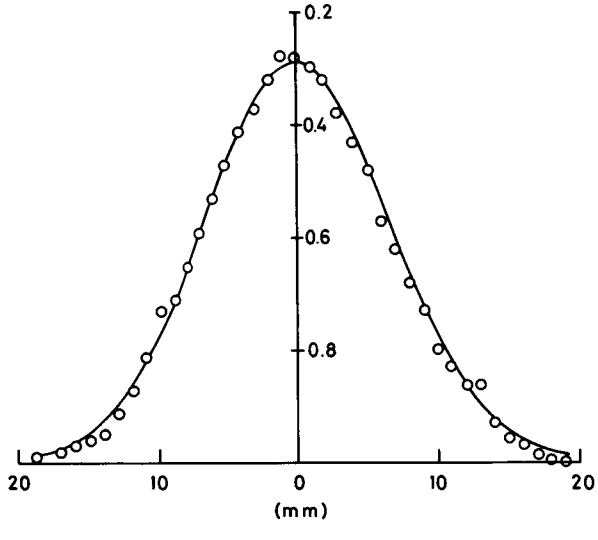

RADIAL TRANSMISSION PROFILE OF GAUSSIAN MIRROR
(fit to curve w = 9.33 mm)

Figure 9.

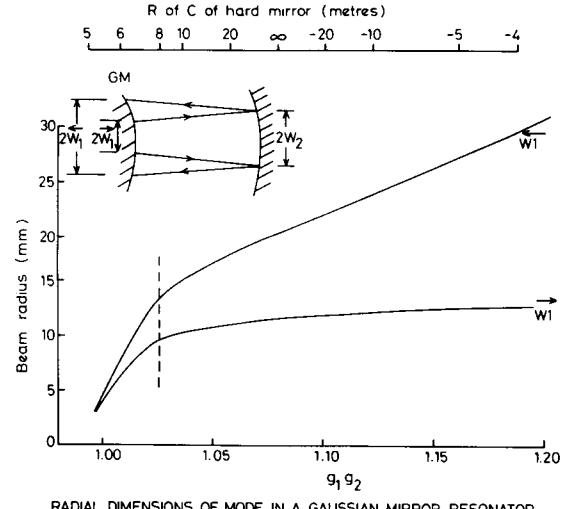

RADIAL DIMENSIONS OF MODE IN A GAUSSIAN MIRROR RESONATOR
(R OF C = 5m VEX, WINT = 10 mm)

Figure 10.

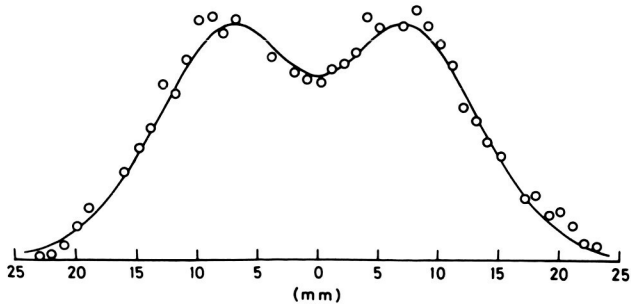

NEAR FIELD (d = 1.2 m) TRANSVERSE PROFILE OF GAUSSIAN MIRROR RESONATOR

Solid line calculated assuming w = 15.9 mm, w_{int} = 11.5 mm, R_{max} = 0.74

Figure 11.

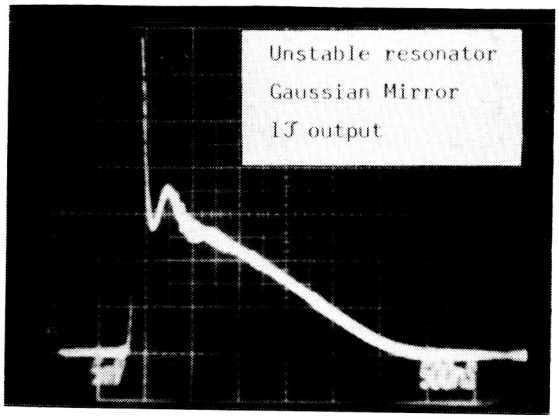

Figure 12.

Beat signal between L.O. and pulsed laser with Gaussian Resonator. Output energy = 1.1 J, horizontal time scale = 1 μs/div

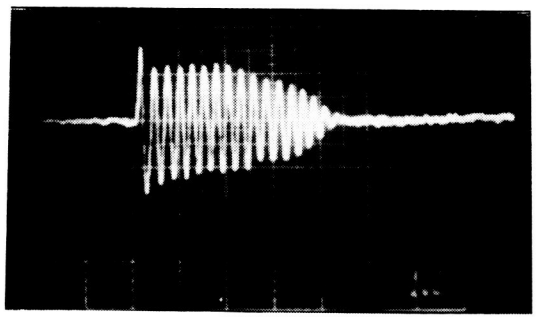

Figure 13.

WIND VELOCITY MEASUREMENT ACCURACY WITH HIGHLY STABLE 12 mJ/PULSE HIGH REPETITION RATE CO_2 LASER MASTER OSCILLATOR POWER AMPLIFIER

James W. Bilbro and Steven C. Johnson
Marshall Space Flight Center, AL

Jeffry Rothermel
University Space Research Associates
Huntsville, Alabama

SUMMARY

A coherent CO2 lidar operating in a master oscillator power amplifer configuration (MOPA) is described for both ground-based and airborne operation. Representative data taken from measurements against stationary targets in both the ground-based and airborne configurations are shown for the evaluation of the frequency stability of the system. Examples of data are also given which show the results of anomalous system operation. Overall results demonstrate that velocity measurements can be performed consistently to an accuracy of ±0.5 m/s and in some cases ±0.1 m/s.

INTRODUCTION

The pulsed coherent CO_2 lidar is shown in figure 1. This system has been operated in both ground-based and airborne configurations since 1971. Extensive modifications have been made and numerous measurements have been performed to obtain better understanding of the operation of the lidar and its inherent measurement accuracy. Ideally, the measurement accuracy should be determined primarily by the signal-to-noise ratio. To that end, many contributing errors must be overcome. Since many of the errors are due in part to system configuration, the ground-based operation of the system will be described first, followed by a description of airborne operation. A more detailed description of the system, its operation and associated errors will be found in references 1 and 2.

GROUND-BASED CONFIGURATION

A simplified block diagram of the lidar in its ground-based configuration is shown in figure 2. The master oscillator laser is an eight watt continuous wave CO_2 laser operating at a wavelength of 10.6 microns. Briefly, a small portion of the laser output is split off and directed to a pyroelectric detector where it is combined with the local oscillator laser. The beat signal out of this detector is used in a locking loop to lock the

local oscillator laser to a 10 MHz offset from the master oscillator laser. The main portion of the master oscillator laser is directed through an electro-optic modulator, an isolator, a beam expander and into a series of six longitudinal discharge tubes which serve as the power amplifier. The output of the power amplifier passes through a Brewster window, a quarter-wave plate and into the telescope where it is expanded to a diameter of 24 cm (measured to the 1/e2 points). The return beam, scattered by the target, is collected by the same telescope, directed through the quarter-wave plate, then reflected off the Brewster window to the detector where it is combined with the local oscillator beam. The output of the detector is then processed to extract the Doppler velocity and associated information. Velocity errors arise primarily from four different areas within this process. These are discussed in greater detail as follows.

A. Electro-optic modulator

The electro-optic modulator consists of two Cadmium Teluride crystals nested in a series of Brewster plates. Modulation of the beam is accomplished by applying a voltage to the first crystal which rotates the polarization of the beam such that it is passed by the central Brewster plates. At a selectable time later (1, 2, 4, or 8 microseconds), voltage is applied to the second crystal which rotates the polarization so that the beam is blocked by the final set of Brewster plates. Failure of the second crystal in the 1984 flight tests described in reference 1 produced the pulse shape shown in figure 3. The arrow at the top of the figure indicates the point at which the second crystal would normally have terminated the pulse. The exponential decay following the arrow is the relaxation of the crystal while the long tail is the result of acoustic ringing. An amplitude plot of the return in the vicinity of a mountain peak is shown in figure 4. Five traces are shown in this figure, one up wind of the mountain where there are no aerosols and hence no signal, one on the downwind side where aerosols from the mountain have been entrained and three traces where the mountain was hit. The shelf, which is evident just prior to the peak in signal return from the mountain, is due to pre-pulse leakage, whereas the ringing after the peak is due to the pulse tail caused by acoustic ringing in the first crystal. It is apparent that significant errors can result due to contributions from both the pre-pulse shelf and the tail. While it is not evident from looking at the trace of the aerosol return, the apparent range to which measurements have been made has been greatly extended due primarily to the integrating effect of the long tail in particular. Hence, velocity measurements beyond approximately 8 km are in reality the results of an average over the entire length of the tail and are not from the primary pulse. Refurbishment of the modulator with improved mounting techniques has reduced this problem, but a double crystal is still used to provide a well-defined pulse shape. The modulation frequency is variable from 100 to 200 Hz.

B. Isolator

The isolator is an Indium Antimonide crystal embedded in a permanent magnet. The isolator prevents radiation which has been scattered from optical surfaces downstream from the master oscillator from reentering the laser and causing frequency pulling in the master oscillator. The isolator provides approximately 12 dB of isolation with 3 dB of loss. A plot of the apparent Doppler velocity of a mountain approximately 15 km from the lidar with the isolator removed is shown in figure 5. As can be seen from this plot, significant velocity excursions occur with a periodicity of approximately 90 seconds. This is in contrast to the plot shown in figure 6 with the isolator in place. In this case the velocity excursions are less than ±0.5 m/s.

C. Local oscillator

The primary difference between the airborne and ground-based configurations is that in the case of the ground-based configuration, a separate local oscillator laser is locked to the master oscillator laser at a frequency offset of 10 MHz. This allows the velocity sense (i.e., the direction of the motion) to be determined by noting on which side of the 10 MHz local oscillator the Doppler shifter signal occurs. In the offset local oscillator case, error is a function of how well the two lasers can be locked. The locking loop is designed for ±100 kHz; however, in practice considerable variability is experienced depending upon how well the locking loop is tuned under a given set of ambient conditions. Figure 7 shows velocity measurements of the signal return from a mountain at a range of 4350 meters. In this figure, the locking loop has been tuned to produce a variation of only ±0.1 m/s. This corresponds to a frequency stability of approximately ±18 kHz; however, this is the result of a 50 pulse average. If we allow for a n improvement in variance, where n is the number of shots averaged, this results in a single pulse frequency stability of ±50 kHz. Figure 8 illustrates momentary loss of lock resulting in sharp excursions in the measured velocity. A 30 minute time history is shown in figure 9, demonstrating the long-term stability of the system. The slight offset from zero is a function of how well the loop has been tuned to the 10 MHz offset. As can be seen from this figure there is a long-term drift of approximately 0.25 m/s plus occasional short-term oscillations of ±0.25 m/s. Excluding the momentary losses of lock, the overall accuracy of the measurement is determined by the short-term oscillations of ±0.25 m/s.

D. Zero Doppler shift measurement

Ordinarily it is not possible to perform measurements of a stationary target with a coherent lidar such as has been described. This is due to the fact that leakage from the master oscillator laser heterodynes with the local oscillator to produce an extremely strong beat signal at the offset frequency. This beat signal will obscure any return from a stationary target

which also occurs at the offset frequency. Therefore, in order to perform the measurements previously described, it is necessary to remove the offending beat signal. This is accomplished by applying a voltage "kick" to the pzt of the master oscillator laser shortly after pulse transmission. When this occurs, the frequency of the laser is driven to a point where the beat signal between the master oscillator and the local oscillator is outside the bandpass of the signal processing electronics. Scattered radiation from stationary targets will then be heterodyned with the local oscillator and will appear as a beat signal at the offset frequency without contamination from the master oscillator leakage. If this process is not done carefully, errors will be introduced into the measurements. Figure 10 illustrates the frequency excursion of the master oscillator laser as it is driven out of band. It is apparent from this figure that if the master oscillator laser is not driven sufficiently far off, frequency and oscillations appear at the edge of the pass band of the signal processing electronics creating large errors in velocity measurement.

AIRBORNE CONFIGURATION

The primary difference in the basic lidar configuration between ground-based and airborne operation is that instead of using an offset local oscillator, a portion of the master oscillator is used as a local oscillator in a homodyne configuration as shown in figure 11. In the airborne case there is no need to have an offset local oscillator. The Doppler shift due to the aircraft provides the offset necessary to determine the sense of the wind velocity. There are, however, additional factors contributing to the error in that the velocity of the aircraft must be known as well as the attitude of the lidar and the pointing accuracy of the scanner. All of these factors are critical to the wind measurement accuracy.

In operation, an inertial platform is attached directly to the lidar, and the entire assembly is shock mounted to the aircraft. The data from the inertial platform (i.e. pitch, roll, drift angle and true heading, true airspeed) are transmitted to a central computer which calculates the desired scanner settings for pointing the lidar beam. The resulting scanner settings, along with ground speed and true airspeed, are then used to calculate the wind velocity relative to the ground. Typically, the lidar beam is scanned forward 20 degrees and then aft 20 degrees in a horizontal plane at the altitude of the aircraft. This is depicted in figure 12. Data are collected for each range gate of the lidar and averaged for 50 pulses. As can be seen from this figure, each aft scan intersects a number of prior forward scans. At each intersection point a vector velocity can be calculated. The results of such a calculation in a uniform flow field are shown in figure 13. Relative accuracy on the order of 0.2 m/s has been calculated in similar conditions by comparing adjacent

forward scans for variations in velocity measurements. The absolute accuracy of the airborne measurements can be determined by examining ground hits when the beam is given a slight angle of depression. This case is shown in figure 14, where adjacent forward scans are displayed. These scans have a 3-degree depression angle, and the ground hits can be clearly seen as a narrow line separated from the wind data. These ground hits were isolated by amplitude discrimination and their velocity plotted as a function of time. The result is shown in figure 15. Large excursions on the order of 2.0 m/s can be seen in this data. These excursions correspond to heading changes of the aircraft. Extensive investigations are under way to determine the cause of these excursions, but so far no satisfactory explanation has been found. The most likely cause currently under study concerns the potential misalignment due to increased g-loading during aircraft bank. Error in ground speed calculation by the inertial platform may also be a contributor in some cases. In spite of the undesirable excursions, the velocity variation in those time periods between heading changes is quite satisfactory. The time segment from 22:30 to 23:00 is shown expanded in figure 16. In this case the variation is less than ±0.5 m/s which is on the order of the accuracy obtained in ground-based operation.

CONCLUDING REMARKS

A number of examples have been given of the various errors which can occur in coherent lidar data from the instrument standpoint. It is hoped that these examples will serve as a demonstration of the care that must be taken in interpreting data from such an instrument since these errors can often times be mistaken for real data. In addition to the areas addressed, there are significant problems involved in taking into account the various atmospheric effects as well as the different methods of signal processing. While all of these problems are difficult and extreme care must be taken in dealing with them, coherent lidars can provide highly accurate velocity data and can serve as a very useful tool for performing atmospheric research.

REFERENCES

1. Bilbro, J.; DiMarzio, C.; Fitzjarrald, D.; Johnson, S.; Jones, W.: Airborne Doppler Lidar Measurements. Appl. Opt. Nov. 1, 1986.

2. McCaul, Eugene W.,Jr.; Bluestein, Howard B.; and Doviak, Richard J.: Airborne Doppler Lidar Techniques for Observing Severe Thunderstorms. Appl. Opt., Vol. 25, p.698 Mar. 1, 1986.

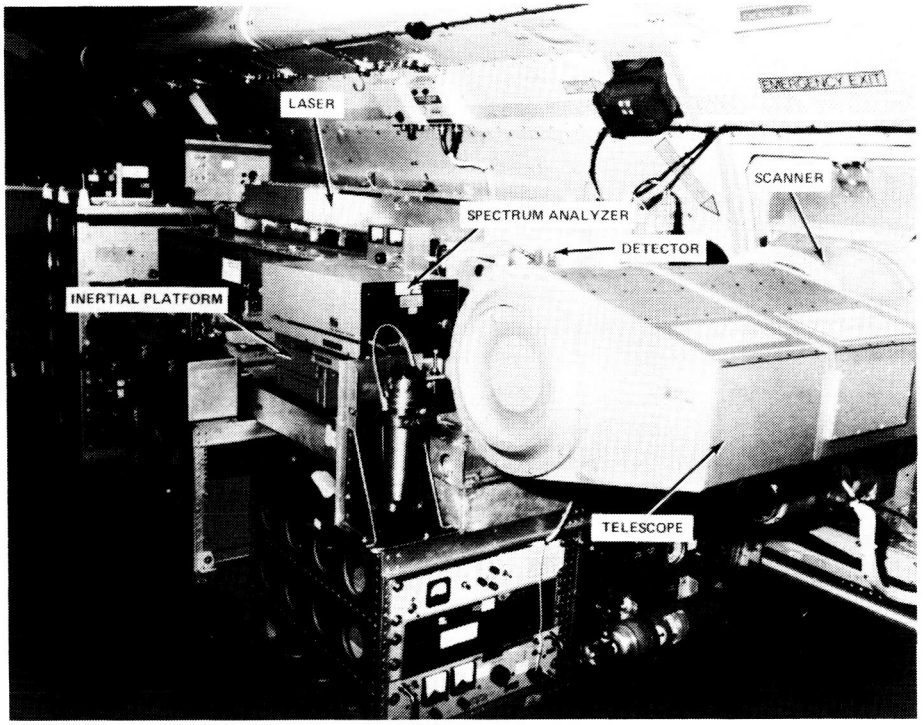

Figure 1. PULSED COHERENT CO_2 LIDAR.

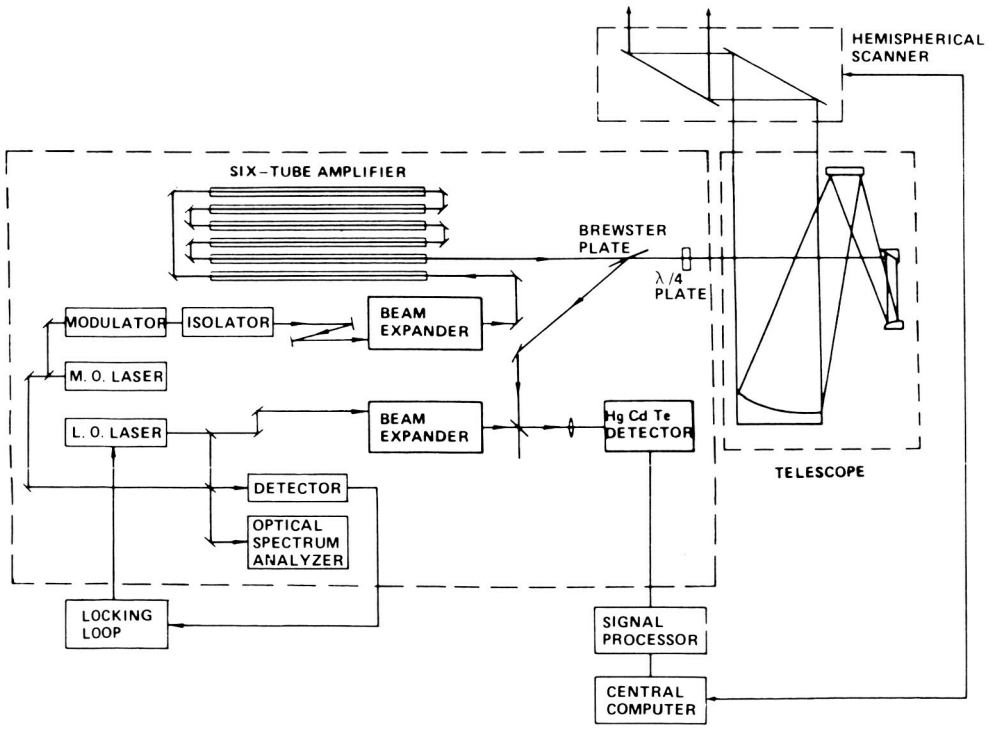

Figure 2. SIMPLIFIED BLOCK DIAGRAM OF GROUND-BASED CONFIGURATION.

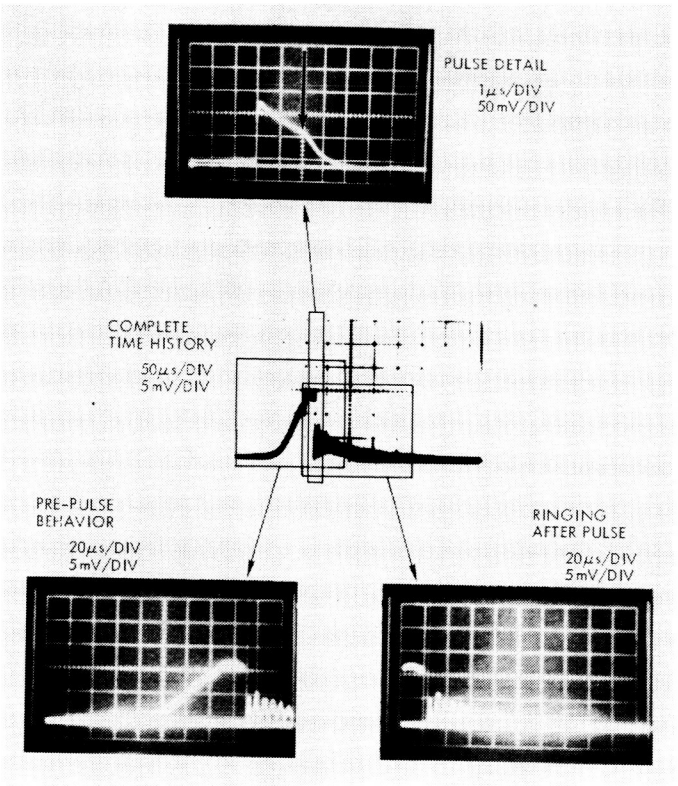

Figure 3. PULSE SHAPE DUE TO MODULATOR FAILURE.

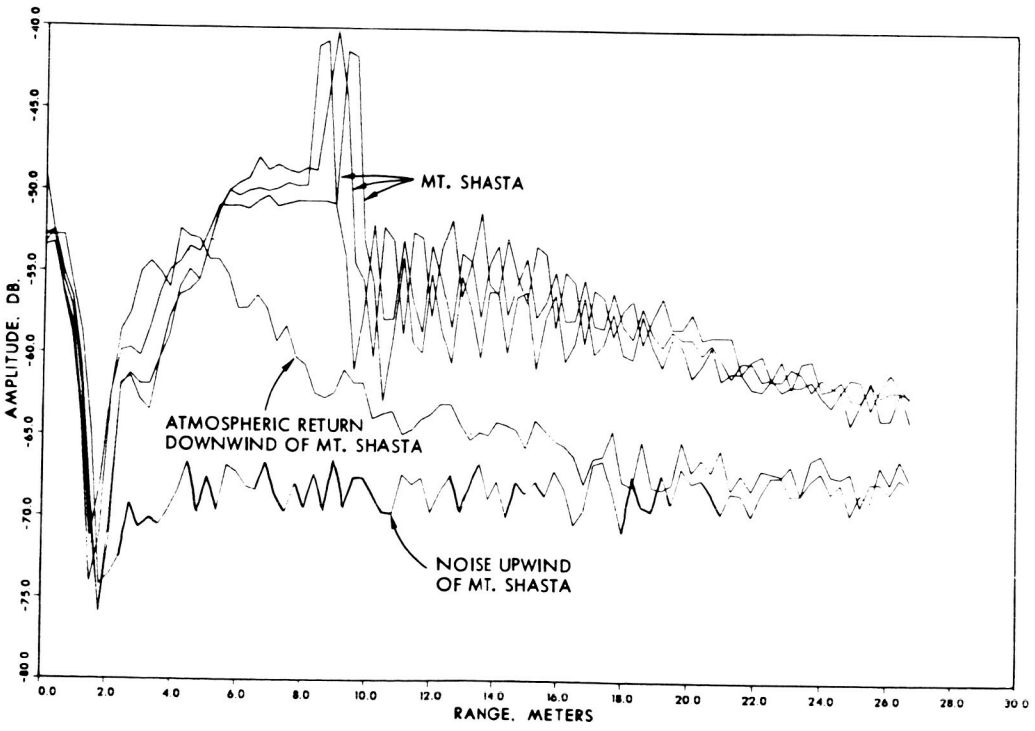

Figure 4. AMPLITUDE RETURN IN THE VICINITY OF A MOUNTAIN AFTER MODULATOR FAILURE.

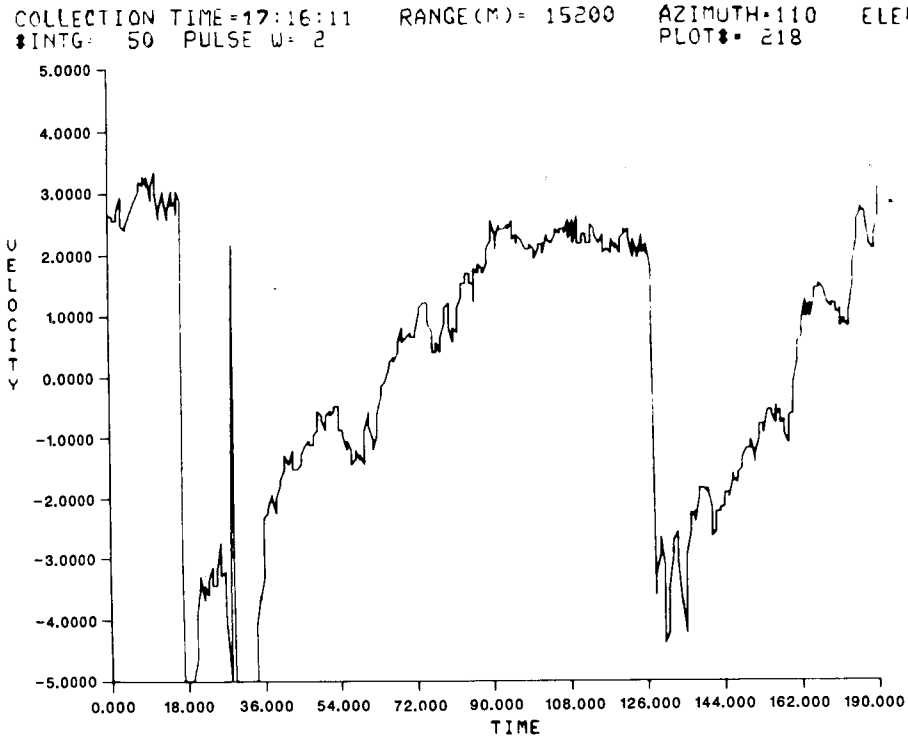

Figure 5. APPARENT DOPPLER VELOCITY OF A MOUNTAIN AT A RANGE OF 15 KM WITH ISOLATOR REMOVED.

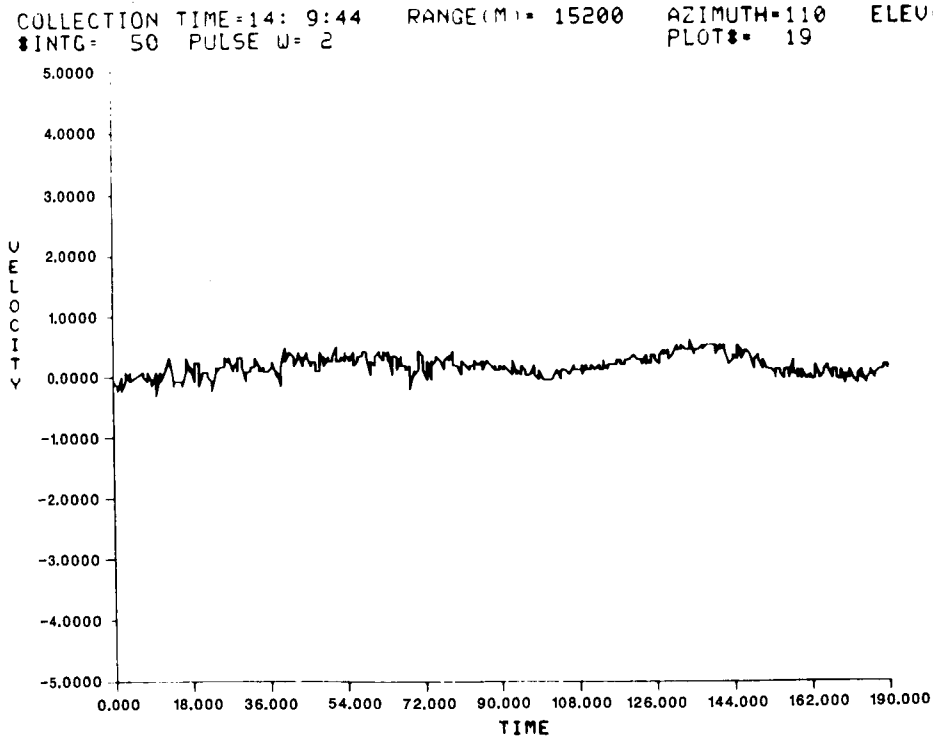

Figure 6. APPARENT DOPPLER VELOCITY OF A MOUNTAIN AT A RANGE OF 15 KM WITH ISOLATOR IN PLACE.

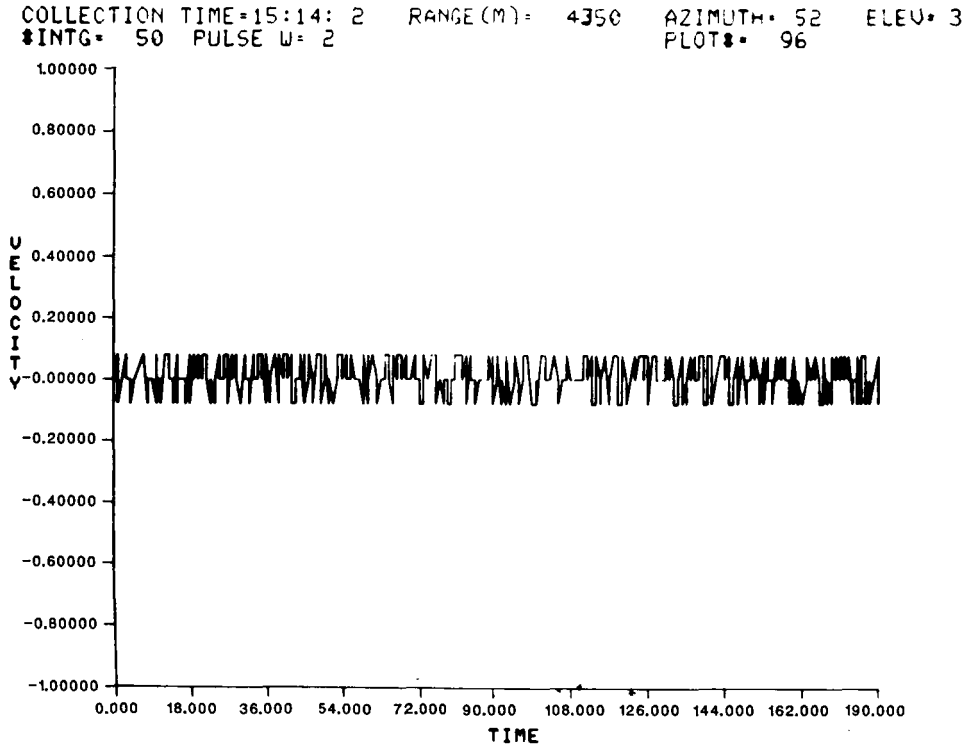

Figure 7. APPARENT DOPPLER VELOCITY OF A MOUNTAIN AT A RANGE OF 4 KM.

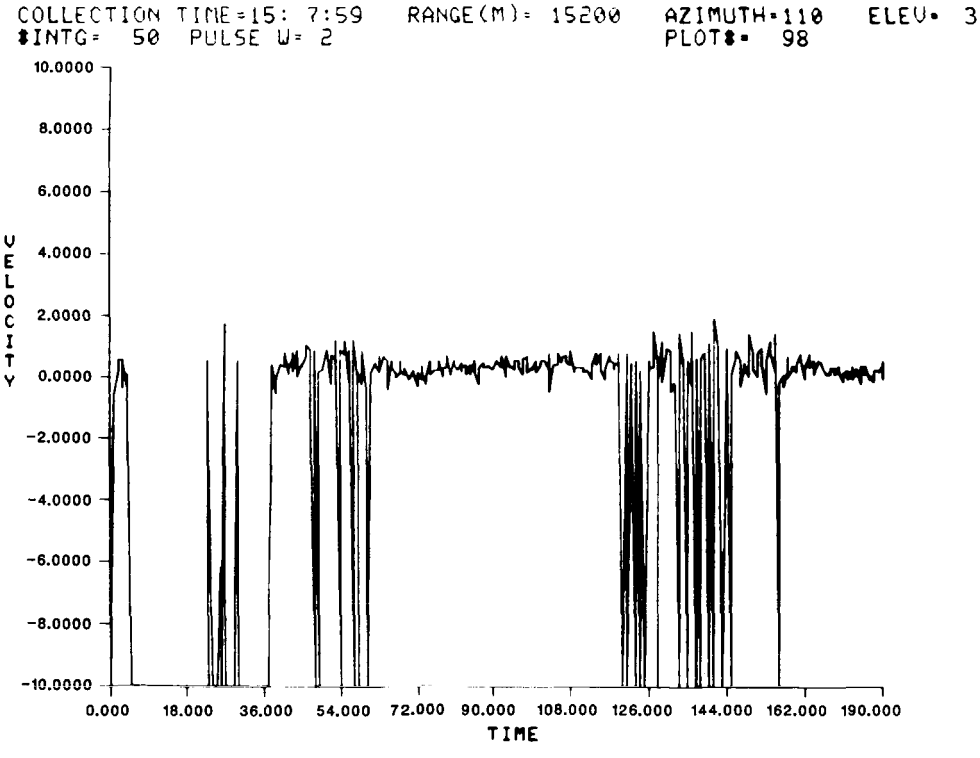

Figure 8. EFFECTS OF MOMENTARY LOSS OF LOCK ON VELOCITY MEASUREMENT.

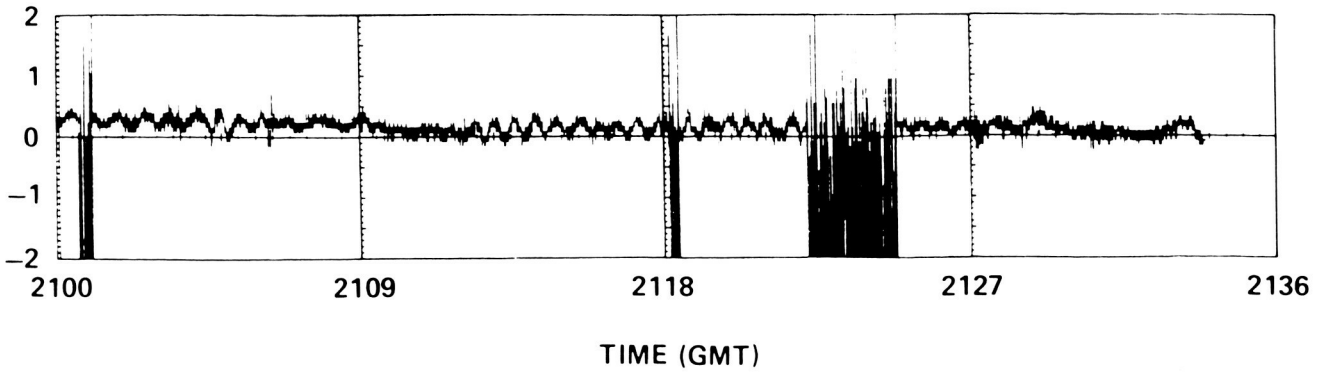

Figure 9. LONG-TERM STABILITY OF VELOCITY MEASUREMENT AGAINST A STATIONARY TARGET.

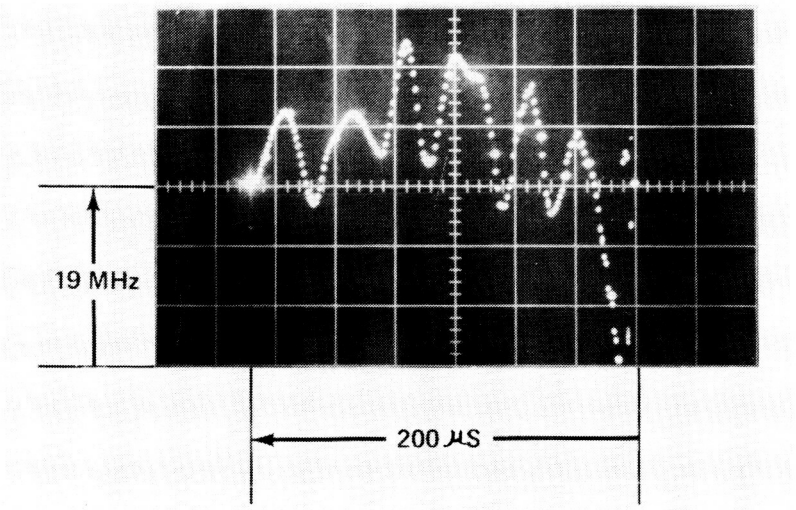

Figure 10. FREQUENCY EXCURSION OF MASTER OSCILLATOR LASER BEING DRIVEN OUT OF THE PASS BAND OF THE SIGNAL PROCESSOR ELECTRONICS.

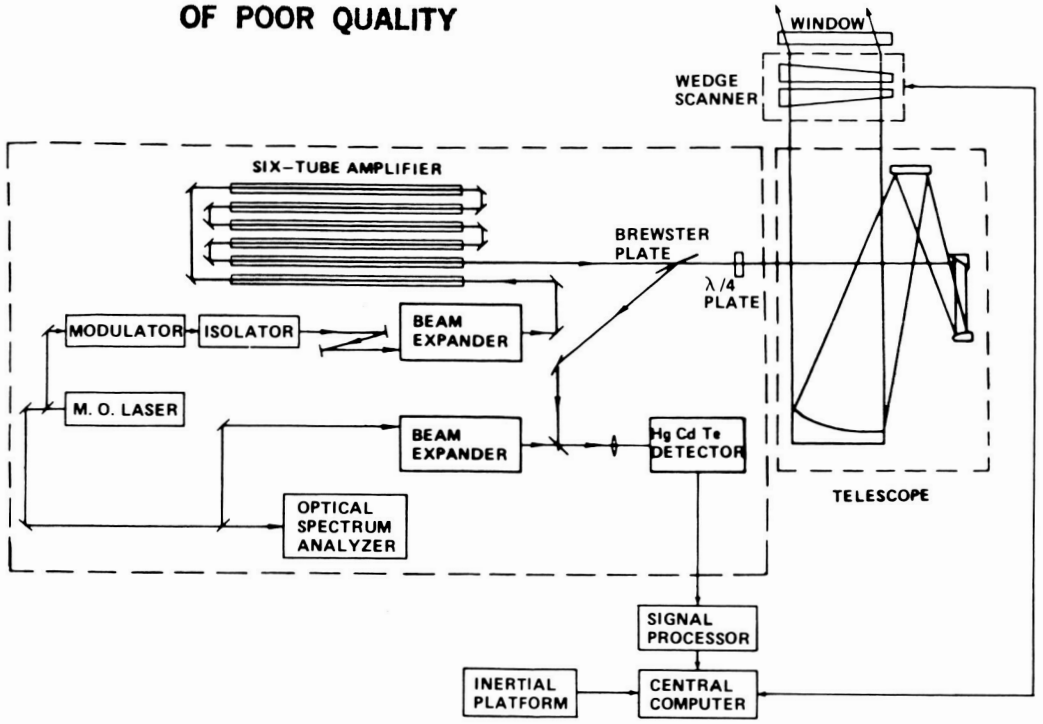

Figure 11. SIMPLIFIED BLOCK DIAGRAM OF AIRBORNE CONFIGURATION.

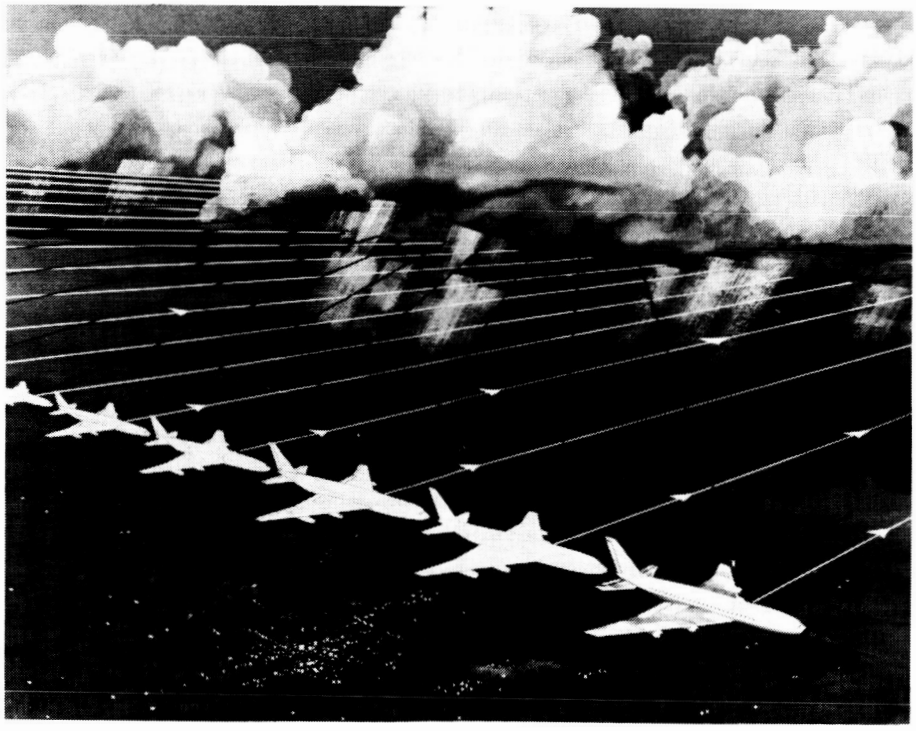

Figure 12. SCAN PATTERN OF THE AIRBORNE LIDAR.

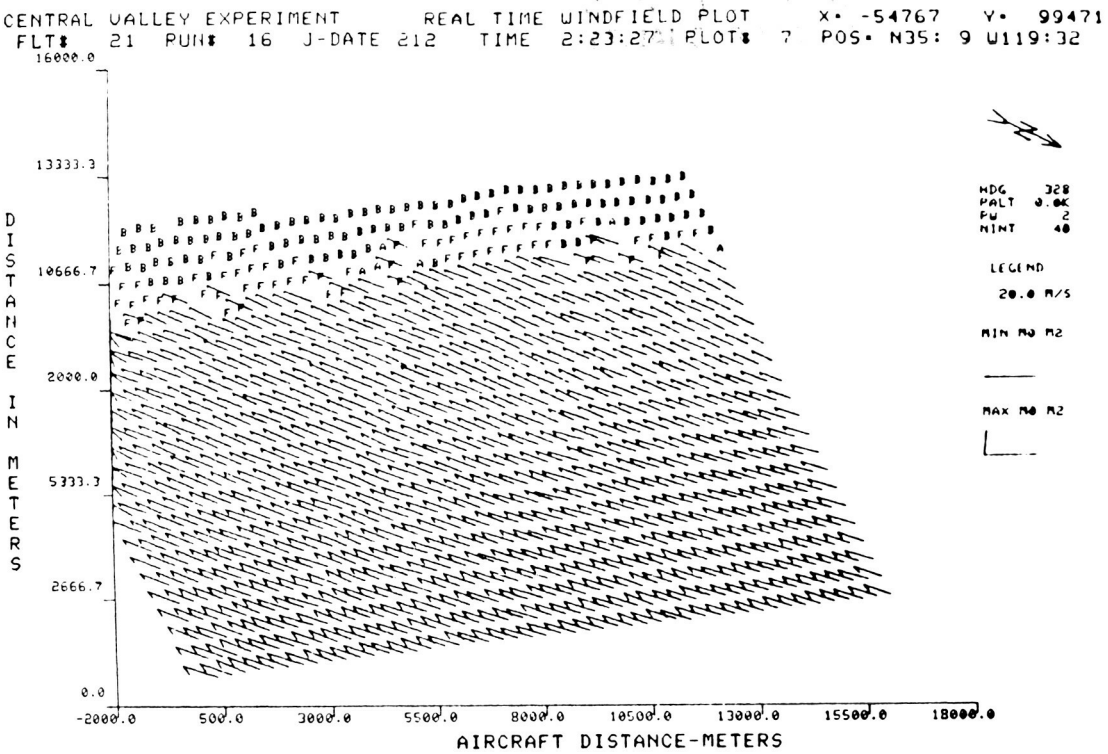

Figure 13. VECTOR VELOCITY MAP OF A UNIFORM FLOW FIELD IN A HORIZONTAL PLANE AT THE ALTITUDE OF THE AIRCRAFT.

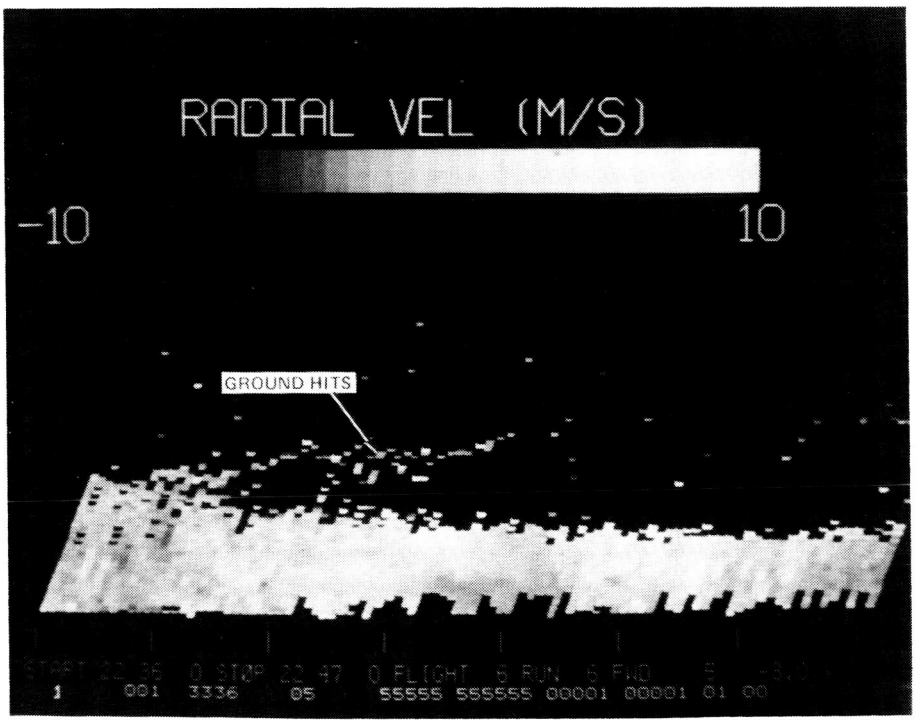

Figure 14. PLAN VELOCITY DISPLAY OF AIRBORNE MEASUREMENTS SHOWING GROUND RETURN FROM ADJACENT FORWARD SCANS HAVING AN ANGLE OF DEPRESSION OF 3 DEGREES.

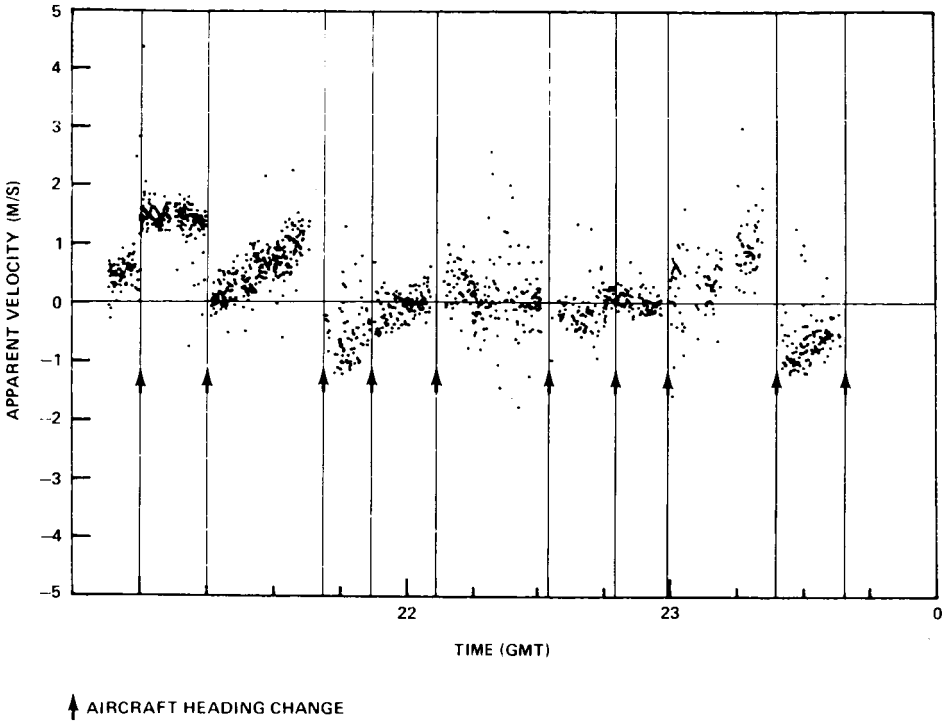

Figure 15. APPARENT DOPPLER VELOCITY OF GROUND AS A FUNCTION OF TIME.

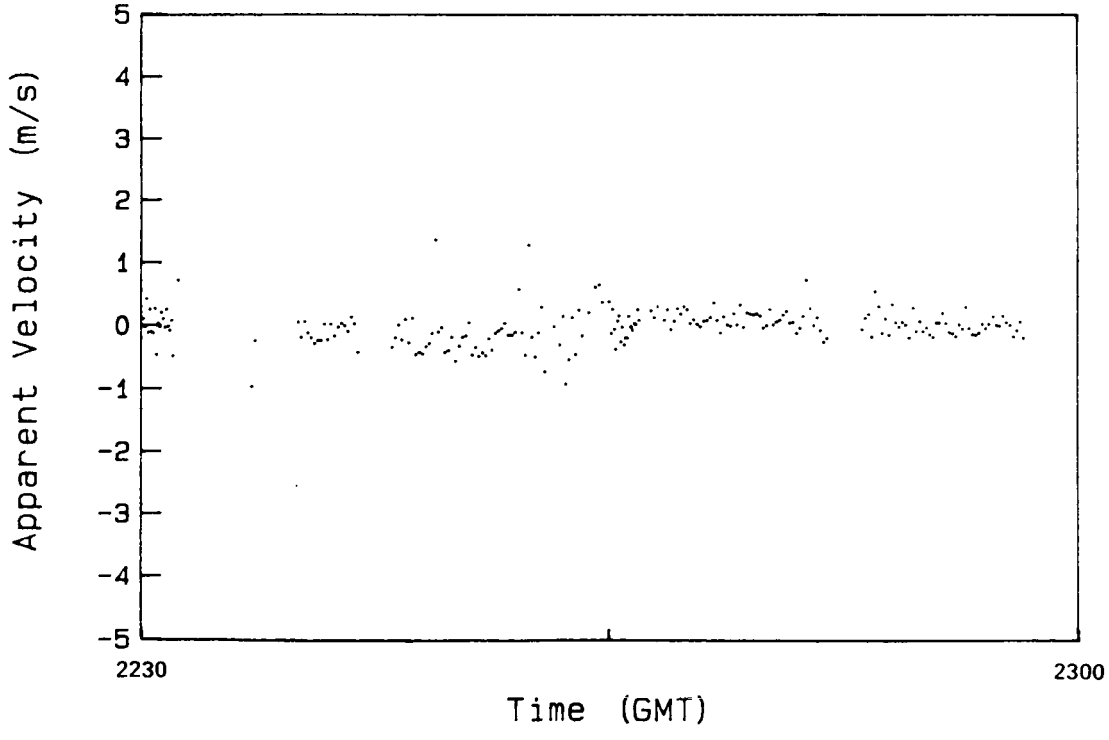

Figure 16. EXPANDED VIEW OF APPARENT DOPPLER VELOCITY OF GROUND AS A FUNCTION OF TIME.

ANALYSIS OF INTRAPULSE CHIRP IN CO_2 OSCILLATORS

Stephen E. Moody, Russell G. Berger, and William J. Thayer III
Spectra Technology, Inc.
Bellevue, Washington

SUMMARY

Pulsed single-frequency CO_2 laser oscillators are often used as transmitters for coherent lidar applications. These oscillators suffer from intrapulse "chirp", or dynamic frequency shifting. If excessive, such chirp can limit the signal-to-noise of the lidar (by generating excess bandwidth), or limit the velocity resolution if the lidar is of the Doppler type. This paper describes a detailed numerical model that considers all known sources of intrapulse chirp. Some typical predictions of the model are shown, and simple design rules to minimize chirp are proposed.

INTRODUCTION

Pulsed CO_2 lasers are one important technology for application as coherent laser radar (or lidar) transmitters. Given today's technological resources, the CO_2 laser remains the tool of choice for coherent lidar applications. However, the performance of real-world coherent lidar systems is more often than not limited by unwanted intrapulse frequency sweeping ("chirp"). To understand and minimize intrapulse chirp in short-pulse TEA CO_2 laser oscillators is an essential ingredient of high-performance coherent lidar design.

There appears to be a well-accepted concensus within the community as to the physical origins of dynamic refraction and, hence, chirp.[1] This paper is an attempt to incorporate this existing understanding into a more accurate tool for the prediction of laser chirp.

Chirp is believed to result from dynamic changes of refractive index within the laser medium on time scales comparable to the laser pulse length. Probable causes of such index changes are discussed in the following section. An intracavity index change maps into a time-varying laser output frequency:

$$\delta\nu(t) = \nu_0 \frac{\ell}{L} \delta n(t) \qquad [1]$$

where $\delta\nu$ is the frequency shift ("chirp"), ν_0 is the laser frequency, ℓ is the gain medium length, L the total resonator length, and δn the index variation within the gain region.

The frequency change in the laser output can be viewed either as a drift in the longitudinal resonator mode frequency, or as a cumulative Doppler shift in the frequency of the trapped radiation in the resonator. Both pictures produce equivalent predictions for the relation between index change and chirp, as long as the index change is sufficiently slow. The condition defining "slow" changes is:

$$\ell \frac{\delta n(t)}{\delta t} << c \frac{\lambda_0}{L} \qquad [2]$$

Here c is the speed of light and λ_0 is the operating wavelength, corresponding to ν_0.

Chirp Mechanisms

There are three distinct generally accepted causes of dynamic refractive index and, hence, laser chirp. These are **time-varying** electron density in the laser plasma, **time-varying** gas density because of a thermal expansion, and time variation of inversion density. Each of these three causes has a characteristic signature that makes **it** readily distinguishable from the others.

In most pulsed CO_2 lasers, the electron density is falling rapidly during the early part of the optical output pulse, which coincides with the trailing edge of the electrical excitation pulse. This effect causes a down chirp, which levels out as the electron density becomes small. The electron driven component is often called the "early" chirp. Its magnitude is typically of order 1 MHz.

After lasing begins, a radial thermal distribution develops due to optical extraction. Each extracted photon leaves behind a vibrationally excited CO_2 molecule, which is eventually converted to heat. There is a thermal maximum coinciding with the intensity maximum (usually on axis) of the laser mode. This thermal maximum drives a fluid dynamic expansion, which eventually results in a drop in gas density, hence, index near the center line of the resonator. An upchirp results with frequency increasing, typically, quadratically with time. This fluid dynamic effect is sometimes called the "late" chirp, because it increases quadratically or cubically with time, and becomes most evident late in the pulse. The magnitude of the late chirp can vary from 0.5 to greater than 5 MHz in typical CO_2 oscillators.

The final chirp component results from anomalous dispersion, due to the laser inversion. For typical CO_2 lasers systems, which operate near line center where the anomalous dispersion component goes through zero, this effect **can be ignored.** However, for certain applications, there may be externally imposed constraints forcing operation away from line center. For a given offset frequency, the magnitude of the anomalous dispersion component decreases monotonically throughout

the pulse, as the inversion is depleted. The sign of the inversion driven term changes on opposite sides of line center.

Estimation of Chirp Magnitude

Rough estimates of the plasma and anomalous dispersion contributions to chirp can be made by using the end point values of the driving terms, and the characteristic times over which they change. The fluid dynamic term is more difficult to estimate, since it is sensitive to very small changes in gas density, which in turn can vary wildly depending on the laser configuration.

Fortunately, the fluid dynamic component of chirp is amenable to a useful analytical model, if certain simplifying assumptions are made. Figure 1 shows the predictions of such a model, which treats the special case of Gaussian beams. The time behavior of the heat input is also treated in a very simplified fashion; the heat addition resulting from the extracted laser energy is presumed to be all deposited at the beginning of the pulse. The resultant predicted quadratic chirp can be described by a single coefficient, which is found to scale with a single parameter depending on the laser aperture (σ), longitudinal resonator fill factor (ℓ/L), the gas Gladstone-Dale coefficient (K) and ratio of specific heats (γ), and the laser energy (E_L). There is a particularly strong dependence on the tranverse dimension σ of the laser resonator. Larger apertures lead to lower chirp, since the thermal gradients are smaller in magnitude when spread over a larger area. As seen in Figure 1, there is good qualitative agreement between this scaling model and the measured performance of a number of dissimilar laser systems.

Detailed Chirp Model

While these rough estimates and scaling analyses are useful, they are insufficient to support detailed predictions of the complete time dependent output waveform of a given laser. Such predictions are often needed as input to a lidar system model, which will ultimately predict the performance of the complete lidar. Therefore, a detailed numerical model has been constructed to include all of the known chirp inducing mechanisms. Our goal was to arrive at the highest possible degree of quantitative accuracy within the resources available.

Figure 2 shows the structure of the resultant model. An existing laser kinetics model (upper left) serves as the point of departure. This model predicts laser output, given the geometry, gas mixture, and pump conditions. Internally, this model carries time dependent values for electron density and inversion density. Time dependent heating is modeled by applying a finite V-T relaxation rate to the lower state population which results from lasing. Because of the full rate

equation approach used, the correct time relationships are maintained between cause and effect throughout the kinetics model.

The electron density and inversion densities lead directly to index changes via the appropriate dispersion relations. The temperature change is used as the source term in a 2-D transient fluid solver, which predicts gas density. The gas density then is fed to the transient index calculation. The index calculation leads directly to a prediction of frequency, following Equation 1. More detailed mode modeling has been built into the structure of the model, but not yet implemented. The utility of better mode models is discussed below.

Figure 3 shows typical predictions of the chirp model. Only the operating pressure was changed between the two cases shown. Both frequency and intensity time histories are included in the figure. The frequency is displayed as the change in resonator mode relative to the pre-pump value. There is a large upchirp in the mode frequency during pumping, due to the rapid rise in electron density. This effect is responsible for the large offset from zero seen at the beginning of the frequency trace. If excessive, this effect can result in a failure of frequency selection in an injection locked system. In a hybrid system, the frequency scale used is realistic if the cw lasing frequency before pumping is treated as the zero reference.

The modeled case was 300 MHz above line center, to maximize the anomalous dispersion component. For positive offsets, the anomalous dispersion tends to cancel the other terms and slightly reduce the peak excursion in the frequency time history. This effect is most clearly visible at 0.5 atm, where anomalous dispersion causes the double minimum behavior seen in the frequency history.

The value of the detailed chirp model is most obvious in the lower pressure case, where the specifics of the time history substantially change the implications of the various chirp mechanisms. Lasing always lags the pump pulse, by an amount that increases at lower pressure. This lag increases by a few tenths of a microsecond as the pressure is decreased from 1 to 0.5 atm. While seeming minor, this additional lag is sufficient to drastically reduce the significance of the early chirp component at lower pressure. In contrast, the 1 atm case shows the highest rate of frequency change during the highest intensity part of the output pulse. The difference between these two cases, which results from a subtle difference of time relationships, cannot be readily predicted by simpler analyses of chirp behavior.

DIRECTIONS FOR FUTURE WORK

The results that have been shown have so far used an ad-hoc Gaussian intensity distribution as a model of the transverse resonator mode structure. In the presence of the saturation, or for unstable resonators, such a model is clearly not accurate. These details are important in defining the extraction-induced thermal gradients, which drive the fluid dynamic chirp component. Figure 4 shows an example of the detailed radial intensity distribution calculated for an unstable resonator equipped CO_2 transmitter, as recently built by Spectra Technology, Inc. (STI) for the National Oceanic and Atmospheric Administration. Clearly, there are very large small-scale gradients near the center of the resonator, where the laser frequency is in some sense determined. We believe that future chirp models should include such a resonator as one component so that the thermal gradients can be better modeled.

REFERENCES

1. Willetts, D.V., Harris, M.R.: Scaling Laws for the Intrapulse Frequency Stability of an Injection Mode Selected TEA CO_2 Laser. IEEE J. Quantum Electron. (USA), Vol. QE-19, No. 5, May 1983, pp. 810-14.

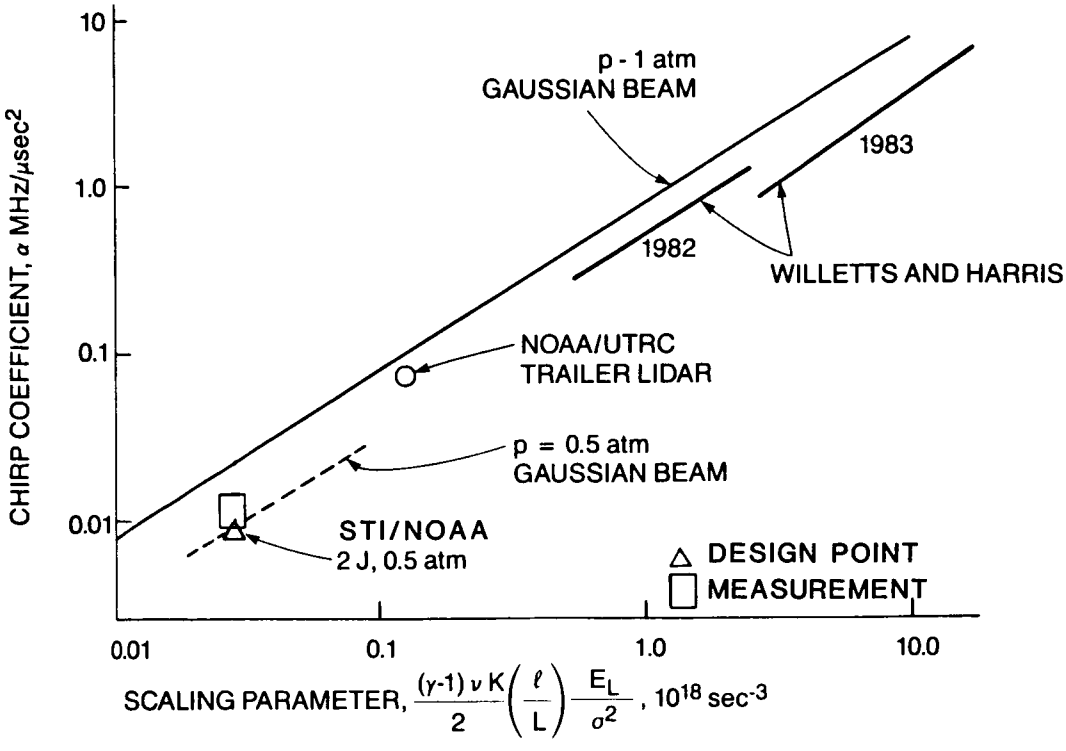

Figure 1. Predictions of Fluid Dynamic Chirp Scaling Model

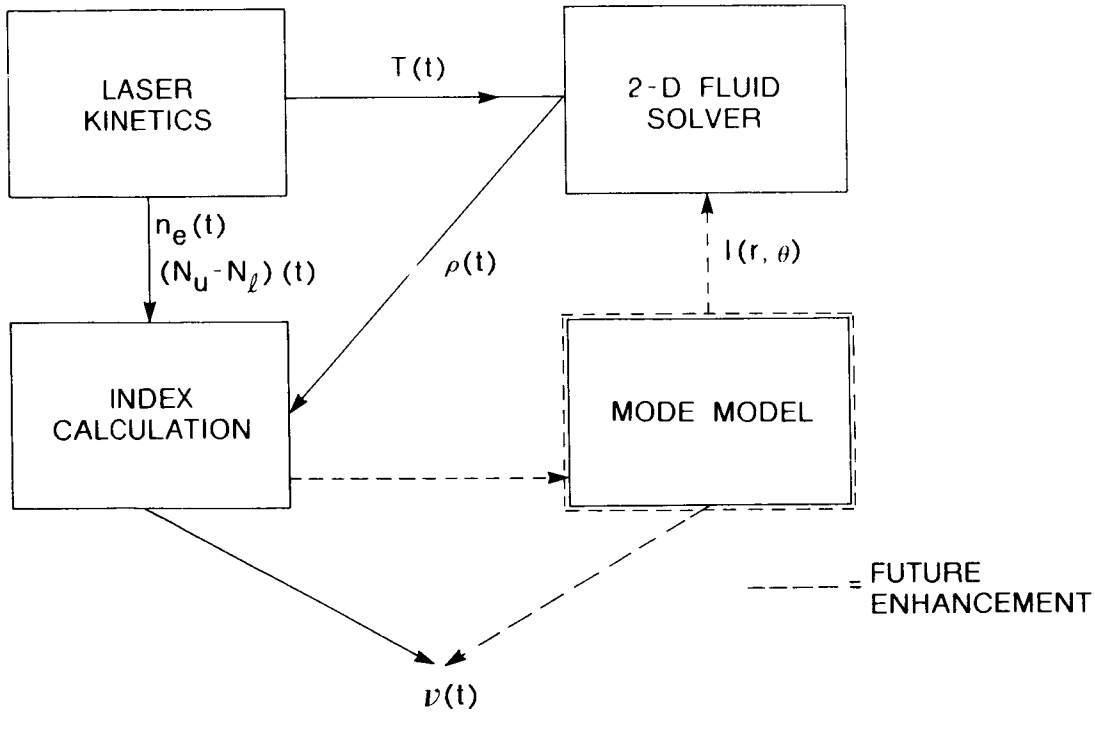

Figure 2. Structure of Detailed Numerical Chirp Prediction Model

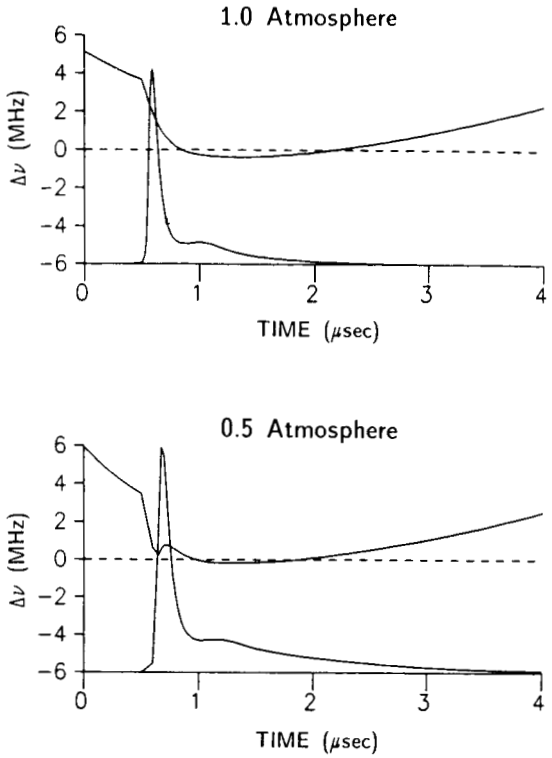

- Chirp (frequency shift) vs time overlaid on laser output intensity plot.
- Chirp scale was offset so that output spectrum peaked at $\Delta\nu = 0$.
- Injected frequency was at 300 MHz higher than line center (anomalous dispersion component was thus negative).

Figure 3. Sample Predictions of Chirp Model

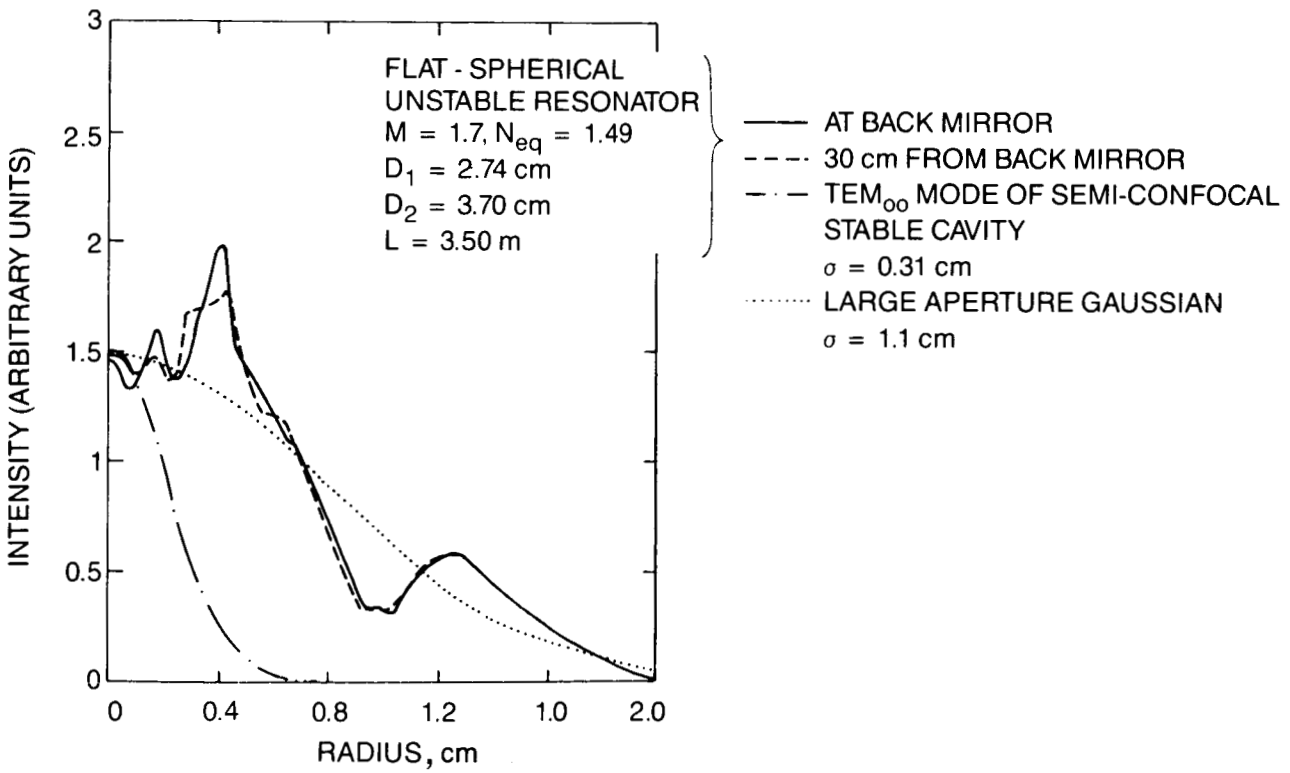

Figure 4. Calculated Intensity Distribution in Unstable Resonator

FREQUENCY STABILIZATION IN INJECTION CONTROLLED PULSED CO_2 LASERS WITH UNSTABLE RESONATOR CAVITIES

Robert T. Menzies and Gerard M. Ancellet
Jet Propulsion Laboratory
California Institute of Technology
Pasadena, California

SUMMARY

Longitudinal mode selection by injection has been demostrated as a viable technique for tailoring a TEA-CO_2 laser with pulse energies of a Joule or greater to fit the requirements of a coherent lidar transmitter. Once reliable generation of single-longitudinal-mode (SLM) pulses is obtained, one can study the intrapulse frequency variation and attempt to determine the sources of frequency sweeping, or chirp. These sources include the effect of the decaying plasma, the thermal gradient due to the energy dissipation associated with the laser mechanism itself, and the pressure shift of the center frequency of the laser transition. The use of the positive-branch unstable resonator as an efficient means of coupling a discharge with transverse spatial dimensions of the order of centimeters to an optical cavity mode introduces another concern: namely, what can be done to emphasize transverse mode discrimination in an unstable resonator cavity while maintaining high coupling efficiency. These issues are briefly discussed in the paper, and representative experimental examples are included.

DESCRIPTION OF EXPERIMENTAL APPARATUS

Mode selection in a TEA-CO_2 laser cavity through the use of injection techniques provides high peak-power SLM pulses with relatively low intensities of injected radiation [refs. 1,2]. Provided the selected mode is near the center of the pressure-broadened TEA-CO_2 gain transition and the frequency proximity requirements are met, as little as 10 μw of injected power is sufficient to ensure a single-frequency pulse with peak power of several Megawatts.

An experimental coherent CO_2 lidar has been developed at JPL which uses an injection-controlled TEA-CO_2 transmitter. The injection control technique has been refined to the level at which this lidar has been used to measure vertical profiles of atmospheric backscatter and atmospheric wind velocity on several occasions, with particular emphasis on collecting vertical aerosol backscatter profile with enough frequency during the past four years to permit a statistical analysis of seasonal differences, trends, etc. The studies of injection control of the laser have been reported in the literature [refs. 1-4]. The lidar optical block diagram, indicating the front-end injection, is displayed in Figure 1. A brief description follows. The TEA-CO_2 laser is a modified Lumonics model 102-2 normally operated at pressures around 760 torr with a flowing gas mixture of He:CO_2:N_2 (85:9:6). The gain section is 80 cm and the total cavity length is 2.4 m, corresponding to a longitudinal mode spacing of 62.5 MHz. The optical cavity is formed from a Littrow mounted reflection grating (150 lines/mm) and a germanium meniscus convex output coupler. The inside

and outside radii of curvature of the Ge coupler are 15 m and 41.5 m, respectively, and both surfaces are AR coated for 10.6 μm to a diameter of 40 mm. The central 14.6 mm square area of the inside surface is uncoated yielding an intensity reflection coefficient for normal incidence of approximately 40%. This positive branch unstable resonator cavity has a magnification of approximately 2.2 (fractional power loss per roundtrip = 80%) and provides a near-diffraction limited far-field pattern. The injection oscillator is a CW CO_2 waveguide laser operated at a pressure near 200 torr. The waveguide laser energy which is reflected by the TEA laser optical cavity is focused onto a cooled HgCdTe photodetector. This detector signal is used as a diagnostic for automatic (feedback loop) control of the relationship between the waveguide laser frequency and the longitudinal mode frequencies (mc/2L) of the TEA cavity.

The frequency stability of the injection-controlled TEA-CO_2 laser was examined by a heterodyne technique, schematically illustrated in Fig. 2. The signal was recorded at 30 MHz intermediate frequency corresponding to the center frequency of the filter/amplifier. In order not to use the transient digitizer at a speed higher than 50 MHz, where the A/D conversion was not accurate enough for our purpose, the 30 MHz IF signal was converted to 10 MHz through an RF mixer followed by a 20 MHz filter. The time evolution of the period of the IF signal was calculated with a temporal resolution equivalent to 2 periods (200 ns) in order to improve the accurancy of the frequency measurement (300 kHz). Representative examples of results will be shown following a brief discussion of sources of frequency sweeping.

INTRAPULSE FREQUENCY SWEEPING

The frequency sweeping of the laser follows any changes in the cavity refractive index, n, at the selected mode frequency. The three major potential sources of phase shifting due to refractive index temporal variations are briefly discussed in the following paragraphs.

The refractive index variation associated with the time dependent electron density in the decaying discharge plasma occurs mainly during the initial part of the pulse build-up time but may still represent a substantial refractive index perturbation at the time of the peak of the optical pulse [ref. 5]. This effect also causes the mode selection zone to be offset slightly with respect to the frequency of the selected mode of the pre-discharge TEA laser cavity [ref. 3]. Assuming for our laser an average electron density of 10^{13} cm^{-3} during a 0.5μs excitation pulse, the plasma frequency ν_p is 2.10^{10} Hz. The frequency change, in the laser cavity, due to this electron density is calculated to be about 5 MHz. (The observed frequency deviation near the time of the appearance of the gainswitched-spike-maximum (GSSM) is approximately 2 MHz).

One should also consider the mode pulling effect arising from the frequency difference between the TEA molecular gain curve maximum ν_o and the injected radiation frequency ν_i coincident with the resonant mode of the empty resonator. The equivalent frequency pulling is:

$$\Delta\nu_i = \frac{c}{4\pi} \frac{\nu_o - \nu_i}{\Delta\nu_o} \frac{g\ell}{L}$$

where c is the light velocity, $\Delta\nu_o$ is the half width half maximum of the TEA molecular gain curve, g is the gain of the medium in the cavity, and ℓ/L is the filling factor. The injected laser frequency normally corresponds to the center frequency of a low pressure (10 torr) CO_2 laser tuned to the same line as that of the TEA laser. A careful study of the pressure shift of CO_2 transition frequencies was done by SooHoo et al. [ref. 6] with the pressure ranging from 10^{-2} torr to 1 torr, but little is known about the pressure shift between 10 torr and 1 atm. The problem is further complicated by the dependence on the gas mixing composition. Referring to Agalakov's work [ref. 7], one may calculate a shift of +240 MHz for a 10% CO_2 90% He gas mix and lines in the P branch. Hollins and Jordan [ref. 8] measured a very small shift of -5 MHz for a 40% CO_2, 20% N_2, 40% He gas mix. This small shift appears to be consistent with Agalakov's work, because it can be attributed to a cancellation of shifts of opposite sign caused by CO_2 - CO_2 (or CO_2 - N_2) and CO_2 - He collisions. A pressure shift of +240 MHz is large enough to induce a 2MHz mode pulling when the gain coefficient g is changing from 0 to 2.10^{-2} cm^{-1}. The mode pulling due to the saturation of the CO_2 molecules in the non-active region of the cavity is an order of magnitude smaller and can be neglected.

Finally, laser-induced medium perturbation (LIMP) has been found to be a major cause of changes in frequency ν during the optical pulse and is related in the following way to the output energy E, the beam radius σ, and the cavity length L [9]:

$$\Delta\nu = \frac{2KR\nu}{\pi\ C_v}\ \frac{E}{\sigma^4 L}\ t^2 = \alpha\, t^2$$

where K is the Gladstone-Dale constant and R, C_v the usual thermodynamic constants. For a cavity with transverse dimension of its spatial modes larger than 1 cm, and output energy of 1J (assuming 100% loss), α is smaller than 50 kHz/μs.

The salient features of this qualitative analysis of frequency sweeping mechanisms are depicted in Figure 3. Although frequency variations appearing before the gain switch spike maximum (GSSM) are presented, only those occurring near or after the GSSM contribute to the spectral broadening of the laser pulse.

TRANSVERSE MODE DISCRIMINATION

It is important to analyze the properties of the lowest order transverse modes in an unstable resonator cavity which is appropriate for a TEA-CO_2 laser. Often the mode loss separation of the first 2-3 modes is small enough such that if the lowest-loss mode suffers incrementally due to spatial hole burning or some other spatial nonuniformity, the appearance of another tranverse mode during a portion of the pulse duration may result. It has been pointed out by Weiner [ref. 10] that the unstable resonator mode loss discrimination is sensitive to tilt, such that the optical axis, which is determined by the line through the centers of curvative of the cavity defining mirrors, intersects the output coupler at an off center position. The degree of tilt can be described by the normalized off-axis distances $\varepsilon_{x,y} = h_{x,y}/\alpha_{2x,2y}$, as depicted in Figure 4. (In Figure 4 the reflective portion of the output coupling optic is represented by the shaded square, which is offset with respect to the laser output intensity pattern.) The optical axis intersects the output coupler at the origin of coordinates. Weiner analyzed the effects of

off-axis tilts on mode-loss discrimination for a high equivalent-Fresnel-number example (N_{eq}=9.6), using calculations based on the asymptotic technique.

To analyze the transverse mode properties of the TEA laser positive branch unstable resonator in a more general fashion, we use the Huygens-Fresnel integral equation for a one-dimensional (strip resonator) case [ref. 11] to define eigenfunctions $\mu_m(x)$ and eigenvalues $\gamma_m = \gamma_m \exp(i\phi_m)$, corresponding to the mode amplitude distributions and the energy losses and phase shifts per round trip in the cavity. Applying symmetry arguments to the orthogonal dimension, the two-dimensional transverse mode shape, fractional power loss and mode frequency are given by:

$$u_{mn}(x,y) = u_m(x)\, u_n(y)$$

$$\delta_{mn} = 1 - (\gamma_m \gamma_n)^2$$

$$\nu_{mnq} = \frac{cq}{2L} + c\frac{(\phi m + \phi n - 2kL)}{2\pi L}$$

In order to solve the integral equation, an iterative method (the Prony method) was used. This was first applied by Siegman and Miller [ref. 12] to the case of a symmetric resonator with circular mirrors. An iterative method is preferable to the asymptotic method for low Fresnel number.

To illustrate an example of the effects of a slight off-axis tilt on mode-loss separation, we have tabulated in Table I the results of the mode loss calculations for the three lowest order modes, comparing the on-axis case with the case for which $\varepsilon = 0.3$. The $N_{eq} = 1.3$ and the magnification factor M = 2.2 for this case. It is noteworthy that the lowest order mode loss separation is quite small for the on-axis case but changes dramatically for $\varepsilon = 0.3$. In fact, our analysis indicates that experimental alignment tolerances which result in a small but non-zero value for ε, even when onaxis symmetry is the goal, will result in a much larger mode-loss separation than is indicated in the ideal $\varepsilon = 0$ case. However, an intentional tilt in order to achieve a value for ε in the neighborhood of 0.25 - 0.5 should definitely help to ensure single transverse mode oscillation throughout the laser pulse.

TABLE I. UNSTABLE RESONATOR MODE LOSSES (%)

Mode index, (m,n)	On-axis (even symmetric)	Off-axis (α=0.3)
(0,0)	80.0	65.2
(0,1)	80.9	80.0
(1,1)	81.8	88.5

EXPERIMENT RESULTS AND DISCUSSION

Two examples which are typical displays of the TEA-CO_2 laser pulse shape and corresponding chirp record are shown in Figures 5 and 6. The decreasing frequency characteristic at the beginning of each pulse can be attributed to the plasma

decay. The dotted line on the figure represents the expected plasma decay effect. As expected, the chirp due to the LIMP mechanism is less than 100 kHz. The same results were obtained when we shifted the injection frequency by 60 MHz with respect to the transition center frequency of the atmospheric pressure broadened TEA line. In other words, any effect of mode pulling towards the line-center frequency was not discernible. The record shown in Figure 5 reveals a large frequency shift (7-8 MHz) which appears just after the gain-switched-spike and disappears synchronously with the sharp amplitude spike at 1.5 μs. The occurrence of such sudden frequency shifts was found to be strongly dependent on the alignment of the laser cavity in the region near the "on-axis" configuration. These frequency shifts were not observed for a slightly misaligned "off-axis" configuration, which was a surprise to us until the transverse mode studies were accomplished. The numerical analysis of the transverse modes of the unstable resonator with characteristics matching our TEA-CO_2 laser provides a plausible interpretation of these rather large frequency shifts. The significant difference in spatial intensity distributions of the two most dominant transverse modes provides a reasonable mechanism for the sudden appearance and disappearance of the next higher mode just after the GSS. The medium is highly saturated just after the GSS, and spatial variation in the degree of saturation might allow the second mode to gain the advantage for a period of time. This would be most probable when the mode-loss separation is small.

The research described in this paper was carried out by the Jet Propulsion Laboratory, California Institute of Technology, under contract with the National Aeronautics and Space Administration and was performed while Gerard Ancellet held a NRC-NASA Resident Research Associateship award at the Jet Propulsion Laboratory.

REFERENCES

1. U. P. Oppenheim, R. T. Menzies, and M. J. Kavaya, "Dependence of Injection Locking of the TEA-CO_2 Laser on Intensity of Injected Radiation", IEEE J. Quantum Electron. QE-18, 1332 (1982).

2. P. H. Flamant and R. T. Menzies, "Mode Selection and Frequency Tuning by Injection in Pulsed TEA-CO_2 Lasers", IEEE J. Quantum Electron. QE-19, 821 (1983).

3. P. H. Flamant, R. T. Menzies, M. J. Kavaya, U. P. Oppenheim "Pulse Evolution and Mode Selection in a TEA-CO_2 Laser Perturbed by Injection of External Radiation", Optics Comm. 45, 105 (1983).

4. R. T. Menzies, P. H. Flamant, M. J. Kavaya, and E. N. Kuiper, "Tunable Mode and Line Selection by Injection in a TEA-CO_2 Laser", Appl. Opt. 23, 3854 (1984).

5. D. V. Willetts and M. R. Harris "A Plasma Effect in Injection-Mode Selection of TEA-CO_2 Lasers", Appl. Phys. B. 33, 91 (1984).

6. K. L. SooHoo, C. Freed, J. E. Thomas, H. A. Haus: IEEE J. of Quant. Electron., QE-21, 1159 (1985).

7. Y. G. Agalakov, M. D. Bulanin, V. V. Bertsev, A. P. Burtsev, Y. A. Rubinov: Opt.Spectrosc. (USSR) 58, 298 (1985).

8. R. C. Hollins and D. L. Jordan, J. Phys. B. 15, L491 (1982).

9. D. V. Willetts and M. R. Harris, IEEE J. Quantum Electron. QE-21, 188 (1985).

10. M. M. Weiner, "Modes of Empty Off-Axis Unstable Resonators with Rectangular Mirrors", Appl. Optics 18, 1828 (1979).

11. R. L. Sanderson, W. Streifer: Appl. Opt., 8, 2129 (1969).

12. A. E. Siegman, H. Y. Miller: Appl. Opt., 9, 2729 (1970)

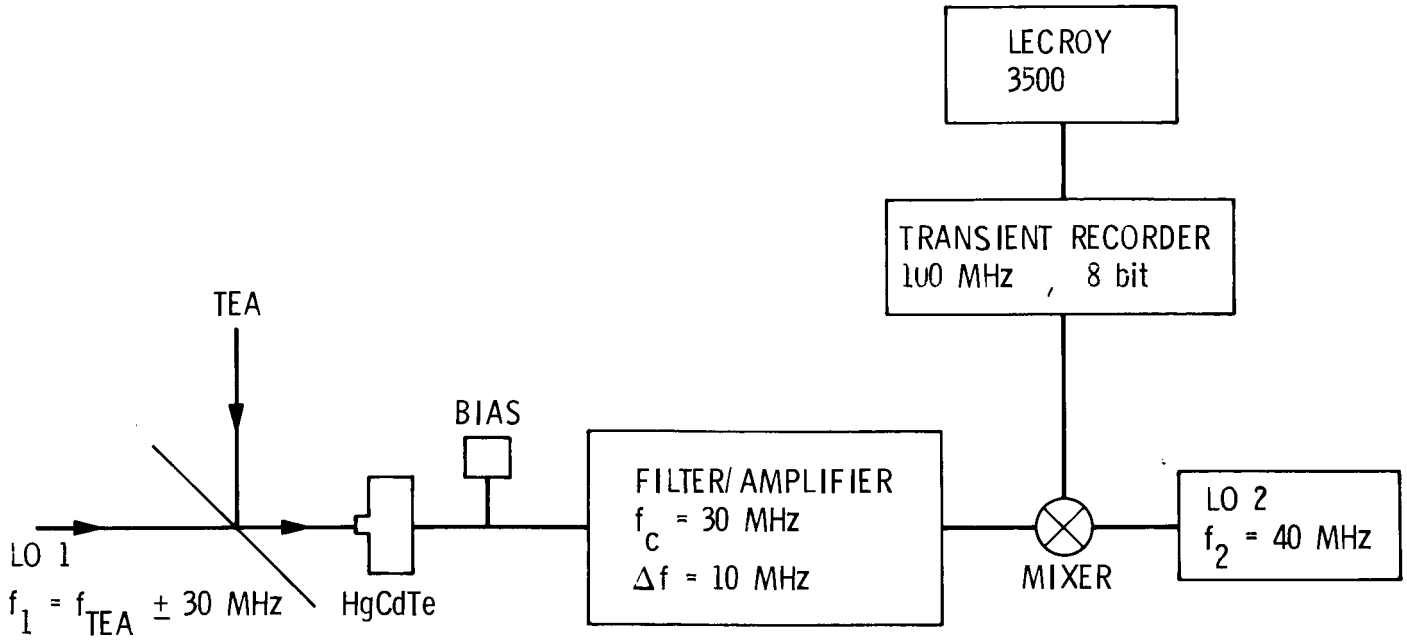

Figure 1. Optical block diagram of coherent lidar system using an injection-controlled TEA-CO_2 laser transmitter with an unstable resonator cavity.

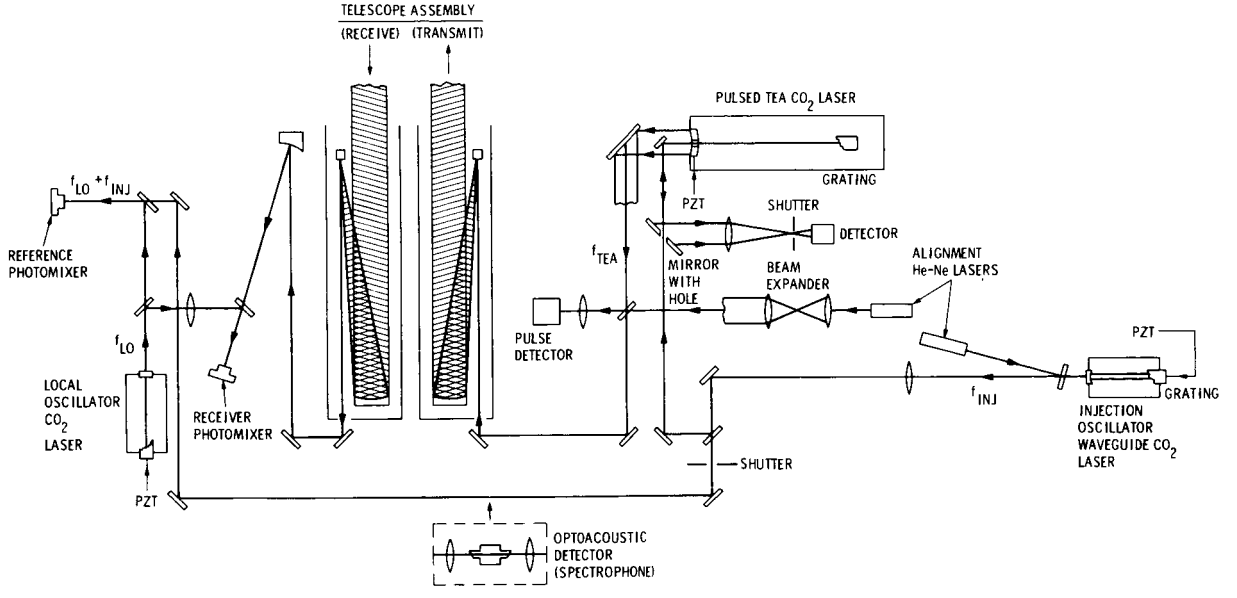

Figure 2. Block diagram of heterodyne detection apparatus for frequency chirp measurement of TEA-CO_2 laser pulse.

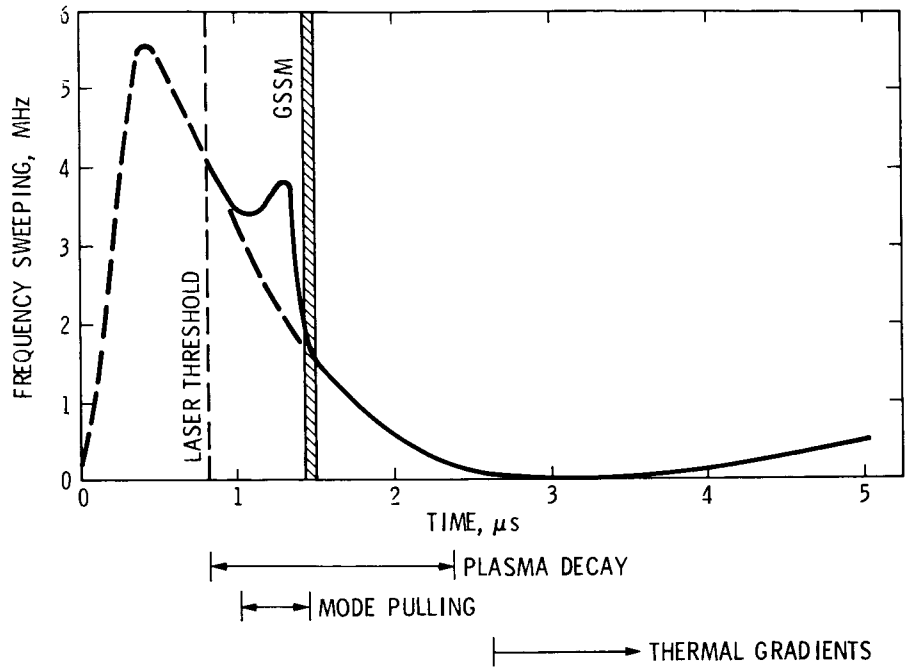

Figure 3. Semi-quantitative depiction of the temporal dependence of the pulse output frequency, assuming a selected cavity mode near the low-pressure laser transition center frequency.

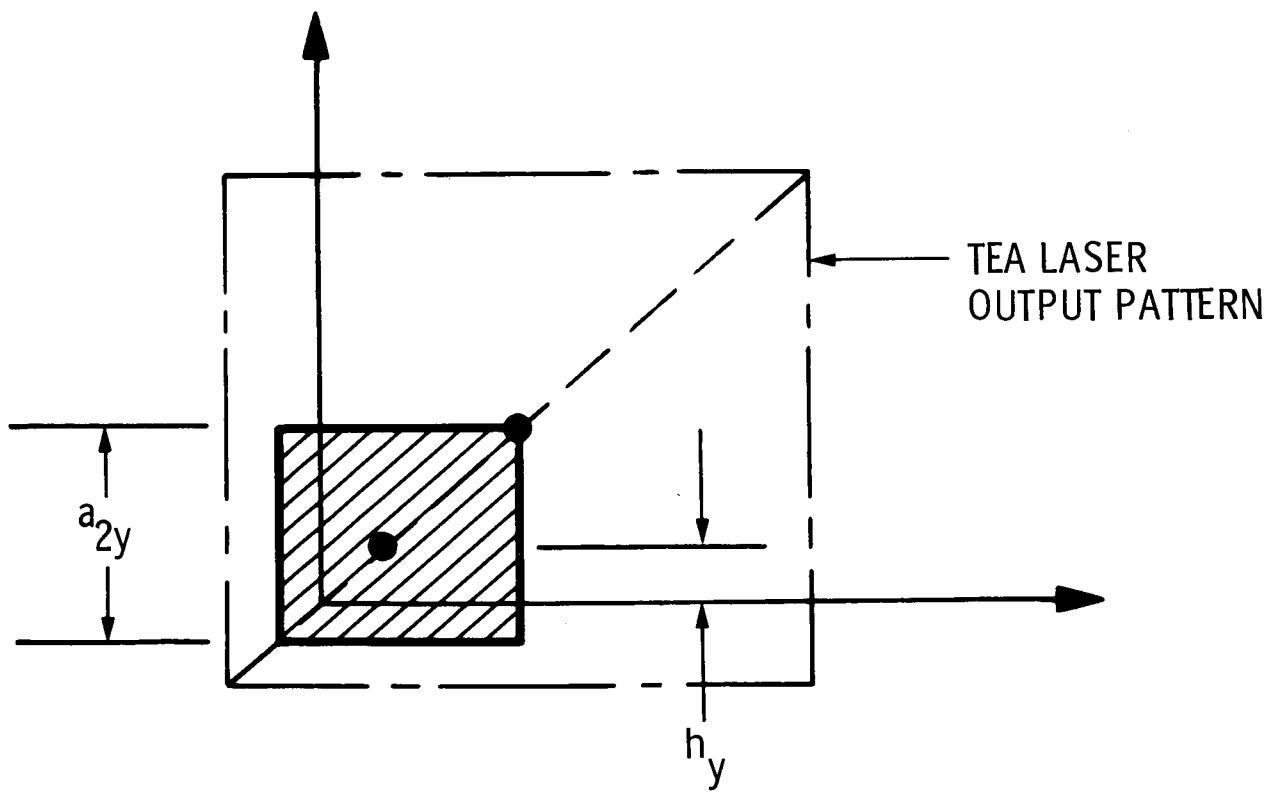

Figure 4. Geometry of the off-axis case in which the output intensity pattern (with approximately square exterior dimensions) is displaced from the central reflective patch (also square) of the output coupler.

- LARGE PLASMA DECAY EFFECT
- INADEQUATE MODE LOSS DISCRIMINATION

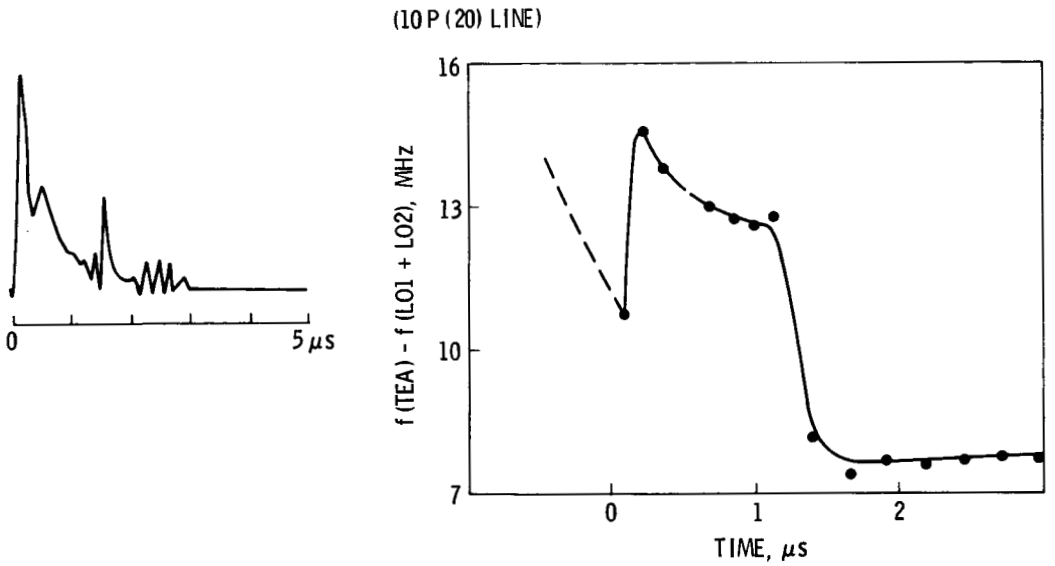

Figure 5. Example of the intrapulse frequency variation when a sudden jump to a second transverse mode occurred just after the GSSM.

- LARGE PLASMA DECAY EFFECT
- ADEQUATE MODE LOSS DISCRIMINATION

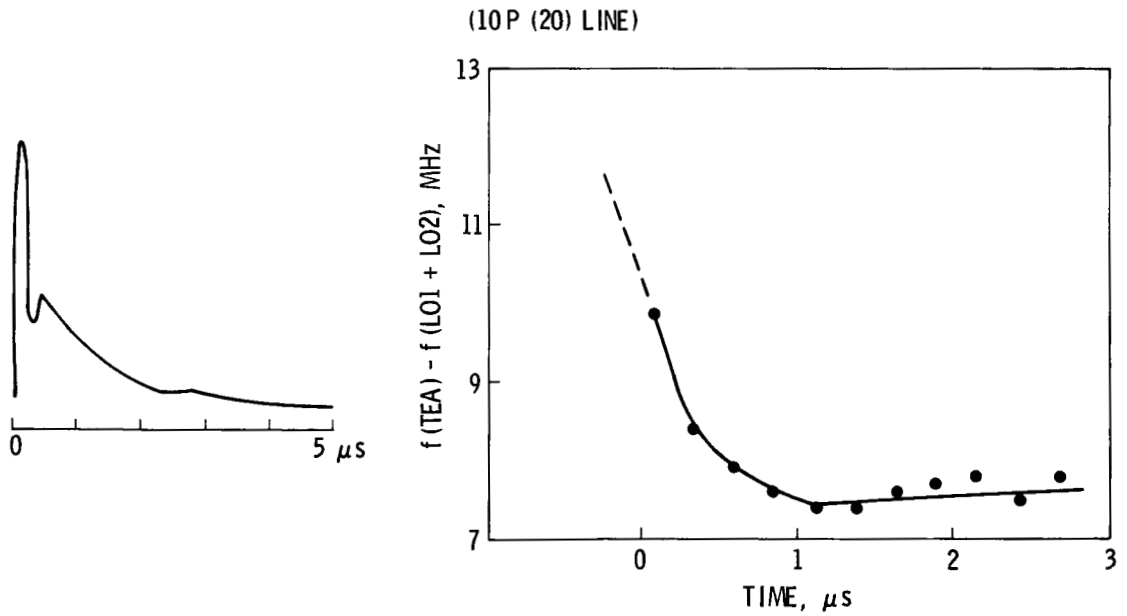

Figure 6. Example of the intrapulse frequency variation when oscillation was maintained on a single transverse mode as well as single longitudinal mode.

THE OXIDATION OF CARBON MONOXIDE USING A TIN OXIDE CATALYST

Christopher F. Sampson and Nicholas J. Gudde
United Kingdom Atomic Energy Authority
A.E.R.E. Harwell, Didcot, Oxon.
United Kingdom

SUMMARY

This paper outlines some of the steps involved in the development by the United Kingdom Atomic Energy Authority (UKAEA) of a catalytic device for the recombination of carbon monoxide and oxygen in a CO_2 laser system.

It contrasts the differences between CO oxidation for air purification and for laser environmental control, but indicates that there are similarities between the physical specifications. The principal features of catalytic devices are outlined and some experimental work described. This includes measurements concerning the structure and mechanical properties of the artifact, the preparation of the catalyst coating and its interaction with the gaseous environment. The paper concludes with some speculation about the method by which the reaction actually occurs.

INTRODUCTION

During the late 1970's, the United Kingdom Atomic Energy Authority at Harwell became involved in sol-gel technology as a result of oxide fuel development. The sol-gel method was found to be suitable for the preparation of catalytic materials which eventually led to their use in car exhaust catalytic converters and for air purification catalysts. Such catalysts were usually in the form of coatings applied to supporting artifacts such as monoliths, formed from either cordierite or from a corrosion resistant metal such as Fecralloy steel (R). The UKAEA has experience in the use of sol-gel catalysts for CO removal from air and so has a technological link to a system intended to recombine O_2 and CO formed in sealed CO_2 lasers.

Table 1 gives typical specifications for CO oxidation in breathing gear and in a laser recombination system. The main difference lies in the gas composition; the air purifier will be exposed to CO and O_2 concentrations considerably higher than those seen by the recombination catalyst, but will only encounter a fraction of the CO_2. In a laser environment, the CO_2 concentration might be as much as 40% by volume, whereas the CO_2 content of air is $< 1\%$. The operating requirements are very similar, however. Carbon monoxide oxidation is an exothermic process, but both catalytic systems must have a low exhaust temperature. The production of hot air by a breathing appliance can cause respiratory difficulties (catalysts sometimes have very human failings), whereas heated gases within the laser could result in optical distortion. Similarly, mechanical integrity is important to prevent dust and debris from the catalyst becoming inhaled or obscuring the optical system.

(R) Fecralloy steel is a registered trademark of the UKAEA.

CATALYST TEST RIG

The catalyst device had to be designed to fit within the case of a recycle laser system without impeding the circulation of the laser gas, yet providing sufficient catalytic activity to effect the recombination. To achieve these goals, several types of catalyst artifacts were considered, the final choice being a ceramic monolith coated with a strongly adherent catalyst. An example is shown in figure 1.

The laser test rig is shown in figure 2. The laser cavity, which normally contains the electrode assembly, is at the top, and gas circulation is provided by a tangential fan situated at the left hand side. The gas mixture flows clockwise through the electrode assembly, through the catalyst artifact and may be cooled, if necessary, before returning to the fan. A typical gas velocity through the laser cavity is 7 m/s, which is sufficient to pass three laser volumes per laser pulse. The monolith typically had dimensions of 10 cm long by 5 cm wide by 2 cm deep.

CATALYST PREPARATION AND PERFORMANCE

The initial stages of catalyst development concerned the production of a tin sol. Of the catalyst formulations tried, tin oxide with two precious metal coatings was found to be the best. Several factors had to be considered:

1. The viscosity of the sol must be low enough that there is adequate penetration of the material into the pores of the substrate.
2. The concentration of the sol must be high so that enough catalyst is deposited in a practical number of coating steps.
3. The sol must form a catalyst with a high surface area.
4. The final catalyst coating must adhere to the ceramic substrate.
5. The precious metal should be uniformly distributed over the surface of the catalyst.

Some of these requirements are incompatible, and so a compromise must be sought, for example between concentration and viscosity. It is not just the physical properties which may be altered, one may influence the properties of the catalyst by chemical means. Viscosity, for instance, depends on the concentration of the sol but may be influenced by adjusting the pH of the mixture.

Once the coating has been deposited, the physical and chemical structure of the catalyst control the way in which the reactor behaves. Figure 3 shows the three main processes occurring in a chemical reactor.

Firstly, reactants must pass from the flowing gas stream to the surface of the artifact, in this case the walls of the monolith channel. Such mass transfer is controlled by the linear velocity of the gas, and the channel diameter (hence channel density.) However, these factors also determine the pressure drop required across the monolith in order to maintain the required flow rate. It is apparent that one must compromise between rapid mass transfer and low flow resistance.

The second step involves the diffusion of reactant molecules through the pores of the catalyst until they encounter a catalytic active site. Generally, a high surface

area support will give more active sites per unit volume of catalyst. Unfortunately, high surface areas are normally associated with pores of small diameter which restrict diffusion more than would large pores. Again, a balance must be attained. The structural stability of the coating may also be effected by the pore structure.

Finally, the recombination reaction occurs at the active site. Chemical factors are very important; impurities may poison the reaction, the form of the precious metal may be influenced by the precious metal salt used for deposition, the purity and structure of the tin oxide may effect both the dispersion of the precious metal and the reaction itself.

The removal of products may also play a part, especially if the products can react with the catalyst. If product molecules remain attached to the catalyst surface, they may impede the reaction by blocking the diffusion of reagents or by changing the chemical properties of the catalyst.

EXAMPLES OF CATALYST OPTIMIZATION AND TESTING

Surface Area

Figure 4 shows the results of an experiment which measured the effect of sol concentration on the BET surface area of the catalyst coating. These results have been corrected for the surface area of the cordierite support (ca. $3m^2/g$). The graph shows that the highest surface areas were obtained from the lowest concentration sols. After optimization, an improved sol was prepared. This had a concentration of 200 g/l and gave a coating with a surface area between 150 and 200 m^2/g.

Effect Of High Concentrations Of CO_2

It was not known whether the large partial pressure of CO_2 would have any effect on the activity of the catalyst. The rate of recombination was measured for a stoichiometric mixture of 1% CO, 0.5% O_2 in various He/CO_2 mixtures. The results in figure 5 show the rate at a given CO_2 concentration relative to the rate of recombination in a CO_2-free atmosphere. Carbon dioxide has little inhibiting effect at concentrations below 50 vol%. Even above 90 vol% CO_2, the rate was only reduced to 70% of the CO_2-free value.

Reduction Of The Support By CO

The presence of CO in the gas mixture could have modified the surface of the tin oxide. Mossbauer spectroscopy can distinguish between Sn(IV) and Sn(II), so an experiment was undertaken to observe the effect of CO on a catalyst at room temperature. Significant reduction of the catalyst would have introduced a Sn(II) peak in addition to the Sn(IV). The spectra in figure 6 show that no Sn(II) could be observed. This suggests that either CO did not reduce the catalyst, or that the catalyst had reverted to its original form because of oxygen in the environment.

Catalyst Distribution

The catalytically active material (precious metal on tin oxide) was coated on a porous cordierite monolith. For maximum activity, one must ensure that the device supports the maximum amount of catalyst, ie. ensure that all the pores

of the cordierite have been coated with catalyst. If this condition has been fulfilled, then the precious metals will be uniformly distributed throughout the wall of the monolith. Figure 7 shows an electron microprobe trace across the thickness of a finished monolith wall. The tin signal shows that the tin oxide profile is matched closely by the precious metal, and decreases slightly towards the center of the wall. Although the profiles are not uniform, they do show that the substrate is porous and that the catalytic materials have penetrated well within the substrate.

Mechanical Properties

The inclusion of a catalyst in the laser device may effect the stability of the instrument by creating dust or obstructing the flow of gas. To study the latter, pressure drop measurements were made by measuring the differential pressure across the catalyst artifact as shown in figure 8. Measuring ports were located before and after the monolith holder in the laser case, and the gas velocity measured using a pitot tube fitted into the laser cavity. Figure 9 shows two curves of pressure drop versus cell density for monoliths of different depth. The gas linear velocity was kept constant throughout. For both monolith depths, the pressure drop for the higher cell densities was approximately twice that of the lower densities.

Mechanical strength and resistance to dusting of the applied coating are very important because of potential damage to the optical system. Shock and vibration tests were carried out by weighing the catalyst artifacts before and after various treatments. The shock test used a 981 m/s^2 half-sine 6 ms pulse applied three times along three mutually perpendicular planes. The vibration test used a 20-500 Hz, 19.8 m/s^2 acceleration for two hours, again along three mutually perpendicular planes. No loss of weight was detected in either test.

MECHANISTIC STUDIES

The mechanism of a catalytic reaction can often indicate how the catalyst works, and so indicate which aspects if its formulation will most benefit its performance. Figure 10 shows the rate of formation of CO_2 for different concentrations of CO in air. The solid curve is from a catalyst reduced in hydrogen before use; the dashed curve is from an unreduced catalyst. Both curves show that there is a maximum rate of reaction which occurs between 1.0 and 1.5 vol% of CO, and that higher concentrations of CO do not cause an increase in the rate as would be expected from a simple (pseudo) first-order process (i.e., in air, the oxygen is always in stoichiometric excess. This is simply explained in terms of strong adsorption of CO. At low CO pressures, the rate of oxidation of CO is high enough to keep the surface of the catalyst fairly free of adsorbed CO. At high pressures, the surface becomes covered with unreacted CO which blocks the supply of oxygen and so causes a reduction in the overall rate even though there is plenty of CO available.

To observe the effect of CO and O_2 partial pressures, two experiments were conducted using powdered samples of catalyst held at 30°C in a differential reactor. The test gas contained CO and O_2 in a helium carrier. Figures 11a and 11b show the rates of CO_2 production as functions of CO and O_2 partial pressures, respectively. In either case, the other reagent concentration was held constant. The reaction appears to be zero order with respect to CO, but first order with respect to O_2. This indicates that under laser recombination conditions, the surface always holds its maximum amount of CO and the rate limiting step is the supply of oxygen (either atoms or molecules) to combine with the CO.

Prof. Bond (ref. 1) has studied the reaction of CO in air on a Pd/alumina catalyst at 150°C., and has proposed a "spill-over" mechanism to explain the results. Our results are consistent with our technical catalyst operating by this type of mechanism at room temperature. A possible spill-over mechanism is shown in figure 12. In the first step, a CO molecule from the gas phase arrives at a precious metal site, becomes activated (eg. vibrationally) then spills over onto the tin oxide surface. The CO molecule abstracts an oxygen atom and forms a CO_2 molecule which desorbs back into the gas phase. An oxygen vacancy is left in the surface. Reoxidation of the surface occurs by a similar process in step 2. Oxygen may spill over either as atoms or molecules (eg. dissociative redox or Mars-van Krevelen models); the important step is the refilling of the vacancy. Inhibition occurs when adsorbed CO blocks the resupply of the oxygen. This would indicate that the catalyst can be improved if the CO bond to the surface could be weakened (choice of precious metal, additives, and pretreatment).

CONCLUSIONS

This paper indicates how a catalytic device is developed. There are considerations to be made regarding the means of supporting the catalyst, the method of preparation, both chemical and physical, and an understanding of the way in which the final device will work. None of these can be treated truly in isolation as their interaction is surprisingly complex.

Reference

1. Bond G.C., Fuller M.J., Molloy L.R., Proc. 6th Int. Congr. Cat. 1, 356 (1977).

Acknowledgment

The United Kingdom Atomic Energy Authority would like to thank the D.C.V.D. Ministry of Defense for their cooperation throughout this period of development.

TABLE 1

SPECIFICATION

	AIR PURIFICATION	LASER
Gas composition: CO	few %	< 1%
O_2	20%	< 1%
CO_2	few %	20-40%
Temperature :	ambient	ambient
Other requirements:	low $\Delta\rho$	low $\Delta\rho$
	low dust	low dust
Reactor configuration:	single pass	recycle

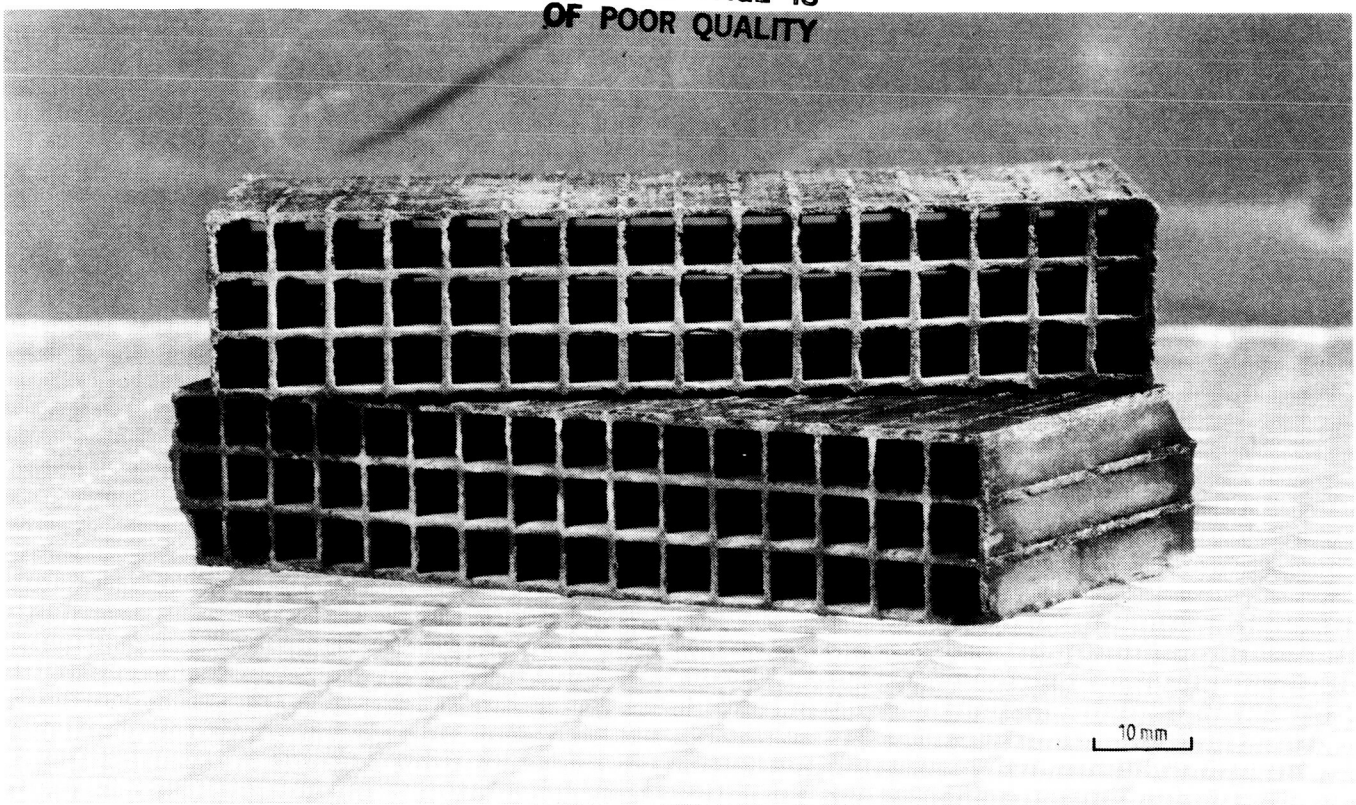

Figure 1. Ceramic monolith coated catalyst.

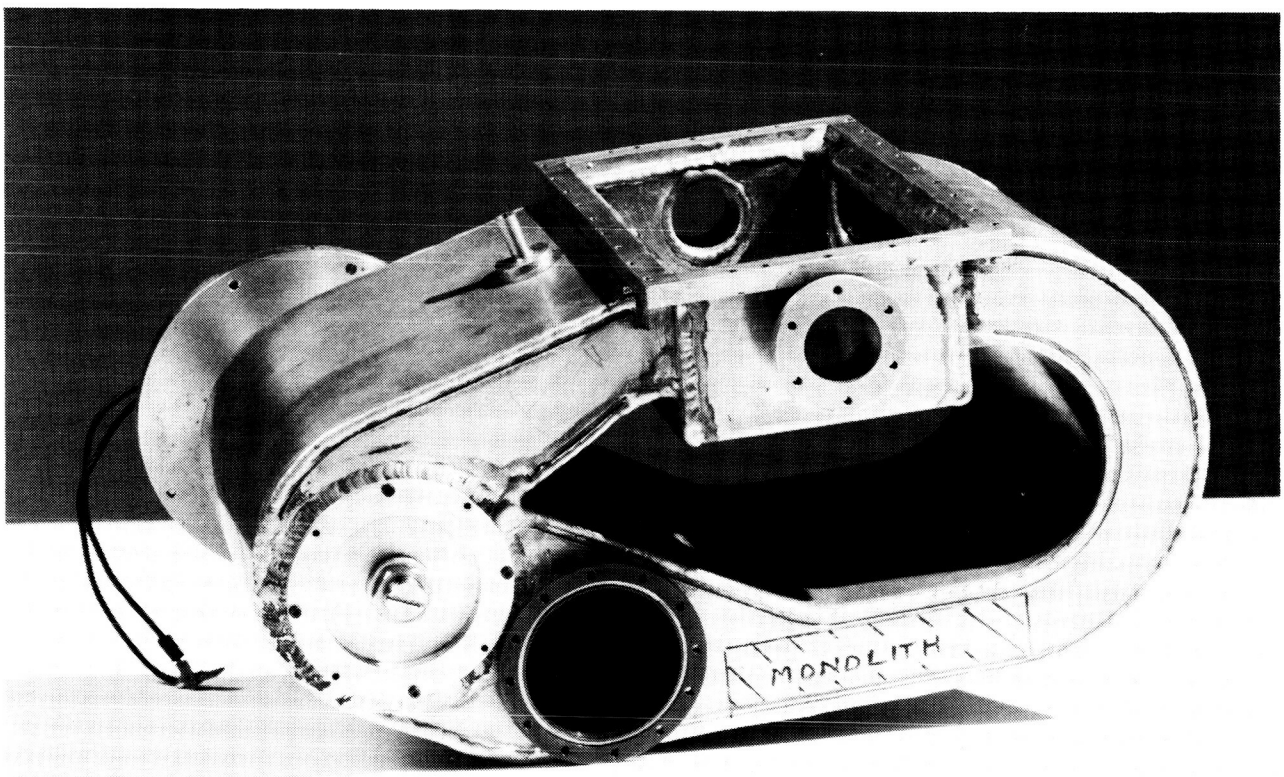

Figure 2. Laser test apparatus.

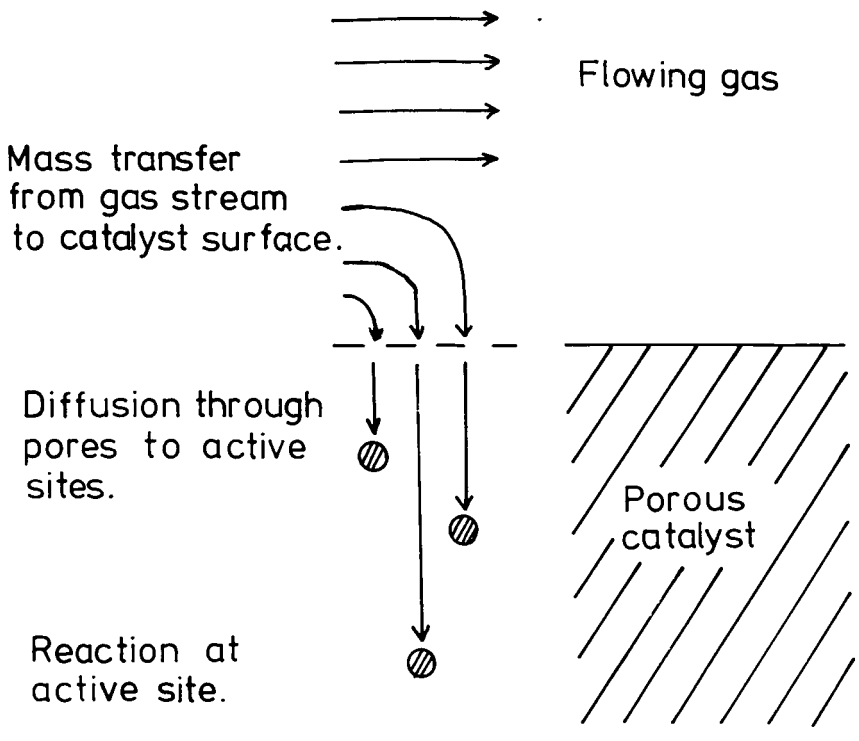

Figure 3. Physical processes in catalysis.

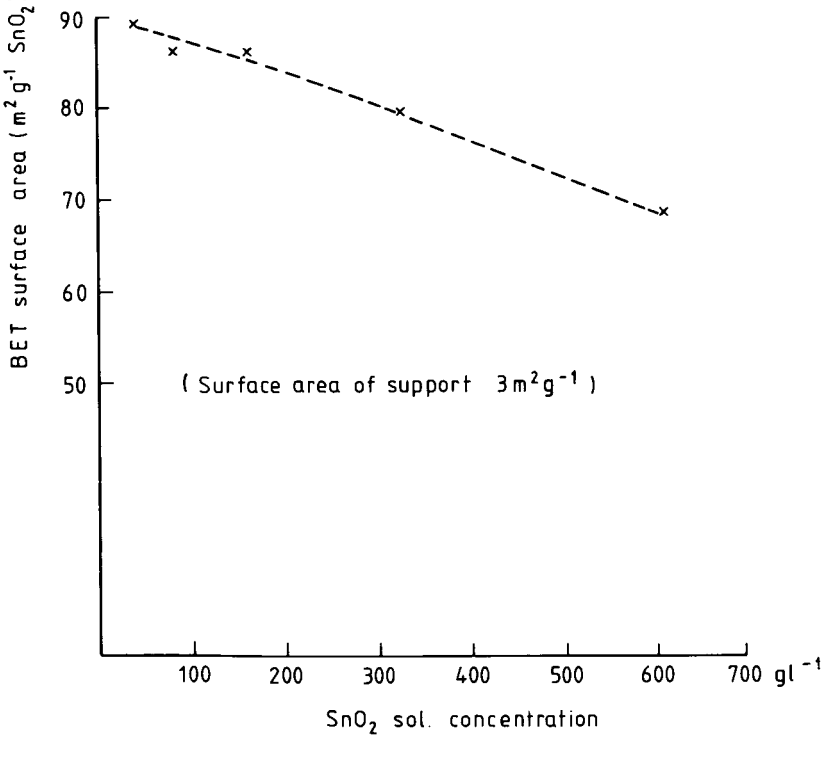

Figure 4. Surface area of SnO_2 calcined on monolith versus SOL concentration used for coating.

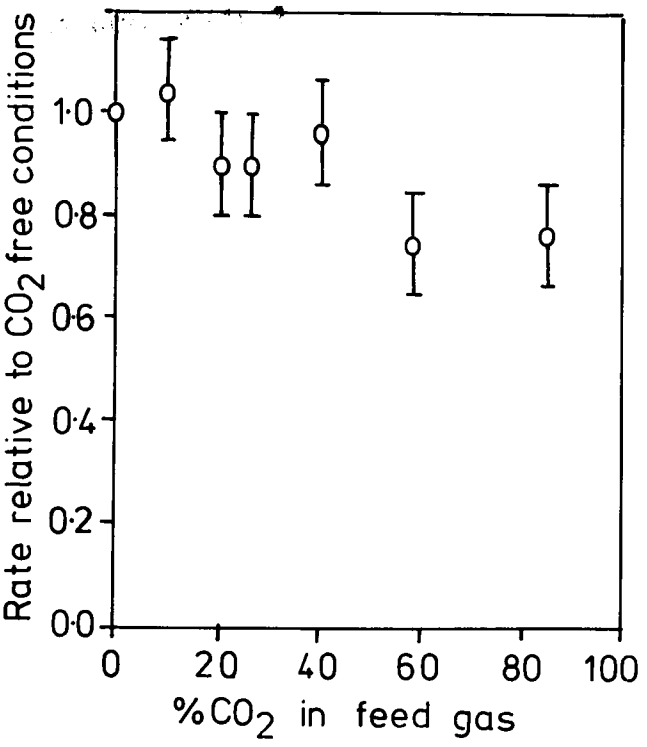

Figure 5. Effect of added CO_2 on the rate of $CO-O_2$ recombination.

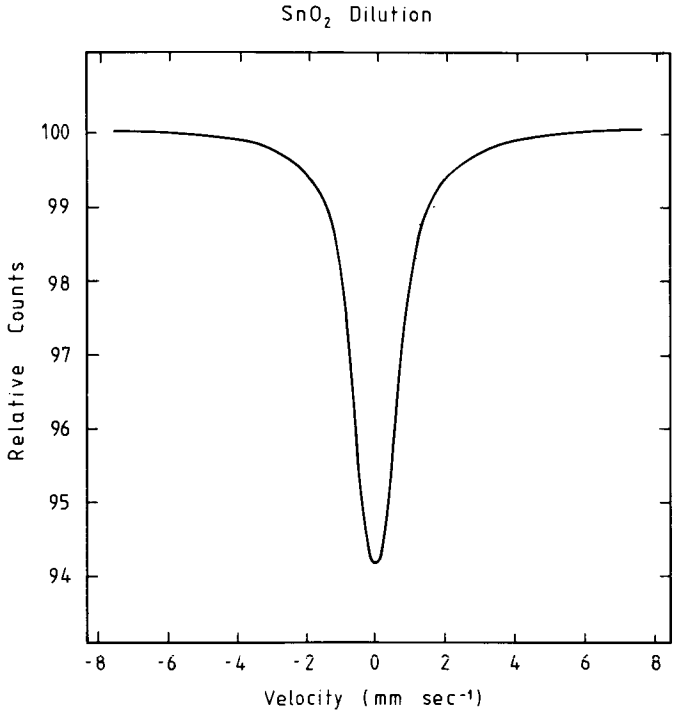

Figure 6. Mössbauer peak position of Sn^{4+}.

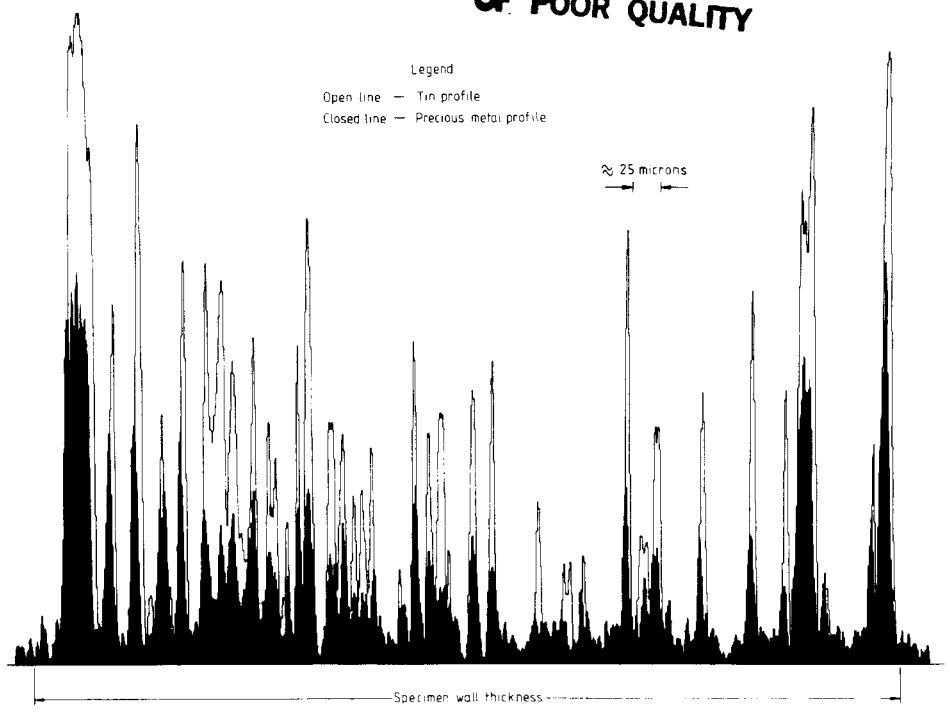

Figure 7. Electron microprobe trace across wall thickness of monolith.

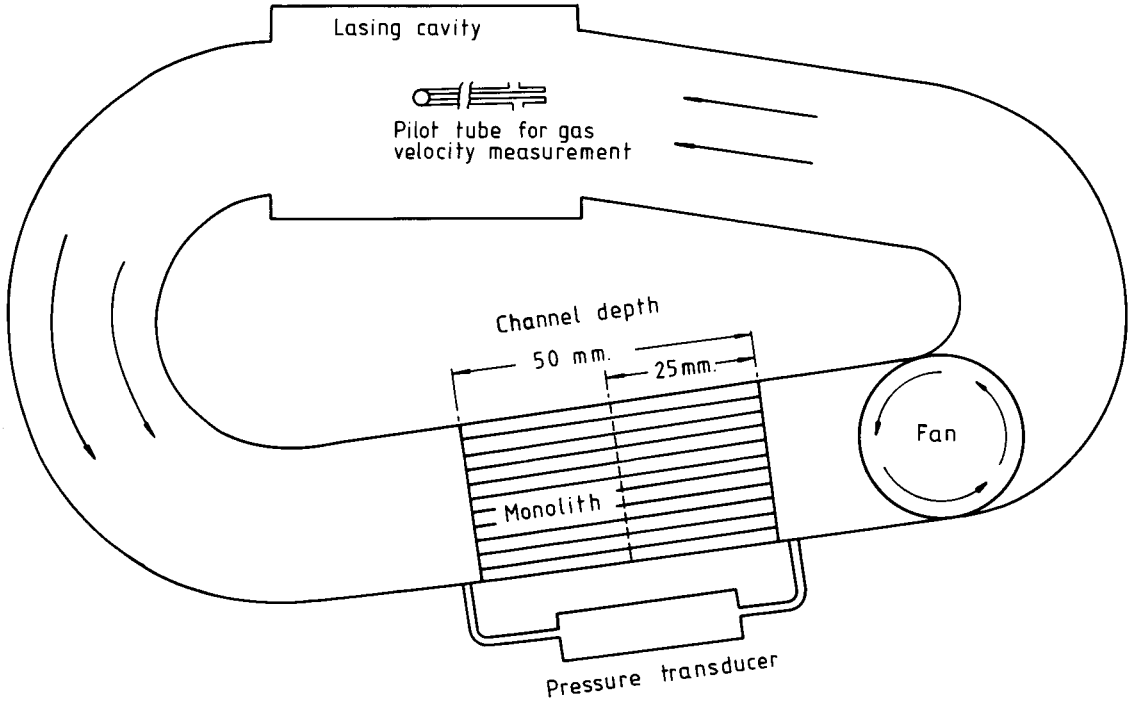

Figure 8. Diagram of pressure drop measurement system.

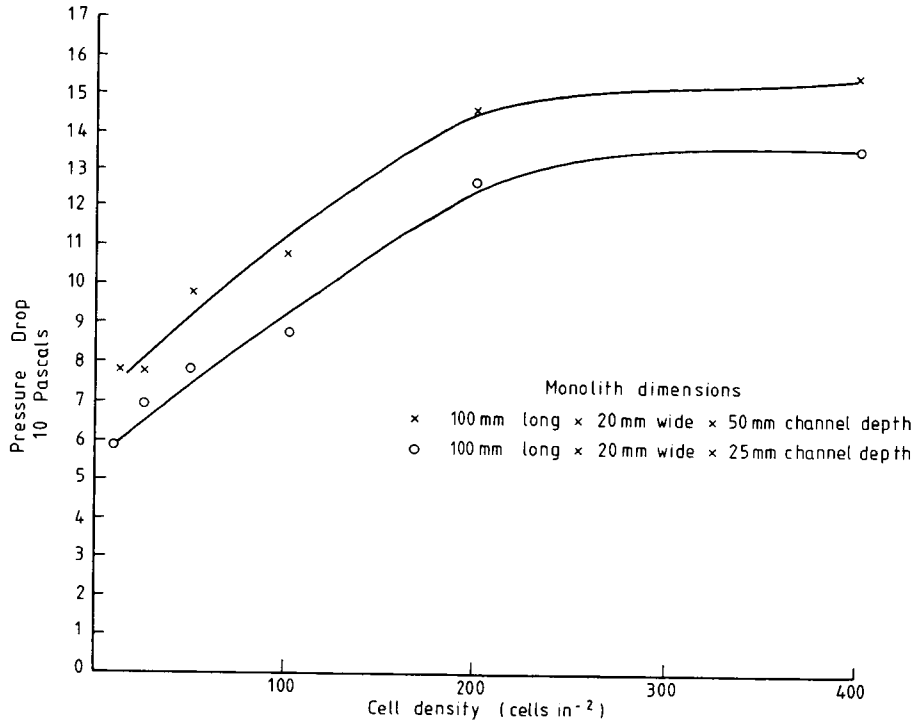

Figure 9. Pressure drop across monolith versus cell density at constant gas velocity (7 mm sec^{-1}).

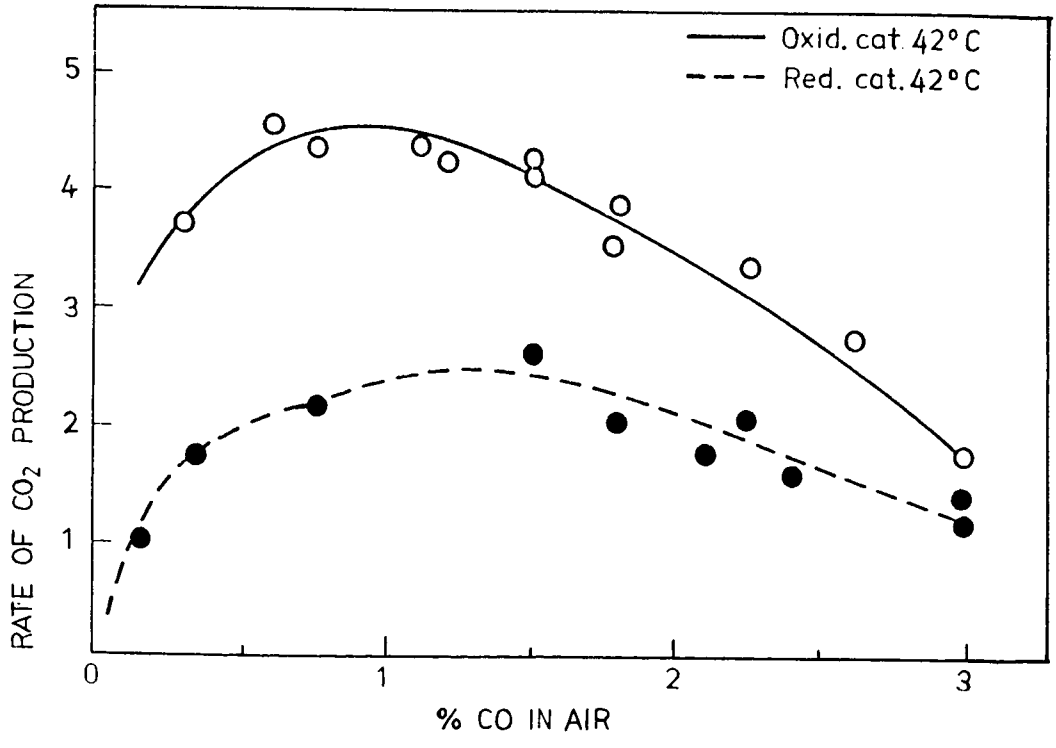

Figure 10. Rate of CO_2 production versus CO in air.

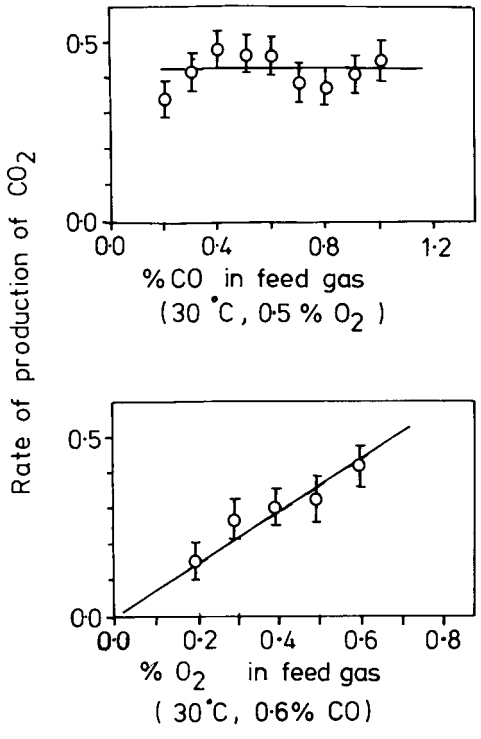

Figure 11. Effect of CO and O_2 partial pressure on the rate of recombination.

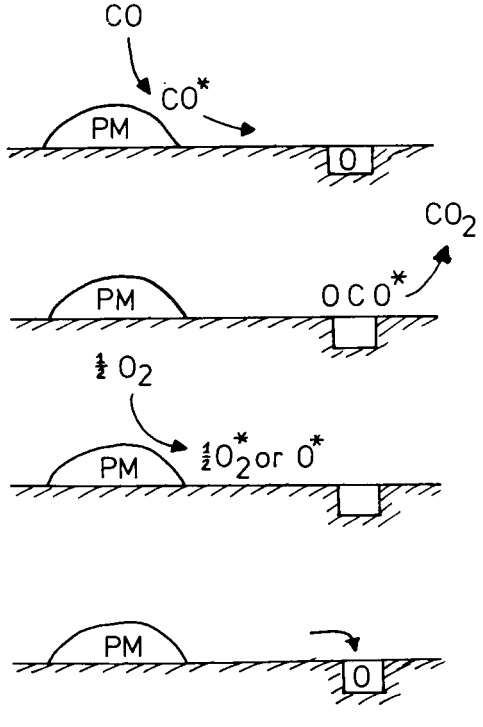

Figure 12. Spillover model (Bond et al.).

HIGH REPETITION RATE SEALED CO_2 TEA LASERS USING HETEROGENEOUS CATALYSTS*

H. T. Price and S. R. Shaw
Applied Physics Division, GEC Avionics Limited
Borehamwood, Herts
United Kingdom

INTRODUCTION

The significant operational advantages offered by CO_2 lasers, operating in the 10.6 micron region of the spectrum, over current solid state lasers, emitting in the near I.R. region of the spectrum, have prompted increased interest in the development of compact, reliable, rugged CO_2 laser sources. Perhaps the most critical aspect associated with achieving a laser compatible with military use is the development of lasers which require no gas replenishment.

Sealed, single shot, CO_2 TEA lasers have been available for a number of years. Stark et al were first to demonstrate reliable sealed operation in single shot CO_2 TEA lasers in 1975 (reference 1) using gas catalysis. GEC Avionics reported the compact, environmetally qualified, MKIII CO_2 TEA laser with a pulse life of greater than 10^6 pulses in 1980 (reference 2).

A sealed laser lifetime of greater than 10^6 pulses is acceptable for single shot cases, such as direct detection rangefinders for tank laser sights. However, in many other applications, such as tracking of fast moving targets, it is essential that a repetition rate of typically 30Hz to 100Hz is employed. In such cases, a pulse lifetime of 10^6 pulses is no longer sufficient and a minimum pulse lifetime of 10^7 pulses is essential to ensure a useful service life. In 1983 Stark et al (reference 3) described a sealed, 100Hz CO_2 TEA laser, with a life of $>2.6 \times 10^6$, which employed heterogeneous catalysis. Following this pioneering work, GEC Avionics has been engaged in the development of a sealed high repetition rate lasers and in the following a pulse lifetime of 20 million pulses is demonstrated.

FACTORS INFLUENCING LIFETIME

The single most critical factor dictating the attainment of a sealed lifetime is the chemical reactions which occur in the discharge of the pulsed CO_2 TEA laser. The electrical discharge dissociates CO_2 forming CO and oxygen, primarily as a result of direct electron impact (2 body attachment). A typical three gas mixture, tends to dissociate linearly with the number of pulses and a glow to arc transition is obtained whenever the negative ion concentration becomes comparable with the electron concentration. Thus, to control arcing in these lasers, steps must be taken to control the negative ion concentration, which in turn means the O_2 concentration must be controlled. Typically the oxygen concentration must be limited to <1% in order to guarantee prevention of arcing (though the actual oxygen tolerance of a particular system is a strong function of the laser design).

In lasers employing low concentrations of CO_2 (i.e. <15%) gas additives are a particularly successful technique to control the oxygen buildup. For high CO_2 concentrations, more effective forms of catalysis can be employed. In this case the

*This work was supported by the Procurement Executive, Ministry of Defence, sponsored by DCVD

catalytic recombination rate must be matched with the dissociation rate, dictated by the CO_2 concentration and the repetition rate. However, it would be incorrect to imply that the gas chemistry effects outlined above are the sole factor influencing laser lifetime. Many additional factors are important including:

a) Gas contamination
b) Excess or slow electrical excitation
c) Electrode assembly and condition
d) Inadequate or limited preionization
e) Optical deterioration

where items b) to d) tend to enhance the criticality of controlling the gas chemistry. Also important are aspects of the laser construction including materials employed, mechanical sealing techniques used, and cleaning and processing schedules. Thus successful sealed laser performance is related to the optical, mechanical and electrical design of the laser, the design of the external drive circuit, and the control of the gas chemistry.

LIFETEST LASER DESIGN

The basic design of the test-bed laser constructed for sealed lifetime studies is indicated in Figure 1. This shows a schematic cross section of the laser normal to the optic axis. The electrode structure consists of a pair of solid metal electrodes preionized by either sliding arc arrays or semiconductor plates. The electrodes are profiled so that the field decreases uniformly in all directions away from the uniform field region between the electrodes. The arc array preionizer geometry is similar to that described previously (reference 1) while the semiconductor preionizers consist of slabs of low resistivity silicon mounted close to the high voltage electrodes. The total discharge volume is $11cm^3$.

A tangential fan is used to provide the closed cycle gas circulation necessary for operation at high repetition rates. A gas flow velocity of typically $2ms^{-1}$ is used to provide a clearing ratio of greater than 2. The fan is driven from an external motor via a magnetic fluid leadthrough. Since the laser operates continuously, fluid cooling of the laser is provided to remove the heat dissipated by the discharge.

A room temperature, tin-oxide/precious metal CO oxidation catalyst is placed in the gas flow. Two forms of catalyst have been tested. The first is supplied by UOP Limited (UK) and is in pellet form. The pellets are supported on a suitable substrate and the mass of catalyst pellets is selected to provide sufficient recombination for the conditions under which the laser will be operated. The second form of catalyst is supplied by AERE (Harwell) and in this case the catalyst is supported on a ceramic monolith. Both forms of catalyst are mechanically strong and are resistant to powdering.

The cavity reflectors consist of a plane, 100% gold on copper mirror and a plane, zinc selenide, partial reflector, both of which are mounted on an internal optical frame. The intracavity aperture constrains the laser to the fundamental mode. The cavity reflectors for the test-bed lasers are easily removed to facilitate inspection and can be aligned during the lifetests without opening the laser. The cavity is designed such that the internal power density is limited to a value significantly lower than the measured laser damage threshold of the optics.

The gas envelope of the laser head is a welded stainless steel structure, which has been designed to give maximum experimental flexibility during the ongoing experimental program. As a consequence the physical size of the laser at 2.4 liters is significantly larger than is required for the nominal design performance of a 1MW peak power, 100mJ pulse energy.

The lifetests were conducted with the laser operated in the test set-up illustrated in figure (2). The laser is driven from a standard, spark gap switched, single energy storage capacitor, pulse forming network, charged to typically 30kV. The laser is connected to an IR CO analyser and a paramagnetic O_2 analyzer. This permits the gas composition in the laser to be monitored in situ during the lifetest, thus avoiding interference with the experiment. Measurement of the pumping speed of the catalyst can also be made.

The pumping speed is determined periodically during a lifetest by switching the laser off and measuring the change in O_2 partial pressure with time. The partial pressure, P at time, t, is give by

$$P=P_o \bar{e}^{mAt/V}$$

Where P_o is the partial pressure at t_o
V is the volume of the laser
A is the specific volumetric pumping speed
m is the mass of catalyst.

The oxygen volumetric pumping speed is thus the rate of removal of oxygen per gram of catalyst and is a useful measure of the activity of the catalyst in relation to oxygen recombination. From a semi-logarithmic plot of oxygen partial pressure and time, 'A' may be readily determined from the slope.

In addition to gas compositions and catalyst activity, the laser output power, energy, divergence and discharge characteristics are monitored throughout the lifetests.

The system described has been used to conduct a series of sealed lifetests and the results obtained are indicated below. In all the tests discussed the gas mixture employed was a 1:1:1 mixture of CO_2, N_2 and He, and the repetition rate was 30Hz to 50Hz.

RESULTS

Figure (3) shows the variation in output energy of the laser as a function of the number of pulses. In this test the laser was preionized by a pair of sliding arc-arrays, and a UOP catalyst was employed. Over the 10^7 pulses of the test the output remained essentially constant, and at the termination of the experiment the laser was completely stable.

Similarly, figures (4), (5) and (6) show the performance of the laser over a 10^7 lifetest using a Harwell catalyst and arc-array preionization. The peak power and pulse energy exhibit little degradation over the duration of the test, while, the pumping speed of the catalyst is unchanged at the end of the test, though there is an increase observed during the first 2.0×10^6 pulses. Thus the initial pumping speed of 32 cc/s/g is maintained over the 10^7 pulses, indicating the

catalytic activity is not degraded. Figures (7) and (8) show the behavior with the UOP catalyst and arc array preionization over a 20 million pulse lifetest. The critical laser parameters are only reduced by typically 10%. The same performance is also obtained in the complementary tests using the Harwell catalyst.

The above tests all employed arc-array preionization. Results obtained using semiconductor preionization have been equally successful.

During the lifetest program we have also demonstrated a cumulative life of 10^8 pulses for some of the major components of the laser. This includes laser resonator optics and arc array preionizers. In the latter case, arc array erosion over the 10^8 pulses resulted in an increase in arc gap and a consequent increase in the delay of the arc array preionizing discharge. This latter effect would not present a difficulty where the arc arrays and main discharge arc fired independently. However the accumulation of eroded material within the laser could result in deleterious effects if remedial action is not taken.

CONCLUSIONS

In the course of the lifetest program described it has clearly been demonstrated that our essential lifetime requirement of 10^7 pulses has been achieved and that the desirable lifetime of 10^8 pulses appears feasible. To obtain such a lifetime reliability, or even extended it further, additional work is required to investigate, for example, the long term stability of the catalyst and identify any catalyst effects which have not yet become to manifest, to study accumulated optical effects to resonator reflectors, and to address engineering factors such as erosion products of active elements in the laser.

REFERENCES

1. D. S. Stark, P. H. Cross and H. Foster IEEE J. Quant. Elect. QE11 774, (1975).

2. H. T. W. Price SPIE Vol 227 CO_2 Laser Devices and Applications, 48, (1980).

3. D. S. Stark, A. Crocker and G. J. Steward J. Phys. E. Sci Instrum 16 (1983) 158.

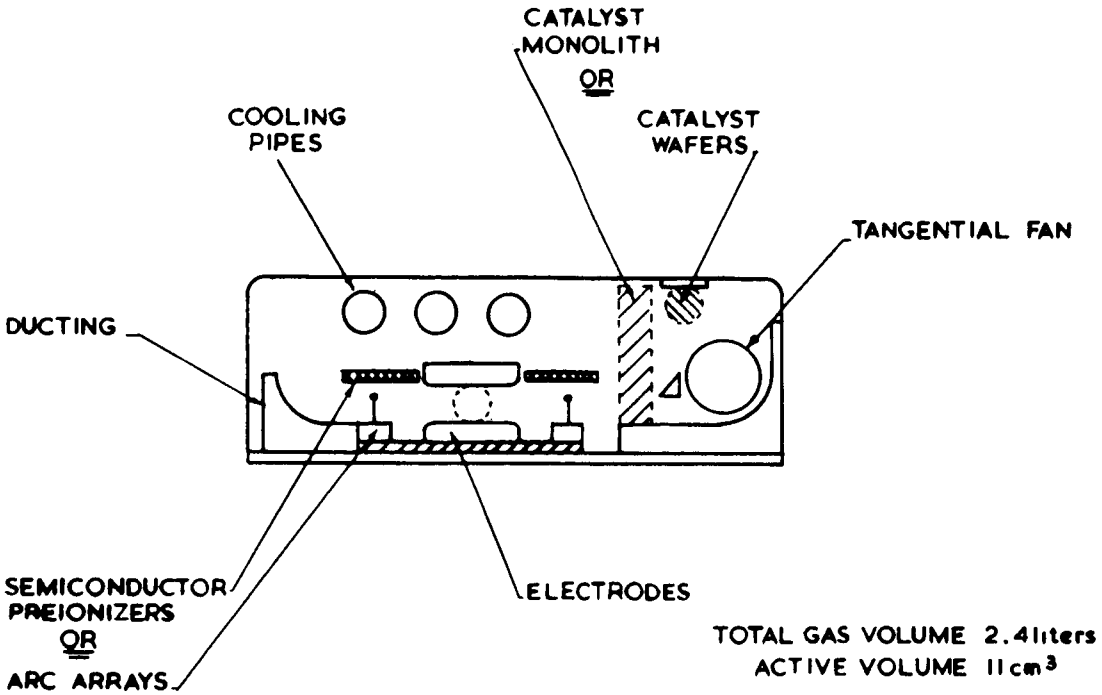

SCHEMATIC OF LIFETEST LASER

Figure 1

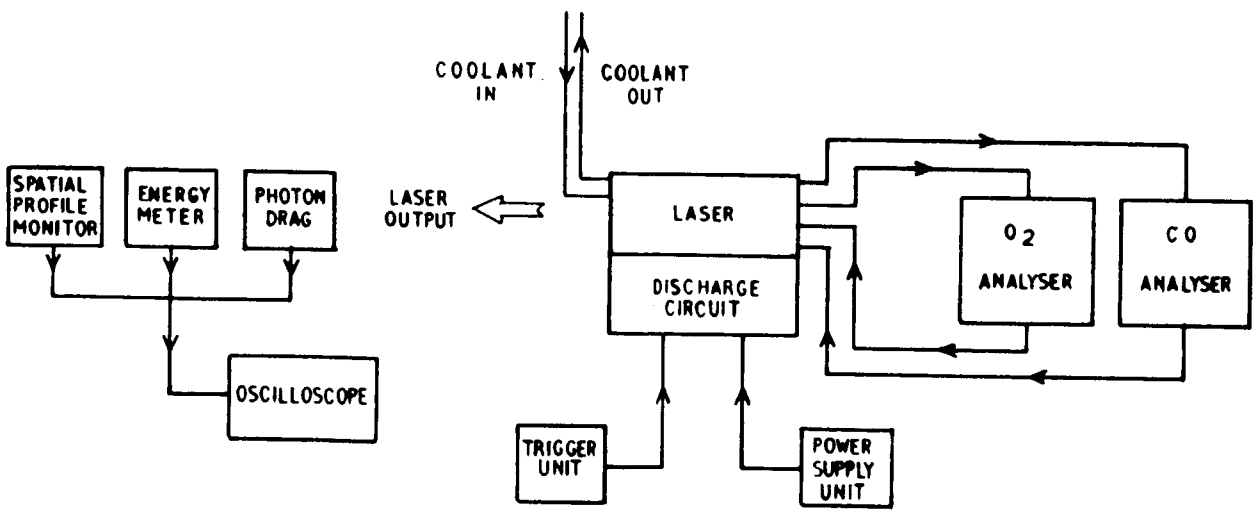

LIFETEST LASER TEST SET-UP

Figure 2

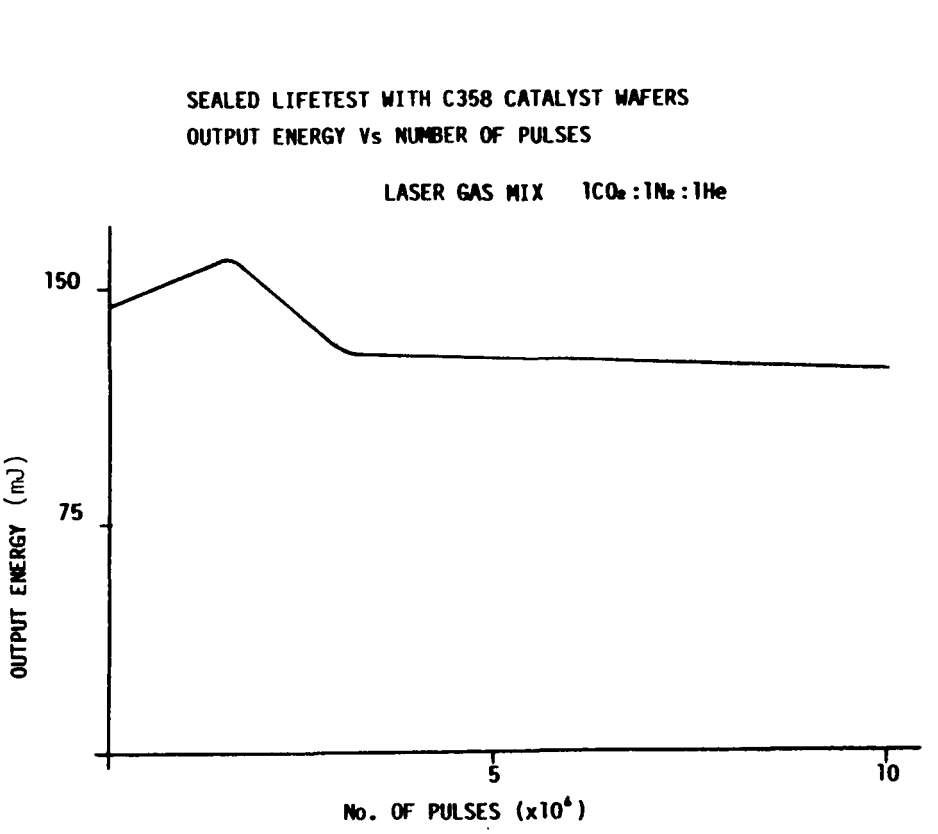

Figure 3

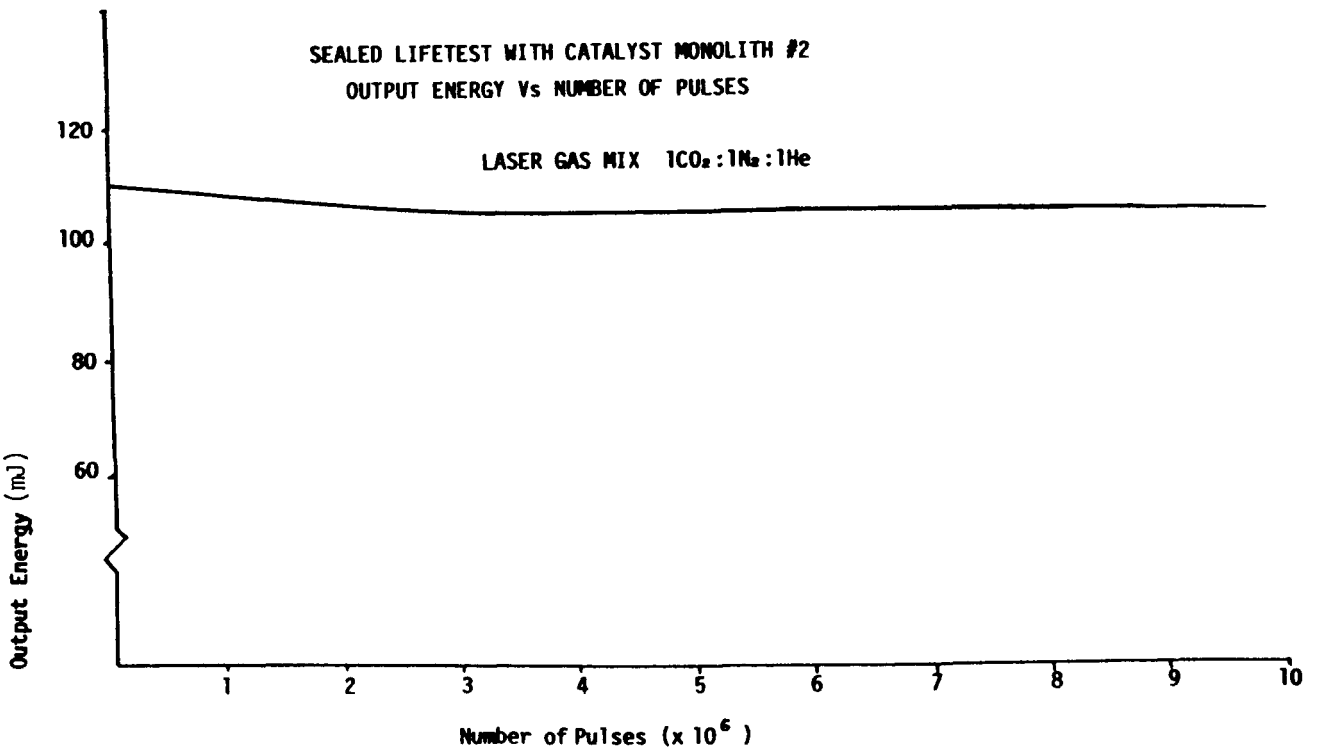

Figure 4

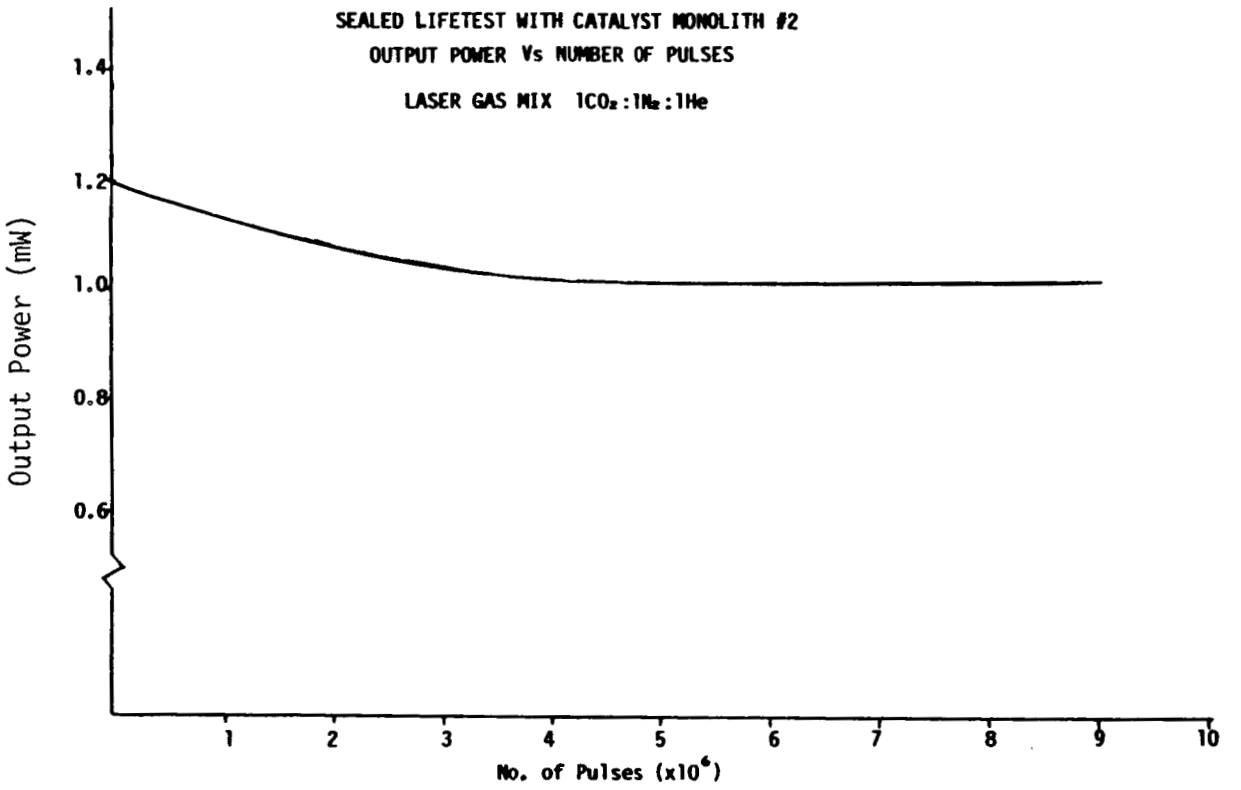

Figure 5

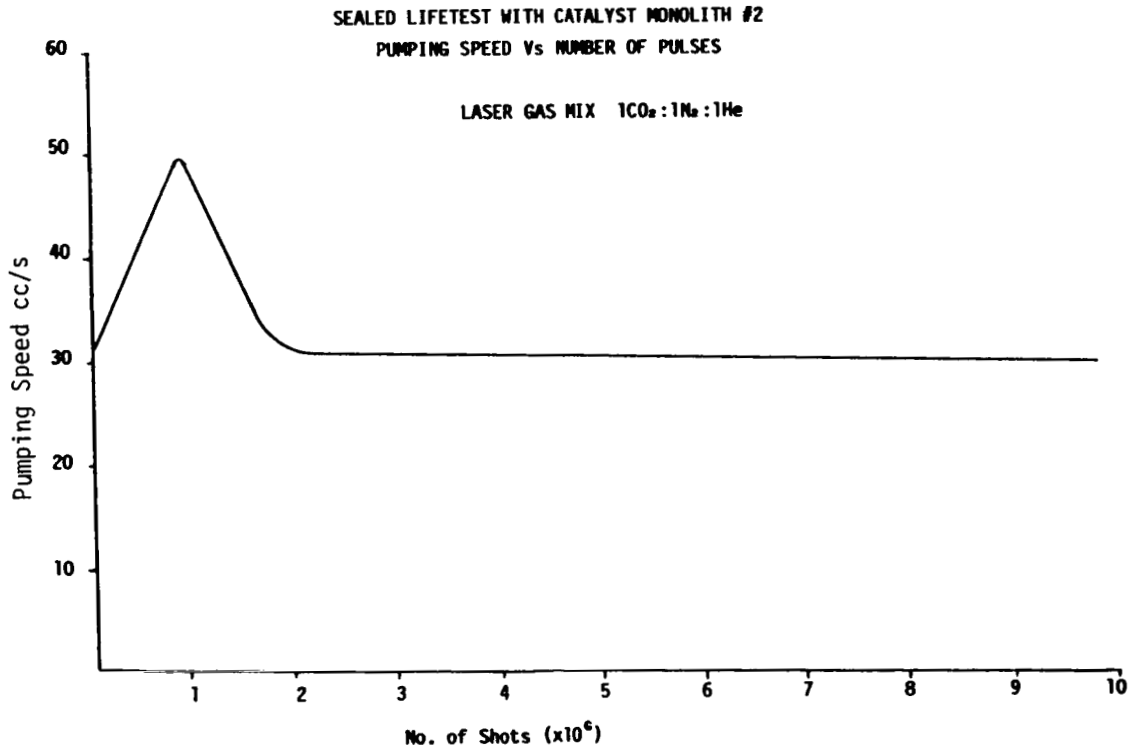

Figure 6

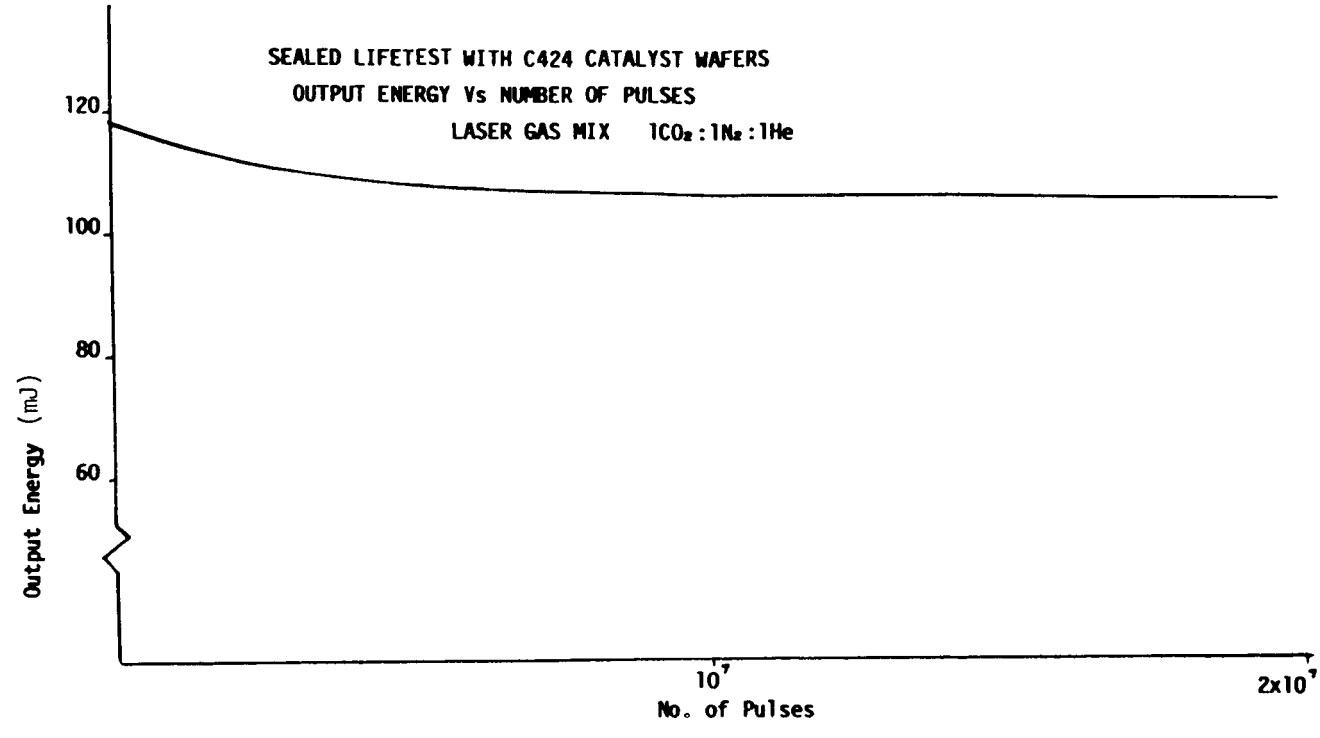

Figure 7

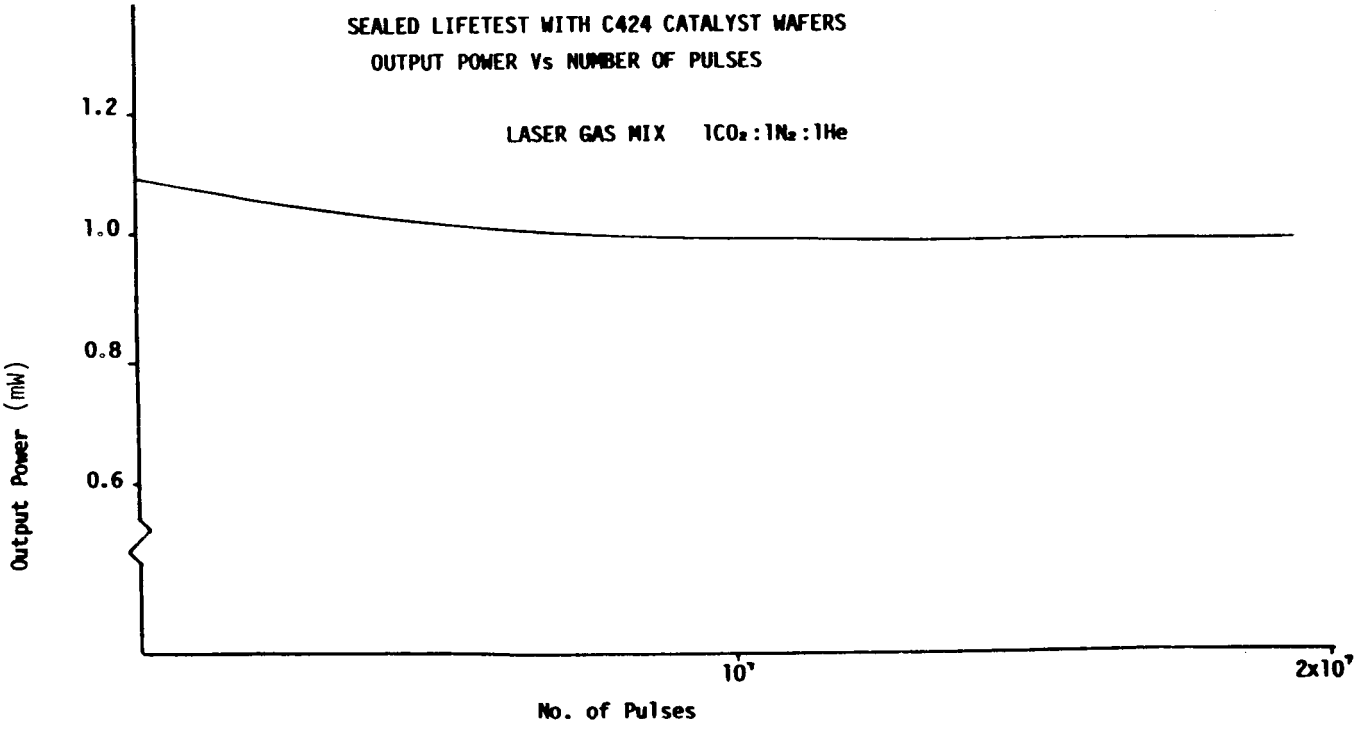

Figure 8

CO Oxidation Studies Over Supported Noble Metal Catalysts and Single Crystals: A Review

Dirk Böcker and Richard D. Gonzalez
The University of Illinois at Chicago
Chicago, Illinois 60680

SUMMARY

The catalytic oxidation of CO over noble metal catalysts is reviewed. Results obtained on supported noble metal catalysts and single crystals both at high pressures and under UHV conditions are compared. The underlying causes which result in surface instabilities and multiple steady-state oscillations are considered. In particular, the occurrence of hot spots, CO islands of reactivity, surface oxide formation and phase transformations under oscillatory conditions are discussed.

INTRODUCTION

The oxidation of CO over noble metal catalysts has been one of the most frequently studied catalytic reactions and is also perhaps the best understood of all catalytic reactions. This reaction is a problem which has attracted both the industrial and the academic sector and has fascinated catalytic chemists for many years. It is of immense importance in the control of emissions from automotive exhaust gases, enviromental cleanup and a variety of industrial applications of significant economic importance. A number of excellent reviews have recently appeared in the literature which deal with the reaction on both well-defined crystal surfaces [1,2] and on supported noble metal catalysts [3]. Of particular interest in the case of supported Pt is the occurrence of multiple steady states [4], the presence of self-sustained oscillations [3 & ref. therein], the existence of CO islands of reactivity [5,6] and induced metal and adlayer phase transitions. The importance of considering intraparticle diffusion in the case porous catalysts has been pointed out by HEGEDUS et al. [7]. More recently HERZ and MARIN [4] have shown quite convincingly that multiple steady states can arise as a result of coupling between nonequilibrium adsorption and surface kinetics.

CO oxidation studies on supported noble metal catalysts other than Pt and Pd have received less attention. CANT et al. [8] have performed CO oxidation studies on five noble metal catalysts in an attempt to bridge the gap between low pressure studies on well defined crystal surfaces and high pressure studies on supported metal powders. In these studies, the rather anomalous behavior of Ru was noted. It was suggested that the extensive catalyst deactivation might be due to the incorporation of oxygen into the Ru crystal lattice. Recently, OH and CARPENTER on the basis of an XPS study, reported that the rate of CO oxidation over Rh/Al_2O_3 was strongly dependent on the oxidation state of Rh [9].

C-2 *

The current review is by no means exhaustive. However, we feel that an overview of the following areas in the catalytic oxidation of CO should serve to broaden the view of the conferees present at this meeting on pulsed CO_2 lasers: (1) reactions on supported metal catalysts, (2) reactions on selected well-defined single crystal surfaces, (3) surface instabilities and oscillatory behavior on supported noble metal catalysts at high pressures, (4) surface instabilities and oscillatory behavior on noble metals foils and under UHV conditions and, (5) surface reconstructions under UHV conditions.

REACTIONS ON SUPPORTED METALS

The catalytic oxidation of CO on supported noble metal catalysts displays a typical behavior regarding the pressure dependence of CO. The turnover frequency for the rate of CO_2 formation is plotted as a function of the ratio of the partial pressure of CO to that of O_2 in figure 1 for a 5% Ir/SiO_2 catalyst [10]. Exept for the p_{CO}/p_{O_2} ratio which corresponds to the inhibition by CO, the shape of the curves is identical for all of the supported noble metal catalysts studied. At low CO/O_2 partial pressure ratios, the surface coverage of oxygen is at its maximum. Because the sticking coefficient for CO on noble metals is not a function of oxygen surface coverage, the reaction rate is controlled by the rate of CO adsorption. Following inhibition of the reaction by CO, the surface is almost completely covered by CO. In this regime, the reaction rate is controlled by the CO desorption rate and by the sticking coefficient of oxygen which is strongly dependent on the surface coverage of CO. Kinetically, in this regime, the rate can be expressed by [2]:

$$r = k\Theta_{CO}\Theta_O = k'S(O_2)p_{O_2}$$

where Θ_{CO} and Θ_O represent the fraction of the surface covered by CO and oxygen respectively, and $S(O_2)$ is the sticking coefficient for the dissociative adsorption of oxygen on the supported noble metal. It is important to note that the sum of Θ_{CO} and Θ_O does not necessarily add up to 1. The monolayer surface coverage has been shown to depend quite critically on the composition of the adlayer [11]. The *role over* region between low and high p_{CO}/p_{O_2} partial pressures is characterized by rapidly changing CO and oxygen surface coverages. In this region the apparent activation energy for the reaction changes from 0 to about 100 kJ/mole and the reaction rate orders in CO and O_2 change from about +1 and -1 to -1 and +1 respectively [12]. Surface coverages of CO in both of these regimes have been substantiated by numerous *in-situ* infrared studies [10].

When the p_{CO}/p_{O_2} pressure loop is reversed by increasing the partial pressure of oxygen and decreasing that of CO, a hysteresis loop develops in which the rate of CO_2 formation is observed to be considerably less than that found during increasing p_{CO}/p_{O_2} partial pressure ratios [10]. A simple explanation of this observation can be rationalized on the dual site requirement for oxygen dissociation. Additionally, the sticking coefficient for oxygen dissociation is low at high surface coverages of CO. The possibility that heat transfer limitations may play a role in multiple steady–state reactions cannot be discounted. In the low CO surface coverage regime the surface may be considerably hotter than in the high CO surface coverage regime. This might be due, in part, to the higher heat of adsorption of oxygen in addition to the heat released as a result of the higher reaction rate.

The area under the hysteresis curve is a function of temperature and the particular metal under study. When the temperature is increased, the inhibition of the reaction rate is observed to occur at higher p_{CO}/p_{O_2} partial pressure ratios. This is undoubtedly due to the competitive nature of the CO and oxygen adsorption and desorption rate. At higher temperatures the desorption rate of CO increases. For this reason, higher pressures of CO are required to bring about an inhibition in the rate of reaction. Since CO is more weakly adsorbed, the lower branch of the hysteresis curve disappears due to a more facile displacement of chemisorbed oxygen by CO. CO oxidation studies on supported Pt [13] and supported Ir [10], which have about the same catalytic activity, show that at temperatures above 423 K, the hysteresis loop disappears.

CO oxidation reaction rates on supported metal catalysts should be compared at similar reactant gas phase compositions. This is of the utmost importance due to the dependence of reaction rates on the formation of strongly bound oxygen or the possible formation of subsurface oxides which may inhibit the reaction. Additionally , under oxidizing conditions, the formation of higher noble metal oxidation states may have a significant effect on catalytic activity. CO oxidation rates on Rh/SiO_2 catalysts for example [14], are inhibited by the formation of Rh(I) under net oxidizing conditions.

Reaction rates under net oxdizing, stoichiometric and net reducing reactant gas compositions at 373K are shown in table 1. Under both net reducing and stoiciometric conditions, the following catalytic sequence is observed: Ru>Ir>Pt>Rh>Pd. Under net oxidizing conditions, this sequence becomes: Rh>Ru>Pd>Ir [15]. From these results we conclude that Rh, while not a particularly active catalyst for CO oxidation, retains its activity under net reducing conditions. However, it rapidly looses its activity when exposed to oxidizing conditions [8,16].

DEACTIVATION OF SUPPORTED NOBLE METAL CATALYSTS

All supported noble metal catalysts deactivate to some extent following time on stream. Ru is the worst actor in this regard. Catalyst deactivation continues for several hours even under net reducing conditions. When a Ru/SiO_2 catalyst was exposed to a p_{CO}/p_{O_2} partial pressure of 0.25 for 12 hours, the catalyst was completely deactivated [16]. Its initial activity could only be restored following reduction in H_2 at 673 K. The buildup of unreactive oxygen, possibly in the form of unreactive chemisorbed oxygen or through the formation of a bulk subsurface oxide was offered as a reason for the observed deactivation. These results were in part confirmed using temperature programmed desorption following exposure of the catalyst to an oxygen rich reactant gas mixture for an extended period of time [16].

Catalytic CO oxidation studies on Rh/SiO_2 [14] show that Rh is quite resistant to deactivation. However, the results of a recent *in situ* infrared study show that CO oxidation rates depend to some measure on the oxidation state of Rh [9,14]. Reaction rates decrease in the following sequence: Rh(0)>Rh(I)>Rh(III). Recent studies on Ru-Rh/SiO_2 bimetallic clusters are encouraging. Evidently the formation of Ru-Rh bimetallic clusters appear to inhibit deactivation nearly completely [17].

On Pt/SiO_2, CANT et al. [18] suggest that deactivation occurs as a result of the buildup of nonreactive oxygen. To substantiate this suggestion, using *in situ* infrared methods, they observed the appearance of an unreactive infrared band centered at 2120 cm^{-1}, which he assigned to CO adsorbed on an oxidized Pt surface site. Because the decline in the catalytic activity appears to be concomittant with the appearance of this

infrared band, it can be concluded that all Pt surface sites capable of chemisorbing oxygen are not equally reactive in the oxidation of CO. In fact, because the dissociation of O_2 occurs preferentially on edges, steps and centers of low surface coordination, the blockage of these sites by unreactive chemisorbed oxygen would, in all likelihood, result in an overall decrease in the catalytic activity.

SUPPORT AND PARTICLE SIZE EFECTS

There has not been widespread agreement with respect to the effect of particle size on the rate of CO oxidation and the subject is quite controversial. SARKANY and GONZALEZ support the view that the oxidation of CO is a facile reaction on Pt/SiO_2 [19]. CO_2 turnover numbers measured at 373 K were insensitive to an overall increase in the Pt dispersion by a factor of 4. On Pt/Al_2O_3 the situation was not clean cut [19]. When Pt dispersions were increased from 0.17 to 0.90, the reaction rate increased by a factor of 3. Because CO oxidation results performed on Rh and Ru single crystals [20] are in excellent agreement with studies performed on supported Rh [14] and Ru [16] it appears that the reaction is, in fact, facile. In a recent CO oxidation study on supported Pd, BOUDART and ICHIKAWA [21] reported that reaction rates appeared to be faster on small particles. However, they also reported that because small particles were considerably more active in promoting the BOUDOUARD reaction, an additional route to CO_2 formation through dissociated carbon was possible. When a correction for this observation was made, they concluded that the reaction on supported Pd was facile.

Recent studies on Pt/SnO_2 have shown this catalyst to have a very high low temperature activity [22]. This property makes it useful for use in applications of pulsed CO_2 lasers. In a pulsed CO_2 laser, CO_2 is decomposed to CO and O_2. Because it is necessary to maintain a constant CO_2 pressure, a catalytic recycle system is necessary to reoxidize CO back to CO_2. Unfortunately, the SnO_2 support exchanges oxygen with CO_2 [23] and, therefore, does not maintain the isotopic integrity of the CO_2 which requires labeling with ^{18}O. This results in the instability of the lasing frequency.

REACTIONS ON SINGLE CRYSTALS

Because of the facile nature of the catalytic oxidation of CO it is of interest to compare studies on single crystal surfaces to similar studies on supported metals. In a survey study, similar activation energies (~100 kJ/mole) and kinetic orders (+1 in O_2 and -1 in CO) were found for supported Pd, Rh [15] and Ir [10] catalysts. For Ru, the situation appears to be more complex. Furthermore, Ru has been reported to be the most active catalyst for the series of supported noble metal catalysts [15] while under UHV conditions it is the least active [20].

In a recent surface science study performed under more realistic pressure conditions, GOODMAN and PEDEN [20] and OH et al. [24], have reexamined the catalytic oxidation of CO on Ru(0001) and Rh(111). In these studies, the reactor could be withdrawn from the high pressure reaction system at any time and examined using UHV methods.

Turnover frequencies for CO_2 formation on Rh(111) and Rh(100) as a function of temperature are shown in figure 2. They are in exellent agreement with similar rates obtained on highly dispersed Rh/Al_2O_3 catalyst [25]. Apparent activation energies of 121 kJ/mole were obtained on Rh(111) compared to 125 kJ/mole on Rh/Al_2O_3. A similar

agreement was obtained in studies performed on Ru(0001) and Ru/SiO_2 [20]. Apparent activation energies of 83.6 kJ/mole on Ru(0001) compare favorably with those obtained on Ru/SiO_2 (94.05 kJ/mole) [16]. Furthermore, Ru(0001) was considerably more active than Rh(111) in agreement with studies on supported metal catalysts.

The dependence of the rate of CO oxidation on the partial pressure of CO on Rh(111) decreases linearly with with increasing partial pressure of CO, figure 3 [20]. The behavior of Ru(0001) is considerably more complex. However, it too is in excellent agreement with results obtained on Ru/SiO_2 [16]. At low partial pressures of CO, the reaction is positive order in O_2.

The dependence of the CO oxidation rate on the partial pressure of oxygen on Rh(111) increases until a partial pressure ratio p_{O_2}/p_{CO} of about 30 is reached [20]. The rate roles over and is inhibited by a further increase in the partial pressure of O_2. These results are in good agreement with similar studies on NAFION supported Rh catalysts [25]. Perhaps a catalyticly inactive Rh surface oxide is formed at sufficiently high partial pressures of oxygen. Surface analysis of the oxygen adlayer using Auger Electron Spectroscopy (AES) showed that the role over in the reaction rate occurred following the formation of a monolayer of oxygen on Rh(111) [20]. Presumably this oxygen, whatever its nature, deactivates the catalyst.

Similar experiments on Ru(0001) [20] show that when a monolayer of oxygen is obtained, the reaction rate reaches its maximum value and becomes zero order in the partial pressure of O_2. This result is in striking variance to studies on Ru/SiO_2 [16]. For the case of supported Ru catalysts the reaction rate is strongly inhibeted by excess O_2. Surface AES studies show that the maximum rate of CO oxidation on Ru(0001) coincides with the maximum concentration of surface oxygen [20]. Thus, in this respect, there appears to be a significant difference in the results of the Ru single crystal studies and the supported Ru studies. Further work is needed to resolve this apparent inconsistency.

In conclusion, similar activity trends are obtained on single crystals and on supported noble metal catalysts. However, important differences also exist with respect to the dependence of the rate on the partial pressure of the reactants.

REACTIONS IN MOLECULAR BEAMS

Recent studies using molecular beams focused onto Pt(111) single crystals [26] and Pt foils [27] have led to a significant understanding of the nature of the adsorbed transition state complex which leads to the formation of gas phase CO_2.

When the reaction was run using a mixed molecular beam consisting of CO and O_2 molecules under steady state conditions [27], the infrared emission spectra of the resulting CO_2 product molecules showed that there vibrational frequencies corresponded to temperatures which were considerably higher than that of the surface. When the composition of the beam had excess oxygen [28], the vibrational temperature of CO_2 was considerably higher than that observed in a CO rich molecular beam. Perhaps, as noted earlier, the higher heat of adsorption of oxygen might result in higher surface temperatures on an oxygen covered surface.

The results of a pulsed CO molecular beam in the presence of a constant pressure of oxygen showed that the vibrational temperature was a function of oxygen surface coverage [28]. The vibrational temperature of the product CO_2 molecules was observed to decrease with decreasing oxygen surface coverage. Because the rotational temperature

decreased at a much faster rate than the vibrational temperature, it was concluded that the product CO_2 molecules were vibrationally excited. It would appear that a transition state with a CO_2 molecule oriented perpendicular to the surface would account for this observation. In all likelihood the excess vibrational energy is stored in the asymmetric stretching mode of CO_2.

NAGAI et al., have recently made similar observations in a transient CO oxidation study over a Pt/SiO_2 catalyst [29]. Using an *in situ* infrared cell reactor, these authors observed that the antisymmetric stretching vibration of CO_2 was red shifted by 10 cm^{-1}. Additionally the P-branch and the R-branch in the resulting transient infrared spectra could not be resolved suggesting vibrationally exited CO_2. In these studies, a pulse of CO was added to a Pt surface covered by oxygen. The resulting transient response giving rise to the infrared spectrum of CO_2 lasted for about 10 seconds during which time 10 scans were made. Future studies will be aimed at fitting the resultant transient response data of CO_2, preferably in the emission mode, to vibrational and surface temperatures.

SURFACE INSTABILITIES AND SELF-SUSTAINED OSCILLATIONS

Supported metals

Given a set of time-dependent differential equations, multiplicity is obtained when there is more than one stable, physically realizable solution to the steady-state form of the equations for a given set of parameters [3]. This characteristic is rather easily obtained for mathematical models if heat and mass transfer influences are considered. However, the underlining cause which leads to oscillatory behavior has not as yet been unambiguously determined.

Even though self-sustained oscillations during the oxidation of CO have been the most widely studied, reaction rate instabilities are by no means limited to this reaction. Self-sustained oscillations have been observed for a wide variety of surface catalyzed reactions which include: H_2+O_2, NH_3+O_2, $C_2H_4+O_2$, $CO+NO$, CH_3OH+O_2, $NO+NH_3$ and $C_6H_{12}+O_2$ [3]. It is noteworthy that most of these reactions are highly exothermic in nature and generally involve catalytic oxidations. However, several cases of reaction rate instabilities which involve reductions have also been reported [3]. For the purposes of discussion, we will limit ourselves here only to a consideration of self-sustained oscillations observed during the oxidation of CO.

The various kinetic regimes during the oxidation of CO are summarized in figure 4. In region (I) the reaction rate is controlled by the rate of CO adsorption [13]. The reaction rate in this regime is approximately first order in CO and zero order in oxygen. Under these conditions, the fraction of the surface covered by oxygen is at its maximum and the apparent activation energy is close to zero. In region (III), the reaction rate is strongly inhibited by adsorbed CO. Under these conditions, the apparent activation energy is close to 100 kJ/mole on most noble metals and the reaction rate is approximately first order in oxygen and negative first order in the partial pressure of CO.

The existence of self-sustained oscillations is limited to region (II). In this region, surface coverage of CO and oxygen vary over the pressure domain in which the oscillations occur. Apparent activation energies also change sharply as the partial pressure of CO is increased. The amplitude of the oscillations are a function of both the

partial pressure of CO and temperature [13]. This behavior is outlined in figure 5 for a Pt/SiO_2 catalyst. As the temperature is increased from 488 K to 544 K, the amplitude of the oscillations is observed to decrease. The dependence of the ampliutude of the oscillations on the CO partial pressure is also shown in figure 6. This amplitude increases until the surface is predominantly covered by CO and the reaction rate is rapidly quenched. The dependence of the oscillatory period on the partial pressure of CO is shown in figure 6. As the partial pressure of CO is increased, the frequency of the oscillations is observed to decrease.

A recent *in situ* infrared study by KAUL and WOLF [30] shows that these self-sustained oscillations are accompanied by large surface temperature fluctuations. A summary of their results on Pt/SiO_2 is shown in figure 7. Surface temperature fluctuations of up to 100 K are observed during these oscillations. Of interest in their results is that the rate of CO_2 production and the surface temperature do not oscillate in phase. This apparent inconsistency was resolved by inserting a second thermocouple on the surface at a location which was remote from the first. Because both thermocouples reported temperatures which differed by as much as 100 K, they concluded that hot spots were formed throughout the pressed catalyst pellet. When the temperature fluctuations were integrated over the entire surface of the catalyst pellet, the rate of CO_2 production, the surface oxygen coverage and the surface temperature oscillated in phase.

The occurrence of hot spots has elegantly been demonstrated by SCHMITZ and co-workers [31] using infrared thermograms. These authors observed temperature inhomogeneities during the oxidation of H_2 and CO over a series of Pt/Al_2O_3 catalysts.

Apparently, the relatively non-conducting support inhibits heat transfer between various locations on the catalyst bed. The reason underlying the formation of hot spots is not entirely clear. Reactor design appears to be an important variable and the occurrence of local gas phase concentration fluctuations has been offered as a possible reason for the fluctuating hot spots. Whether the oscillations are thermally or kinetically driven is a matter which is still open to debate. In order for self-sustained oscillations to occur, there must be an autocatalytic and an inhibition step. It would seem to us that these requirements should be intimately linked to changes which occur in the surface mechanism. If this were not the case, all exothermic catalytic reactions would oscillate given the right set of conditions. This is most certainly not the case.

The formation of CO islands and centers of reactivity has also been suggested as a possible mechanism which can lead to self-sustained oscillations [5,6]. This possibility is nicely illustrated in a recent *in situ* FTIR study by BÖCKER and WICKE on Pd/TiO_2 [6,32]. The catalytic reaction cycle which incorporates both an autocatalytic and an inhibition step is shown in figure 8. Initially, figure 8a, the surface is covered by oxygen in a (2x2) adsorbate layer configuration. Small isolated patches of CO give rise to a single wide CO infrared band centered at 1900 cm^{-1}. This vibration is due to CO adsorbed in a bridging configuration with each CO coordinated to about three surface Pd atoms. This assignment is due to the recent EELS work of BRADSHAW and HOFFMAN [33,34]. As the CO islands grow in size, the reaction rate increases to a maximum as shown in figure 8b. Because the reaction occurs at the perimeter of these CO islands, the reaction rate decreases as the CO islands increase in size. By forming these CO islands an increasing number of surface sites are lost to the reaction due to the inability of oxygen to adsorbe inside an organized CO surface structure. Concomitant with this increase in CO island size a second sharp absorption band centered at 1980 cm^{-1} is observed in the infrared spectrum of CO. This band has been assigned by

BRADSHAW and HOFFMAN [34] to CO coordinated to two Pd surface atoms. This surface species can be related to the adsorbate phase changes occurring during the CO island formation. A further increase in CO island size leads to a compression of surface oxygen into a more dense ($\sqrt{3}x\sqrt{3}$) adlayer structure. Because this surface oxygen which has undergone a phase transition of sorts has been shown to be considerably more reactive than oxygen adsorbed in a (2x2) adlayer configuration [1], the reaction rate again increases thus completing the reaction cycle. It appears, therefore, that surface phase transformations could lead to self-sustained oscillations.

Recent CO oxidation results in our laboratory [10] on highly dispersed Ir/SiO_2 (66%)have also shown the occurrence of self-sustained oscillations. Because small metal particles are unlikely to support large CO islands of reactivity it appears that different mechanisms may be responsible for the self-sustained oscillatory behavior during CO oxidation Additionally, recent studies on the CO adsorption of CO and NO [35] show that the resulting adlayers are intimately mixed. Because this reaction also oscillates [36], it is unlikely that the concept of CO islands of reactivity can be applied to this reaction.

Recent *in situ* infrared studies on Pt/Al_2O_3 [37] and Ru/SiO_2 [16] have also shown oscillatory behavior during CO oxidation. In these studies the formation and disappearance of reducible surface oxides were cited as possible causes for oscillatory behavior. A weakness in the concept of reducible surface oxides is that there is no built in autocatalytic and inhibitory step in the mechanism.

From the above discussion several possibilities for oscillatory behavior have been suggested. However, it is also clear that a mechanism capable of explaining all of these observations has not yet emerged. Any realistic mechanism which attempts to explain oscillatory behavior should at a minimum have built into it an accelerating autocatalytic step in addition to an inhibitory step.

Reaction on single crystals under UHV conditions

Reaction rate instabilities and self-sustained oscillations have also been observed by several workers on single crystals under UHV conditions [1,38,39]. The oscillatory behavior of the CO oxidation reaction has recently been related to phase tranformations of both the metal and the adsorbate phase [40]. (100) crystalographic planes of Au, Pt, Ir, V, Cr, Mo and W have been shown to reconstruct under the influence of both CO and oxygen adsorption [ref. in 41]. The (110) planes of Pt and Ir do not reconstruct and do not exhibit oscillatory behavior during CO oxidation.

At low CO surface coverages the Pt(100) surface exhibit a reconstructed hexagonal (5x20) surface [40]. When the CO surface coverage is increased to about half of a monolayer, a surface phase transition to an unreconstructed (1x1) surface occurs. Using a novel scanning LEED technique, ERTL has followed CO oscillatory behavior while monitoring both the metal reconstruction and the phase transformation of the CO and oxygen adlayer. The reconstructed (5x20) structure can be correlated with a high CO oxidation activity, while the unreconstructed (1x1) structure has a low CO oxidation activity. During the low point in the reaction rate, the CO adsorbate layer consists of patches of CO adsorbed in a (2x2) surface adlayer.

Changes in the sticking coefficient of oxygen following phase transition to the unreconstructed (5x20) structure may also play an important part in the acceleration of the reaction rate. Sticking coefficients for the dissociative adsorption of oxygen have

been shown to be orders of magnitude larger on the unreconstructed (5x20) structure than on the reconstructed (1x1) structure [42]. ERTL et al. [40] have shown that the onset of oscillations obtained experimentally as a function of temperature agree well with the predicted reconstruction of the metal surface.

Several attempts have been made to extend the UHV results to high pressure oscillatory behavior on supported metal catalysts. However, the point should be made that these attempts are invalid because under high CO and oxygen partial pressures, the metal surface must always be present as an unreconstructed (1x1) structure.

CONCLUDING REMARKS

The results of numerous studies allow us to conclude the following regarding the catalytic oxidation of CO over supported noble metal catalysts: (1) The catalytic oxidation of CO over noble metal catalysts appears to be a facile reaction. However, support effects, particularly SnO_2, cannot be completely overlooked. (2) Reaction rates over single crystals agree favorably with results over supported metal catalysts. (3) The occurrence of self-sustained oscillations has been observed by a large number of workers. However a single mechanism which accounts for all of the experimental observations has yet to emerge. Causes of self-sustained oscillations may include: (1) the formation of CO islands combined with a compression of the remaining oxygen adlayer structure, (2) hot spots caused by fluctuations in gas phase concentrations, (3) the formation and disappearance of reducible surface oxides, (4) heat and mass transfer effects and (5) surface phase transformations. CO oxidation studies under UHV conditions unequivocally relate phase transformations to oscillatory behavior.

In summary, much has been accomplished. However, inconsistencies reported between different laboratories abound in the literature. Further experimentation in the area of CO oxidation is encouraged in the hope that a consistent picture will emerge regarding the mechanism for this very important reaction. In particular, surface instabilities and self-sustained oscillations should be studied by different investigators under comparable conditions. Reactor geometry, mass and heat transfer effects, fluctuations in gas phase reactant concentrations are important variables which could be minimized by well planned experiments.

REFERENCES

[1] Ertl, G.; Engel, T.; *The chemical physics of solid surfaces and heterogeneous catalysis* 4, 73; King, D. A.; Woodruff, J. P.; Elsevier Sci. Publ. Comp.; Amsterdam, New York, 1982.

[2] Ertl, G.; Engel, T.; Advances in Catalysis, 28, Academic Press, New York, London, Toronto, Sydney, San Franzisco, 1979.

[3] Razon, L. F.; Schmitz, R. A.: *Intrinsically unstable behavior during the oxidation of carbon monoxide on Platinum* Cat. Rev-Sci. Eng., 28 (1), pp. 89-164, 1986.

[4] Herz, R. K.; Marin, S. P.: *Surface chemistry models of carbon monoxide oxidation on supported Platinum catalysts* J. Cat., 65, pp. 281-296, 1980.

[5] Haaland, D. M.; Williams, F. L.: *Simultanous measurement of CO oxidation rate and surface coverage on* Pt/Al_2O_3 *using infrared spectroscopy rate hysteresis and CO island formation* J. Cat., 76, pp. 450-465, 1982.

[6] Böcker, D.; Wicke, E.: *In-Situ IR study during oscillations of the catalytic CO oxidation* Ber. Bunseng. Phys. Chem.; 89, pp. 629-633, 1985.

[7] Hegedus, L. L.; Oh, S. H.; Baron, K.: *Multiple steady states in an isothermal, integral reactor: The catalytic oxidation of carbon monoxide over Platinum-Alumina* A.I.Ch.E., J., 23 (5), pp 632-642, 1977.

[8] Cant, N. W.; Hicks, P.C.; Lennon, B. S.: *Steady state oxidation of carbon monoxide over supported noble metals with particular reference to Platinum* J. Cat., 54, pp. 372-383, 1978.

[9] Oh, S. H.; Carpenter, J. E.: *The oxidation state and catalytic activity of supported Rhodium* J. Cat., 80, pp. 472-478, 1983.

[10] Savmeh, R. A.; Gonzalez, R. D.: *Oxidation of carbon monoxide over* Ir/SiO_2. *An in-situ infrared and kinetic study* J. Phys. Chem., 90, pp. 622-627, 1986.

[11] Sarkany, J.; Bartok, M.; Gonzalez, R. D.: *The modification of CO adlayers on* Pt/SiO_2 *catalysts by preadsorbed oxygen. An infrared and pulse measurement study* J. Cat., 81, pp. 347-357, 1983.

[12] Wicke, E.; Keil, W.: *Uber die kinetischen Instabilitaten bei der CO Oxidation an Platin Katalysatoren* Ber. Bunseng. Phys. Chem., 84, pp. 377-383, 1980.

[13] Wicke, E.; Kummann, P.; Keil, W.; Schiefler, J.: *Instable and oscillatory behaviour in heterogenous catalysis* Ber. Bunseng. Phys. Che., 84, pp. 315-323, 1980.

[14] Kiss, J. T.; Gonzalez, R. D.: *Oxidation of carbon monoxide over* Rh/SiO_2. *An in-situ and kinetic study* J. Phys. Chem., 88, pp. 898-904, 1984.

[15] Kiss, J. T.; Gonzalez, R. D.: *A catalytic oxidation of CO over Rh/SiO_2, Ru/SiO_2, Pd/SiO_2. An in-situ infrared and kinetic study* Proceedings of the 8th Intern. Congress on Catalysis, Berlin-(West), July 2-4th, 1984; II, pp 635-644; Verlag Chemie; Weinheim, Deerfield Beach, Florida, Basel.

[16] Kiss, J.; Gonzalez, R. D.: *The catalytic oxidation of CO over Ru/SiO_2. An in-situ infrared and kinetic study* J. Phys. Chem., 88 (5), pp. 892-898, 1984.

[17] McLaughlin McLory, M. L.; Gonzalez, R. D.: *The catalytic oxidation over well characterized supported Ru-Rh bimetallic clusters* J. Phys. Chem., 90, pp. 628-633, 1986.

[18] Cant, N. W.; Donaldson, R. A.: *Infrared spectral studies of reactions of CO and oxygen on Pt/SiO_2* J. Cat., 71, pp. 320-330, 1981.

[19] Sarkany, J.; Gonzalez, R. D.: *Support and dispersion effects on silica and alumina supported Pt catalysts. II. Effects on the CO-oxygen reaction* J. Appl. Cat., 5, pp. 85-97, 1983.

[20] Goodman, W.; Peden J.: *CO oxidation over Rh and Ru: A comparative study* J. Phys. Chem., in press.

[21] Boudart, M.: *Structure insensitive reactions on metallic catalysts* I, pp. 13 ff., 1984; 9th Iberoamerican Symposium on Catalysis; Lisbon, Portugal.

[22] Batten, C. E.: *Studies of CO oxidation on Pt/SnO_2 catalyst in a surrogate CO_2 Laser Facility* NASA CP-**2456,1987.**

[23] Schryer, D. R.: **NASA-*LaRC* research on catalysts for long-life closed-cycle CO_2** *lasers*, NASA CP-**2456, 1987.**

[24] Oh, S. H.; Fisher, G. B.; Carpenter, J E.; Goodman, D. W.: *Comparative kinetic studies of CO-O_2 and CO-NO reactions over single crystal and supported Rhodium catalysts* J. Cat., 100, in press, 1986.

[25] Matera, V. D. Jr.; Barms, D. M.; Chaudhuri, S. N.; Risen, W. M. Jr.; Gonzalez, R. D.: *A kinetic study of the catalytic oxidation of CO over PFSA (NAFION) supported Rh, Ru and Pt* J. Phys. Chem., vol. 90, # 20, Sept. 1986, pp. 4819-4824.

[26] Ertl, G.; Campell, C. T.; Kneipers, H.; Segner, J.: *A molecular beam study of the catalytic oxidation of CO on a Pt (111) surface* J. Chem. Phys., 73 (11), pp. 5862-5873, 1980.

[27] Mantell, D. A.; Ryali, S. B.; Haller, G. L.; Fenn, J. B.: *Distribution of internal energy in carbon monoxide vibrationally excited by a hot Platinum surface* J. Chem. Phys., 78, pp. 4250-4255, 1983.

[28] Mantell, D. A.; Kunimori, K.; Ryali, S. B.; Haller, G. L.: *Carbon monoxide oxidation on Platinum: Coverage dependence of the product internal energy* Prepr.-Am. Chem. Soc., Div. Pet. Chem., 29, pp. 904-907, 1984.

[29] Nagai, M.; Lucietto, L. L.; Li, Yao-En; Gonzales, R. D.: *An improved cell reactor for use in transient response studies. The catalytic oxidation of CO reexamined* J. Cat., in press, 1986.

[30] Kaul, D. J.; Wolf, E. E.: *FTIR studies of surface reaction dynamics* J. Cat., 89, pp. 348-361, 1984.

[31] Schmitz, L. D.; Aris, R.; Takoudis, C. G.: *Isothermal oscillations in a very simple surface reaction* Surf. Sci., **105**, pp. 325-333, 1981.

[32] Böcker, D.; Wicke, E.: *In-Situ FTIR Study during oscillations of the catalytic CO Oxidation* in TEMPORAL ORDER: Proceedings of a symposium on oscillations in heterogenous and biological systems; University of Bremen, West-Germany, Sep. 17-22th, 1984; ISBN: 3-540-15274-1; Springer–Verlag, Berlin, Heidelberg, New York, Tokyo.

[33] Bradshaw, A. M.; Hoffman, F. M.: *The chemisorption of CO on single crystal surfaces: IR spectroscopic evidence for localized site adsorption* Surf. Sci., 72, pp. 513-535, 1978.

[34] Bradshaw, A. M.; Ortega, A.; Hoffman, F. M.: *The adsorption of CO on Pd (100) studied by IR reflection absorption spectroscopy* Surf. Sci., 119, pp. 79-94, 1982.

[35] Sarkany, J. R.; Bartok, M.; Gonzalez, R. D.: *The co-adsorption of CO and NO on Pt/SiO_2: An infrared study* J. Phys. Chem., 1987.

[36] Adlhoch, W.; Lintz, H. G.; Weisker, T.: *Oszillationen der Reaktionsgeschwindigkeit bei der Reaktion von NO mit CO an Pt im Knudsen Gebiet* Surf. Sci., 103, pp. 576-585, 1981.

[37] Tsotsis, T. T.; Elhaderi, A.: *Reaction rate oscillations during the CO oxidation reaction over Pt/Al_2O_3 catalysts: An IR transmission spectroscopy study* Chem. React. Engng., 7, pp. 77 ff., 1982.

[38] Ertl, G.; Norton, P. R.; Ruestig, J.: *Kinetic oscillations in the Platinum catalyzed oxidation of CO* Phys. Rev. Let., 49, pp. 177-180, 1982.

[39] Haul, R.; Barkowski, D.; Kretschmer, U.: *Studies on oscillations in the Pt catalyzed CO oxidation by means of omegatron mass probe* Surf. Sci., 107, pp. L329-L333, 1981.

[40] Ertl, G.; Cox, M. P.; Imbihl, R.: *Spatial self organization of surface structure during an oscillating catalytic reaction* Phys. Rev. Let., 54 (15), pp. 1725-1728, 1985.

[41] Böcker, D.: *Zur oszillierenden CO Oxidation an Platin und Palladium Katalysatoren: Eine IR-Untersuchung in-situ* Dissertation, Münster, West-Germany, 1985.

[42] Ertl, G.; Thiel, P.A.; Behm, R.J.; Norton, P. R.: *Mechanism of an adsorbate induced surface phase transformation: CO on Pt (100)* Surf. Sci. Let., **121**, pp. L553-L560, 1982.

TABLE 1

CO Oxidation Reaction Rates on
Supported Noble Metal Catalysts at 373 K

Catalyst	CO/O_2	TOF molec/site sec X 10^3	EA KJ/mole
Rh/SiO_2	0.5	15.3	96
Ru/SiO_2	0.5	9.9	90
Pd/SiO_2	0.5	0.98	92
Ir/SiO_2	0.5	0.60	40
Ru/SiO_2	2.0	17.0	100
Ir/SiO_2	2.0	3.0	46
Pt/SiO_2	2.0	1.53	54
Rh/SiO_2	2.0	0.674	110
Pd/SiO_2	2.0	0.474	90
Ru/SiO_2	4.0	13.2	96
Ir/SiO_2	4.0	1.5	40
Pt/SiO_2	4.0	1.0	56
Rh/SiO_2	4.0	0.5	93
Pd/SiO_2	4.0	0.29	102

Oxidizing Conditions	Rh > Ru > Pd > Ir
Reducing Conditions	Ru > Ir > Pt > Rh > Pd
Stoichiometric Conditions	Ru > Ir > Pt > Rh > Pd

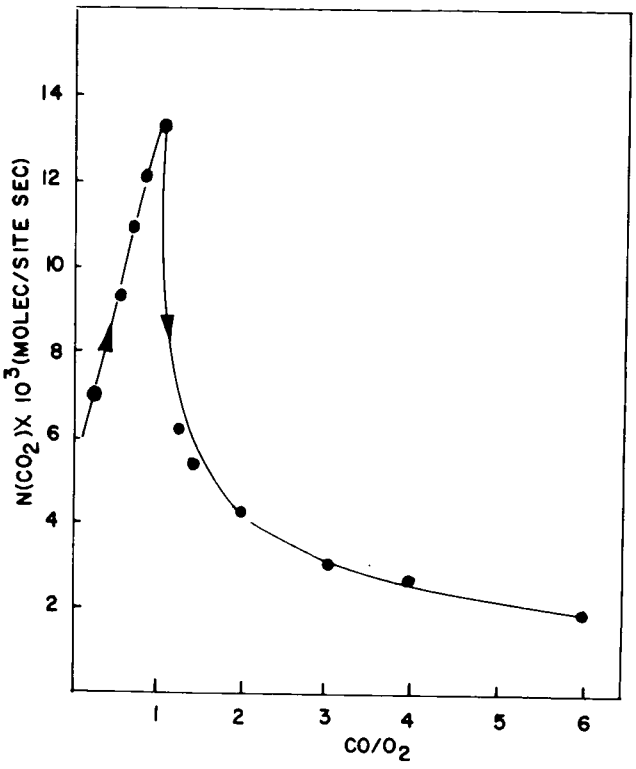

Fig. 1: *Turnover frequency for CO_2 formation as a function of the CO/O_2 partial pressure ratio at 393 K;* [10]. Copyright 1986 ACS.*

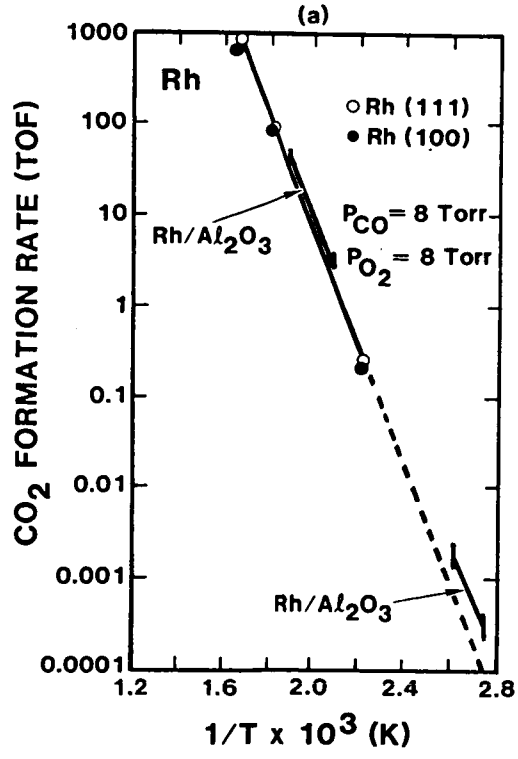

Fig. 2: *Arrhenius Plot CO oxidation on Rh(111), Rh(100) and Rh/Al_2O_3;* reproduced with permission from W. Goodman and J. Peden [20]. Copyright 1986 ACS.*

*Reprinted with permission.

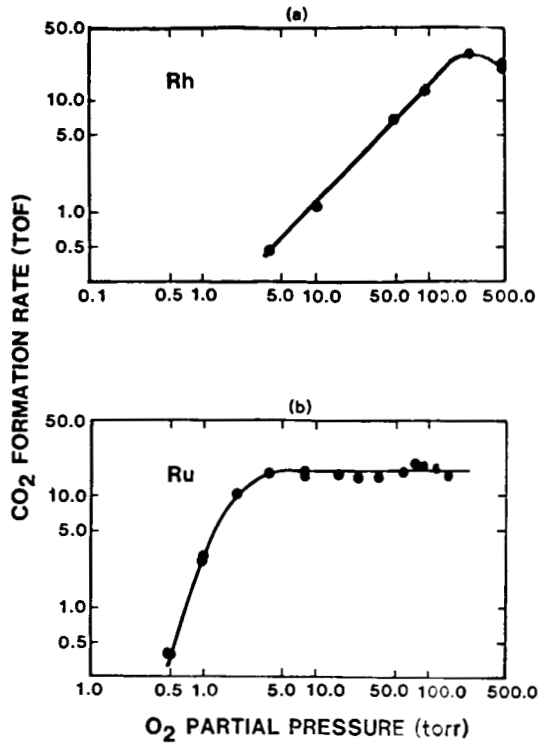

Fig. 3: *The rate of CO_2 formation as a function of oxygen partial pressure;* reproduced with permission from W. Goodman and J. Peden [20]. Copyright 1986 ACS.*

*Reprinted with permission.

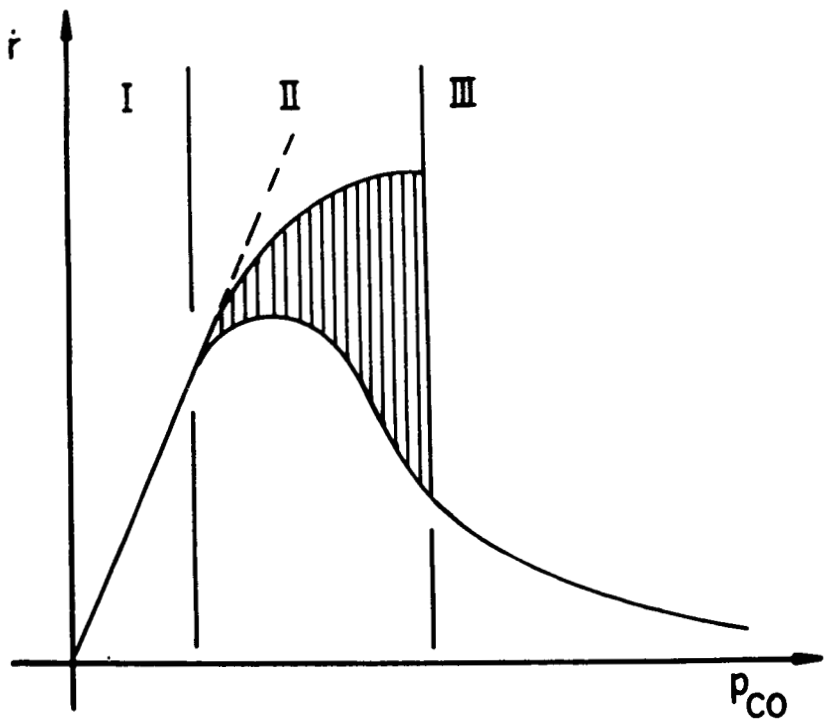

Fig. 4: *Kinetic regimes which occur during the oxidation of CO;* reproduced with permission from E. Wicke et al. [13] Copyright 1980 VCH.*

*Reprinted with permission.

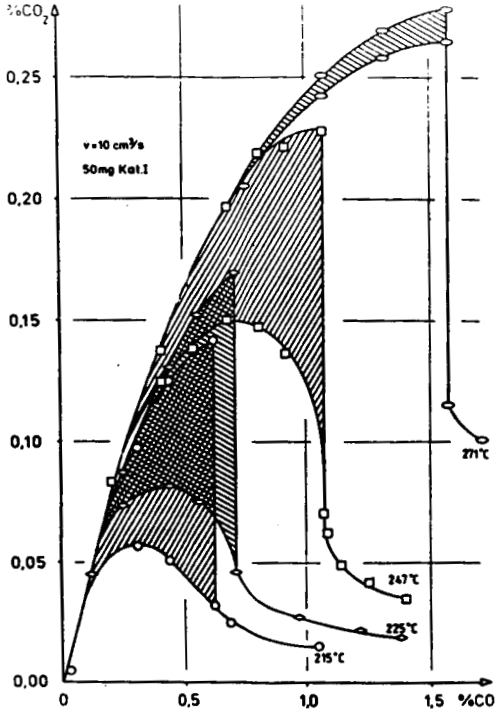

Fig. 5: *Regimes of oscillating behavior during the CO oxidation over Pt/SiO_2* [41].

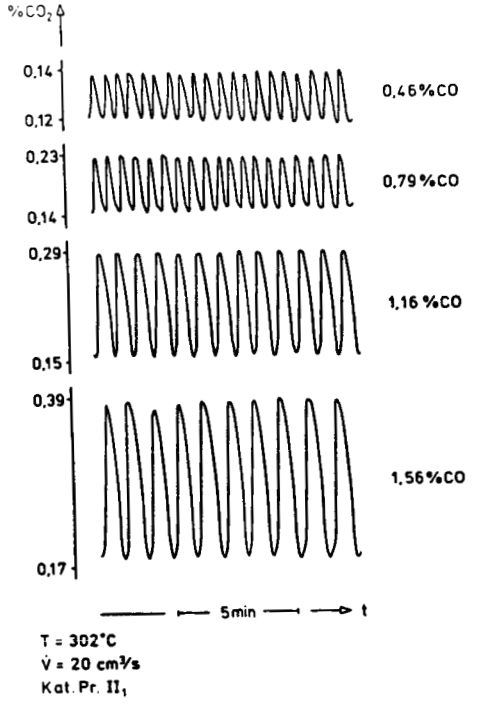

Fig. 6: *Reaction rate oscillations during the CO oxidation over Pt/SiO_2* [41].

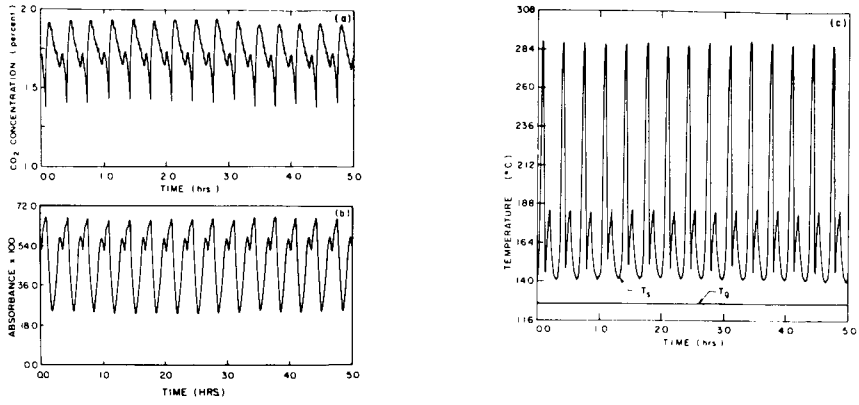

Fig. 7: *Self-sustained oscillations obtained by stopping the oxygen programming at 8 cm3/min; (a) CO_2 production, (b) spectragram of adsorbed CO, (c) surface temperature;* reproduced with permission from D. J. Kaul and E. E. Wolf in J.Cat. 91 216-230 (1985).Copyright 1985 ACS.*

*Reprinted with permission.

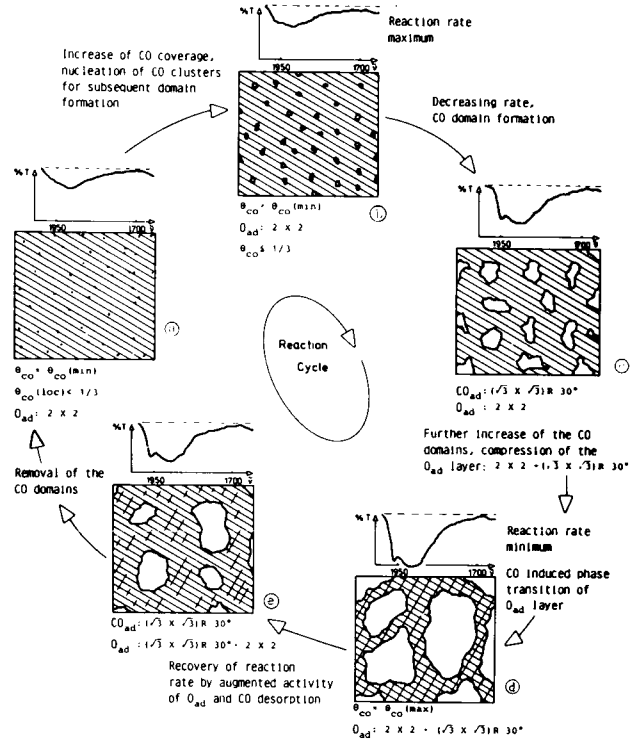

Fig. 8: *Reaction cycle of an oscillation period derived from the IR spectra and supposed structures of chemisorbed layers* [32]. Copyright 1984 Springer-Verlag.

N87-20531

Chemical Engineering Design of CO Oxidation Catalysts

Richard K. Herz
Dept. AMES/Chemical Engineering
University of California at San Diego
La Jolla, CA

INTRODUCTION

The purpose of this paper is to present the way that a chemical reaction engineer would approach the challenge of designing a CO oxidation catalyst for pulsed CO_2 lasers. CO oxidation catalysts have a long history of application, of course, so it is instructive to first consider the special requirements of the laser application and then to compare them to the characteristics of existing processes that utilize CO oxidation catalysts.

All CO_2 laser applications require a CO oxidation catalyst with the following characteristics: (a) active at stoichiometric ratios of O_2 and CO, (b) no inhibition by CO_2 or other components of the laser environment, (c) releases no particulates during vibration or thermal cycling, (d) long lifetime with a stable activity. In all applications, low consumption of power is desirable, a characteristic that is especially critical in aerospace applications and, thus, catalyst activity at low temperatures is highly desirable. High power lasers with high pulse repetition rates inherently require circulation of the gas mixture and this forced circulation is available for moving gas past the catalyst. Low repetition rate lasers, however, do not inherently require gas circulation, so a catalyst that did not require such circulation would be favorable from the standpoint of minimum power consumption. Lasers designed for atmospheric penetration of their infrared radiation utilize CO_2 formed from rare isotopes of oxygen and this application has the additional constraint that normal abundance oxygen isotopes in the catalyst must not exchange with rare isotopes in the gas mixture.

These are the target characteristics. To judge the possibility of using existing CO oxidation catalysts for this application, it is instructive to compare the CO_2 laser application to current applications of CO oxidation catalysts.

One of the major applications of CO oxidation catalysts is removing CO from the exhaust of combustion systems. In this emission control application, the thermal energy needed to raise the catalyst to operating temperatures is naturally present and excess oxygen, which tends to accelerate CO oxidation, is either already present or can easily be added by injecting air. Both of these characteristics are not present in the laser application.

Another major use of CO oxidation catalysts is removing low levels of CO that contaminate breathing air. The CO would be present primarily as the partial oxidation product of a combustion process. Situations where contamination of breathing air may occur are in underground mines, inside burning buildings, and aboard submarines. This application differs from the laser application in that it has the advantage that there is always a great excess of oxygen available. However, it also has a disadvantage in common with the laser application in that CO oxidation has to occur at relatively low temperatures (with the exception of the submarine application where power is available for heating).

Thus, the primary challenges of the application of CO oxidation catalysts in CO_2 lasers are the need to maximize catalyst activity (a) at low temperatures, (b) in the presence of low relative oxygen concentrations (at or near stoichiometric ratios), and (c) with minimal need for forced convection of gas past the catalyst, in some applications.

On the other hand, there are some nice things about the laser application in comparison with the other applications of CO oxidation catalysts: CO concentrations are initially very low in the laser, sintering and loss of active surface area during operation at high temperatures will not occur, and the gas atmosphere is very clean - for example, in comparison to automotive exhaust gas.

The outline of the next sections of this paper will follow the order that is typically used in the design of any catalytic reactor. First, the mechanism and kinetics of the CO oxidation reaction will be discussed, with indentification of the directions that catalyst development should pursue and recommendations for characterization of catalyst activity. Next, the method of design of a catalytic reactor will be outlined using two different examples relevant to CO_2 lasers but using very simple kinetics for illustration.

MECHANISM OF CO OXIDATION

CO oxidation - or CO-O_2 recombination - can occur solely in the gas phase through homogeneous mechanisms, or the reaction can occur on the surface of a solid catalyst through a heterogeneous mechanism. Solid catalysts that catalyze reactions of fluids are called heterogeneous catalysts. Although a heterogeneous catalyst will be required for the laser application, it is instructive to first consider homogeneous mechanisms of CO oxidation.

In almost all systems where the homogeneous reaction of CO with O_2 occurs, hydrogen is also present as H_2 and/or H_2O. This presence of hydrogen has a dramatic effect on the mechanism of CO oxidation in the gas phase. The major steps in this chain reaction mechanism are shown below (ref. 1):

"Wet" Homogeneous Mechanism

Initiation		$\rightarrow$	OH, H
Branching	$H + O_2$	$\rightarrow$	$OH + O$
	$O + H_2$	$\rightarrow$	$OH + H$
Propagation	$OH + CO$	$\rightarrow$	$CO_2 + H$

The most difficult step that occurs in any type of CO-O_2 reaction is the dissociation of O_2. In the presence of hydrogen, this dissociation in the gas phase occurs by the reaction of O_2 with H atoms. Also, CO_2 is formed not through the reaction of CO with O_2 or O atoms but through the reaction of CO with OH radicals. Homogeneous recombination of CO and O_2 was accelerated by addition of H_2 in the first sealed CO_2 TEA laser (ref. 2).

As one would expect, the mechanism is dramatically different in the absence of hydrogen and is much slower:

"Dry" Homogeneous Mechanism

Initiation	$CO + O_2$	$\rightarrow$	$CO_2 + O$
Branching	$CO_2^* + O_2$	$\rightarrow$	$CO_2 + 2O$
Propagation	$O + CO$	$\rightarrow$	CO_2^*

where CO_2^* represents an excited CO_2 molecule and the branching step is subject to uncertainty. In fact, some researchers maintain that trace quantities of hydrogen may have been present in most or all published kinetic studies of the "dry" reaction and, thus, that the "dry" reaction may have not been accurately studied to date (ref. 1).

In the reaction of CO and O_2 over the surface of a heterogeneous catalyst, the interaction of O_2 with the catalyst surface serves to provide the critical step of O_2 dissociation. The mechanism can occur easily in the absence of hydrogen on a catalyst surface. There are two major classes of heterogeneous CO oxidation catalysts: (a) "noble metal" or "precious metal" catalysts, and (b) base metal oxide catalysts, or simply "base metal" or "oxide" catalysts. Here, the mechanism for the reaction over a precious metal catalyst such as platinum is shown (ref. 3):

Heterogeneous Mechanism over Precious Metal

$$O_2 + 2S \rightarrow 2O\text{-}S$$
$$CO + S \leftrightarrow CO\text{-}S$$
$$CO\text{-}S + O\text{-}S \rightarrow CO_2 + 2S$$

where "S" is a "site" or area on the metal surface that can adsorb one CO molecule or one O atom. The adsorption of oxygen is essentially irreversible at temperatures below 500 °C and the formation and desorption of CO_2 is essentially irreversible at all conditions of interest. The fact that CO adsorption requires a smaller area on the metal surface (one S) than does O_2 adsorption (2S) is responsible for the strong inhibition of CO oxidation by CO at high CO concentrations or low temperatures. The readily reversible nature of CO adsorption is responsible for the changes in reaction kinetics that occur with changes in temperature, as discussed below.

The contrast between the homogeneous and heterogeneous mechanisms is further emphasized by the following qualitative comparison of the energetics of the two reactions:

Homogeneous Mechanism

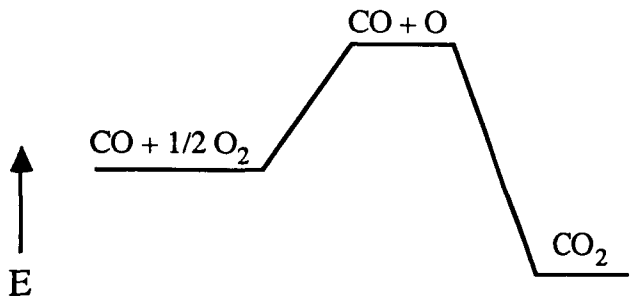

Heterogeneous Mechanism over Precious Metal

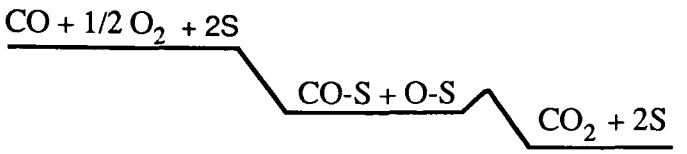

As shown above, the mechanism over a precious metal catalyst occurs with O_2 chemisorbing dissociatively as O atoms bonded on top of the metal atoms that form the surface of the metal. CO molecules adsorb over the same metal surface atoms. Thus, CO and O_2 compete for the same surface atoms when they adsorb. This competitive adsorption is responsible for producing the characteristic kinetics (variation in rate with changes in temperature and gas composition) of CO oxidation over precious metals.

The enthalpy or "strength" of adsorption of oxygen atoms is somewhat greater than the strength of adsorption of CO molecules. An O_2 molecule, however, requires a large open area on the metal surface in order for it to be able to adsorb than does a CO molecule. As a result of this difference in adsorption area requirements, CO can be said to adsorb "more readily" than O_2. This characteristic of CO and O_2 adsorption on precious metals means that at ambient temperatures in a stoichiometric mixture of CO and O_2, the surface of the metal catalyst will be almost completely covered by adsorbed CO molecules. The rate of reaction will be negligible at this condition of relatively low temperature because O_2 molecules can not adsorb on the CO-covered surface and, thus, cannot react. The large CO concentration on the surface is in equilibrium with the CO in the gas. As the temperature of the catalyst is raised, the coverage of the surface by CO will start to decrease since CO adsorption is exothermic. This decrease in surface coverage by CO opens up space on the metal for O_2 to dissociatively adsorb. The rate of reaction between adsorbed CO molecules and oxygen atoms is relatively fast, even at ambient temperature, so that once the CO coverage drops such that O_2 can adsorb, the rate of reaction will become significant. At a constant and relatively low temperature, the rate of reaction decreases with increasing CO concentration and increases with increasing O_2 concentration. The reaction is said to be strongly inhibited by CO at relatively low temperatures. At higher relative temperatures, the surface is primarily covered by adsorbed O atoms and the reaction rate increases with an increase in CO concentration and becomes independent of O_2 concentration (refs. **4,5**).

The mechanism of CO oxidation over base metal oxide catalysts is qualitatively different from that over precious metals. The mechanism is complex over oxide catalysts, so only general features will be discussed here. Over metal oxides, the reaction proceeds (at least at higher temperatures) through a "redox" mechanism. CO adsorbs on the surface and reacts with oxygen atoms bound in the surface layer of the metal oxide, locally reducing the metal oxide. O_2 in the gas phase reacts with and re-oxidizes the metal oxide (ref. 6):

Heterogeneous Mechanism over Base Metal Oxide

$$O_2 + 2\square \rightarrow 2\boxed{O}$$

$$CO + * \rightarrow CO\text{-}*$$

$$CO\text{-}* + \boxed{O} \rightarrow CO_2 + \square + *$$

where * is an adsorption site for CO and $\square$ is an oxygen vacancy in the oxide surface.

The "slow" step in the reaction is the reduction of the oxide by CO. At constant temperatures, the rate of reaction increases with increasing CO concentration and does not change with O_2 concentration. These kinetics are dramatically different than those which apply to precious metal catalysts.

The dominant factor in CO oxidation over precious metals is the kinetic competition between CO and O_2 for adsorption sites on the metal surface. CO and O_2 interact with different locations or sites on oxide catalysts with no competition. The dominant factor in oxide catalysts is the relatively strong bonding that holds oxygen atoms in the oxide and that limits the rate of CO oxidation.

One can say that, in order for reaction to occur at low temperatures, oxygen doesn't adsorb readily enough over precious metal catalysts and adsorbs readily but too strongly over oxide catalysts.

There are two major functions that must be performed by any CO oxidation catalyst:

- adsorb O_2 dissociatively,
- adsorb CO next to reactive oxygen atoms.

These critical functions of a CO oxidation catalyst can be used as a framework for catalyst analysis and design of improved catalysts. An optimal catalyst will perform both of these two functions to the correct extent. That is, it will chemisorb O_2 readily but not hold the oxygen atoms too strongly, and it will adsorb CO in a manner that CO doesn't compete directly with O_2 adsorption.

This framework leads to several ideas for design of an improved catalyst. Starting with a precious metal catalyst, one might try to lower the strength of CO adsorption. While not eliminating the competition between CO and O_2, this approach would decrease the extent to which CO inhibits the reaction at a given temperature. Pt and Pd are the precious metals most frequently used in CO oxidation catalysts. They are used because of their resistance to sintering at high temperatures and because of their relative abundance relative to other precious metal catalysts. The relatively low temperature, low volume laser application allows consideration of other metal elements which might have more favorable CO adsorption characteristics. Several additives to metal surfaces have been shown to lower the desorption temperature of CO (ref. 7). CO adsorption over Rh and Pt has been shown to be suppressed when the metal is supported over TiO_2 and the support and metal subjected to a high temperature reduction treatment in H_2 (ref. 8). Recent research has shown that partial oxides of Ti, or TiO_2, migrate from the support to the surface of the metal particles and suppress the adsorption of CO (refs. 9,10). Another possible metal-support interaction that might affect CO adsorption is charge transfer between the support and the metal (refs. 11-13).

Starting with a metal oxide, one would like to lower the strength of the bonds that hold oxygen atoms in the surface of the oxide. One possibility is that there are metal oxides that are suitable for the laser application that are not used for other CO oxidation applications because of the different operating conditions. Another possibility is that additives might be found that lower the metal-oxygen bond strength in metal oxides.

So far we have considered modifications to pure precious metal or metal oxide catalysts. The fact that there are two distinct functions that a CO oxidation catalyst must perform suggests that a "compound" catalyst should give improved performance. That is, improved performance should be obtained by an intimate mixture, at the atomic level, of two different materials with optimal properties for the two different catalytic functions required.

Oh and Carpenter (ref. 14) have found that Pt/Rh alloy particles supported on alumina catalyze the CO oxidation reaction at lower temperatures than either of the separate metals. Rh interacts with O_2 more strongly than Pt does (refs. 15,16). Thus, it is likely, as suggested by Oh and Carpenter, that the mixed-metal catalyst separates the two functions to some extent, with CO adsorbing primarily on Pt atoms and O_2 adsorbing primarily on Rh atoms, thus, reducing the inhibition of O_2 adsorption by CO.

Currently, the most promising catalyst for the CO_2 laser application is a precious metal supported on SnO_2 (ref. 17). It is likely that this catalyst is an example of the type of "complex" catalyst that we seek. The primary function of the precious metal may be to adsorb CO. The primary function of the SnO_2 may be to adsorb O_2. Alternatively or in addition, SnO_2 may reduce the strength of CO adsorption over the precious metal, and the metal may reduce the strength of O_2 interaction with the oxide. Research needs to be performed to identify the actions of the two components of metal/SnO_2 catalysts. Research is also needed to determine the types of contact between the metal and the oxide, e.g., whether oxide species are present on the surfaces of the metal particles, as seems to be the case for the Pt/TiO_2 system.

KINETIC MEASUREMENTS

Once a specific catalyst has been selected for used in a CO_2 laser, the next step is to determine the kinetics of the reaction over the catalyst. By this we mean that experimental measurements are performed over the relevant ranges of gas composition and temperature in order to develop a "rate

expression." A rate expression (or "equation" or "law") is a mathematical expression that gives the rate of reaction as a function of gas composition and temperature. When performing kinetic studies with heterogeneous catalysts, one must be aware of the fact that heat and mass transfer effects are often present and can interfere with kinetic measurements. Ideally, one would like to determine the reaction rate under conditions where the temperature and composition of the bulk gas is the same as the temperature and composition of the gas immediately near the external surface of the catalyst and within the internal pores of porous catalysts. In some cases, internal transport effects are effectively impossible to eliminate and only "apparent" or "global" kinetics can be measured. However, in that case, it is critical that one is aware of the presence of the heat and mass transport limitations. Kinetic measurements on heterogeneous catalysts are discussed in standard texts (refs. 18,19).

One temptation that understandably occurs during the development of many processes is to make measurements only on working prototypes of the actual system. In this case, measurements would be made only on catalysts installed in working lasers or the bodies of lasers in which synthetic mixtures are injected. The trouble with this approach is that such measurements do not allow for prediction of the magnitude of improvements required or design of other sizes or configurations of the system. We feel that it is imperative that careful kinetic studies be performed in reactors designed for kinetic studies in addition to tests of prototypes.

There are several types of reactors that are used for kinetic studies of heterogeneous catalysts:

- batch reactors
- plug flow reactors
- recycle reactors operating at high recycle ratios.

Each of these types is described in standard texts (refs. 18,19). We suggest that a recycle reactor be considered for kinetic studies of CO oxidation catalysts for CO_2 lasers. External temperature and concentration gradients are most easily minimized in recycle reactors and the reaction rate under given conditions of steady-state operation is determined simply by an algebraic equation.

When the performance of different formulations of catalyst is to be compared, it is critical to consider the basis of comparison. For example, for supported precious metal catalysts, the reaction rate per exposed metal atom is the proper measure of performance under given conditions. Different batches of the same composition of catalyst may give different conversions of CO because the metal in each batch is dispersed over the support to a different extent. Alternatively, the metal dispersion may be the same and a chemical difference may account for the difference in conversion. In this case, one must make measurements of the metal particle size and/or metal chemisorption capacity in addition to performing reaction rate measurements.

DESIGN OF THE LASER/CATALYTIC REACTOR

Once the kinetics of a catalyst have been determined, design of the laser in its function as a catalytic reactor can proceed. Here we illustrate reactor design for two simple cases. First, consider the design of a reactor in which the gas is circulated by a blower past the laser electrodes and past the catalyst in a closed loop. We assume the following:

- isothermal conditions,
- a flat gas velocity profile through the catalyst,
- the rate of CO oxidation is proportional to the weight of catalyst (i.e., no diffusional limitations) and the CO concentration but is independent of the O_2 concentration.

All of these assumptions most probably will not hold in a real laser. For example, the gas may be in laminar flow past heated catalyst surfaces on which the reaction kinetics are more complicated than the first-order kinetics assumed.

Our objective in this example will be to obtain an expression for the volume of catalyst, V_{cat}, required as a function of:

- the gas flow rate, Q (cm^3/s),
- the rate of production of CO in the electrode discharge region, r_{prod} (mol/s),
- the rate constant for the CO oxidation reaction over the catalyst, k (1/s), and
- the maximum allowable concentration of CO leaving the discharge zone and entering the catalyst, C_{max} (mol/cm^3).

The first step in reactor design is to write molar conservation equations (mole balances) for each key species and to write an energy balance. Since isothermal conditions have been assumed, an energy balance is not required. Mole balances are performed around volumes with uniform conditions, in this case, a differential volume element of the catalyst bed, which may consist of catalyst pellets, for example:

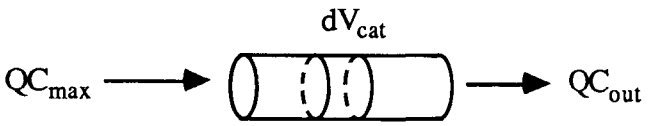

$$\text{accumulation} = \text{in} - \text{out} - \text{reaction}$$

$$0 = QC - Q(C+dC) - kC\,dV_{cat}$$

where C is the concentration of CO at any point. Of course, the concentration of O_2 at any point can be determined from the concentration of CO since they will always be in a stoichiometric ratio. More complex rate equations **can** be substituted in for the rate of reaction without increasing the difficulty of the problem. Separating variables and integrating:

$$\int_0^{V_{cat}} dV_{cat} = -\frac{Q}{k}\int_{C_{max}}^{C_{out}} \frac{dC}{C}$$

$$V_{cat} = -\frac{Q}{k}\ln(C_{out}/C_{max})$$

C_{max} is specified and C_{out} is determined from the rate of production in the discharge:

$$r_{prod} = Q(C_{max} - C_{out})$$

$$V_{cat} = -\frac{Q}{k} \ln (1 - r_{prod} / Q C_{max})$$

And the desired result is obtained. The volume of catalyst required decreases as:

- the activity of the catalyst per unit volume is increased (i.e., k increases),
- the rate of dissociation of CO_2 in the discharge decreases,
- the maximum allowable concentration of CO, C_{max}, (and, thus, concentration of O_2) increases

Rearranging the equation, one can see that, for a fixed volume of catalyst, the steady-state concentrations of CO and O_2 will increase if the repetition rate of the laser discharge is increased. The utility of such a design equation can readily be seen for evaluating the effects of changes in laser design or operation.

Next we consider a case where there is no forced convection of the laser gas and transport of CO and O_2 must occur by diffusion only. This configuration might be feasible in a low repetition rate laser that is constrained to having a small volume and power consumption. In this case, we continue to assume isothermal conditions and a reaction that is first-order in CO and zero-order in O_2. However, here we allow for the possibility that the rate of diffusion of CO and O_2 in the porous catalyst may be slow with respect to the rate of reaction. The configuration of this laser is shown below in schematic form:

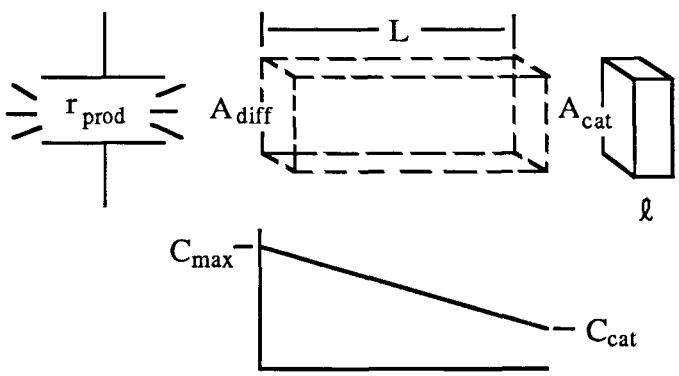

where C_{cat} is the concentration of CO at the external surface of the porous catalyst that has external area A_{cat} (cm^2), thickness ℓ (cm) and volume $V_{cat} = A_{cat} \times \ell$. Diffusion of CO, O_2, and CO_2 occur between the discharge and the catalyst over a one dimensional diffusion path with length L (cm) and cross sectional area $A_{diff} = A_{cat}$.

At steady-state conditions, the rate of production of CO has to equal the rate of consumption of CO at the catalyst:

$$r_{prod} = r_{rxn} = k C_{cat} V_{cat} \eta$$

For brevity we do not show the derivation that describes the diffusion and reaction of CO within the porous catalyst. This derivation is contained in standard texts (refs.18,19). As a result of diffusional

limitations, the concentration of CO and O_2 may be lower inside the porous catalyst than at the external surface. The "effectiveness factor" η corrects for the lower concentrations of reactants inside the porous catalyst and its value ranges between 0 and 1. For a first-order reaction in a one-dimensional catalyst layer:

$$\eta = \frac{\tanh \phi}{\phi} \qquad \text{where} \qquad \phi = \ell \sqrt{k/D_{eff}}$$

and where ϕ is the "Thiele modulus," which gives a measure of the relative rates of reaction and diffusion, and D_{eff} is the "effective diffusivity" of reactants within the catalyst. The volume of catalyst required is:

$$V_{cat} = \frac{r_{prod}}{k\, C_{cat}\, \eta}$$

From the steady-state molar conservation equation for CO in the bulk gas:

$$r_{prod} = r_{diff} = D\, A_{diff}\, (C_{max} - C_{cat})/L$$

$$C_{cat} = C_{max} - r_{prod}/(DA / L)$$

where D is the diffusivity in the bulk gas. And, thus:

$$V_{cat} = \frac{r_{prod}}{k\, \eta\, (C_{max} - r_{prod}/(DA / L))}$$

Again, the complexity of the problem is not increased by using more complex rate expressions than the first-order equation shown here. The required catalyst volume is now a function of the parameters describing diffusion of CO in the stagnant bulk gas and within the porous catalyst.

There are two limits to effects of diffusion within the porous catalyst. First consider the case where diffusion of reactants is fast relative to the rate of reaction. For this case $\phi << 1$ and $\eta \rightarrow 1$:

$$V_{cat} = \frac{r_{prod}}{k\, (C_{max} - r_{prod}/(DA / L))}$$

The other limit is the case where the rate of reaction is fast relative to the diffusion of reactants within the catalyst. For this case $\phi >> 1$ and $\eta \rightarrow 1/\phi$:

$$V_{cat} = \frac{r_{prod}}{(k^{0.5}\, D_{eff}^{0.5} / \ell)\, (C_{max} - r_{prod}/(DA / L))}$$

In this case, quadrupling the activity (i.e., the rate constant, e.g., by adding more precious metal)

within a porous catalyst layer of constant thickness ℓ only halves the amount of catalyst required. For constant activity, increasing the thickness of the catalyst layer increases the volume of catalyst required. This design equation also serves to illustrate the care that must be taken when trying to measure kinetics over porous catalysts where the effects of diffusion may be important. As another example, note that the rate constant occurs to the 0.5 power. Measurement of overall rates at different temperatures in order to determine an activation energy for the reaction will give a result that is approximately equal to one-half of the real activation energy (D_{eff} is relatively weakly temperature dependent).

SUMMARY

This brief introduction to catalytic reactor design has emphasized the following points:

- The optimal low temperature catalyst will be a "complex" formulation in which the critical catalytic steps of dissociative O_2 adsorption and CO adsorption are performed on separate but intimately mixed catalytic sites.

- It is important to determine rate expressions for catalysts in the absence of heat and mass transport limitations whenever possible.

- Reactors designed specifically for kinetic studies of heterogeneous catalysts should be used, whenever possible, rather than prototype lasers. Once a rate expression is determined for a given catalyst formulation, mathematical models can be developed to explore the use of that catalyst in a variety of different lasers, rather than having the measurements only apply to the specific prototype measurements were made in.

- The performance of different catalyst formulations should be compared on the correct chemical basis - such as comparing rate per exposed metal atom or per unit surface area of metal oxide - rather than on an arbitrary basis such as rate per weight of metal.

- Accurate kinetic measurements allow the development of reactor models that allow exploration of a range of design alternatives.

REFERENCES

1. Mulcahy, M. F. R.: "Gas Kinetics," John Wiley and Sons, New York (1973).
2. Stark, D. S.; Cross, P. H.; and Foster, H.: IEEE J. Quantum Electron., QE-11, 774 (1975).
3. Engel, T.; and Ertl. G.: Adv. in Catal., 28, 1 (1979).
4. Herz, R. K.; and Marin, S. P.: J. Catal., 65, 281 (1980).
5. Creighton, J. R.; Tseng, F. H.; White, J. M.; and Turner, J. S.: J. Phys. Chem. 85, 703 (1981).
6. Thomas, J. M.; and Thomas, W. J.: "Introduction to the Principles of Heterogeneous Catalysis," Academic Press, New York (1967).
7. Goodman, D. W.: Applic. Surf. Sci., 19, 1 (1984).
8. Tauster, S. J.; Fung, S. C.; Baker, R. T. K.; and Horsley, J. A.: Science, 211, 121 (1981).
9. Chung, Y. W.; Xiong, G.; and Kao, C. C.: J. Catal. 85, 237 (1984).
10. Rasasco, D. E.; and Haller, G. L.: J. Catal., 82, 279 (1983).
11. Fung, S. C.: J. Catal. 76, 225 (1982).
12. Sexton, B. A.; Hughes, A. E.; and Foger, K.: J. Catal., 77, 85 (1982).
13. Fleisch, T. H.; Hicks, R. F.; and Bell, A. T.: J. Catal., 87, 398 (1984).
14. Oh, S. H.; and Carpenter, J. E.: J. Catal., 98, 178 (1986).
15. Schmidt, L. D.; and Wang, T.: J. Vac. Sci. Technol., 18, 520 (1981).
16. Wang, T.; and Schmidt, L. D.: J. Catal., 66, 301 (1980).
17. Stark, D. S.; Harris, M. R.: J. Phys. E: Sci. Instrum., 16, 492 (1983).
18. Carberry, J. J.: "Chemical and Catalytic Reaction Engineering," McGraw-Hill, New York (1976).
19. Fogler, H. S.: "Elements of Chemical Reaction Engineering," Prentice-Hall, New Jersey (1986).

NASA-LaRC RESEARCH ON

CATALYSTS FOR LONG-LIFE CLOSED-CYCLE CO_2 LASERS

David R. Schryer, Barry D. Sidney, Irvin M. Miller, Robert V. Hess,
George M. Wood, Carmen E. Batten, Lewis G. Burney, Ronald F. Hoyt,
and Patricia A. Paulin
Langley Research Center
Hampton, Virginia

Kenneth G. Brown and Jacqueline Schryer
Old Dominion University
Norfolk, Virginia

Billy T. Upchurch
Chemicon, Inc.
Virginia Beach, Virginia

SUMMARY

Long-life, closed-cycle operation of pulsed CO_2 lasers requires catalytic CO - O_2 recombination both to remove O_2, which is formed by discharge-induced CO_2 decomposition, and to regenerate CO_2. Platinum metal on a tin (IV) oxide substrate (Pt/SnO_2) has been found to be an effective catalyst for such recombination in the desired temperature range of 25°C to 100°C. This paper presents a description of ongoing research at NASA-LaRC on Pt/SnO_2 catalyzed CO - O_2 recombination. Included are studies with rare-isotope gases since rare-isotope CO_2 is desirable as a laser gas for enhanced atmospheric transmission. Results presented include (1) achievement of 98% - 100% conversion of a stoichiometric mixture of CO and O_2 to CO_2 for 318 hours ($> 1 \times 10^6$ seconds), continuous, at a catalyst temperature of 60°C and (2) development of a technique, verified in a 30-hour test, to prevent isotopic scrambling when $C^{18}O$ and $^{18}O_2$ are reacted in the presence of a common-isotope $Pt/Sn^{16}O_2$ catalyst.

INTRODUCTION

Pulsed CO_2 lasers have several potential remote sensing applications, both military and non-military, which require long-life operation with high conversion-efficiency and good power-stability. However, two problems are associated with such applications.

One problem is that the electrical discharge normally used to excite pulsed CO_2 lasers inevitably decomposes some of the CO_2:

$$CO_2 \xrightarrow[\text{Disch.}]{\text{Elec.}} CO + 1/2\ O_2$$

This decomposition is harmful to long-life laser operation both because of the loss of CO_2 and because of the buildup of O_2. The loss of CO_2 results in a corresponding gradual loss of laser power. The buildup of even relatively small concentrations (0.1% - 1.0%) of O_2 molecules can cause rapid power loss and even complete laser failure.

The second problem has nothing to do with CO_2 lasers themselves; it is caused by the fact that the atmosphere contains a significant concentration, about 300 ppm, of common-isotope CO_2 ($^{12}C^{16}O_2$). If common-isotope CO_2 is used in a CO_2 laser intended for atmospheric transmission, the emission frequencies available to the laser will correspond to the absorption frequencies of the atmospheric CO_2 and poor transmission will result.

The solutions to these two problems are superficially quite simple: (1) continuously remove O_2 as it is formed and replenish CO_2 and (2) use some form of rare-isotope CO_2 (such as $^{12}C^{18}O_2$, $^{13}C^{16}O_2$, or $^{13}C^{18}O_2$) in all lasers intended for applications involving atmospheric transmission so that the emisson frequencies of such lasers will differ from the absorption frequencies of atmospheric $^{12}C^{16}O_2$. Actual implementation of these two solutions, however, is far from simple.

Removal of O_2 and replenishment of CO_2 can be achieved in certain applications simply by operating the laser open-cycle with a continuous flow-through of fresh laser gas and the consequent removal of dissociation products. However for space-based applications or other applications involving weight and/or volume constraints, the amount of gas required for open-cycle operation would be unacceptable and, instead, closed-cycle laser operation with recycling of the laser gases would be imperative. Closed-cycle operation would also be highly desirable for any applications where rare-isotope CO_2 is used for enhanced atmospheric transmission because of the expense of the large volumes of rare-isotope gas which would be required for flow-through operation.

Closed-cycle CO_2 laser operation with removal of O_2 and regeneration of CO_2 can be achieved, in principle, simply by accomplishing CO-O_2 recombination.

$$CO + 1/2\ O_2 \longrightarrow CO_2$$

However, this recombination is negligibly slow at steady-state temperatures (about 50°C to 100°C) achieved by the gas mixture in a typical CO_2 laser. Thus, although some recombination can occur in the region of the electric discharge where effective temperatures are quite high, no significant recombination can occur in the main body of the laser gas unless a catalyst is used. Several materials have been found to catalyze CO-O_2 recombination under various conditions. Most such catalysts utilize noble metals (especially Pt and/or Pd), metal oxides, or both. Catalysts consisting of Pt or Pd on a tin (IV) oxide substrate (Pt/SnO_2, Pd/SnO_2) have been shown to be much more efficient than Pt, Pd, or SnO_2 alone at moderate temperatures (Refs. 1 and 2).

At the NASA Langley Research Center (NASA-LaRC) we have investigated several catalysts for potential use with long-life, closed-cycle CO_2 lasers including Pt/SnO_2, Pt/SiO_2, unsupported Pt, Pd/C, and $Cu/Cu_2O/CuO$ (Refs. 2 and 3). The most promising of these catalysts has been found to be Pt/SnO_2 and so a detailed investigation of this catalyst has been undertaken and is currently in progress. Studies of this and other catalysts are being carried out in several laboratory reactors as well as in a pulsed CO_2 laser.

TEST FACILITIES

Laboratory Reactors

Laboratory reactors are used for catalyst study under controlled conditions. Three laboratory reactors are presently operational, all of which are flow-through reactors. In these reactors a test-gas mixture flows through a reactor tube containing a catalyst sample which is situated in a temperature-controlled oven. The gas which exits the reactor tube is quantitatively analyzed with either a gas chromatograph (GC) or mass spectrometer (MS) and from this analysis the amount of CO and O_2 converted to CO_2 by the catalyst sample is determined. The test-gas mixtures used are purchased premixed in a high-purity He carrier, typically 1.00% CO and 0.50% O_2 plus 2.00% Ne (as an internal calibration standard for gas analysis).

Two of the flow-through reactors are used with common-isotope gases and use GC's for gas analysis. These GC's are fully automated so that tests with common-isotope gases can be conducted in the flow-through reactors around-the-clock without an operator present. The third flow-through reactor is used with rare-isotope gases and uses an MS for gas analysis.

Studies performed in the flow-through reactors are (1) parametric studies to determine the effect of such parameters as catalyst mass, temperature, reactor residence-time, etc., on the performance of a given catalyst material, (2) comparison of different catalyst compositions (such as Pt/SnO_2, Pd/SnO_2, and Pt + Pd/SnO_2) and concentrations to determine the optimum catalyst formulation, (3) long-term performance tests (using the automated-GC reactors) to determine how a catalyst performs with long-term exposure to the test gases, and (4) isotopic studies (using the MS reactor) to determine the interaction of a given catalyst with rare-isotope gases.

A recirculating reactor is presently being assembled and should be operational shortly. In this reactor a gas mixture will be continuously recirculated through a temperature-controlled reactor tube containing a sample of catalyst, and the conversion of CO and O_2 to CO_2 monitored as a function of time. Gas analysis will be performed with a GC. This reactor will be used to determine the rate of $CO-O_2$ recombination using various catalyst materials and also to study the mechanism of catalysis. Knowledge of these factors is important for optimization of catalyst performance.

Also to be assembled shortly will be a system to quantitatively measure chemisorption of gases on a catalyst surface when some of the chemisorbed species undergo desorption as a product gas.

Laser Reactor

A Lumonics model TEA-820 pulsed CO_2 laser (.7Joule/pulse, 1-20 pulses/second) is available for catalyst testing under actual laser operating conditions. The laser is operated closed-cycle with an external catalyst bed (in a temperature-controlled oven) and the results are compared with the open-cycle performance of the laser at the same flow rate. It is intended that ultimately the

laser will be operated with no heating of the catalyst other than by the laser gas. Gas analysis is performed with a GC in current common-isotope tests. An MS will be used when the laser is operated with rare-isotope CO_2.

RESULTS AND ON-GOING RESEARCH

This section presents a summary of results obtained to date using the currently operational reactors described in the previous section as well as a synopsis of work currently in progress or planned.

Laboratory Reactor Studies

Common-Isotope Gases

(1) Conversion of 1% CO and .5% O_2 to CO_2 at an efficiency of 98%-100% has been achieved in a laboratory reactor with 1.5 grams of 2% Pt/SnO_2 at 60°C and 10 std. mL/minute flow rate. This efficiency was maintained for 318 hours (> 10^6 seconds or 13 days). The test was terminated because of a GC failure not because of a loss of catalyst efficiency. Tests at lower temperatures are in progress. Scheduled are laser tests to verify this result in actual laser operation, and laboratory-reactor tests involving non-stoichiometric gas mixtures (both CO and O_2 rich).

(2) At a given catalyst temperature, catalyst surface-area-to-mass ratio, and gas flow rate, the conversion of CO and O_2 to CO_2 over a Pt/SnO_2 catalyst appears to be an approximately linear function of catalyst mass until 100% efficiency is achieved. (See Figure 1)

(3) The conversion efficiency per unit mass of Pt/SnO_2 has been approximately doubled (or the catalyst mass halved) by pretreating the catalyst with flowing 1% CO in He for one hour at 225°C relative to pretreatment for the same time and temperature with He alone. The conversion efficiency per unit mass of Pt/SnO_2 has been more than doubled (or the mass more than halved) by pretreating the catalyst with flowing He at 225°C for twenty hours relative to pretreatment with He at the same temperature for only one hour. Tests are scheduled to determine the optimum pretreatment time and temperature to achieve maximum catalyst efficiency. Also to be investigated is whether combination of extended He pretreatment with CO pretreatment will further increase catalyst efficiency.

(4) The catalytic efficiency of 2% Pt/SnO_2 at 100°C has been found to be nearly twice that of 1% Pt/SnO_2 of equal sample mass and surface area. The optimum loading of noble metal to SnO_2 will be determined in future tests.

(5) Initial tests comparing 2% Pt/SnO_2 with 2% Pd/SnO_2 and 1% Pt + 1% Pd/SnO_2 have been performed at 75°C. More than twice the conversion efficiency was achieved with 2% Pt/SnO_2 than was achieved with 2% Pd/SnO_2. A slightly higher conversion efficiency was achieved with 1% Pt + 1% Pd/SnO_2 than was achieved with 2% Pt/SnO_2. Comparison of various catalyst materials will continue including both comparison of Pt/SnO_2 with other catalysts and comparison of Pt/SnO_2 prepared at this laboratory and by Prof. Gar Hoflund at the University of Florida with the commercially available products used in our studies to date.

Rare-Isotope Gases

(1) Exposure of common-isotope $Pt/Sn^{16}O_2$ to 1% $C^{18}O$ and .5% $^{18}O_2$ at 100°C yields about 85%-90% $C^{18}O_2$ and 10%-15% of the mixed-isotope species, $C^{16}O^{18}O$. This result tends to imply that two competing reactions occur when CO and O_2 are oxidized with a Pt/SnO_2 catalyst. The reaction which yields $C^{18}O_2$ appears to involve reaction of $C^{18}O$ and $^{18}O_2$ on the catalyst surface but no reaction of these species with the surface. The reaction which yields $C^{16}O^{18}O$ implies oxidation of $C^{18}O$ by ^{16}O atoms in the surface lattice and then, presumably, reoxidation of the surface by $^{18}O_2$. Further isotopic studies will be performed to verify the occurrence of two competing reactions and to determine their mechanisms in detail.

(2) A technique has been developed to prevent formation of the mixed isotope species $C^{16}O^{18}O$ when $C^{18}O$ and $^{18}O_2$ are recombined using a $Pt/Sn^{16}O_2$ catalyst (as in the preceding item). The technique involves reducing the catalyst surface with a measured quantity of H_2 to remove all reactive ^{16}O atoms and then reoxidizing the surface with $^{18}O_2$. The net effect is to replace all reactive ^{16}O atoms on the catalyst surface with ^{18}O atoms so that any exchange of oxygen atoms between the gaseous species and the catalyst surface does not result in isotopic scrambling of the gases. This technique (for which a Patent Application has been filed) has been validated in a 30-hour test.

Laser Studies

The Lumonics Model TEA-820 laser has been operated closed-cycle with a catalyst bed of 150 g of 2% Pt/SnO_2 at 100°C. The laser achieved 96.5% (± 2.5%) of steady-state open-cycle power for 28 hours (1×10^6 pulses at 10 pulses/second). (See Figure 2) A test of 10^7 pulses at a catalyst temperature <100°C is planned for 1987.

CONCLUDING REMARKS

Pt/SnO_2 has been shown to be an effective CO - O_2 recombination catalyst at steady-state temperatures achieved by the gas mixture in pulsed CO_2 lasers. Its catalytic efficiency can be enhanced by suitable pretreatment techniques and optimum metal loading. Even though the substrate SnO_2 contains predominantly common-isotope oxygen, it appears that reduction of the catalyst surface with H_2 and reoxidation with $^{18}O_2$ renders the catalyst compatible with rare-isotope $C^{18}O_2$ and its rare-isotope dissociation products. A systematic research project, described in this report, is in progress at NASA-LaRC to further evaluate and enhance the catalytic properties of Pt/SnO_2 and other catalysts for use in long-life, closed-cycle CO_2 lasers.

REFERENCES

1. Bond, Geoffrey C.; Moloy, Leslie R.; and Fuller, Martin J.: Oxidation of Carbon Monoxide over Palladium-Tin (VI) Oxide Catalyst: An Example of Spillover Catalysis. Journal of the Chem. Soc. Chem Comm., 1975, pp. 796-797.

2. Brown, K. G.; Sidney, B. D.; Schryer, D. R.; Upchurch, B. T.; Miller, I. M.; Wood, G. M.; Hess, R. V.; Batten, C.; Burney, L. G.; Paulin, P. A.; Hoyt, R.; and Schryer, J.: Catalytic Recombination of Dissociation Products with Pt/SnO_2 for Rare and Common Isotope Long-Life, Closed-Cycle CO_2 Lasers. Laser Radar Technology and Applications, Proceedings of SPIE, Vol. 663, 1986, pp. 136-144.

3. Rogowski, R. S.; Miller, I. M.; Wood, G.; Schryer, D. R.; Hess, R. V.; and Upchurch, B. T.: Evaluation of Catalyst for Closed Cycle Operation of High Energy Pulsed CO_2 Lasers. Coherent Infrared Radar Systems and Applications II, Proceedings of SPIE, Vol. 415, 1983, pp. 112-117.

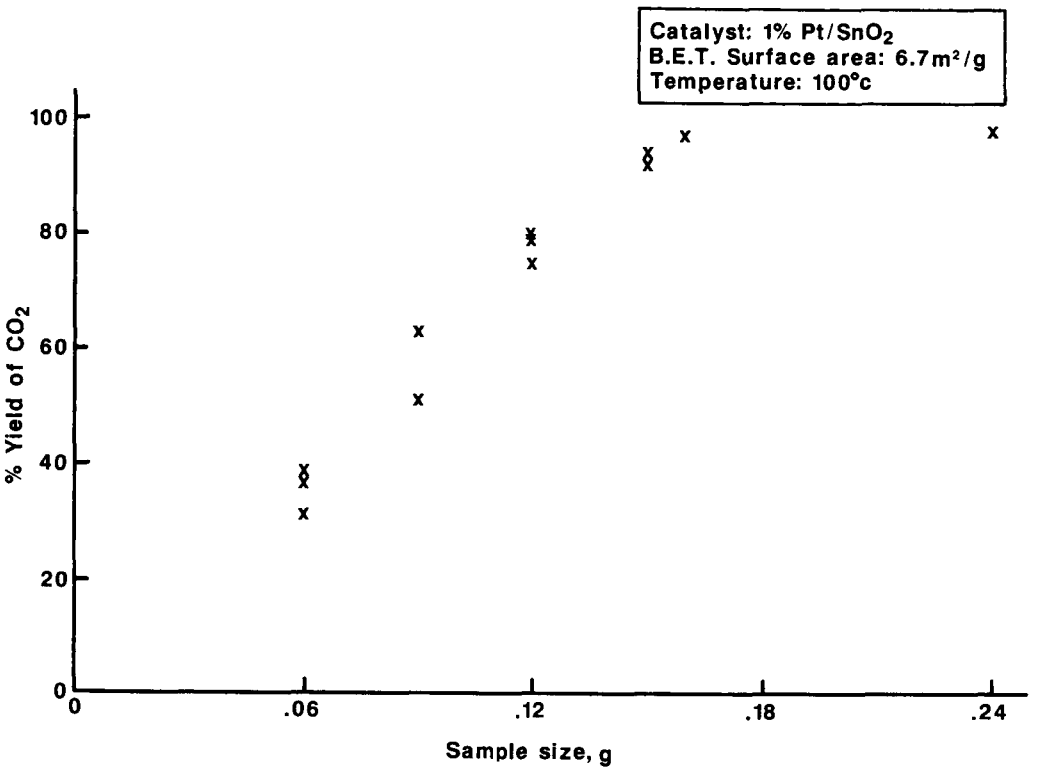

Figure 1. Conversion efficiency of catalyst versus sample weight.

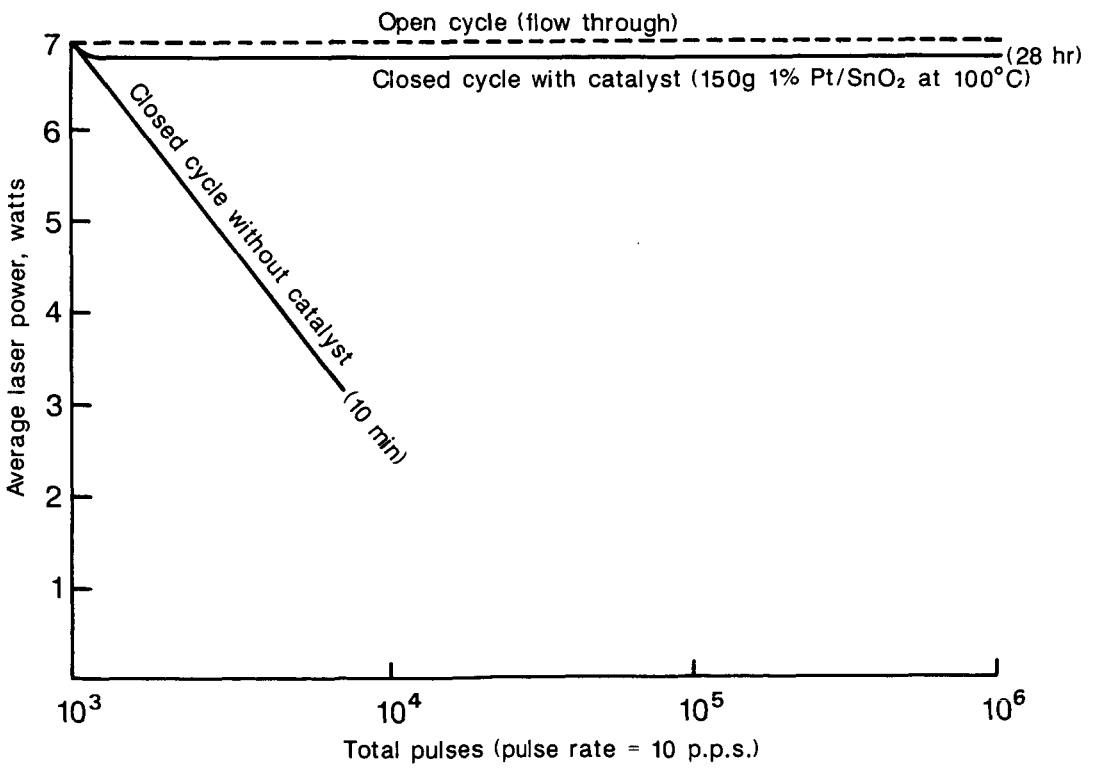

Figure 2. Performance of pulsed CO_2 layer with and without recombination catalyst.

STRONG METAL-SUPPORT INTERACTIONS

M. Albert Vannice
Department of Chemical Engineering
The Pennsylvania State University
University Park, PA 16802, USA

If bifunctional catalysts are discounted, i.e., metals dispersed on acidic oxides in which the metal provides hydrogenation-dehydrogenation activity and the oxide support induces carbonium ion chemistry (1), the number of well-documented examples of rate enhancement by the support is not large. One major reason for this is that the requirement of specific activities (molecules per second per unit metal surface area) or turnover frequencies (molecules per second per surface metal atom) was not fulfilled. It should be stressed at this time that observed changes in catalytic activity as the support is varied cannot automatically be attributed to metal-support interactions. First, artifacts created by heat and mass transfer limitations must be ruled out by conducting experiments at low conversions and using tests to verify the absence of these transport effects (2). Second, metal crystallite size effects must be ruled out. Third, in CO hydrogenation reactions in particular, chromatographic effects by the porous support must be eliminated. Finally, any influence of impurities, poisons and promoters must be eliminated, and the possibility of the support acting as a getter must be considered. In the absence of any direct spectroscopic evidence that a metal-support interaction exists, it is only after all other possibilities have been ruled out that the explanation of metal-support effects can safely be accepted.

Evidence that a dispersed phase on a substrate could have its catalytic behavior altered by that substrate was first reported by Schwab and co-workers (3-5) and Szabo and Solymosi (6,7); however, effects on specific activity of metals were not determined in these early studies. Later investigations by Sinfelt and co-workers provided some of the first evidence that the support could affect the specific activity of the dispersed metal (8), and the possibility of electronic interactions between the metal and the support was discussed in an early review (9). After this, Sagert and Pouteau showed that the degree of graphitization of the carbon support had a major effect on both the activation energy and the specific activity of the hydrogen-water deuterium exchange reaction over Pt (10,11).

However, it wasn't until the work of Tauster and co-workers that the effect of the support on chemisorption properties was observed (12,13), with titania, in particular, inhibiting the chemisorption of H_2 and CO on the Group VIII noble metals after high temperature reduction (HTR) at 773 K. A low temperature reduction (LTR) near 473 K provided normal chemisorption behavior. This behavior, which could be reversed by exposure to oxygen, was attributed to a Strong Metal-Support Interaction (SMSI). Catalytic studies of CO hydrogenation over TiO_2-supported metals by Vannice and co-workers showed the specific activity, i.e., the turnover frequency (TOF), was markedly enhanced over many, but not all, of the Group VIII metals (14-21). In some systems, such as Ni/TiO_2, significant changes in selectivity to heavier paraffins were also found (14,16). Since these initial publications, many subsequent

investigations have been directed toward these catalytic systems, principally titania-supported metals, in an effort to better understand this phenomenon (22-67), and an international meeting was held on this topic in 1982 (68).

Perhaps the most apparent manifestation of "SMSI" behavior is the inhibition of H_2 and CO chemisorption on Group VIII noble metals dispersed on titania, as illustrated in Table 1, and certain other supports such as Ta_2O_3, and Nb_2O_5 after high temperature reduction (HTR) at 773 K (10,11). Explanations such as sintering, contamination and encapsulation by the support were initially ruled out (12), and later CAEM (Controlled Atmosphere Electon Microscopy) studies by Baker et al. on Pt/substrate systems under UHV conditions provided further evidence that this behavior was a consequence of a metal-support interaction (33). This latter study was of particular interest because it showed: (1) morphological changes occurred for the Pt crystallites on titania and 2-dimensional "pill-box" structures were formed after HTR; (2) this change could be reversed by exposure to O_2 or H_2O to form thicker hemispherical particles, and (3) reduction of the TiO_2 to Ti_4O_7 occurred and appeared to be closely associated with "SMSI" behavior. Interestingly, oxygen adsorption on TiO_2-supported noble metals does not seem to be greatly affected (36) and may provide a useful chemisorption technique for these systems. This has been already proposed for Ni/TiO_2 catalysts (22). Recent work by Baker and co-workers has provided additional evidence that a reduced phase of titania, again presumably Ti_4O_7, is present when "SMSI" behavior exists (49). However recent studies have provided overwhelming evidence that the decrease in chemisorption capacity is principally due to the migration of TiO_x species onto the metal surface during the high temperature reduction step and that physical blockage of the surface metal atoms occurs (36,69).

Significant enhancements in specific activity have been found for CO hydrogenation over TiO_2-supported Group VIII metals although not all metals are affected in a favorable manner (19). The much lower activity for iron may be a consequence of migration into the titania structure, as found by Tatarchuk and Dumesic (64-66). Titania-supported nickel catalysts are the most active reported to date for CO hydrogenation, as shown in Table 2, and the higher TOF values first reported by Vannice and co-workers (14-21) have subsequently been observed for Ni by other investigators (24,34,35,57). The high TOF values shown in Tables 3 and 4 for Pd and Pt, especially on Pt, are important because they vary by over two orders of magnitude even if the metal surface area is assumed equal to that existing after a LTR, which produces normal chemisorption behavior (18,21). Crystallite size effects were shown to be absent in both studies. However, significant changes in the adsorbed state of CO were detected by IR spectroscopy. Whereas H_2 has little effect on CO adsorbed on typical Pd and Pt catalysts, it significantly decreased the IR band intensities on the TiO_2-supported metals, as shown in Figures 1 and 2 (20,58). Under steady-state reaction conditions, almost no IR-active CO existed on the TiO_2-supported metals, in sharp contrast to the behavior of these metals dispersed on common supports, as shown by a comparison of Figures 1a and 1b and of Figures 2a and 2b. Additional examples are shown in Figure 3. Although there is common agreement that CO hydrogenation reaction rates are higher over most TiO_2-supported metals (53,68), similar rate enhancements usually do not occur in other hydrogenation reactions and in hydrogenolysis reactions. In fact, after HTR to induce "SMSI" behavior, large decreases in activity have been observed for ethane hydrogenolysis (37,56), n-butane hydrogenolysis (36,70), benzene hydrogenation (36,71,72), n-hexane reactions (71) and cyclohexane dehydrogenation (36). Some of these results are reported

in Tables 5 and 6. Although normal activities for benzene hydrogenation, hexane reactions and ethane hydrogenolysis have been reported over Ni/TiO_2 catalysts (53,57,73), Pd/TiO_2 catalysts reduced at low temperature had enhanced benzene hydrogenation activity compared to typical Pd catalysts (72). A treatment in oxygen tends to restore the typical catalytic properties of these metals (36).

In addition to significant rate enhancements for CO hydrogenation, (and perhaps of greater importance) pronounced changes in selectivity can occur for some TiO_2-supported metals. The changes in Ni/TiO_2 catalysts to produce long-chain paraffins are quite vivid (14,16), as shown in Tables 7 and 8. Vannice and Garten also found that olefin formation was enhanced over TiO_2-supported Ru, compared to typical Ru catalysts (15), and Morris et al. later found similar behavior (74). Under certain reaction conditions, methane formation constituted less than 15 wt% of the hydrocarbon product (12-14).

The chemistry responsible for SMSI behavior is still not completely understood, especially since the occurrence of inhibited chemisorption does not always parallel an increase in catalytic activity (21,74). A number of explanations have been proposed for "SMSI" behavior, and they include: (1) changes in structure, i.e., formation of thin rafts; (2) intermetallic compound formation; (3) electron transfer to Pt via Ti^{3+} cations formed during reduction; (4) electron transfer to Pt from the Fermi level of bulk titania via a metal/semiconductor interface (i.e., a Schottky barrier); (5) titania migration onto the metal surface: and (6) increased, rather than weakened, metal-H bond strengths. To explain the higher activity for CO hydrogenation, additional proposals invoking special sites in the adlineation region, i.e., at the metal-support interface (53,69) and H_2 spillover during reaction have also been made. At the present time, little evidence has been found to support the notion of surface intermetallic compound formation in metal/titania systems (36) and, in actuality, bulk intermetallic compounds have been found to convert to metal/metal oxide systems under CO hydrogenation reaction conditions (75,76). Enhanced hydrogen adsorption, i.e., stronger H-metal bonding, has also been discounted (33).

The CAEM studies by Baker and co-workers on supported Pt and AgPt have clearly shown that the morphology of Pt crystallites changes on reduced titania, and they appear to wet the support surface by forming thin rafts, as depicted in Figure 4 (33,49). This structural change could have a effect on adsorption and catalytic properties even if no electron transfer occurred and, in addition, such wetting of the surface would also increase the metal-support interface and facilitate electron transfer as proposed in explanation 3 or 4. The Exxon workers have favored direct metal atom-support cation (Ti^{3+}) interactions (32) - a more localized bonding model - whereas others have proposed electron transfer dependent upon electronic properties of the bulk oxide support via a Schottky barrier (28-30,36). Although behavior indicating electron transfer from the titania to the metals has in some cases been observed by using a variety of techniques such as XPS (23-27) and electrical conductivity measurements (28-30), as shown in Figures 5 and 6, such results have not always been obtained (38).

The ability of TiO_2-supported metals to selectively enhance the rate of CO hydrogenation, but not other hydrogenation or hydrogenolysis reactions, implies that the effect responsible has a strong influence on adsorbed CO. The two most likely possibilities are a structural effect due to electron transfer and particle morphological changes, or the creation of unique sites at the metal/support interface, or possibly a combination of the two

(21,53,69). This proposal of special active sites in the metal/support interface region, i.e., the theory of adlineation, is an old concept first proposed by Schwab (3). The migration of TiO_2 onto the metal surface would tend to enhance this effect and also minimize any metal crystallite size effect governing interfacial area (21). Although special active sites for the CO molecule could play a role, an enhanced surface concentration of hydrogen under reaction conditions may also account for the much higher activities observed (18,21); however, recent studies have provided strong support for the creation of unique active sites at the metal-support interface, for instance, note the high turnover frequencies shown in Table 9 (69). The model resulting from this study is shown in Figure 7, and it invokes special sites at the metal-titania interface which interact with the oxygen end of the CO molecule to facilitate bond rupture, which is the slow step on Pt and Pd catalysts.

A model invoking special active sites on the titania surface which are outside the adlineation region, but participate in CO hydrogenation reactions via hydrogen spillover (i.e., surface migration), has not been supported by recent studies (63). Regardless, the role of spillover under reaction conditions is presently obscure. Under low temperature conditions with active hydrogenation catalysts, predicted rates of hydrogen transport on the support surface, using calculated surface diffusion coefficients, are too low to be significant compared to rates of reaction on the metal surface (77-79). In contrast, under typical reaction conditions for methanation over the less active metals (1 atm, 275°C, $H_2/CO=3$), calculated rates of hydrogen transfer to the support per metal crystallite can be comparable to rates of reaction per crystallite. For example, using the solution to the equation describing 2-dimensional surface diffusion (77), calculating a diffusion coefficient of 7×10^{-18} $cm^2 \cdot s$ at 275°C from the work of Kramer and Andre (79), and assuming 1 nm Pt crystallites containing 20 Pt atoms with a hydrogen coverage of $\theta_H=0.1$, a maximum transport rate to the support of 0.03 H atoms per second per crystallite can be estimated. The rate of H consumption during methanation on Pt/Al_2O_3 catalysts is 0.13 H atoms per second per Pt crystallite (21). This comparison is made to show that although hydrogen spillover does not seem to be adequate to explain the higher turnover frequencies found on TiO_2-supported metals, if comparable diffusion coefficients are assumed, this process could enhance the rate in the adlineation region because this transport process involves only a very short jump distance. Despite this exercise to ascertain the possible contribution of H_2 spillover to reaction rates, its actual role has not yet been determined. Although hydrogen spillover alone does not appear to provide an explanation for enhanced CO hydrogenation activity, it is clearly important in facilitating "SMSI" behavior by catalyzing the reduction of TiO_2 (25,33,49,80). The reduction of other metal oxides at lower than normal temperatures via hydrogen spillover from a metal capable of activating H_2 has also been reported (81-94).

At the present time there is much interest in metal-support effects, particularly with regard to their role in CO hydrogenation reactions. The chemistry inducing "SMSI" behavior and activity enhancement is still not yet completely resolved and future studies are needed to determine: (1) the extent of electron transfer between metal and support, should it occur; (2) whether this is localized behavior at the surface or best described by metal/semiconductor bulk properties; (3) the effect of structural (morphological) changes in the metal crystallites; (4) the contribution of the adlineation region to the catalytic process; (5) the importance, if any, of hydrogen spillover in the catalysis of CO hydrogenation reactions; and (6)

whether metal-support effects occur in other reactions involving CO, such as oxidation.

In view of the interest in CO oxidation, a short comment pertaining to crystallite size effects seems appropriate. Recent studies of integral heats of adsorption on Pd catalysts have shown that Q_{ad} values for CO and O_2 increase markedly on crystallites smaller than 3 nm, as shown in Figures 8 and 9 (95-97). Such a large change has not been observed for supported Pt catalysts, but the support has a significant influence on CO heats of adsorption (98). Such changes in heats of adsorption can have a large effect on the kinetics of reactions involving these species; consequently, it seems important to study the influence of these parameters on CO oxidation over noble metals like Pt and Pd.

In summary, it has now been unambiguously demonstrated that synergistic metal-support effects can occur which markedly enhance specific activity and alter selectivity in certain reactions. Because of the presence of such effects in certain reactions conducted under reducing conditions (that is, under H_2 pressure), but not others, the creation of unique sites at the metal-support interface seems to be the best model at the present time to explain this behavior. The postulation of these sites, which are specific for a certain reactant such as CO, provides an effective explanation for the higher methanation rates that have been reported over some catalysts. The creation of these sites in the adlineation zone is facilitated by hydrogen spillover from the metal surface, and this same process can also enhance the reduction of many oxide supports. Although oxygen spillover is much less probable due to its higher heat of adsorption, it is much less well understood and the possibility of rate enhancements in CO oxidation caused by special interface sites cannot be discounted at the present time. Consequently, this seems to be an important area of research in the future.

REFERENCES

1. Sinfelt, J. H., Adv. Chem. Eng. 5, 37 (1964).

2. Madon, R. J. and Boudart, M., I&EC Fund. 21, 438 (1982).

3. Schwab, G-M., Adv. Catal. 27, 1 (1978).

4. Schwab, G-M., Block, J., Muller, W. and Schultze, D., Naturwiss, 44, 582 (1957).

5. Schwab, G-M., Block, J. and Schultze, D., Angew. Chem. 17, 101 (1959).

6. Szabo, Z. G. and Solymosi, F., Act. Deux. Cong. Inter. Catalyse, Paris 1627 (1961).

7. Solymosi, F., Cat. Rev. 1, 233 (1967).

8. Sinfelt, J., Cat. Rev. 3, 175 (1969).

9. Slinkin, A. A. and Fedorovskaya, E. A., Russ. Chem. Rev. 40, 860 (1971).

10. Sagert, N. H. and Pouteau, R. M. L., Can. J. Chem. 50, 3686 (1972).

11. Sagert, N. H. and Pouteau, R. M. L., Pt Metals Rev. 19, 16 (1975).

12. Tauster, S. J., Fung, S. C. and Garten, R. L., J. Am. Chem. Soc. 100, 170 (1978).

13. Tauster, S. J. and Fung, S. C., J. Catal. 55, 29 (1978).

14. Vannice, M. A. and Garten, R. L., J. Catal. 56 236 (1979).

15. Vannice, M. A. and Garten, R. L., J. Catal. 63, 255 (1980).

16. Vannice, M. A. and Garten, R. L., J. Catal. 66, 242 (1980).

17. Vannice, M. A., Moon, S. H. and Twu, C. C., ACS Prepr.-Petr. Chem. Div. 25, 303 (1980).

18. Wang, S-Y., Moon, S. H. and Vannice, M. A., J. Catal. 71, 167 (1981).

19. Vannice, M. A., J. Catal. 74, 199 (1982).

20. Vannice, M. A., Twu, C. C. and Moon, S. H., J. Catal. 79, 70 (1983).

21. Vannice, M. A. and Twu, C. C., J. Catal. 82, 213 (1983).

22. Smith, J. S., Thrower, P. A. and Vannice, M. A., J. Catal. 68, 270 (1981).

23. a) Bahl, M. K., Tsai, S. C., Chung, Y. W., Phys. Rev. B21, 1344 (1980). b) Kao, C. C., Tsai, S. C., Bahl, M. K., Chung, Y-W. and Lo, W. J., Surf. Sci. 95, 1 (1980).

24. Kao, C-C., Tsai, S-C. and Chung, Y-W., J. Catal. 73, 136 (1982).

25. Sexton, B. A., Hughes, A. E. and Foger, K., J. Catal. 77, 85 (1982).

26. Chien, S. H., Shelimov, B. N., Resasco, D. E., Lee, E. H. and Haller, G. L., J. Catal. 77, 301 (1982).

27. Fung, S. C., J. Catal. 76, 225 (1982).

28. Chen, B-H. and White, J. M., J. Phys. Chem. 86, 3534 (1982).

29. Herrmann, J-M. and Pichat, P., J. Catal. 78, 425 (1982).

30. Disdier, J., Herrmann, J-M. and Pichat, P., JCS Faraday I 79, 651 (1983).

31. Horsley, J. A., J. Am. Chem. Soc. 101, 2870 (1979).

32. Tauster, S. J., Fung, S. C., Baker, R. T. K. and Horsley, J. A., Science 211, 1121 (1981).

33. a) Baker, R. T. K., Prestridge, E. B. and Garten, R. L., J. Catal. 56, 390 (1979);
b) Ibid. 59, 293 (1979).

34. Bartholomew, C. H. and Mustard, D. G., J. Catal. 67, 186 (1981).

35. Bartholomew, C. H., Pannell, R. B., Butler, J. L. and Mustard, D. G., I&EC Prod. Res. Dev. 20, 296 (1981).

36. Meriaudeau, P., Ellestad, O. H., Dufaux, M. and Naccache, C., J. Catal. 75, 243 (1982).

37. Ko, E. I. and Garten, R. L., J. Catal. 68, 233 (1981).

38. Huizinga, T. and Prins, R., J. Phys. Chem. 85, 2156 (1981).

39. Huizinga, T. and Prins, R., J. Phys. Chem. 87, 173 (1983).

40. Ko, E. I., Winston, S. and Woo, C., JCS Chem. Comm. 740 (1982).

41. Mochida, I., Tsuji, K., Suetsugu, K., Fujitsu, H. and Takeshita, K., J. Phys. Chem. 84, 3159 (1980).

42. Praliand, H. and Martin, G. A., J. Catal. 72, 394 (1981).

43. Tsai, W., Schwarz, J. A. and Driscoll, C. T., J. Phys. Chem. 87 1619 (1983).

44. Summers, J. C. and Ausen, S. A., J. Catal. 58, 131 (1979).

45. Chen, B-H., White, J. M., Brostrom, L. R. and Deviney, M. L., J. Phys. Chem. 87, 2423 (1983).

46. White, J. M. and Tanaka, K., J. Phys. Chem. 86, 3977 (1982).

47. Tanaka, K. and White, J. M., J. Catal. 79, 81 (1983).

48. DeCanio, S. J., Apple, T. M. and Dybowski, C. R., J. Phys. Chem. 87, 194 (1983).

49. Baker, R. T. K., Prestridge, E. B. and Murrell, L. L., J. Catal. 79, 348 (1983).

50. Bossi, A., Garbassi, F., Petrini, G., Zanderighi, L., JCS Faraday Tr I 78, 1029 (1982).

51. Brenner, A. and Hucal, D. A., J. Phys. Chem. 85, 496 (1981).

52. Briggs, D., Dewing, J., Burden, A. G., Moyes, R. B. and Wells, P. B., J. Catal. 65, 31 (1980).

53. Burch, R. and Flambard, A. R., J. Catal. 78 389 (1982).

54. Gonzales, A. R., Soria, J. and Munuera, G., J. Catal. 76, 254 (1982).

55. Haller, G. L. and Resasco, D., JCS Chem. Comm. 1150 (1980).

56. Haller, G. L., Resasco, D. E. and Rouco, A. J., Faraday Disc. 72, (7) (1981).

57. Burch, R. and Flambard, A. R., JCS Chem. Comm. 123 (1981).

58. Vannice, M. A., Wang, S-Y. and Moon, S. H., J. Catal. 71, 152 (1981).

59. Vannice, M. A. and Wang, S-Y., J. Phys. Chem. 85, 2543 (1981).

60. Vannice, M. A. and Twu, C. C., J. Chem. Phys. 75, 5944 (1981).

61. Apple, T. M., Gajardo, P. and Dybowski, C., J. Catal. 68, 103 (1981).

62. Conesa, J. C. and Soria, J., J. Phys. Chem. 86, 1392 (1982).

63. Vannice, M. A. and Vasco-Jara, J., Studies in Surface Science and Catalysis, Vol. 11, B. Imelik et al., Eds., Elsevier, p. 185 (1982).

64. Tatarchuk, B. J. and Dumesic, J. A., J. Catal. 70, 308 (1981).

65. Tatarchuk, B. J. and Dumesic, J. A., J. Catal. 70, 323 (1981).

66. Tatarchuk, B. J. and Dumesic, J. A., J. Catal. 70, 335 (1971).

67. Tatarchuk, B. J., Chludzinski, J. J., Sherwood, R. D., Dumesic, J. A. and Baker, R. T. K., J. Catal. 70, 443 (1981).

68. Studies in Surface Science and Catalysis, Vol. 11, "Metal-Support and Metal-Additive Effects in Catalysis," B. Imelik et al., Eds., Elsevier, 1982.

69. Vannice, M. A. and Sudhaker, C., J. Phys. Chem. 88, 2429 (1984), and reference therein.

70. Resasco, D. E. and Haller, G. L., Ref. 68, p. 105.

71. Meriadeau, P., Dutel, J. F., Dufaux, M. and Naccache, C., Ref. 68, p. 95.

72. Vannice, M. A. and Chou, P., Proc 8th Inter. Cong. on Catal. V-99, DECHEMA, Frankfurt, 1984.

73. Burch, R. and Flambard, A. R., Ref. 68, p. 193.

74. Morris, S. R., Moyes, R. B., Wells, P. B. and Whyman, R., Ref. 68, p. 247.

75. Imamura, H. and Wallace, W. E., J. Catal. 65, 127 (1980).

76. Chin, R. L., Elattar, A., Wallace, W. E. and Hercules, D. M., J. Phys. Chem. 84, 2895 (1980).

77. Vannice, M. A. and Neikam, W. C., J. Catal. 27, 207 (1972).

78. Fleisch, T. and Abermann, R., J. Catal. 50, 268 (1977).

79. Kramer, R. and Andre, M., J. Catal. 58, 287 (1979).

80. Vannice, M. A., Odier, P., Bujor, M. and Fripiat, J. J., ACS Symp. Series 228, 98 (1985).

81. Boudart, M., Vannice, M. A. and Benson, J. E., Z. physik. Chem. NF 64, 171 (1969).

82. Vannice, M. A., Boudart, M. and Fripiat, J. J., J. Catal. 17, 359 (1970).

83. Levy, R. B. and Boudart, M., J. Catal. 32, 304 (1974).

84. Bolivar, C., Charcosset, H., Frety, R., Primet, M., Tournayan, L., Betizeau, C., Leclercq, G. and Maurel, R., J. Catal. 39, 249 (1975).

85. Bond, G. C. and Tripathi, J. B. P., JCS Faraday I 72, 933 (1976).

86. Ekstrom, A., Batley, G. E. and Johnson, D. A., J. Catal. 34, 106 (1974).

87. Frety, R., Charcosset, H. and Trambouze, Y., Ind. Chim. Belg. 38, 501 (1973).

88. Erre, R., Van Damme, H. and Fripiat, J. J., Surf. Sci. 127, 48 (1983).

89. Erre, R., Legay, M. H. and Fripiat, J. J., Surf. Sci. 127 69 (1983).

90. Gentry, S. J., Hurst, N. W. and Jones, A., JCS Faraday I, 77, 603 (1981).

91. Sancier, K. M., J. Catal. 23, 298 (1971).

92. Viswanath, R. P., Viswanathan, B. and Sastri, M. V. C., React. Kin. Catal. Lett. 2, 51 (1975).

93. Nowak, E. J. and Koros, R. M., J. Catal. 7, 50 (1967).

94. Nowak, E. J., J. Phys. Chem. 73, 3790 (1969).

95. Vannice, M. A. and Chou, P., ACS Symp. Ser. 298, 76 (1986).

96. Chou, P. and Vannice, M. A., Calorimetric Heat of Adsorption Measurements on Palladium. Part 2. Influences of Crystallite Size and Support on CO Adsorption., J. of Catal, 1987.

97. Chou, P. and Vannice, M. A., Calorimetric Heat of Adsorption Measurements on Palladium. Part 3. Influences of Crystallite Size and Support on O_2 Adsorption., J. of Catal, 1987.

98. Sen B., Chou, P. and Vannice, M. A., J. Catal., vol. 101, p. 517, 1986.

TABLE 1

(From Ref. 12)*

Hydrogen and CO Sorption at 25 ± 2 °C on TiO_2-Supported Metals

Metal	Redn temp, °C	H/M	CO/M	BET area, $m^2 g^{-1}$
2% Ru	200	0.23	0.64	45
	500	0.06	0.11	46
2% Rh	200	0.71	1.15	48
	500	0.01	0.02	43
2% Pd	175	0.93	0.53	42
	500	0.05	0.02	46
2% Os	200	0.21		
	500	0.11		
2% Ir	200	1.60	1.19	48
	500	0.00	0.0	45
2% Pt	200	0.88	0.65	
	500	0.00	0.03	
Blank TiO_2	150[a]	*b*		51
Support	500	*b*		43

[a] Evacuated for 2 h at 150 °C; no reduction prior to BET area determination. [b] H_2 uptake on these samples exhibited Henry's law behavior and was zero at $P_{H_2} = 0$ by extrapolation.

*Reprinted with permission, copyright ©, 1978, American Chemical Society.

TABLE 2

(From Ref. 14)*

Specific Activities of Ni/TiO_2 Relative to Other Ni Catalysts for the $CO-H_2$ Reaction[a]

Catalyst	N_{CO} ($sec^{-1} \times 10^3$)		N_{CH_4} ($sec^{-1} \times 10^3$)	
	H_2 (fresh)	H_2 (used)	H_2 (fresh)	H_2 (used)
1.5% Ni/TiO_2	500	1142	231	528
1.5% Ni/TiO_2 (100)[b]	16		7.4	
10% Ni/TiO_2	1607	2500	196	305
10% Ni/TiO_2 (100)[b]	90		11	
5% Ni/η-Al_2O_3	19.6	44	16.4	37
8.8% Ni/η-Al_2O_3	10.7	128	7	85
42% Ni/α-Al_2O_3	58	109	23.8	43
30% Ni/α-Al_2O_3	32.3	35	16.6	18
16.7% Ni/SiO_2	14.8	47	10.7	34
20% Ni/graphite	43.1	79	27.8	51
Ni powder	30	18	26.6	16

[a] Reaction conditions: 548°K (275°C), 103 kPa (1 atm), $H_2/CO = 3$.
[b] Calculated assuming 100% nickel metal exposed.

*Copyright ©, 1979, by Academic Press, Inc.

TABLE 3

(From Ref. 18)*

Kinetic Properties of Palladium Catalysts[a]

Catalyst	Rate (μmole CH_4/s · g cat.)	N_{CH_4} ($s^{-1} \times 10^3$) (b)	N_{CH_4} ($s^{-1} \times 10^3$) (c)	E_a (kcal mol^{-1})	Average particle size[c] (nm)
1.98% Pd/η-Al_2O_3 (C)	0.200	4.6	3.0	13.8 ± 0.6	3.2
(F) 2% Pd/Al_2O_3[d]	—	12	—	19.7 ± 1.6	4.8[e]
(G) 2% Pd/η-Al_2O_3[f]	0.125	3.1	3.2	19.2 ± 0.8	5.4
1.98% Pd/η-Al_2O_3	0.108	4.8	2.8	19.7 ± 1.3	5.7
(G) 2% Pd/Al_2O_3[d]	—	7.4	—	23.6 ± 1.9	8.2[e]
1.79% Pd/η-Al_2O_3	0.109	8.8	5.9	19.4 ± 0.7	10.2
(H) 9.5% Pd/Al_2O_3[d]	—	7.4	—	21.0 ± 0.8	12.0[e]
(H) 9.5% Pd/η-Al_2O_3[f]	0.257	3.2	4.0	24.5 ± 1.1	15.7
10.28% Pd/Al_2O_3 (S)	0.25	8.5	4.7	19.0 ± 1.0	20.0
10.28% Pd/Al_2O_3 (C, S)	0.09	5.1	2.2	22.8 ± 0.6	26.3
2.12% Pd/SiO_2–Al_2O_3	0.11	4.1	3.4	19.9 ± 0.3	7.0
(J) 4.75% Pd/SiO_2[d]	—	0.32	0.23	26.9 ± 1.8	3.1[e]
(K) 4.75% Pd/SiO_2[d]	—	0.26	—	—	4.9[e]
1.93% Pd/SiO_2	0.0013	0.12	0.11	27.7 ± 2.6	18.0
8.78% Pd/SiO_2 (C, S)	0.00103	1.0	0.34	19.2 ± 1.8	153
1.86% Pd/TiO_2 (448 K) Sample 1	0.168	4.1[g]	5.2[h]	19.7 ± 1.2	6.2[g]
Sample 2	0.187	4.5[g]	5.8[h]	22.4 ± 0.6	—
1.86% Pd/TiO_2 (SMSI) Sample 1	0.128	18 3.1[g]	32 4.0[h]	24.3 ± 1.9	—
Sample 2	0.187	27 4.6[g]	47 5.8[h]	23.6 ± 0.7	—

[a] T = 548 K, P_T = 1 atm, H_2/CO = 3.
[b] Based on $CO_{(ad)}$ on used sample.
[c] Based on $H_{(ad)}$ on used sample.
[d] Results previously reported in Reference (4).
[e] Based on $CO_{(ad)}$ on used sample assuming CO/Pd_s = 0.5.
[f] Results obtained in this study with fresh catalysts so designated in Reference 4.
[g] Based on $CO_{(ad)}$ on fresh, reduced sample.
[h] Based on $H_{(ad)}$ on fresh, reduced sample.

TABLE 4

(From Ref. 21)*

Kinetic Behavior of Platinum Catalysts[a]

Catalyst[b]	Rate $\left(\frac{\mu\text{mole } CH_4}{s \cdot g \text{ cat}}\right)$	$N_{CH_4}(s^{-1} \times 10^3)$ (c)	$N_{CH_4}(s^{-1} \times 10^3)$ (d)	E_a (kcal mole^{-1})	Diameter (nm) (c)	CO conversion range (%)
t/Al_2O_3						
1.75% Pt[h]		1.7		16.7	1.2	
A—2.1%						
I	0.134	1.7	3.5	16.2 ± 0.7	1.6	1.0–3.8
II	0.164	2.1	4.3	—	1.6	0.2–1.0
B—2.0%	0.040	1.6[e]	2.4[e]	16.5 ± 1.2	4.7[e]	0.2–1.0
E—10.0%	0.092	1.4	2.4	16.7 ± 1.0	8.7	0.3–1.3
D—2.0%	—	—	—	—	38	—
C—2.0%	0.0024	1.7	2.3	17.6 ± 0.8	80	0.03–1.0
F—10.0%	0.0028	0.73	1.0	18.6 ± 1.4	160	0.05–0.2
t/SiO_2						
J—2%	0.0084	0.14	0.31	—	1.9	<0.01
H—1.3%	0.0024	0.17	0.19	—	5.4	0.01–0.03
I—2%	0.0040	0.19	0.24	—	5.6	<0.01
G—1.5%	0.0016	0.19	0.19	16.8 ± 1.1	10	0.01–0.05
/SiO_2–Al_2O_3						
K—1.5%	0.029	1.4	1.6	16.4 ± 1.0	4.2	0.2–1.0
/TiO_2						
N—1.9% (LT)						
I	0.538	10.9	19	19.1 ± 0.6	2.2	2.6–16
II	0.737	14.9	26	20.3 ± 0.3	2.2	1.8–5.0
L—1.9% (LT)						
I	0.064	6.7	9.6	17.2 ± 0.7	11	0.4–1.8
II	0.081	8.4	12	19.0 ± 1.5	11	0.3–1.7
M—1.9% (LT)	0.084	14.5	29	—	19	—
P—1.9% (SMSI)						
I	0.564	59(11.3)[f]	120	20.6 ± 0.8	(2.2)	3.0–15
II	0.659	66(12.7)[f]	130	19.1 ± 1.6		0.7–4.2
O—1.9% (SMSI)						
I	0.150	54(16)[g]	110	17.7 ± 0.8	(11)	1.8–5.0
II	0.355	127(38)[g]	250	23.3 ± 3.2		0.8–4.9

[a] T = 548.2 K, P_T = 101 kPa, H_2/CO = 3.
[b] Roman numerals indicate different samples.
[c] Based on final $H_{(ad)}$.
[d] Based on final $CO_{(ad)}$.
[e] Based on initial $H_{(ad)}$.
[f] Based on final $H_{(ad)}$ on catalyst N.
[g] Based on final $H_{(ad)}$ on catalyst L.
[h] From Ref. 8.

TABLE 5

USE OF TiO_2 AS A SUPPORT REDUCED ETHANE HYDROGENOLYSIS ACTIVITY OVER METALS

(From Ref. 37)*

Specific Activities[a] for Ethane Hydrogenolysis at 205°C

Metal	SiO_2-supported[b]	TiO_2-supported[c]
Fe	1.2×10^{-5}	$<10^{-13}$
Co	3.4×10^{-5}	1.0×10^{-9}
Ni	8.0×10^{-4}	8.0×10^{-7}
Ru	1.8×10^{-3}	1.4×10^{-3}
Rh	2.2×10^{-4}	2.9×10^{-5}
Pd	6.7×10^{-10}	2.6×10^{-13}
Os	4.2×10^{-2}	9.6×10^{-4}
Ir	1.1×10^{-4}	3.0×10^{-7}
Pt	7.2×10^{-10}	$<10^{-13}$

[a] Expressed in units of moles of ethane converted/hr/m^2.
[b] Calculated from Ref. (4).
[c] Calculated from Table 1.

TABLE 6

THE SMSI STATE DECREASES ACTIVITY FOR CERTAIN REACTIONS

(From Ref. 36)*

Catalyst	Treatment (Temp. in °K)	Rate (mmol·H^{-1}·g metal^{-1})	
		C_6H_6 hydrogenation at 288 K	C_6H_{12} dehydrogenation at 523 K
4.8 Pt/TiO_2	H_2-523	40	1740
	H_2-523,O_2-273	56	----
	H_2-773	3.5	217
	H_2-773,O_2-273	29	1087
2.7% Ir/TiO_2	H_2-523	81	1400
	H_2-523,O_2-273	159	----
	H_2-773	0	304
	H_2-773 , O_2-273	18.5	----

TABLE 7

(From Ref. 14)*

Comparison of the Selectivity of Ni/TiO_2 to Other Ni Catalysts for the $CO-H_2$ Reaction

Catalyst	Reaction T (°K)	CO conversion (%)	mole% paraffin of each carbon number				
			C_1	C_2	C_3	C_4	C_{5+}
1.5% Ni/TiO_2	524	13.3	58	14	12	8	7
10% Ni/TiO_2	516	24	50	9	25	8	9
5% $Ni/\eta-Al_2O_3$	527	10.8	90	7	3	1	—
8.8% $Ni/\eta-Al_2O_3$	503	3.1	81	14	3	2	—
42% $Ni/\alpha-Al_2O_3$	509	2.1	76	1	5	3	1
16.7% Ni/SiO_2	493	3.3	92	5	3	1	—
20% Ni/graphite	507	24.8	87	7	4	1	—
Ni powder	525	7.9	94	6	—	—	—

TABLE 8

(From Ref. 16)*

Comparison of 10% Ni/COT and 10% Ni/P-25[a]

Catalyst	CO conversion (%)	Product distribution (mole%)						
		C_1	C_2	C_3	C_4	C_5	C_6	C_7+
10% Ni/COT	4.6	51.3	14.7	7.7	10.5	8.6	4.9	2.3
10% Ni/P-25	5.5	42.5	13.3	10.9	8.8	10.3	8.0	6.2

[a] T = 200°C, H_2/CO = 3, P = 101 kPa.

TABLE 9

(From Ref. 69)*

Effect of Titanium Oxide Deposited on Pt Surface

catalyst[a]	T_R, °C	BET surface area, $m^2\ g^{-1}$	irreversible adsorption, mol/g		TOF,[b] $s^{-1} \times 10^3$		E_a, kcal/mol	
			H_2	CO	CH_4	CO_2	CH_4	CO_2
Pt powder								
initial	500	0.5	2.6	4.0				
final	500	0.4	2.5	3.5	0.11	0.008	16	27
TiO_x/Pt (monolayer)								
initial	500		1.7	3.3				
final	500		1.7	3.1	0.41	0.12	25	38
TiO_x/Pt (multilayer)								
initial	200		1.4	0.9	18	11	22	31
final	500	0.9	0.9	1.6	4.2	2.6	23	29
1.5% Pt/SiO_2	450		4.1	8.0	0.17[c]		16.8	
1.9% Pt/TiO_2	200		24.7	28.0	13[c]		19.7[c]	
1.9% Pt/TiO_2	500		4.8	4.8	63[c] (12)[d]		20[c]	

[a] Final state is after completion of kinetic study. [b] Measured at 548 K, 100 kPa, $H_2/CO = 3$, based on H adsorbed on used sample. [c] Average values from ref 6. [d] Based on Pt_s measured after 200 °C reduction.

*Reprinted with permission, copyright ©, 1984, American Chemical Society.

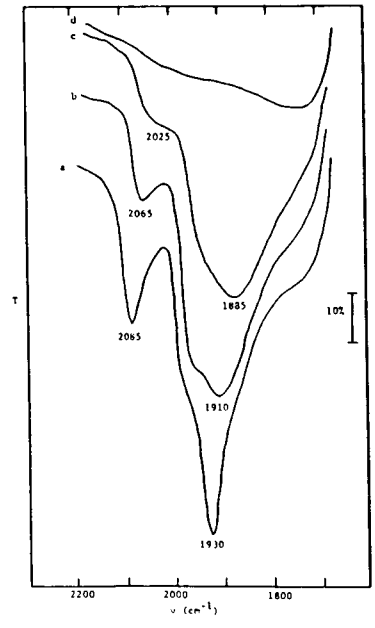

Spectra of CO adsorbed on 1.98% Pd/η-Al_2O_3: P_{CO} = 6.6 kPa, P_{He} = 92 kPa: (a) 300 K, (b) 428 K, (c) 548 K, (d) baseline in He at 300 K.

(A)

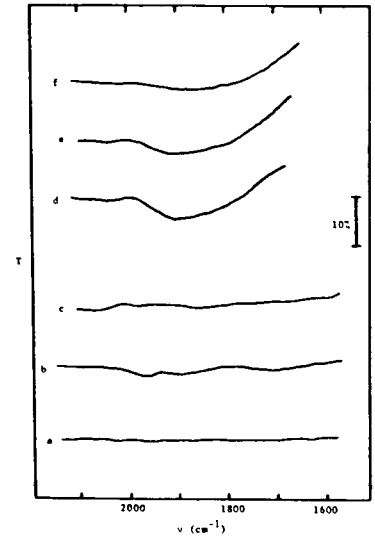

Spectra of CO adsorbed on 1.86% Pd/TiO_2 (SMSI): P_{CO} = 25 kPa, P_{H_2} = 75 kPa: sample 1: (a) 548 K, (b) 300 K, (c) baseline in He at 300 K; sample 2: (d) 300 K, (e) 373 K, (f) 548 K.

(B)

Figure 1. (From reference 18)*

*Copyright ©, 1981, by Academic Press, Inc.

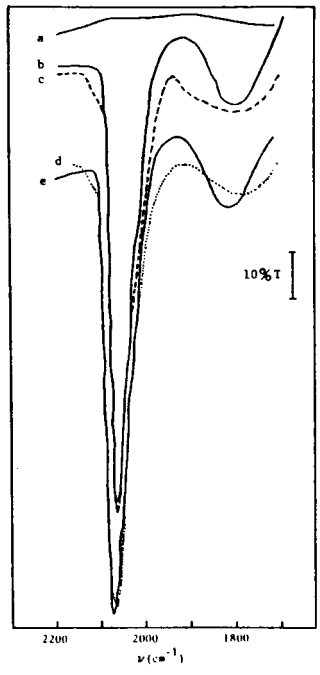

Infrared spectra of CO adsorbed on 1.5% Pt/SiO_2-Al_2O_3 (P_{CO} = 185 Torr, He/CO or H_2/CO = 3): (a) baseline in He, (b) 3000 K in H_2, (c) 548 K in H_2, (d) 548 K in He, (e) 300 K in He.

(A)

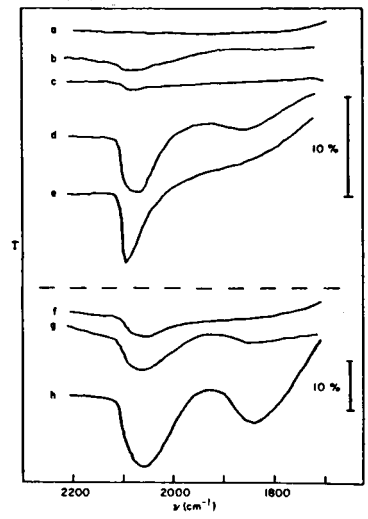

Infrared spectra of CO adsorbed on 1.9% Pt/TiO_2 (P_{CO} = 185 Torr, He/CO or H_2CO = 3): Catalyst O (SMSI)—(a) baseline in He at 300 K, (b) 300 K in H_2, (c) 548 K in H_2, (d) 300 K in He, (e) 548 K in He; Catalyst N (LT)—(f) 473 K in H_2, (g) 300 K in H_2, (h) 300 K in He. Note change in transmittance scale.

(B)

Figure 2. (From reference 20)*

*Copyright ©, 1983, by Academic Press, Inc.

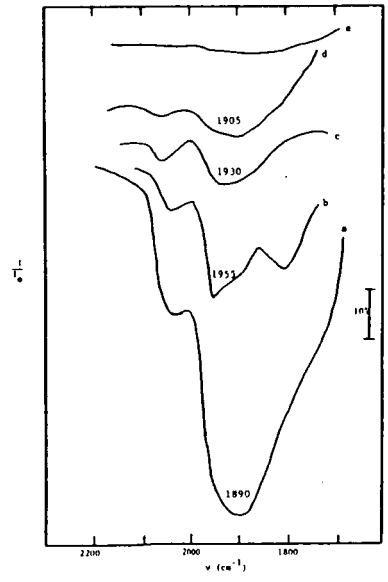

Relative intensities of CO adsorbed under reaction conditions; P_{Total} = 1 atm, H_2/CO = 3, T = 548 K. I_0 is the baseline intensity in pure H_2 at 548 K. (a) 1.98% Pd/η-Al_2O_3, (b) 1.93% Pd/SiO_2, (c) 2.12% Pd/SiO_2-Al_2O_3, (d) 1.86% Pd/TiO_2 (448 K), (e) 1.86% Pd/TiO_2 (SMSI).

Figure 3. (From reference 18)*

*Copyright ©, 1981, by Academic Press, Inc.

Pt Can Undergo Reversible Morphological Changes on Titania

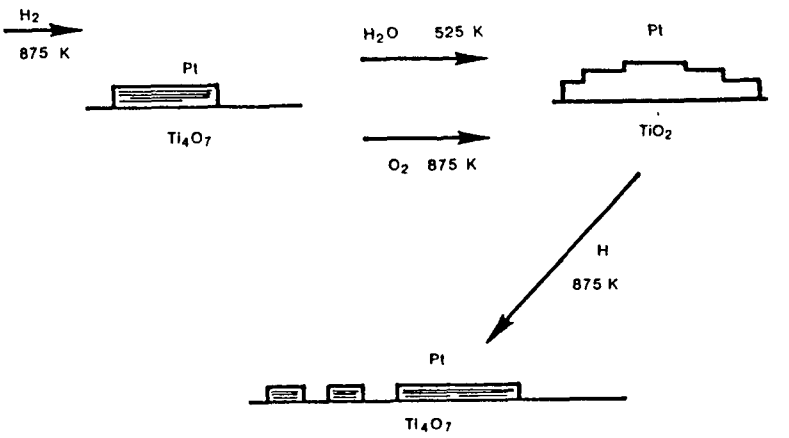

Figure 4. (From reference 33b)*

*Copyright ©, 1979, by Academic Press, Inc.

Evidence Indicates Electron Transfer Occurs from Titania to the Metal

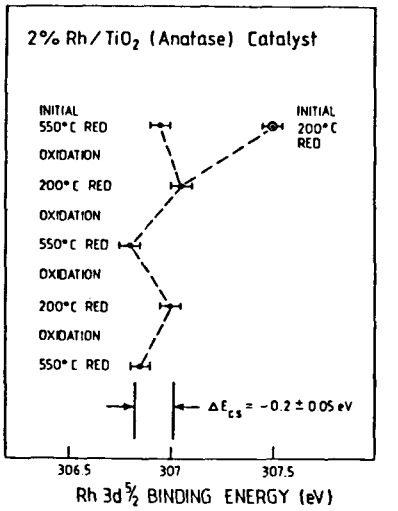

Binding energies of the Rh 3d 5/2 peak on a 2% Rh/TiO_2 catalyst after several cycles of reduction and oxidation. Initially reduction at 200 and 550°C produces a large $\Delta E_B = -0.6$ eV but this changes to −0.2 eV after an oxidation-reduction cycle.

Figure 5. (From reference 25)*

*Copyright ©, 1982, by Academic Press, Inc.

CONDUCTIVITY CHANGES INDICATE OXYGEN TRANSFER FROM TITANIA TO METAL

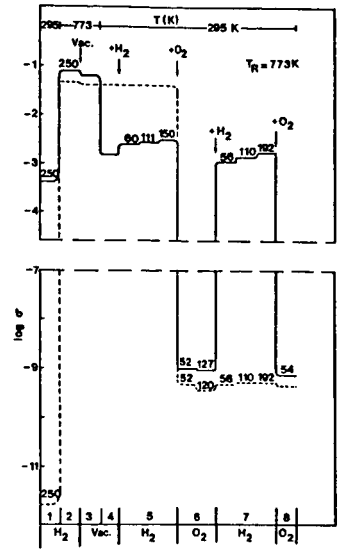

Logarithm of the electrical conductivity (in Ω^{-1} cm^{-1}) of TiO_2 (dotted line) and of the 5-Pt sample (solid line) reduced at 773 K in H_2 as a function of the different phases described in the text; the numbers on the curves indicate the pressures (in Torr) of the corresponding gas.

Figure 6. (From reference 29)*

*Copyright ©, 1982, by Academic Press, Inc.

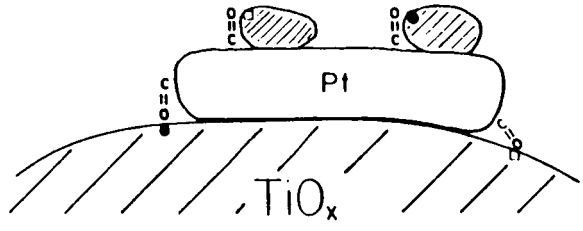

Proposed model for CO hydrogenation active sites in Pt–titania systems: (●) Ti^{3+} cation; (□) oxygen vacancy.

Figure 7. (From reference 69)*

*Reprinted with permission, copyright ©, 1984, American Chemical Society.

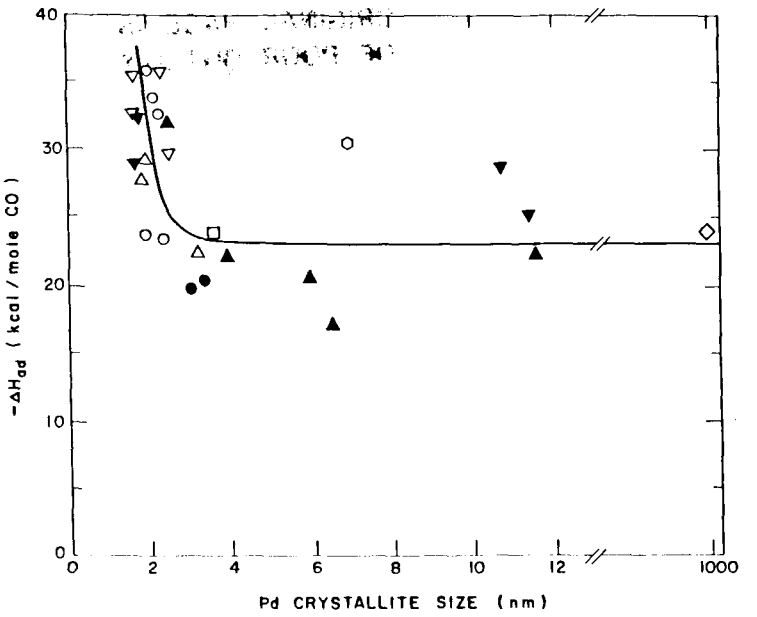

Heats of adsorption of CO on supported and unsupported palladium: Pd/SiO_2 (▼,▽), Pd/SiO_2-Al_2O_3 (▲,△), Pd/Al_2O_3 (●,○), Pd/TiO_2 (□,○), Pd powder (◇). Solid symbols: samples reduced at 673K; Open symbols: samples reduced at 573K or 448K.

Figure 8. (From reference 96)*

*Copyright ©, 1987, by Academic Press, Inc.

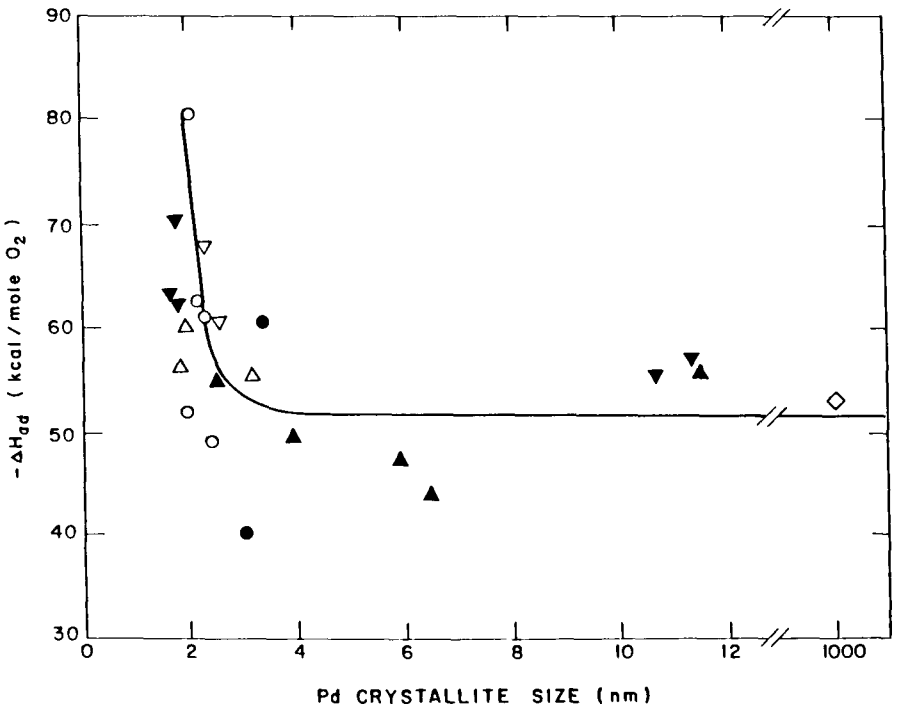

Integral heat of adsorption of oxygen on Pd at 300 K versus crystallite size : Pd/SiO_2 (▼,▽); Pd/SiO_2-Al_2O_3 (▲,△); Pd/Al_2O_3 (●,○); Pd powder (◇); Solid symbols -- T_r = 673 K, open symbols -- T_r = 448 K or 573 K.

Figure 9. (From reference 97)*

*Copyright ©, 1987, by Academic Press, Inc.

REACTION RATE OSCILLATIONS DURING CATALYTIC CO OXIDATION- A BRIEF OVERVIEW.

T. T. Tsotsis and R. C. Sane
Department of Chemical Engineering
University of Southern California
Los Angeles, California

INTRODUCTION

It is not our intent here to present a comprehensive review of the dynamic behavior of the catalytic oxidation of CO. This reaction is one of the most widely studied in the field of catalysis. A review paper by Engel and Ertl [1] has examined the basic kinetic and mechanistic aspects, and a comprehensive paper by Razon and Schmitz [2] was recently devoted to its dynamic behavior. Those interested in further study of the subject should consult these reviews and a number of general review papers on catalytic reaction dynamics [3-12].

Our goal is to present here a brief overview of certain interesting aspects of the dynamic behavior of this reaction and to discuss a few questions and issues, which are still the subject of study and debate.

(I) THE DYNAMIC BEHAVIOR OF THE CO OXIDATION REACTION

Interest in the dynamic behavior of catalytic reactions started in 1968, when for the first time Hugo [13] observed reaction rate oscillations during decomposition of N_2O over a CuO catalyst. Since then, interest in such phenomena has grown and other reactions have been shown to exhibit interesting dynamic behavior, such as simple and complex types of hysteresis behavior, isolas, single-peak, multipeak and chaotic oscillations, propagating waves and spatial patterns.

Among the reactions exhibiting such behavior, one finds industrially important systems such as NH_3 [14] and hydrocarbon [15] oxidations and Fischer-Tropsch synthesis over zeolite-type and other catalysts [16]. The system that has received the greatest attention is CO oxidation over Pt-type catalysts. To date, over eighty experimental and/or review papers have appeared [2] which deal with some aspect of its steady-state and dynamic behavior.

The early studies were primarily of a qualitative character. Compared to more recent studies, relatively little attention was paid to issues such as catalyst cleanliness and preparation techniques, purification of reactants and reactor materials, or to control and monitoring of operating conditions.

The issue of impurities in the gas phase reactant streams became of particular concern to workers in the area for the first time in 1976 [17]. During the 4th ISCRE meeting in Heidelberg, Eigenberger attempted to explain the reaction rate oscillations observed, during CO oxidation, by Beusch et al. [18] by a four

step kinetic scheme, which included CO and oxygen adsorption and desorption steps, a Langmuir-Hinshelwood surface reaction, and a slow buffer step involving an unidentified inhibitor. He pointed out that oscillations can result from the fact that the first three steps lead to multiple steady states for CO surface coverage at a fixed concentration of the unidentified inhibitor. The effect of the buffer step was to drive the value of CO surface concentration around a hysteresis loop. Eigenberger proposed gaseous oxygen as the so-called unidentified inhibitor, which reacts with the catalyst to create an inactive oxide species.

Experimental evidence of the role of gas phase impurities on the oscillatory behavior of this reaction appeared almost simultaneously. At the Sixth International Congress on Catalysis, in the discussion following the paper presented by Belyaev et al. [19], Jones reported that introduction of small amounts of TEP (triethylphosphate) triggered reproducible reaction rate oscillations during CO oxidation over a Pt wire. Similar observations were reported three years later by Gray and coworkers [20]. Jones et al. reported in 1977 [21] that oscillations were also triggered by the introduction of trace amounts of isopropyl methyl phosphofluoridate.

At about the same time additional experimental evidence was also presented by other groups apparently supporting the idea that trace amounts of impurities are primarily responsible for oscillations observed with CO oxidation. Cutlip, Kenney and coworkers [22,23] in their experiments over a 0.5% $Pt/\gamma-Al_2O_3$ catalyst for CO concentrations in the range of 0.5-3.0% and O_2 in the range 2-4% in Ar were unable to observe oscillations. They were, however, able to observe reproducible oscillations with a reaction mixture of 2% CO, and 3% O_2 and 1% Butene in Ar. Varghese et al. [24] reported a startling effect of hydrocarbon impurities on the oscillatory behavior in their system. Oscillations were observed, when an "impure" O_2 was used and disappeared when the "impure" O_2 was replaced by an "ultrapure" O_2. The only apparent difference between the "ultrapure" and "impure" O_2 was a 30 ppm impurity of hydrocarbons. Zhang [25] in 1980 reported that an aluminum coating on the inside reactor walls of the Illinois group [26,27] was the cause of the oscillations. The explanation advanced was that traces of a residual organic solvent entered the vapor phase.

Since then, and in contrast to the above, several published studies have reported oscillations for CO oxidation in the absence of gas phase impurities [28-30] several of them conducted under low-pressure or UHV conditions [31-37]. We have also considered the issue of gas phase impurities a few years ago [29] and attempted to duplicate Varghese's experiments. We found no effect of gas phase impurities in the O_2 stream, and oscillations were observed for both high and low purity O_2. Since then, experiments performed in our laboratories at intermediate and atmospheric pressure conditions (10^{-4} Torr - 1 atm) with elaborate purification techniques, in the absence of gas phase impurities (<1 ppm) and with spectroscopically clean catalyst surfaces have shown a variety of types of oscillatory behavior [28,37]. Based on our data and recent corroborating data of other groups we

concluded in a 1985 paper [28] that "gas phase impurities are not the prime cause for the experimentally observed oscillatory behavior of this system." The issue of gas phase impurities is, of course, by no means closed, and it goes beyond the narrow confines of the field of catalytic reaction dynamics. To quote Razon and Schmitz [2], "It would be legitimate to ask what is the maximum amount of impurities tolerable in an experiment? Absolute purity is impossible. Indeed workers cannot even agree on how to approach the control of impurities as far as catalyst treatment steps are concerned. If ultrapurity levels are required in order to obtain reproducible results, then what resource must chemical engineers take in designing and controlling catalytic reactors for real conditions."

One of the primary reasons that CO oxidation has received attention in the field of catalytic reaction dynamics is its rich dynamic behavior. For a large range of experimental conditions, the reaction exhibits hysteresis behavior, i.e. regions where multiple steady states are observed. The typical steady state behavior reported, in a CSTR flow reactor, is shown in Figs. 1 and 2. Such figures are called bifurcation diagrams, and the independent experimental variable the bifurcation parameter (gas-phase, catalyst temperature in Figs. 1 and 2). The hysteresis behavior in Fig. 1a is of a counter-clockwise type (clockwise when the diagram is plotted in terms of CO surface-coverage, i.e., absorbance, Figs. 1b, 2a, 2b). Counter-clockwise hysteresis behavior, with temperature as the bifurcation parameter, is typical for CO oxidation and contrasts this reaction with other reactions such as H_2 oxidation. Note that multiple steady states (hysteresis behavior) have been observed even under isothermal, low-pressure conditions (Figs. 2a, 2b). This is important because even simple (first order) reactions can exhibit hysteresis behavior under non-isothermal conditions.

When inlet gas phase CO concentration is used as the bifurcation parameter, the behavior, in the presence of temperature gradients between the solid and gas phases, can be very complex, as shown both by our group [28,37] and Harold and Luss [38]. The observed behavior is best summarized in terms of the bifurcation set for this system (see Fig. 3), which is constructed by plotting the ignition and extinction points from the bifurcation diagrams (Figs. 1, 2) as a function of the inlet gas phase concentration.

Fig. 3 is for CO oxidation at atmospheric pressure conditions over a $Pt/\gamma\text{-}Al_2O_3$ catalyst. The upper line is, of course, the line of ignition points. Notice that the line of extinction points has a maximum value. The presence of such maximum implies interesting bifurcation behavior shown schematically in Fig. 4. Note in Fig. 4 steady states not directly connected to the main steady-state branch. The only way these states, commonly referred to as "isolas", can be accessed experimentally is by large perturbations in the operating variables. The behavior shown schematically in Fig. 4 was observed experimentally both by our group [37] and by Harold and Luss [38]. Under isothermal conditions, the maximum in the extinction line disappears and one is left with the clockwise hysteresis behavior [37].

In Figs. 1, 2, 4 there are at most two stable steady states.

This is the behavior reported by most studies of CO oxidation. There are, however, studies [25,38,39] reporting the existence of three stable steady states (five in total). Under non-isothermal conditions three stable states are, in principle, possible for this reaction [40]. In two of the above studies the authors have attributed the existence of three stable states to other causes. Hegedus et al. [39], who performed their experiments in an integral reactor, cite diffusional limitations. Zhang [25] implicates temperature non-uniformities along his Pt ribbon.

CO oxidation has also been shown to exhibit various types of oscillatory behavior. Both single peak and multipeak regular (regular meaning oscillations having a periodic pattern) oscillations have been observed. Several studies report relaxation-type oscillations (Fig. 5) characterized by sudden sharp changes in reaction rate (bursts), followed by periods of relatively constant behavior.

Aperiodic or "chaotic" oscillations have also been reported. The term "chaotic" has been used rather loosely, as Razon and Schmitz have observed [12], to describe oscillations that appear not to have a repeat pattern. Until Razon et al. [41] recently calculated the fractal dimension of the chaotic (strange) attractor they observed for CO oxidation, no analysis had been done to show that the reported aperiodic behavior did indeed conform to the mathematical definition of chaos.

(II) THE MECHANISM RESPONSIBLE FOR OSCILLATIONS

Even amidst the early excitement of discovering new types of dynamic behavior, there were efforts to understand the mechanistic basis for oscillations. There were also hopes that the newly discovered dynamic phenomena would eventually enable one to discriminate amongst rival mechanisms for CO oxidation and other catalytic reactions, in situations where steady-state data cannot. The success of our efforts in this direction is still subject to debate.

As is often the case, most of the initial efforts to understand the causes of rate oscillations and hysteresis behavior for CO oxidation and other catalytic reactions were somewhat misguided. Little experimental data were available, most of it of questionable quality by today's standards. The first effort to bring a sense of order into the fairly confused state of affairs was made by Scheintuch and Schmitz [4]. They critically examined many of the proposed mechanisms for the oscillatory behavior of CO oxidation. Most of these failed the test because they were not able to predict oscillations for realistic values of experimental parameters and/or conditions. The serious reader should consult this work. Most of the mechanisms subsequently proposed to explain oscillations for CO oxidation and other catalytic reactions can either be found in this work or traced back to it.

By the late seventies, it became clear to most workers in the field that if a mechanism for oscillations was ever to be found, elaborate experiments would have to be performed, in which the catalyst surface state would be monitored in situ, during oscillations. Two research groups engaged in this approach and in 1982 almost simultaneously reported their findings on CO oxidation

over supported Pt [29,42]. In these studies IR Transmission Spectroscopy was employed to monitor the catalyst surface during oscillations. A number of issues heretofore unsettled were clarified at this point, not the least of which was the question of whether surface processes were at all responsible for oscillations. Some of the previously suggested mechanisms were put to test and found to fail, for example, that an Eley-Rideal mechanism was responsible for the oscillations [4], that long period oscillations result from a slow interconversion process between bridge and linear adsorbed CO [43] etc. For further details, the reader should consult the original and follow-up publications by the above groups [28,30,37] and others [44] who have since used the same techniques to study the dynamic behavior of the CO oxidation.

The year 1982 also marked the appearance of the first paper [32] in a series [32-36] by Ertl and coworkers, on the dynamics of CO oxidation over Pt single crystals. In their kinetic studies of CO oxidation over Pt(100) using a scanning LEED technique and work function measurements, they observed rate oscillations for a wide range of experimental conditions. They attributed these to a reversible phase transition of the surface structure of Pt(100) between phases (i.e., hex ⟷ 1×1), which both have distinctly different properties towards CO adsorption and oxidation. It was not clear in the beginning, whether this transition was the cause or the outcome of the observed rate oscillations. There were also a number of other questions. Ertl and coworkers have since then, however, refined their mechanistic ideas on low-pressure CO oxidation over Pt(100), culminating with an excellent recent publication [36]. Their proposed mechanism for low-pressure oscillations over Pt(100) single crystals is today well accepted. But what about the oscillations observed at high pressures, where such a phase transition does not occur, or with other crystal planes, which do not undergo such a phase transition? For example, Yeates et al. [45] have observed reaction rate oscillations during CO oxidation over Pt(100), Pt(111) and Pt(13,1,1) crystals at high pressures. What about reaction rate oscillations observed on supported Pt catalysts? The issues here are certainly not resolved.

Our own group has been primarily involved with the study of the dynamics of CO oxidation over supported Pt catalysts. We have observed [27,28,37], both in the so-called "pressure-gap" region and under atmospheric conditions, that at least two types of adsorbed oxygen exist on supported Pt, with different physical and chemical characteristics. It appears that a species responsible for a CO adsorbance band around 2120 cm^{-1} (also observed by other investigators [46-48] and attributed to either CO adsorbed with oxygen atoms on Pt or CO adsorbed on oxidized Pt) is practically inert towards CO oxidation. As such, the formation and reduction of this species is a prime candidate for the slow mechanistic buffer step originally suggested by Eigenberger [17] and since then repeatedly mentioned in the literature as necessary for the generation of reaction rate oscillations. That this is the case is shown in Fig. 5. Note that the 2120 cm^{-1} band oscillates in phase with both the 2060 cm^{-1} (the band corresponding to linearly

adsorbed CO) and the conversion. Note furthermore that both the conversion and the 2060 cm^{-1} band show multipeak oscillatory behavior, characterized by long period relaxation oscillations with superimposed oscillations of small period, the same order of magnitude as the reactor residence time. On the other hand, the 2120 cm^{-1} band shows only large period and apparently more regular oscillations. Such observations are direct evidence of multiple time scale phenomena and are in accord with the theoretical investigations, by Chang and Aluko [49].

There is additional experimental evidence [28,37] on the role of the 2120 cm^{-1} band in the generation of (large period) oscillations during CO oxidation over $Pt/\gamma\text{-}Al_2O_3$. We have observed, in agreement with Sarkany and Gonzalez [50] and Cant [51], that the 2120 cm^{-1} band forms to any appreciable extent only on catalysts with high metal dispersions and small Pt crystallites. In our experiments, we have been unable to observe long period oscillations during CO oxidation on any catalyst not forming a 2120 cm^{-1} band. On the other hand, catalysts that show oscillations, cease to exhibit any oscillations when they lose (by controlled sintering) the ability to form the 2120 cm^{-1} band. At the risk of sounding repetitious, it should be emphasized that the idea that formation and reduction of an "inactive" surface oxide is responsible for oscillations is neither original nor is specific to CO oxidation. Dating from Eigenberger's work, it has been the central theme of several theoretical investigations. Yeates et al. [45] proposed (but did not establish experimentally) the same mechanism for oscillations of CO oxidation at high pressures over single crystal and polycrystalline Pt catalysts. After all, the slow formation and reduction of an inactive surface oxide is probably the most plausible (the hex ⇄ 1×1 transition for Pt(100) notwithstanding) mechanistic scheme to explain phenomena like the oscillations observed in CO oxidation, which are characterized by (long) periods orders of magnitude larger than the reactor residence time and the time constants typical of adsorption and reaction. It is well established [48] by now that noble supported catalysts do form inactive (at least towards CO oxidation) oxides both under intermediate and high (atmospheric) pressure conditions. The issues are, however, not very clear for single crystal and polycrystalline Pt catalysts, where the formation of similar oxide species has been attributed to bulk Si (and Al) impurities [2,28,37,45].

There is still much confusion surrounding the above issues. When it comes to explaining the oscillations, during CO oxidation, the need to postulate slow steps, such as a hex ⇄ 1×1 transition or the slow formation and reduction of an oxide, arises from the clear difference between the time scales characterizing the oscillations (long periods) and the other plausible physico-chemical processes. If the oscillations observed with CO oxidation were of higher frequency, there would be no need to postulate slow mechanistic steps. There are many plausible causes ranging from the fluid mechanics of the process, the presence of diffusional limitations and nonisothermal phenomena to the existence of macroscopic roughness on the catalyst's surface (for polycrystalline catalysts) that could give rise to such

oscillations [12]. The theoretical work of Chang and Aluko [49] should be very informative to anyone interested in further study on the subject.

When it comes to reaction rate oscillations observed for CO oxidation over supported catalysts, especially under isothermal and low-pressure conditions, there still remains a question for which there is no answer at present. For the catalyst to exhibit the observed type of behavior (oscillations, multiple steady states), there must be absolute synchronization in the behavior of all crystallites. The means of such perfect communication among the different crystallites still remains a mystery.

(III) FUTURE WORK

What the future should hold for further studies of the dynamics of CO oxidation and other catalytic reaction dynamics is probably a matter of personal predilection. There are, for example, those who find it difficult to accept that two or more mechanisms are needed to (or can possibly) explain the same type behavior (oscillations) for the same reaction (CO oxidation). For those, who have dealt with the complexities and peculiarities of non-linear systems, catalytic reactions being a prime example, this presents no conflict.

Resolving the issue of perfect communication among crystallites on a supported catalyst during oscillations will certainly occupy the thoughts and work of many. So also will efforts to understand and mathematically model new phenomena, such as propagating waves, chaos, and the phenomena resulting from external forcing of such reaction systems, which are, by themselves, intrinsically unstable.

The field is currently being shaped by two diametrically opposing forces. On one side, the newly observed phenomena are becoming more complex and the mathematical techniques and concepts required to model them are becoming progressively more difficult and esoteric. On the other hand, the experimental surface techniques needed to design and perform new and meaningful experiments are also rapidly becoming more complex, elaborate and expensive. In the face of current trends, the future probably holds little hope for the single investigator and further progress will require well-equipped and funded multidisciplinary efforts.

REFERENCES

1. T. Engel and G. Ertl, Adv. Catal., **28**, 1(1979).
2. L. F. Razon and R. A. Schmitz, Catal. Rev.-Sci. Eng., **28**(1), 89(1986).
3. R. A. Schmitz, Adv. Chem. Ser., **148**, 156(1975).
4. M. Sheintuch and R. A. Schmitz, Catal. Rev.-Sci. Eng., **15**(1), 107(1977).
5. V. Hlavacek and J. Vortruba, Adv. Catal., **27**, 59(1978).
6. M. G. Slinko and M. M. Slinko, Catal. Rev.-Sci. Eng., **17**, 119(1978).
7. G. Eigenberger, Chem. Ing. Tech., **50**, 924(1978).
8. M. G. Slinko and M. M. Slinko, Usp. Khim., **49**, 561(1980).
9. V. Hlavacek and P. van Rompay, Chem. Eng. Sci., **36**, 1587(1981).

10. M. M. Slinko and M. G. Slinko, Kinet. Katal., **23**, 1421(1982).
11. R. A. Schmitz, G. A. D'Netto, L. F. Razon and J. R. Brown, in: Chemical Instabilities, Eds. G. Nicolis and F. Baras (Reidel Dordrecht 1984) p. 33.
12. L. F. Razon and R. A. Schmitz, Chem. Eng. Sci., accepted 1986.
13. P. Hugo, in: Proc., 4th European Symp. Chem. React. Eng., Brussels, 1968, p. 459.
14. M. Flytzani-Stephanopoulos, L. D. Schmidt and R. Caretta, J. Catal., **64**, 346(1980).
15. C. G. Vayenas, B. Lee and J. Michaels, J. Catal., **66**, 36 (1980).
16. T. T. Tsotsis, V. U. S. Rao and L. M. Polinski, AIChE J., **29**, 847(1982).
17. G. Eigenberger, in: Proc 4th Inter. Symp. Chem. React. Eng., Heidelberg, 1976, p. 290.
18. H. Beusch, P. Fieguth and E. Wicke, Advan. Chem. Ser., **109**, 615(1972).
19. V. D. Belyaev, M. M. Slinko amd M. G. Slinko in: Proc. 6th Inter. Congr. on Catalysis, London, 1976, p. 758.
20. P. Gray, J. F. Griffiths and J. S. Rogerson, Joint ASME/AIChE 18th National Heat Transfer Conference, San Diego, 1979.
21. T. Lamb, R. P. Scott, P. Watts, B. Holland, S. J. Gentry and A. Jones, J. Chem. Soc. Chem. Comm., **23**, 882(1977).
22. M. B. Cutlip and C. N. Kenney, Am. Chem. Soc. Symp. Ser., **65**, 475(1978).
23. D. Mukesh, C. N. Kenney and W. Morton, Chem. Eng. Sci., **38**, 69(1983).
24. P. Varghese, J. J. Carberry and E. E. Wolf, J. Catal., **55**, 76(1978).
25. S. X. Zhang, PhD. Thesis, University of Illinois, Urbana (1980).
26. R. T. Plichta and R. A. Schmitz, Chem. Eng. Comm., **3**, 387(1979).
27. M. Scheintuch, AIChE J., **27**, 20(1981).
28. T. H. Lindstrom and T. T. Tsotsis, Surf. Sci., **150**, 487(1985) and **146**, L569(1984).
29. A. El-Haderi and T. T. Tsotsis, Am. Chem. Soc. Symp. Ser., **196**, 77(1982).
30. D. J. Kaul and E. E. Wolf, J. Catal., **91**, 216(1985) and **93**, 321(1985).
31. D. Barkowski, R. Haul and U. Kretschmar, Surf. Sci., **107**, L329(1981).
32. G. Ertl, P. R. Norton and J. Rustig, Phys. Rev. Letters, **49**, 177(1982).
33. M. P. Cox, G. Ertl, R. Imbihl and J. Rustig, Surf. Sci., **134**, 517(1983) and Phys. Rev. Lett., **54**, 1725(1985).
34. P. R. Norton, P. E. Bindner, K. Griffiths, T. E. Jackman, J. A. Davis and J. Rustig, J. Chem. Phys., **80**, 3859(1984).
35. G. Ertl, Surf. Sci., **152/153**, 328(1985).
36. R. Imbihl, M. P. Cox and G. Ertl, J. Chem. Phys., **84**(6), 3519(1986).
37. T. H. Lindstrom and T. T. Tsotsis, Surf. Sci.,

171, 349(1986) and **167**, L194(1986).
38. M. Harold and D. Luss, Chem. Eng. Sci., **40**, 39(1985).
39. L. L. Hegedus, S. H. Oh and K. Baron, AIChE J., **23**, 632(1977).
40. T. T. Tsotsis, A. El-Haderi and R. A. Schmitz, Chem. Eng. Sci., **37**, 1235(1982).
41. L. F. Razon, S. Chang and R. A. Schmitz, Chem. Eng. Sci., **41**, 1561(1986).
42. E. E. Wolf, D. Kaul and R. Ramsey, paper presented at AIChE National Meeting, Los Angeles, 1982.
43. P. Hugo and M. Jakubith, Chem. Ing. Tech., **44**, 383(1972).
44. V. A. Burrows, S. Sundaresan, V. J. Chabal and S. B. Christmann, Surf. Sci., **160**, 122(1985).
45. R. C. Yeates, J. E. Turner, A. J. Gellman and G. A. Somorjai, Surf. Sci., **149**, 175(1985).
46. M. Primet, J. M. Basset, M. V. Mathien and M. Prettre, J. Catal., **29**, 213(1973).
47. H. Heyne and F. C. Tompkins, Proc. Roy. Soc. (London), **A292**, 460(1966).
48. R. K. Herz and E. J. Shinouskis, Appl. Surf. Sci., **19**, 373(1984).
49. H. C. Chang and M. Aluko, Chem. Eng. Sci., **39**, 37(1984) and **39**, 51(1984).
50. J. Sarkany and R. D. Gonzalez, Appl. Catal., **5**, 85(1983).
51. N. W. Cant, J. Catal., **74**, 411(1982).

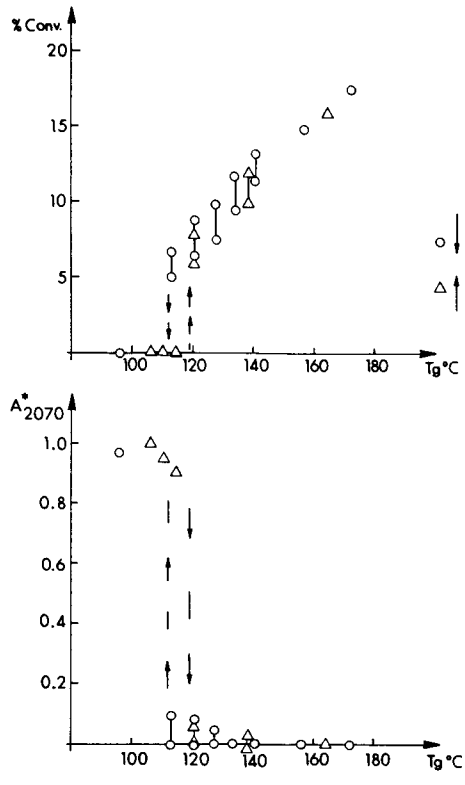

1. Bifurcation diagrams for the CO oxidation over $Pt/\gamma\text{-}Al_2O_3$ in a CSTR, at atmospheric pressures: (a) % conversion versus T_g (gas phase temperature); (b) normalized absorbance ($2070\ cm^{-1}$) versus T_g. From [28].*

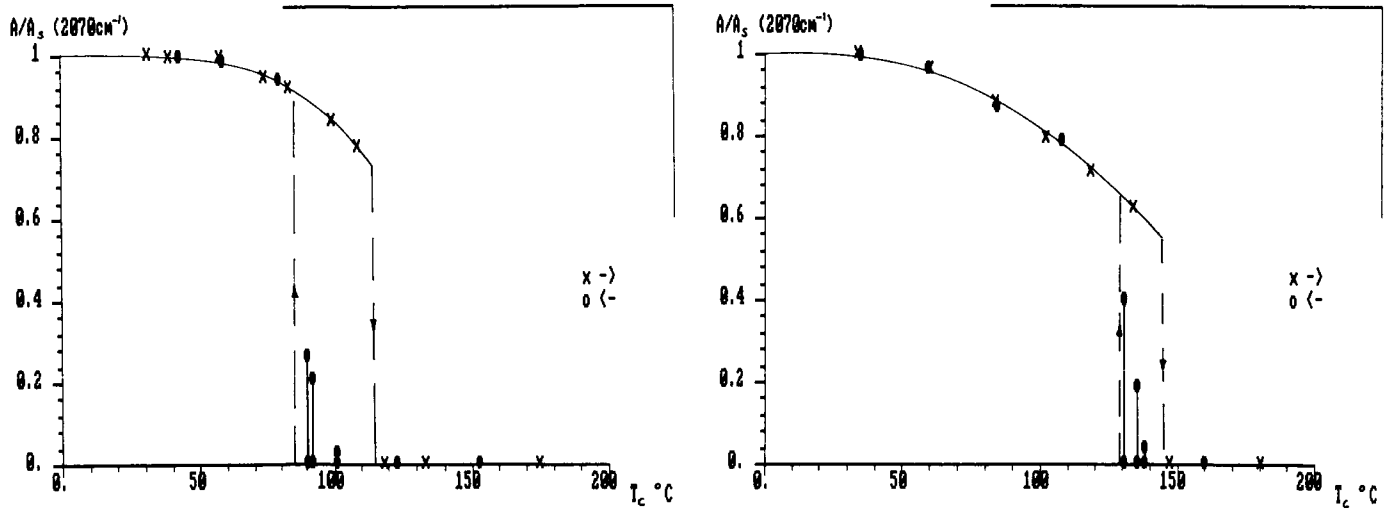

2. Bifurcation diagrams for the CO oxidation in the "pressure-gap" region. Normalized absorbance versus T_c (catalyst temperature): (a) P_t (total pressure) = 2.1 Torr; (b) P_t = 10 Torr. From [37].*

*Reprinted with permission of Elsevier Science Publishers, B.V.

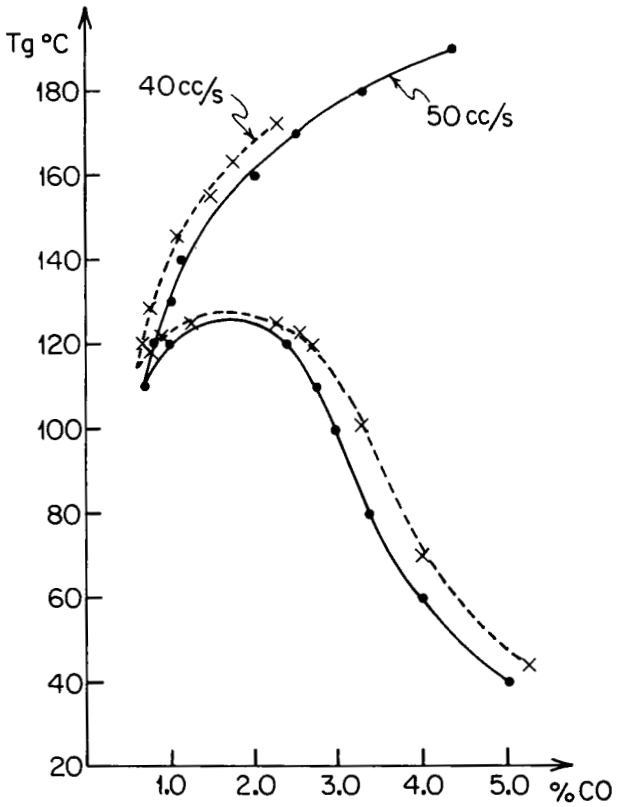

3. Bifurcation set for CO oxidation at atmospheric pressures. T_g versus %CO in inlet stream. From [28].*

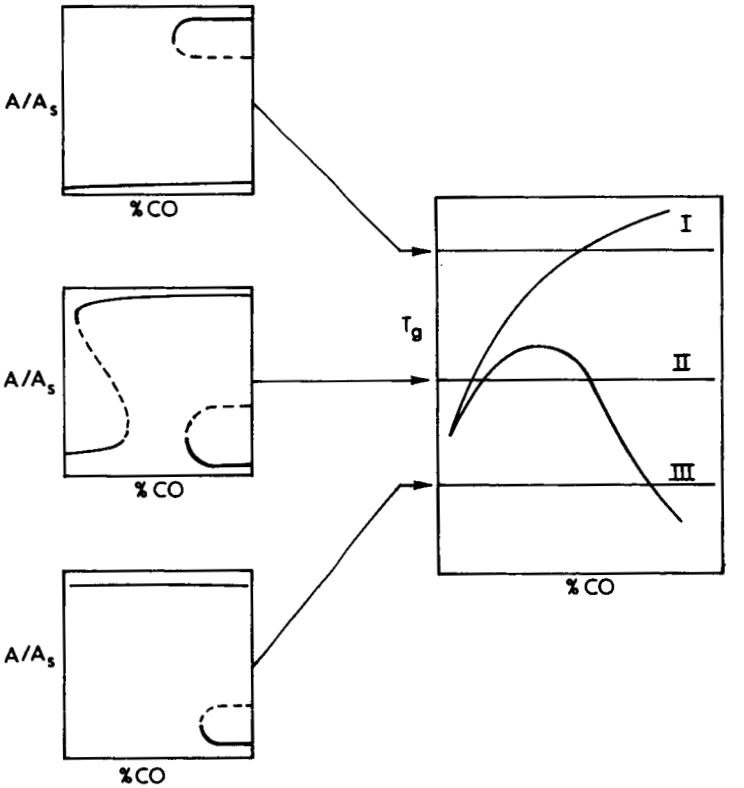

4. Schematic of the bifurcation set and the bifurcation diagrams for CO oxidation. From [28].*

*Reprinted with permission of Elsevier Science Publishers, B.V.

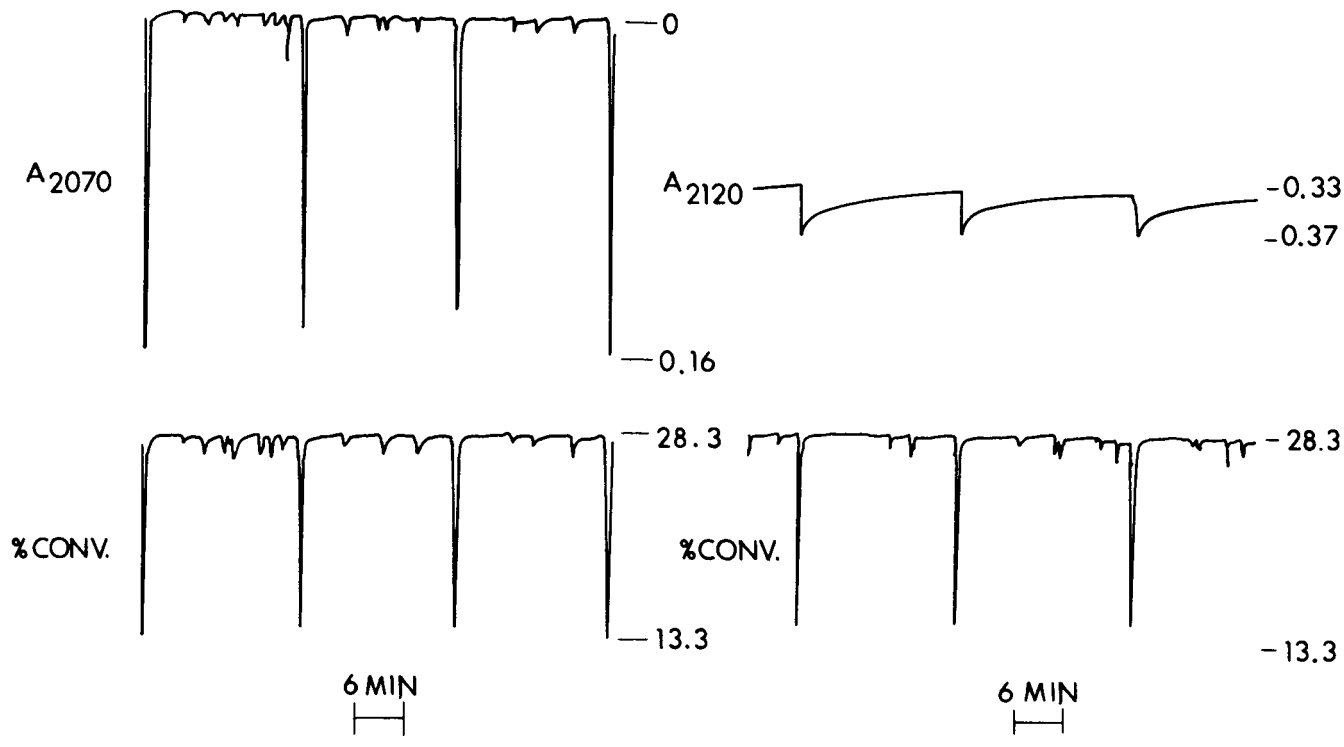

5. Conversion and surface concentration oscillations during CO CO oxidation over Pt/γ-Al_2O_3 in a CSTR at atmospheric pressures. From [28].*

*Reprinted with permission of Elsevier Science Publishers, B.V.

N87-20535

CHARACTERIZATION OF THE LTC CATALYST:

PERFORMANCE AGAINST COMMON AIR POLLUTANTS

Marcia F. Collins
Research & Development, Teledyne Water Pik
Fort Collins, Colorado

SUMMARY

One of the important qualities of the LTC* catalyst is the rapid oxidation of carbon monoxide to carbon dioxide under a wide variety of conditions. The catalytic material is a palladium-copper activated complex which reacts with various contaminant molecules through a continuous oxidation/reduction cycle. The alumina substrate enhances LTC activity with its favorable surface chemistry and very high surface area. About 10 percent surface water is necessary to facilitate the oxidation of CO. This reaction shows a log-log dependence on contact time, suggesting a Langmuir-Hinshelwood mechanism.

In the tube tests, LTC removed 90 to 100 percent of contaminating carbon monoxide in the temperature region of 20° to 400°C, and at ambient over a range of 25 to 65 percent relative humidity. In contrast, NO_2 is chemisorbed by the LTC/alumina material--the amount strongly dependent on temperature increases but independent of humidity.

Performance tests in the Instapure® Air Filtration appliance were done in a sealed room using 300 cfm air flow rate. The CO was 78 percent removed, O_3 100 percent removed, SO_2 and H_2S 100 percent, NH_3 58 percent, NO_2 40 percent, and benzene 8 percent removed. The CO from sidestream tobacco smoke was 34 percent removed by the appliance. Hazardous components of mainstream tobacco smoke were effectively reduced using a small ancillary filter containing LTC.

The LTC catalyst has demonstrated excellent capability to remove an important variety of hazardous pollutant gases which are common factors to poor indoor air quality. The Instapure® Air Filtration System incorporates the LTC catalyst in a 50:50 mixture with activated carbon to effectively remove particulate, odors, and hazardous gages at room temperature and humidities. The ability to remove hazardous gases is unique for the category of portable air filtration equipment. The wide variety of pollutant gases that LTC removes suggests the catalytic technology is adaptable to a considerable range of commercial and industrial applications.

INTRODUCTION

The Environmental Protection Agency has been conducting various studies of indoor air contaminants and their exposure effects.[1,2,3] These results and others indicate that personal exposure to specific pollutants is often significantly greater than outdoor exposure limits. Tightening up of residences for reasons of energy conservation, greater use of synthetic materials in building and furnishing interiors, tobacco smoking, and increased use of solvents all are major contributors to the deterioration of indoor air quality.

---

*Low-Temperature Catalyst (LTC).

Most individuals spend up to 90 percent of their time indoors; about 70 percent is in residential and office environments. The various types of pollutants--as particulate, or harmful gases--have been linked to ill health effects. Currently, the most controversial issue is the effect of sidestream tobacco smoke on non-smokers in the same environment.

As reported in an earlier paper,[4] Teledyne Water Pik has developed a novel room temperature catalyst (LTC) for removal of various gaseous contaminants. In particular, this catalyst oxidizes carbon monoxide to carbon dioxide at very efficient rates. It also has shown good rates of removal for ozone, nitrogen and sulfur oxides, hydrogen sulfide, ammonia, and certain toxic components of cigarette smoke.

LTC CATALYST MATERIAL

In general, the LTC catalyst consists of a solution of copper and palladium salts deposited on a porous alumina substrate. It appears that this substrate material provides a certain enhancement of catalytic activity due to its specific surface chemistry, as well as large surface area for dispersion of the LTC composition. Also a minimum of post-deposition water content, tightly held by the alumina, is necessary to achieve reasonable rates of catalytic efficiency.

Reaction Mechanism

The reaction of LTC with carbon monoxide is analogous to the Wacker commercial process for producing actaldehyde.[5] The oxidation-reduction cycle requires exchange of electrons between the copper and palladium metals of the complex; water is both consumed and returned to the catalytic cycle.

A simplified diagram of this reaction is shown in Figure 1. The deposits of metal salts contain activated complexes which create sites for selective chemisorption of oxygen and carbon monoxide. Present theory holds that "islands of atomic oxygen are adsorbed, surrounded by carbon monoxide molecules and that the oxidation reaction occurs at their interface.[6] The rate of reaction is determined by the catalyst's efficiency.

LTC Activated Complex

Several simple tests imply the formation of a palladium-copper complex, probably stabilized by surrounding anions. This complex is the active species which is responsible for catalytic rates of CO oxidation to CO_2.

A "catalyst" made with only the palladium salt--all else equal--was able to achieve 50 percent CO removal under standard tube test conditions. Likewise, a "catalyst" containing the two copper salts gave only 15 and decaying to 4 percent CO removal. The LTC combination of these three salts consistently removes greater than 85 percent CO.

A series of tests using stepwise additions of the metal salts constituents in various sequences (same final composition) clearly shows the best CO removals occur with the simultaneous deposit of the LTC composition.

SPECIFICATIONS FOR PERFORMANCE TESTS

Tube Test for Catalytic Activity

A one gram sample of LTC catalyst is packed in a glass tube to minimize by-pass and exposed to feed gas flow of known concentration in a single contaminant. Relative humidity in the feed stream may be varied from 10 to 90 percent, while temperature is unregulated ambient. Typical test conditions are 50 parts per million of carbon monoxide and 60 percent relative humidity at a flow rate of 500 cc/minute. The difference in CO concentration between feed gas passed over untreated substrate alumina beads versus over the LTC catalyst measures activity, which can be monitored over time. Equilibrium removal rates are the percentage of pollutant concentration lost after 6 hours. The standard deviation of 8 repetitive test results was a satisfying 2.1.

The actual amount of contaminant removed, of course, depends on physical parameters--the amount of LTC, the size and thickness of the catalyst bed, gas flow rate, length of testing, and initial concentration of contaminant CO. Time of contact with LTC reflects the former variables and is calculated from:

$$\ln (C_o/C_t) = K \cdot t_c \qquad (1)$$

Assuming a first-order reaction rate (oxidation of CO to CO_2), C_t is the contaminant concentration at some time t, C_o is the initial concentration, K is the reaction rate constant, and t_c is contact time. In reality, the reaction rate also varies with the amount of surface coverage of oxygen and carbon monoxide, therefore a first-order reaction scheme is a considerable simplification. The reaction constant is characteristic of catalyst material, independent of test procedures. For example, an LTC catalyst with an equilibrium CO removal rate of 93 percent has a calculated K of about 12 seconds^{-1}.

Room Test of Air Filtration Appliance

The second type of performance test measures contaminant removal in a sealed room, using the LTC catalyst filter in our air filtration appliance. Filters were designed to hold about 230 grams of LTC catalyst in a thin bed with minimal air flow by-pass. This test is conducted in a 1008 cubic foot stainless-steel room with an initially known amount of gaseous contaminant. The rate of decay is subtracted from the performance of the appliance. Air flow through the appliance was 300 cfm for the test duration of 2 hours. The standard deviation of 7 repetitive test results was an excellent 1.4.

TUBE TEST PERFORMANCE

Temperature Dependence

The temperature dependence of LTC performance has been reported previously,[4] but a brief description is included for completeness. Figure 2 maps results of a series of tests for CO removal of LTC at various temperatures. Between room temperature and about 400°C, CO oxidation ranges between 90 and 100 percent. Below about 65°F, the reaction rate drops off sharply, probably as a result of increased dissipation of the heat of reaction.

In contrast, the physical adsorption of NO_2 decreases as the temperature increases. Near 100 percent adsorption occurs between -50° and 25°C, gradually decreasing to 50 percent at 175°C.

Relative Humidity Dependence

The dependence of LTC activity on relative humidity was also reported previously,[4] and is illustrated in Figure 3. The CO oxidation is optimum between about 25 to 70 percent relative humidity. Inadequate water present inhibits the reaction at interfaces of adsorbed "island oxygen" and surrounding CO molecules. Too much moisture fills the micropores of the alumina, effectively "drowning" these active metal deposits.

The physical adsorption of NO_2 is unaffected by humidity, presumably because most of the chemisorption is on the surface of the LTC/alumina bead and in the macropores. A common commercial material, Hopcalite, is severely poisoned by water vapor; it is ineffective above 10 percent relative humidity.

Contact Time

One of the physical parameters which strongly affects the LTC rate of CO oxidation is the time that the contaminant is in contact with the catalyst. Table I shows data for contact times of 0.4 to 0.01 second, achieved by varying the gas flow rate (5 to 0.5 Lpm) and/or the bed depth of LTC packed in the tube. All tests were conducted at room temperature and 60 percent relative humidity with 50 parts per million CO.

TABLE I
Effect of contact time on CO oxidation.

Contact Time (Sec.)	Bed Depth (Inches)	% Average CO Removal
0.4	1.0	84
0.2	0.5	52
0.1	0.5	30
0.08	0.4	28
0.05	0.25	14
0.025	0.25	7
0.01	0.25	2

Although Equation 1 postulates a log-linear plot, the data fit a log-log curve--confirmed by regression analysis. The amount of surface coverage of the active LTC sites with CO and oxygen molecules accounts in large part for the discrepancy, as well as the fact that the oxygen-palladium bonds are weakened by the co-adsorption of CO molecules.[6] Thus, the reaction conforms more closely to the Langmuir-Hinshelwood mechanism rather than a simple first order dependency.[7]

ROOM TEST PERFORMANCE RESULTS

One present application of the LTC catalyst is a portable air filtration appliance for home and office environments. The LTC beads are tightly packed into a thin filter to minimize pressure drop; in the product filters LTC and activated carbon are mixed 50:50. The Instapure® Air Filtration System units used in this series of tests had LTC only (about 230 grams) and an air flow rate of 300 cfm. The contact time is thus approximately 0.02 second, or an order of magnitude less than that in the tube test. All of the following tests were conducted in a 1008 cubic foot sealed room at 40 percent relative humidity and ambient temperature. Initial contaminant concentrations are noted in each test, each of 2 hour duration. Figure 4 summarizes all of the results as adjusted for each species' rate of decay. The Threshhold Limit Value--Short Term Exposure Limit (STEL) values are recommendations issued by the American Conference of Governmental Industrial Hygienists (1983).[8] The STEL values cited are for a 15 minute time-weighted average which should not be exceeded during a work day.

Carbon Monoxide

A filter using 50:50 LTC to activated carbon was tested, using 30 parts per million CO to begin. The STEL limit is 400 parts per million, but 30 parts per million corresponds to the lower limit of the "dangerous" category established by the EPA. After 2 hours running, 55 percent of the CO was removed. Given the brief contact time, a per-pass filter efficiency of 14.6 percent may be calculated. An LTC filter removed 78 percent CO in 2 hours.

Ozone

An LTC-only filter in the appliance was run in the sealed room containing 164 parts per billion ozone (STEL limit is 300 parts per billion). After 38 minutes, 99+ percent was removed. Other tests indicate that the very reactive ozone molecules are decomposed to oxygen by chemisorption and subsequent interaction on the alumina surface, as well as the LTC active sites.

Nitric Oxide

An LTC filter was exposed to 20 parts per million NO at 300 cfm (STEL is 35 parts per million). After 80 minutes, the LTC had removed 20 percent, whereas the LTC/carbon filter was able to remove 40 percent of the initial concentration.

Nitrogen Dioxide

The LTC filter was exposed to 4 parts per million NO_2 (STEL is 5 parts per million). Removal was 40 percent after 100 minutes versus 100 percent removal for the LTC/carbon filter. The NO_2 molecules seem to be more tightly adsorbed to active carbon surfaces than to the LTC/alumina surfaces. As shown in Figure 2, increasing temperatures increase the rate of desorption (tube tests).

Sulfur Dioxide

An LTC filter in our appliance was run in the sealed room containing 5 parts per million SO_2 (STEL is 5 parts per million). Removal of 100 percent was achieved after 90 minutes. Other tube tests[4] have shown that SO_2 is chemisorbed by LTC active Cu(II) sites until saturation.

Hydrogen Sulfide

The LTC filter was subjected to 4 parts per million H_2S (STEL is 15 parts per million). After 60 minutes, about 100 percent of the H_2S was removed. Earlier tube tests (unpublished data, Western Kentucky University, September 1983) indicate an irreversible reaction of H_2S with LTC which results in a gradual poisoning of the active sites. Apparently, copper sulfide is the reaction product.[4]

Ammonia

An LTC filter in the air filtration appliance was run in an atmosphere containing 140 parts per million of ammonia. An STEL recommended limit of 35 parts per million is published. After 60 minutes, 58 percent was removed; 76 percent at the end of the 2 hour test. Subsequent, continuing test runs show that the catalyst is gradually saturated, with NH_3 removal dropping to 6 percent after 6 hours.

Benzene

The LTC filter was exposed to 17 parts per million of benzene vapor in the test room (STEL limit is 25 parts per million). Only 8 percent was removed after 2 hours, whereas the LTC/carbon filter was able to remove greater than 90 percent of the benzene concentration, even after each of five successive test runs. The benzene molecule is non-polar and readily adsorbed by the porous activated carbon. The LTC is relatively unreactive to the benzene structure.

Components of Tobacco Smoke

Chemical components of both mainstream and sidestream tobacco smoke are present in air as particulate or aerosal and a gaseous phase. The major portion of particulate is tar, nicotine, and water; the majority of the gas phase is carbon dioxide, carbon monoxide and methane. Particulate can be removed mechanically from mainstream smoke by a paper filter (cigarettes).

Table II lists some of the higher concentration constituents of tobacco smoke along with their biological effects.

TABLE II
Some cigarette smoke gaseous constituents
Mainstream smoke: unfiltered cigarette[a]

Gas Phase Components	Biological Activity	Wt/Cigarette
Carbon Dioxide		10-60 mg
Carbon Monoxide	Toxic	10-20 mg
Methane		1.3 mg
Acetaldehyde	Toxic	770 mg
Acetone		100-600 mg
Nitrogen Oxides	Toxic	60-600 mg
Isoprene		582 mg
Hydrogen Cyanide	Toxic	430 mg
2 - Butanone		80-250 mg
Acetonitrile		120 mg
Toluene		180 mg
Ammonia	Toxic	80 mg
Benzene	Co-Carcinogen	67 mg
Acetylene		27 mg
Dimethylnitrosamine	Carcinogen	10-65 mg
Nitrosopyrrolidine	Carcinogen	10-35 mg

a - U.S. Dept. of Health, Education & Welfare, "The Health Consequences of Smoking", 1981.

The most acute biological effect of tobacco smoke is suffered first from nicotine, and secondly from carbon monoxide. The latter markedly decreases the oxygen-carrying capacity of the blood and may impair the nervous system functions. Its effects range from inducing headaches and dizziness to implication in heart attacks and strokes.[9]

Room Test for CO From Cigarette Smoke

The test results for CO removal from sidestream cigarette smoke using the Instapure® Air Filter (AF-1) are shown in Figure 5. Two cigarettes were smoked every half-hour in a 1152 cubic foot sealed room to generate the upper curve ending at 48 parts per million CO in 8 hours. The same procedure was followed while running the AF-1 appliance, which gave the center curve (32 parts per million CO at 8 hours). The lower curve is for a repeat of the second test with cigarette smoking terminated after 6 hours. The air filter removes 34 percent of the cumulative CO concentration.

Mainstream Smoking Test

A small filter containing 6 grams of LTC was attached to unfiltered cigarettes to test for removals of mainstream tobacco smoke components. The

tests were conducted by an independent laboratory and are summarized in Figure 6. Oxidation of CO is dramatic--from 17,000 to 430 parts per million with the LTC filter. Referring to Table II, several other hazardous compounds are significantly reduced by use of LTC. Acetaldehyde and ammonia are diminished from 1,600 to 18 and 160 parts per million or less respectively. Likewise, methyl chloride and methyl ethyl ketone are removed in majority. Acetone and methyl alcohol are mechanically removed; several constituents are below the detection level and therefore show no change.

REFERENCES

1. Wallace, L.A., "Results From the First Three Seasons of the Team Study: Personal Exposures, Indoor-Outdoor Relationships, and Breath Levels of Toxic Air Pollutants Measured for 355 Persons in New Jersey." U.S. E.P.A., Research Triangle Park, N.C., 78th Annual A.P.C.A. Meeting, June 16-21, 1985.

2. Wallace, L. A.; Pellizari, E.; Heartwell, T.; Rosenzweig, M.; Erickson, M.; Sparacino, C.; and Zelon, H., "Personal Exposure to Volatile Organic Compounds: Direct Measurement in Breathing-Zone Air, Drinking Water, Food, and Exhaled Breath", Environmental Research, volume 35, 1984.

3. Wallace, L. A.; Pellizari, E.; Leaderer, B.; Heartwell, T.; Perritt, K.; Zelon, H.; and Sheldon, L., "Assessing Sources of Volatile Organic Compounds, in Homes, Building Materials, and Consumer Products", Conference on Characterization of Sources of Indoor Air Contaminants, Raleigh, N.C., May 13-15, 1985.

4. Collins, M. F. "Room Temperature Catalyst for Improved Indoor Air Quality", Transactions of the Air Pollution Control Association, International Specialty Conference-Indoor Air Quality in Cold Climates: Pollutant Abatement Research, Ottawa, April 29 to May 1, 1985, pp 448 - 460.

5. C. Thomas, Catalytic Process and Proven Catalysts, Academic Press, 1970.

6. Gasser, R. P. H., An Introduction To Chemisorption and Catalysis by Materials, Oxford University Press: 1985, pp 220 - 224.

7. Ibid, pp 249 - 252.

8. TLVs® Threshold Limit Values for Chemical Substances and Physical Agents in the Work Environment with Intended Changes for 1983-84. Publisher Amer. Conf. of Governmental Industrial Hygienists. ISBN: 0-936712-45-7, 1983.

9. "Smoking & Health: A Report of the Surgeon General", U.S. Dept. of Health, Education, and Welfare, Part 15, Biological Influences on Cigarette Smoking, 1981.

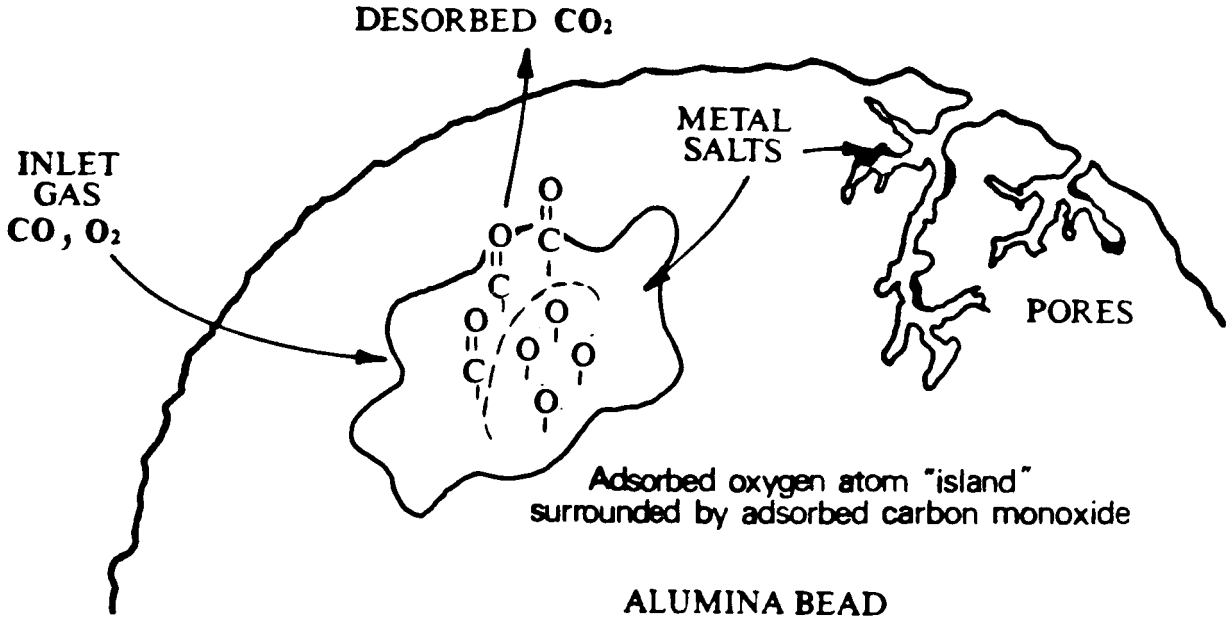

Figure 1. Diagram of catalytic CO oxidation mechanism.

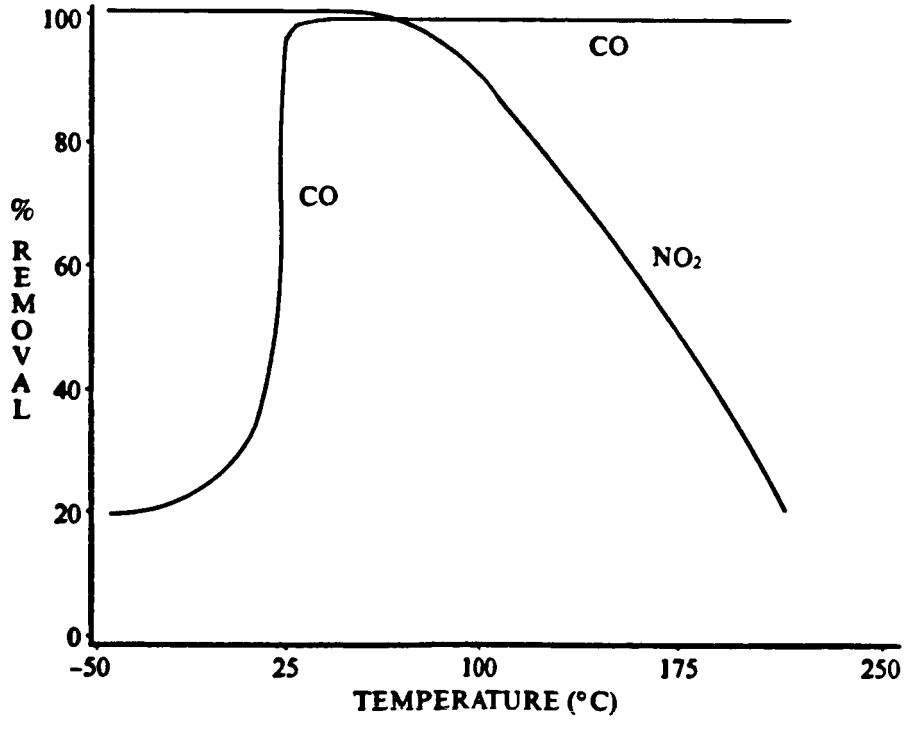

Figure 2. LTC removal of CO and NO_2 as a function of temperature.

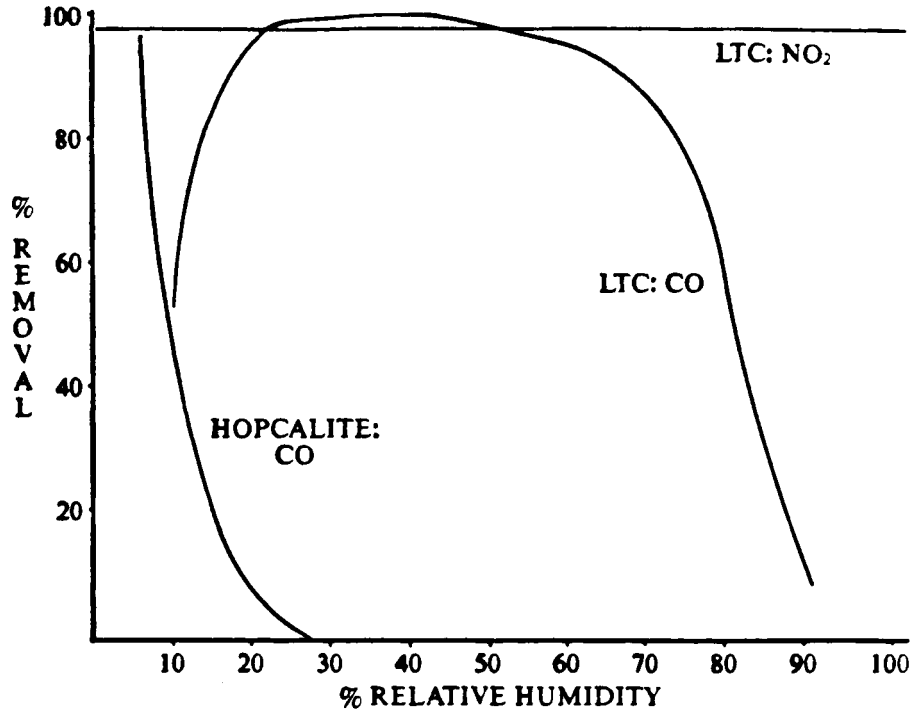

Figure 3. Catalyst removals as a function of relative humidity.

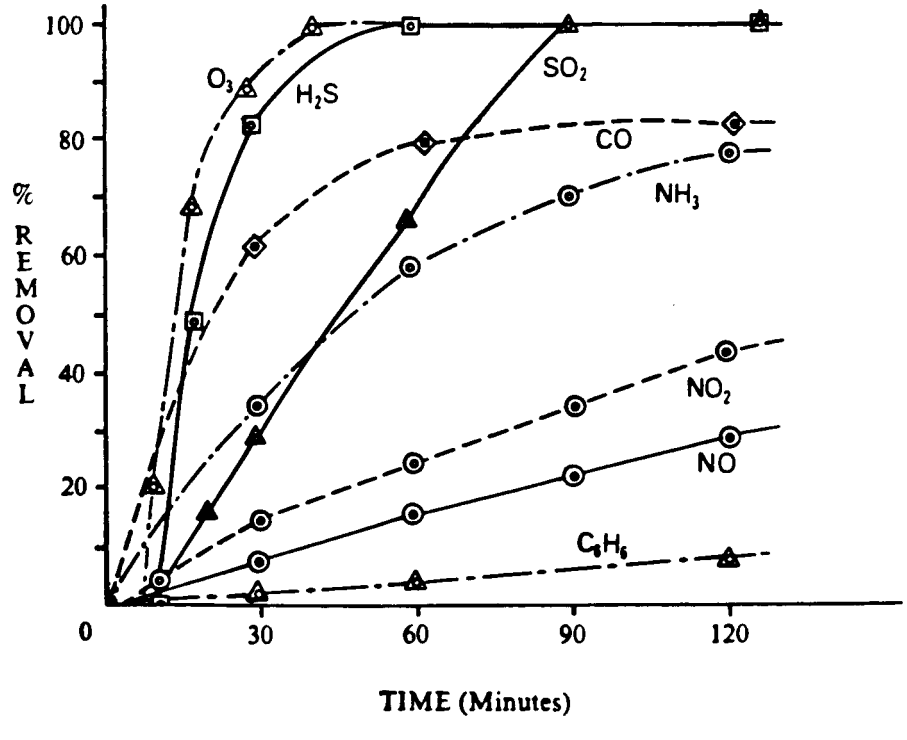

Figure 4. Room test of LTC filter for various contaminants.

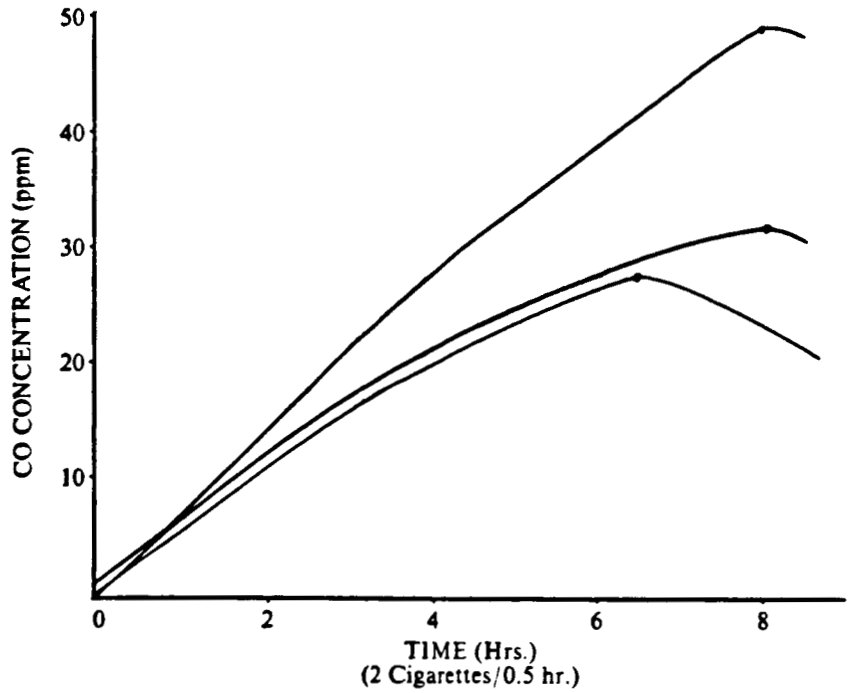

Figure 5. Room tests of product filter for CO (smoke) removal rate.

POLLUTANT	CIGARETTE (ppm)	LTC/CIGARETTE (ppm)
Carbon monoxide	17,000	430
Hydrocarbons	2,700	600
Ammonia	1,600	160
Acetaldehyde	1,600	< 18
Methyl chloride	550	84
Acetone	480	< 7
Methyl alcohol	350	< 60
Methyl ethyl ketone	100	< 6
Hydrogen sulfide	41	< 1

Figure 6. LTC removal of contaminants in cigarette smoke.

ALUMINA-SUPPORTED Pd-Ag CATALYSTS FOR LOW-TEMPERATURE CO AND METHANOL OXIDATION

R. W. McCabe
Physical Chemistry Department
General Motors Research Laboratories
Warren, Michigan

ABSTRACT

Pd-Ag bimetallic catalysts, supported on γ-Al_2O_3, have been evaluated as exhaust catalysts for methanol-fueled vehicles. Laboratory studies have shown that a 0.01% Pd-5% Ag catalyst has greater CO and CH_3OH oxidation activity than either 0.01% Pd or 5% Ag catalysts alone. Moreover, Pd and Ag interact synergistically in the bimetallic catalyst to produce greater CO and CH_3OH oxidation rates and lower yields of methanol partial oxidation products than expected from a mixture of the single-component catalysts. The Pd-Ag synergism results from Pd promoting the rate of O_2 adsorption and reaction with CO and CH_3OH on Ag. Rate enhancement by the bimetallic catalyst is greatest at short reactor residence times where the oxygen adsorption rate limits the overall reaction rate.

INTRODUCTION

Methanol-fueled vehicles differ greatly from gasoline vehicles in their exhaust characteristics. Major differences include the absence of sulfur in methanol exhaust and much lower exhaust temperatures associated with methanol vehicles. The latter provides impetus for developing catalysts that are effective for low-temperature CO and CH_3OH oxidation.

This study is part of a continuing effort in our laboratory to develop catalysts specifically for methanol-fueled vehicles. We begin by reviewing our previous results obtained with single-component catalysts. Those experiments suggested the use of bimetallic catalysts, and this paper focuses on results obtained with a bimetallic Pd-Ag/γ-Al_2O_3 catalyst.

EXPERIMENTAL PROCEDURE

Reactor System

The reactor and experimental methods were identical to those employed previously [1] and are only briefly reviewed here. A schematic diagram of the apparatus is shown in Fig. 1. The reactor was a 2.5 cm o.d. quartz tube

housed in a single-zone furnace. The feed gases passed downward through the reactor and sequentially contacted stacked layers of (1) quartz beads (for preheating and feed), (2) the catalyst pellets, and (3) quartz wool (for supporting the catalyst and quartz beads). Temperatures were measured with a chromel-alumel thermocouple positioned along the reactor centerline with its tip located in the catalyst bed a few millimeters below the top of the bed.

Catalyst activities and selectivities were compared using three feeds: (1) 0.2% CH_3OH, 1% O_2, balance He; (2) 0.2% CO, 1% O_2, balance He; and (3) 0.2% CH_3OH, 0.2% CO, 1% O_2, balance He. The space velocity in most runs was 52,000 h^{-1} (volume basis; standard conditions).

The products were analyzed principally with a Varian 6000 gas chromatograph equipped with both flame ionization and thermal conductivity detectors [1].

Catalysts

All catalysts were supported on 3.5 mm diameter γ-alumina beads from the same lot (Grace Chemical Co., 110 $m^2\ g^{-1}$ BET surface area, 0.5 g cm^{-3} apparent bulk density).

The most notable preparative aspect of our earlier work involving a comparison of Pt, Pd, Rh, Ag, and Cu-Cr catalysts was that the noble metals Pt, Pd, and Rh were prepared and tested under conditions of equal numbers of exposed atoms and identical surface impregnation profiles [1]. In the subsequent comparison of Pd, Ag and Pd-Ag catalysts, the techniques outlined below were employed to achieve a uniform distribution of Pd and Ag throughout the interior of the pellets.

Impregnations were made from aqueous, minimum volume solutions of the metal salts - $Pd(NH_3)_4(NO_3)_2$ and $AgNO_3$. The impregnated catalysts were dried for 12 h at room temperature. The catalysts were subsequently heated in flowing air to 773 K where they were held for 4 h.

The bimetallic 0.01% Pd-5% Ag catalyst was prepared sequentially; the alumina support was first impregnated with $AgNO_3$, dried, and calcined as outlined above, and then the same procedure was repeated for the Pd ammine salt.

The 0.01% Pd catalyst has a dispersion of 42% as measured by static chemisorption at 308 K, assuming a stoichiometry of one CO molecule per exposed Pd atom. The disperson of the air-calcined 5% Ag catalyst was 27% as measured by O_2 chemisorption using techniques similar to those of Vannice and co-workers [2, 3]. Attempts to measure Pd-atom dispersion in the bimetallic catalyst were unsuccessful owing to difficulties in reproducibly distinguishing the small amount of irreversibly adsorbed CO associated with the Pd from the large amount of reversibly adsorbed CO associated with the Ag.

RESULTS AND DISCUSSION

Methanol and CO Oxidation over Selected Catalysts

Figure 2 shows steady-state methanol conversions and product yields as a function of temperature for the Pt catalyst. The Pt catalyst was extremely active and oxidized methanol even at room temperature. CO_2, methyl formate (CH_3OCHO), and H_2CO were the only carbon-containing products. Methyl formate was the principal product at low temperatures, but was replaced by CO_2 at temperatures above 350 K.

Methanol conversion and selectivity were both greatly affected by adding CO to the feed, as shown in Fig. 3. Significant conversion of methanol was not observed below 450 K; moreover, methyl formate was no longer formed.

Similar CH_3OH oxidation experiments were carried out over the Pd, Rh, Ag, and Cu-Cr catalysts both in the presence and absence of CO. A comparison of catalyst activities is shown in Fig. 4. Three conversion versus temperature profiles are shown for each catalyst: (1) methanol conversion in a feed containing CH_3OH and O_2 (solid curve), (2) methanol conversion in a feed containing CH_3OH, CO, and O_2 (dash-dot-curve) and (3) CO conversion in a feed containing CO and O_2 (dotted curve). The behavior of the noble metal catalysts, Pt and Pd, contrasted with that of the base metal catalysts, Ag and Cu-Cr. CH_3OH oxidation was strongly inhibited over the Pt and Pd catalysts by the addition of CO to the feed. This is demonstrated by the 100-150° shift of the CH_3OH conversion profiles to higher temperatures in the presence of added CO.[3] Additionally, the $\underline{CH_3OH}$ conversion profiles observed in the presence of CO superposed almost exactly on the $\underline{CO}$ oxidation profiles, indicating that CH_3OH oxidation is totally dominated by CO oxidation on the Pt and Pd catalysts. This is not unexpected given that CO adsorbs much more strongly on Pt and Pd surfaces than CH_3OH [4-7], and CH_3OH cannot adsorb and react until temperatures are reached where CO begins to desorb.

In contrast to Pt and Pd, CO chemisorption on Ag and Cu-Cr catalysts is very weak [8-14]. Consequently, CO oxidation activities of the Ag and Cu-Cr catalysts are poor compared to Pt and Pd. Because of the weak CO adsorption, however, adsorption and reaction of CH_3OH are not inhibited by CO as in the case of the noble metal catalysts. Thus, the methanol conversion profiles shown for the Ag and Cu-Cr catalysts in Fig. 4. are virtually unaffected by the presence of CO.

Motivations for Utilizing Bimetallic Catalysts

Comparison of the CH_3OH oxidation data of Figs. 4a and 4d, for the Pt and Ag catalysts respectively, indicates that, in the presence of CO, CH_3OH oxidation proceeds more readily on the Ag catalyst at low temperatures than on the Pt catalyst. This comparison is shown more clearly in Fig. 5 where the methanol conversion profiles obtained in the presence of CO are plotted

together. The Ag catalyst is more active at low temperatures (hashed region), but the curves cross at high temperatures. Together, these observations suggest that a bimetallic catalyst containing Ag in combination with either Pt or Pd would show better CH_3OH oxidation activity over the full range of temperatures in automotive exhaust than either Ag, Pt, or Pd catalysts alone.

A bimetallic catalyst such as Pd-Ag might also prove to be a more efficient low-temperature CO oxidation catalyst than the respective single-component catalysts. The basis for this suggestion is shown conceptually in Fig. 6. At low temperatures, CO oxidation rates are low on Pd catalysts because of the high surface coverage of CO which prevents O_2 adsorption. Ag represents the other extreme; CO interacts only weakly with Ag thus its surface coverage is low. A catalyst containing Pd and Ag, intimately mixed in bimetallic crystallites, might promote CO oxidation by effecting more-uniform surface concentrations of CO and atomic oxygen than can be obtained with either Pd or Ag alone.

Design of a Pd-Ag Catalyst

A Pd-Ag/Al_2O_3 catalyst was prepared utilizing a strategy designed to disperse small amounts of Pd over much larger amounts of Ag. The Ag loading was 5% by weight. This loading was chosen because, as shown in Fig. 7, CO conversion activity was found to depend strongly on Ag loading. In contrast, CO conversion activity over Pd catalysts (Fig. 8) did not depend strongly on loading under the conditions of our study. Thus a low loading of 0.01% was chosen and uniform impregnation techniques were employed to highly disperse the Pd and thereby avoid the formation of segregated Pd particles.

Details of the methanol oxidation behavior of the bimetallic catalyst have been reported elsewhere [15]. The activity characteristics and selectivity patterns confirm that the preparative techniques outlined above produce a catalyst where essentially all of the Pd is present in bimetallic crystallites rather than as segregated Pd particles.

CO Oxidation over the Pd-Ag Catalyst

The CO oxidation activity of the 0.01% Pd-5% Ag catalyst was compared to the CO oxidation activities of 0.01% Pd and 5% Ag catalysts alone. Fig. 9 shows data obtained at a space velocity of 195,000 h^{-1}. At temperatures below 500 K, the Pd-Ag catalyst showed higher CO conversions than either of the single-component catalysts. Moreover, the shape of the conversion versus temperature profile closely resembled that of the Ag catalyst, which suggests that the role of Pd in the bimetallic catalyst is to promote CO oxidation on Ag.

CO oxidation was also examined at a space velocity of 52,000 h^{-1}, and results are shown in Fig. 10. In contrast to the data obtained at 195,000 h^{-1}, the Pd-Ag catalyst showed enhanced conversion relative to the Ag catalyst only at temperatures above ~450 K.

Mechanism of Pd Promotion of the Ag Catalyst

The addition of Pd to the Ag catalyst has an effect that is similar to increasing the feed oxygen concentration over an Ag catalyst. This can be seen by comparing Figs. 10 and 11. In Fig. 11, CH_3OH oxidation data are shown for a 2% Ag/Al_2O_3 catalyst at two oxygen concentrations. At low temperatures, CH_3OH conversions are virtually identical, indicating that the rate of O_2 supply is not a limiting factor. At temperatures above 400 K, however, the curves diverge. CH_3OH conversion is greater in the 1% O_2 feed than in the 0.25% O_2 feed, as expected under conditions where the overall reaction rate increases to the point where the supply of oxygen becomes a rate-determining step. Since the same qualitative behavior is observed in comparing CO oxidation over the Pd and Pd-Ag catalysts in Fig. 10 the data suggest that the effect of adding small amounts of Pd to an Ag catalyst is to increase the rate of O_2 adsorption and subsequent reaction on the Ag.

Fig. 12 shows results of temperature-programmed oxidation (TPO) experiments carried out over pre-reduced samples of the 0.01% Pd, 5% Ag, and 0.01% Pd-5% Ag catalysts. The TPO experiments provide additional evidence that the role of Pd in the bimetallic catalyst is to increase the rate of O_2 adsorption and reaction on Ag. No O_2 adsorption was observed on the 0.01% Pd catalyst due to the very low metal loading (any O_2 uptake associated with the 0.01% Pd catalyst would have been below the sensitivity of the thermal conductivity detectors employed in the TPO apparatus). However, the Pd-Ag catalyst showed greater rates of O_2 uptake than the Ag catalyst alone at temperatures below 600 K. The enhanced uptake rate of the Pd-Ag catalyst indicates that Pd enhances the rate of O_2 adsorption on the Ag, since as noted previously, any uptake associated with Pd was below the limits of detectability. This observation is consistent with the relatively high sticking probabilities reported for dissociative O_2 chemisorption on Pd surfaces (s_o ~10^{0}-[16])[4] compared to the extremely low values reported for Ag surfaces (s_o = 10^{-6}-10^{-4} [17, 18]).

SUMMARY

Although a synergistic interaction between Pd and Ag has been achieved in this study, the enhanced rates of CO and CH_3OH oxidation result from Pd promoting the rate of O_2 adsorption and reaction on Ag, rather than from a bifunctional mechanism.

In other words, our data suggest that both CO and CH_3OH oxidation occur nearly exclusively on Ag in the bimetallic catalyst with the role of Pd being to supply oxygen atoms at a rate greater than that of direct dissociative O_2 adsorption on Ag crystallites. This is in contrast to the situation depicted in Fig. 6, where the synergism would result from adsorption of CO and Ag on the different metal components in close proximity.

Thus, in this study, the bimetallic catalyst shows its greatest rate enhancement relative to the single-component catalysts under conditions where the surface reactions are fast relative to the rate of O_2 adsorption. These are not the conditions that would obtain in a low-temperature CO_2 laser application. The surface reaction between adsorbed CO and adsorbed atomic oxygen would likely be rate-limiting, and multimetallic catalysts that adsorb CO and O_2 independently on adjacent sites would appear to offer the greatest rate enhancement.

This sort of configuration has, in fact, been suggested for the structure of Pt-SnO_x catalysts where Pt-O-Sn bonding has been identified. This bonding configuration could represent the active sites for CO and O adsorption and reaction, thereby eliminating the requirement for surface diffusion of either species [19].

REFERENCES

1. R. W. McCabe and P. J. Mitchell, Applied Catalysis 27 (1986) 83.

2. S. R. Seyedmonir, D. E. Strohmayer, G. L. Geoffroy, M. A. Vannice, H. W. Young, and J. W. Linowski, J. Catalysis 87 (1984) 424.

3. S. R. Seyedmonir, D. E. Strohmayer, G. J. Guskey, G. L. Geoffroy, and M. A. Vannice, J. Catalysis 93 (1985) 288.

4. R. K. Herz and S. P. Marin, J. Catalysis 65 (1980) 281.

5. A. Golchet and J. M. White, J. Catalysis 53 (1978) 266.

6. R. W. McCabe and L. D. Schmidt, Surface Sci. 66 (1977) 101.

7. B. A. Sexton, Surface Sci. 102 (1981) 271.

8. R. J. Madix, In "Advances in Catalysis," Academic Press: New York, 1980.

9. C. R. Ryberg, Phys. Rev. Lett. 49 (1982) 1579.

10. T. E. Felter, W. H. Weinberg, G. Ya. Lastushkina, P. A. Zndan, G. K. Boreskov, and J. Hrbek, Appl. Surf. Sci. 16 (1983) 351.

11. I. E. Wachs and R. J. Madix, Surface Sci. 76 (1978) 53.

12. R. Hierl, H. Knozinger, and H.-P. Urbach, J. Catalysis 69 (1981) 475.

13. M. Ayyoob and M. S. Hegde, Surface Sci. 133 (1983) 516.

14. H. Albers, W. J. J. Vander Wal and G. A. Bootsma, Surface Sci. 68 (1977) 47.

15. R. W. McCabe and P. J. Mitchell, J. Catalysis 103 (1987).

16. H. Conrad, G. Ertl, J. Kuppers, and E. E. Latta, Surface Sci. 65 (1977) 245.

17. C. T. Campbell, Surface Sci. 157 (1985) 43; and references therein.

18. H. Albers, N. J. Vander Wal, O. L. J. Gijzeman and G. A. Bootsma, Surface Sci. 77 (1978) 1.

19. G. B. Hoflund and D. A. Asbury, "Thin Solid Films," 129 (1985) 139.

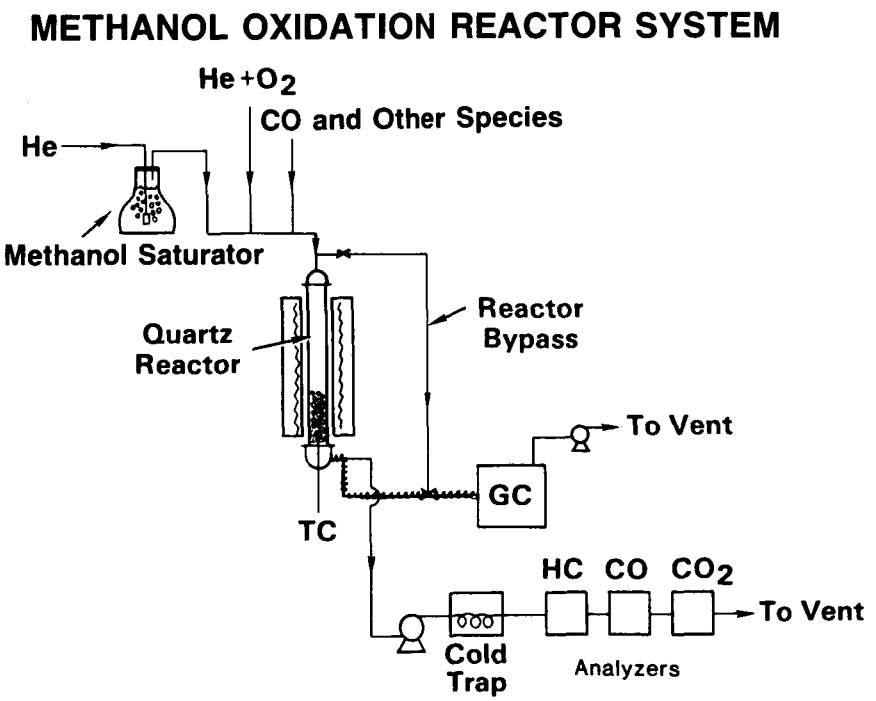

Figure 1. Schematic diagram of reactor apparatus.

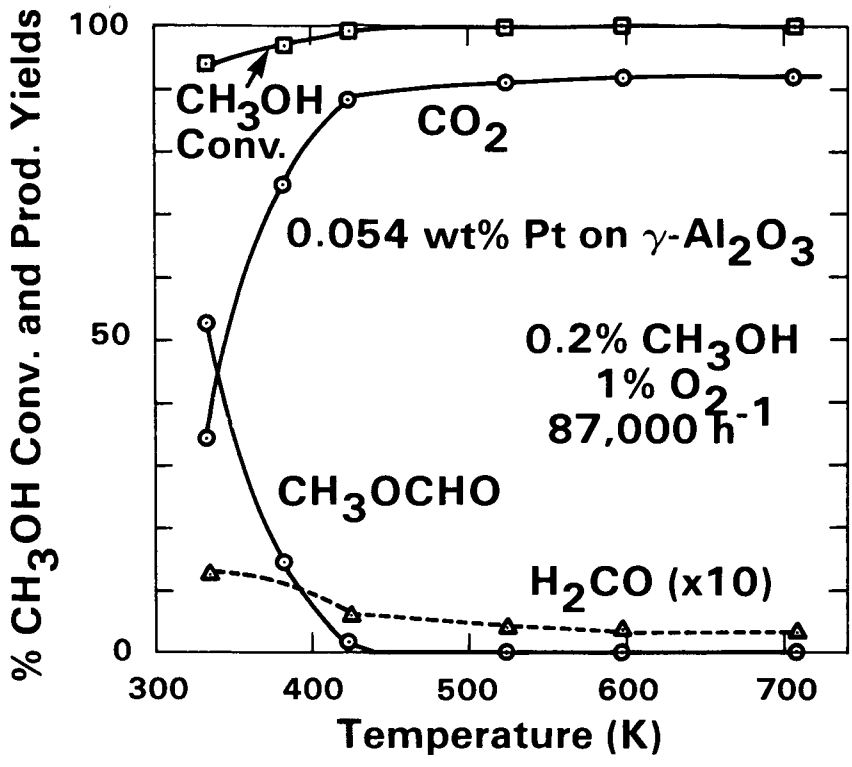

Figure 2. Steady-state methanol conversions and product yields as a function of temperature over a 0.054 wt% Pt/Al_2O_3 catalyst.

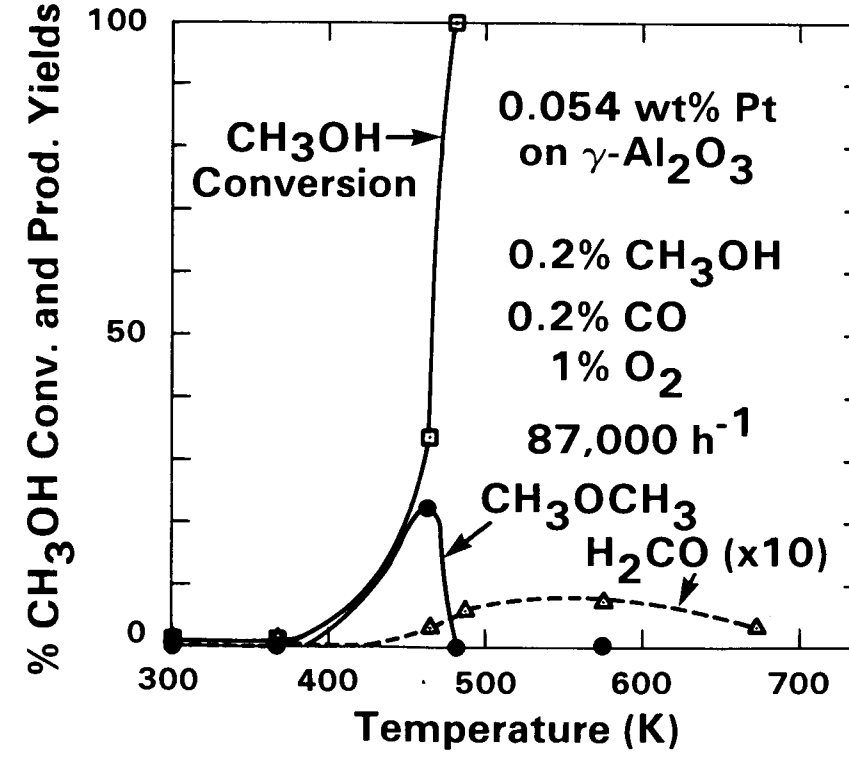

Figure 3. Steady-state methanol conversions and product yields as a function of temperature over a 0.054 wt% Pt/Al_2O_3 catalyst. The experiment was identical to that of Fig. 2 except that 0.2% CO was added to the feed.

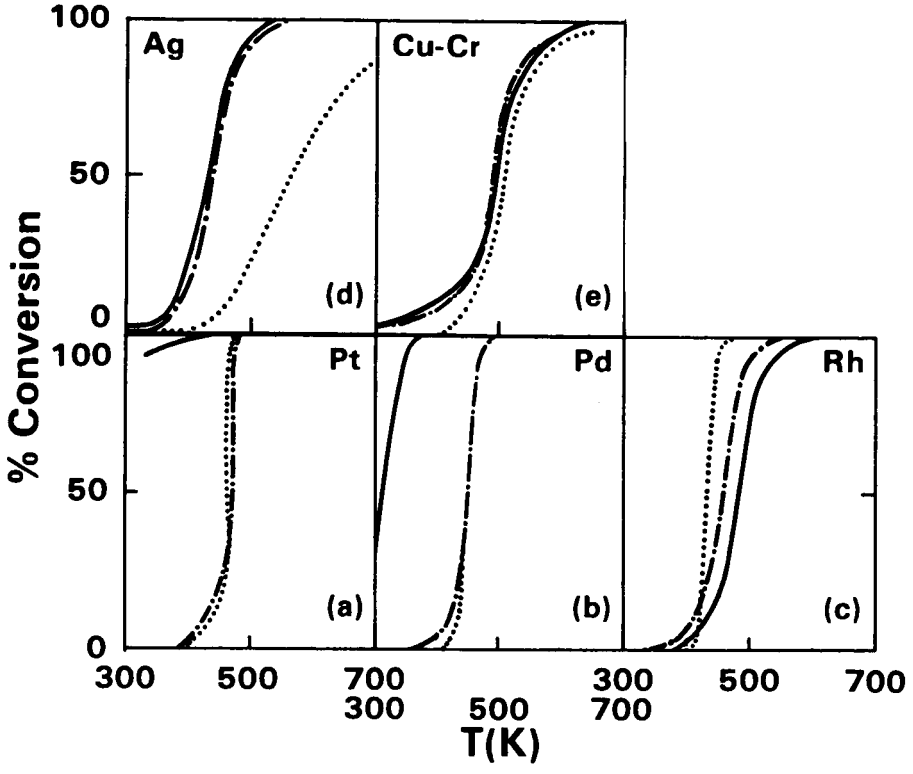

Figure 4. A comparison of conversion versus temperature data obtained over (a) 0.054 wt% Pt, (b) 0.034 wt% Pd, (c) 0.026 wt% Rh, (d) 1.92 wt% Ag, and (e) 4 wt% Cu-2 wt% Cr all supported on γ-Al_2O_3. For each catalyst we show conversion vs temperature data for feeds containing (1) 0.2% CH_3OH/1% O_2 (----), (2) 0.2% CO/1% O_2 (....) and (3) 0.2% CH_3OH/0.2% CO/1% O_2 (--•--). For the mixed 0.2% CH_3OH/0.2% CO/1% O_2 feed, the conversion reported is that of CH_3OH, not CO.

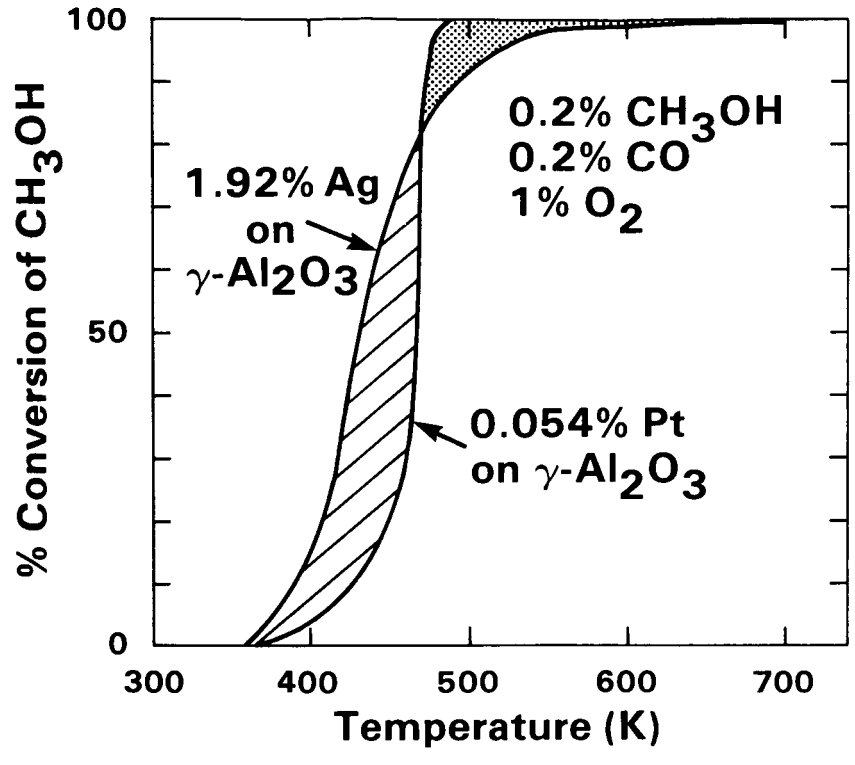

Figure 5. A comparison of methanol conversions over 2 wt% Ag and 0.054 wt% Pt catalysts as a function of temperature.

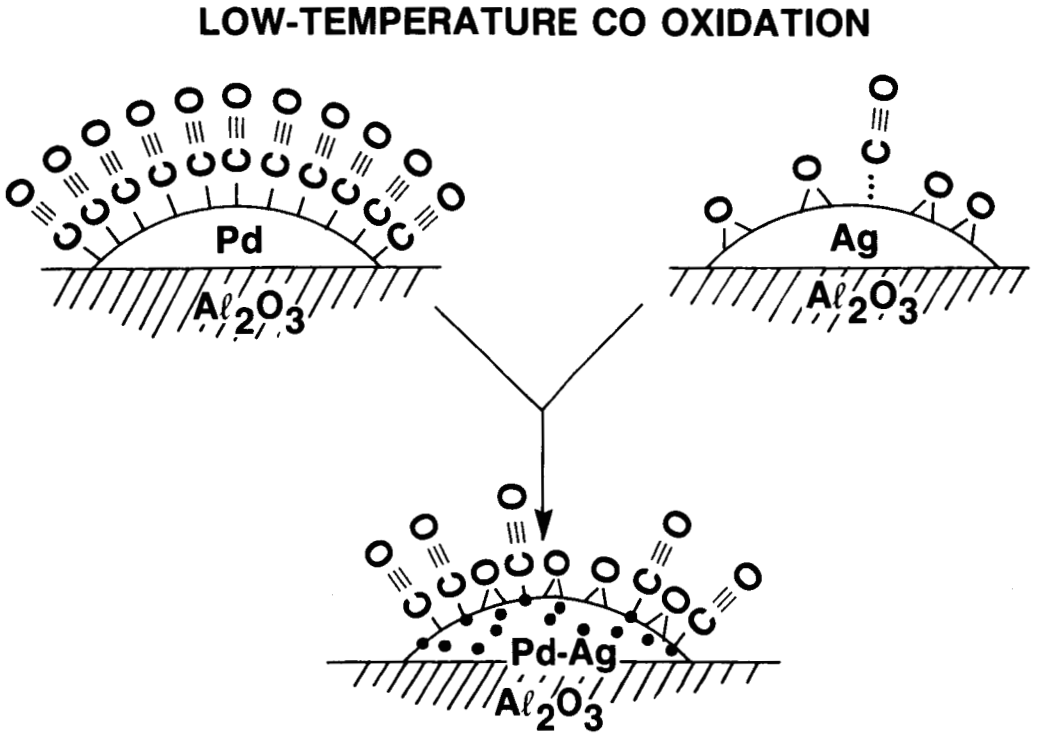

Figure 6. A conceptual representation of surface coverages of adsorbed species expected for CO oxidation on alumina-supported Pd, Ag, and Pd-Ag catalysts at low temperatures. The bimetallic catalyst would be expected to result in a more uniform surface mixture of CO and O than either of the single-component catalysts.

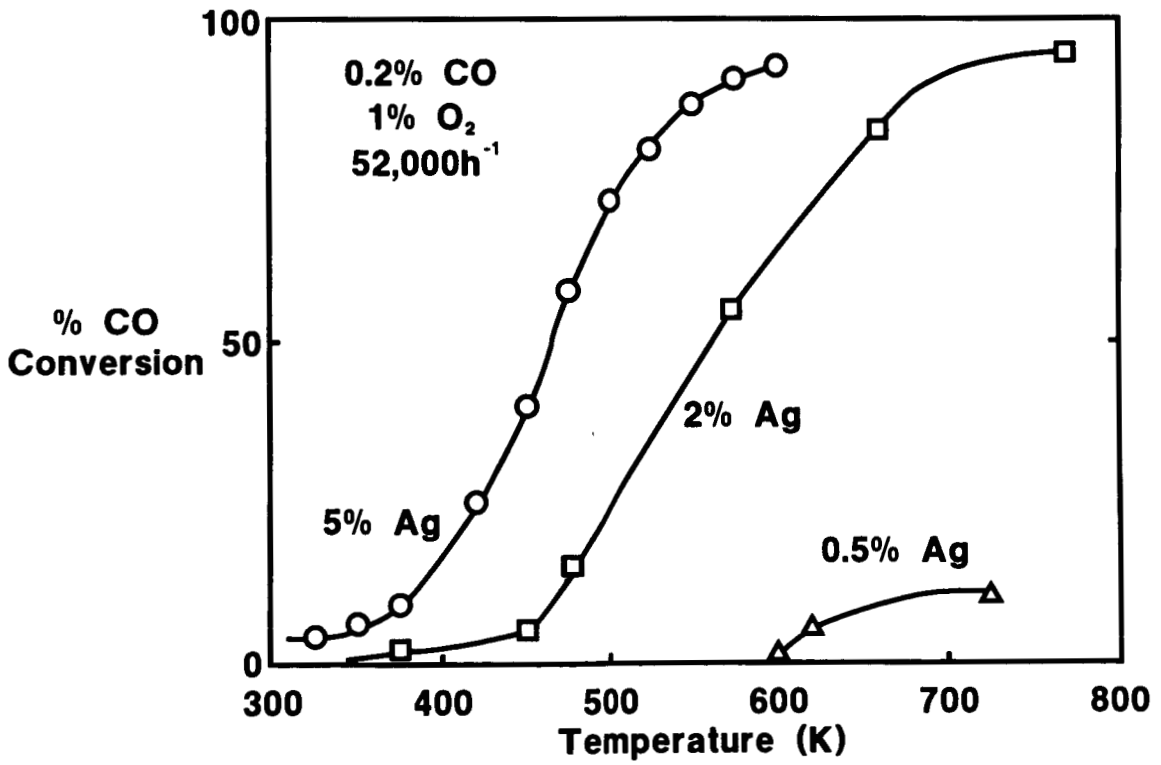

Figure 7. Effect of loading on Ag/γ-Al_2O_3 catalyst CO oxidation activity.

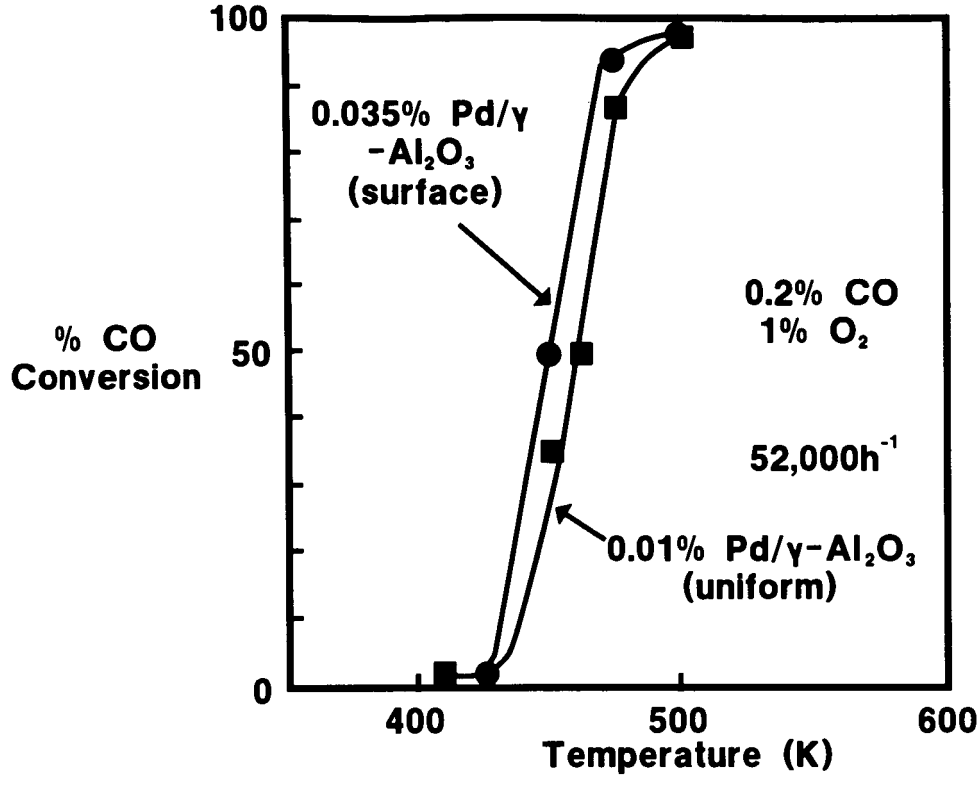

Figure 8. Comparison of CO oxidation activities of two Pd/Y-Al_2O_3 catalysts.

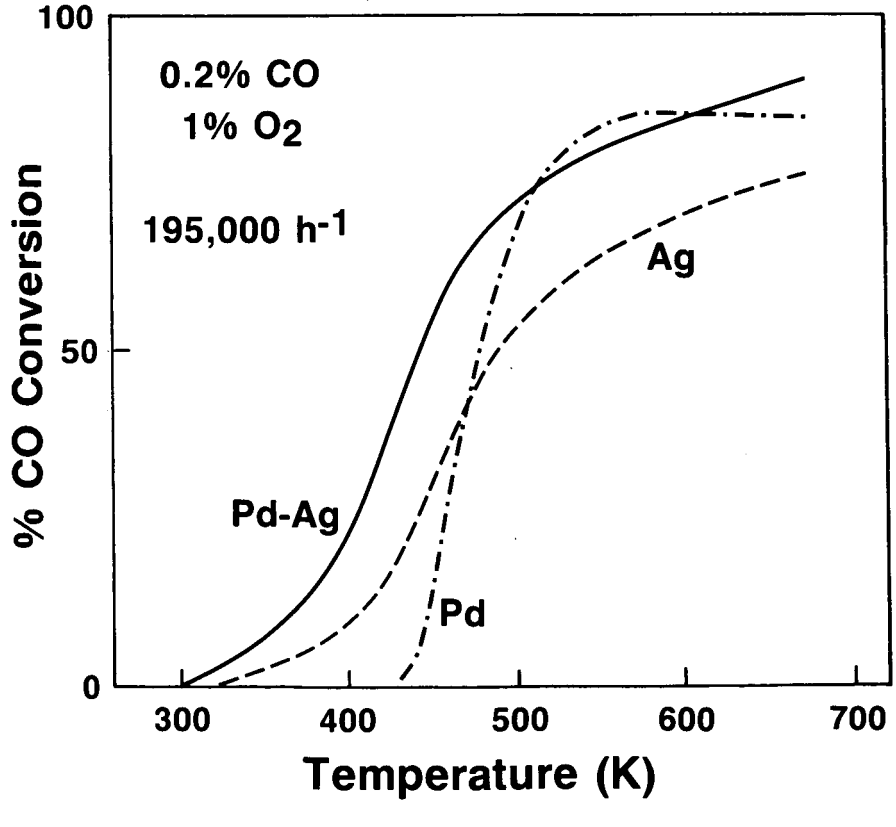

Figure 9. Conversion as a function of temperature for CO oxidation at 195,000 h^{-1} over 0.01 wt% Pd, 5 wt% Ag, and 0.01 wt% Pd-5 wt% Ag alumina-supported catalysts.

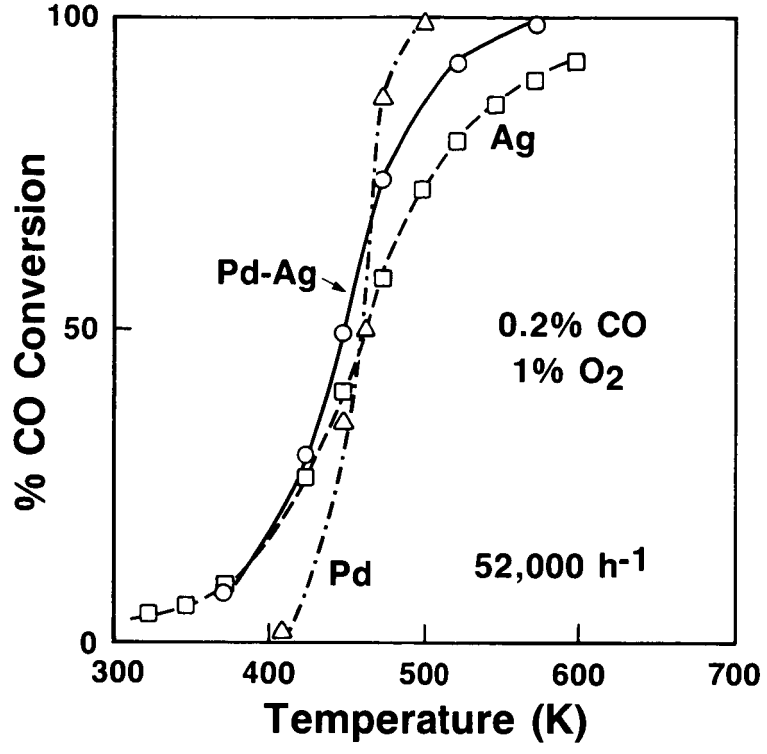

Figure 10. Conversion as a function of temperature for CO oxidation at 52,000 h^{-1} over 0.01 wt% Pd, 5 wt% Ag, and 0.01 wt% Pd-5 wt% Ag alumina-supported catalysts.

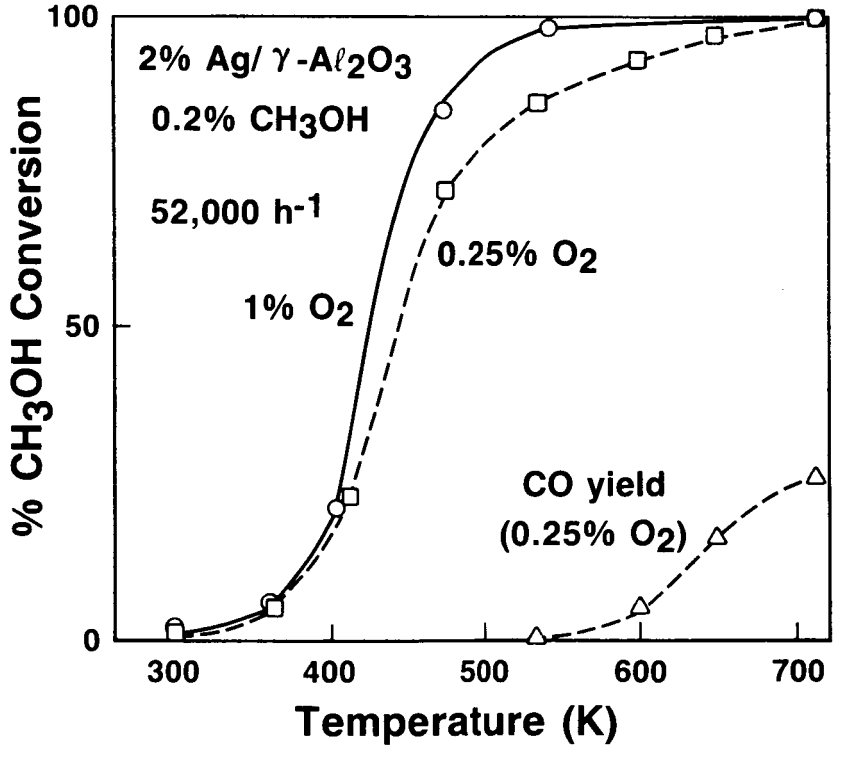

Figure 11. Effect of feed O_2 concentration on CH_3OH conversion profiles obtained over a 2 wt% Ag/Al_2O_3 catalyst.

C-3

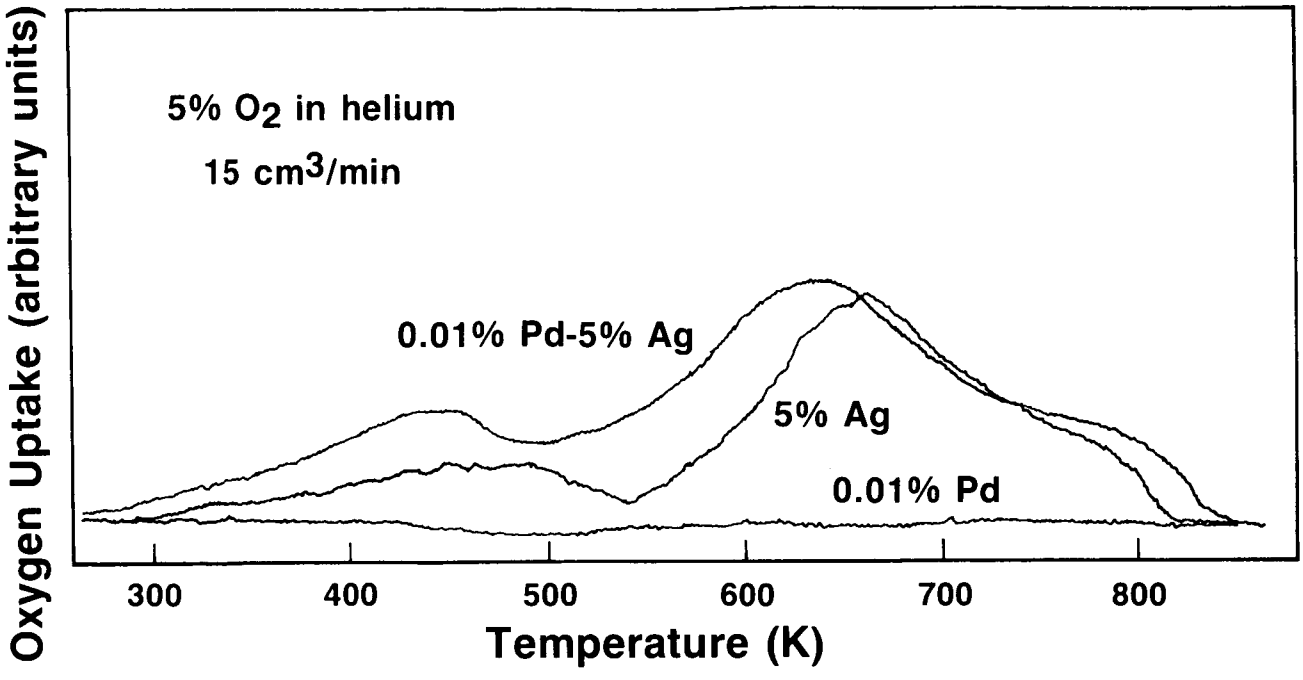

Figure 12. Temperature-programmed oxidation profiles for pre-reduced samples of 0.01 wt% Pd, 5 wt% Ag, and 0.01 wt% Pd-5 wt% Ag catalysts.

A REVIEW OF TIN OXIDE-BASED CATALYTIC SYSTEMS: PREPARATION, CHARACTERIZATION AND CATALYTIC BEHAVIOR

Gar B. Hoflund
Department of Chemical Engineering
University of Florida
Gainesville, Florida

SUMMARY

This paper reviews the important aspects of the preparation, characterization and catalytic behavior of tin oxide-based catalytic systems including doped tin oxide, mixed oxides which contain tin oxide, Pt supported on tin oxide and Pt/Sn supported on alumina. These systems have a broad range of applications and are continually increasing in importance. However, due to their complex nature, much remains to be understood concerning how they function catalytically.

INTRODUCTION

It is only recently that the importance of tin oxide-based catalytic systems has begun to be recognized. These catalysts occur in many forms and are used in a wide range of applications from electrocatalysis to gas-phase reactions. Other than the fact that they all contain tin oxide, a common attribute is their complexity with regard to composition, geometrical structure, electronic structure, redox behavior and catalytic properties. The purpose of this review is to briefly describe some important aspects relating to these catalytic systems and to provide more detailed sources concerning these discussions.

I. OXIDATION OF METALLIC TIN

In these systems it is possible for tin to be present in various forms including metallic oxidic as either stable oxide SnO or SnO_2, alloyed with another metal such as Pt (PtSn or Pt_3Sn), and others. Studying the oxidation of metallic tin using various characterization techniques often allows for the identification of the different species present in more complex environments. Different techniques including Auger electron spectroscopy (AES) (1-4), ultra-violet photoemission spectroscopy (UPS) (5), electron spectroscopy for chemical analysis (ESCA) (3,4,6), electron energy loss spectroscopy (ELS) (1,2,7), low energy electron diffraction (LEED) (2) and thermal gravimetry (8) have been used to examine the oxidation of metallic tin as a function of oxygen exposure (1,2,4,7) and temperature (2,8).

Much information which is useful in characterizing the Pt/SnO_x system is contained in these studies. Both of the two stable oxides SnO and SnO_2 are always present during the oxidation process, and it is very difficult to distinguish

between them using ESCA or AES particularly quantitatively since most of their spectral features are essentially identical. However, it has been demonstrated that valence-band ESCA (6) and ELS (1,2) are capable of distinguishing between SnO and SnO_2. The relative amounts of each oxide present vary considerably with the conditions of oxidation. For heavily oxidized samples, an SnO_2 layer lies beneath an oxygen-depleted or SnO-like layer. Another important point is that the work function of the surface does not change as it becomes oxidized. This fact combined with the fact that SnO and SnO_2 have the same ESCA 3d binding energies provides an excellent means of referencing all spectral features. This eliminates the need to use questionable references such as the C 1s peak (due to contamination) or to make tedious work function corrections.

It is important to understand that both ESCA and AES examine a fairly large number of atomic layers in the surface region and are not as surface sensitive as they are often considered to be. One of the most surface-sensitive techniques is ion scattering spectroscopy (ISS) which is essentially outermost layer sensitive. A recent ISS study carried out in the author's laboratory has demonstrated that a room temperature, saturation exposure to oxygen results in penetration of the oxygen beneath the outermost layer of tin atoms. Scanning Auger microscopy (SAM) shows that this penetration occurs at planar lattice sites and not at grain boundaries.

II. CHARACTERIZATION AND PROPERTIES OF TIN OXIDE

Tin oxide is an n-type, wide-gap, semiconducting oxide material which is transparent to visible light. Consequently, it is important as an electrode material (9-14), in solar cell applications (15,16), as a sensor material (17-19) and as a transparent conductor in electronic displays (20,21). The chemical activity of tin oxide and particularly its redox properties make tin oxide an important catalytic material in both a pure and mixed oxide form for gas-phase reactions (22-37) and for electrocatalytic or photoelectrocatalytic reactions (38-46). Although tin oxide functions as an oxidative catalyst in most of these studies, it is interesting that it can also function in a reductive manner.

Tin oxide is an exceedingly complex material with regard to geometrical structure and composition. Both stable oxides are always present, and each can be in several structural forms including defect-laden structures. Hydrogen is always present in tin oxide in varying amounts and binding states (47), and large quantities of contaminants including C, Ca, K, Na, S and Cl are usually present (48). Furthermore, nearly any treatment of a tin oxide surface alters it in some manner. Based on a large number of characterization studies, it is not possible to understand the complex properties of tin oxide by considering it to be a relatively simple material such as SnO_2. Therefore, it is necessary to develop and utilize characterization techniques which are sensitive to all of the various complex aspects of tin oxide surfaces. Furthermore, the use of multiple techniques on a particular tin oxide surface provides the most complete information about that surface.

AES and secondary ion mass spectrometry (SIMS) are both useful for observing contaminants at tin oxide surfaces. ESCA is often less useful since it is not as surface sensitive as either AES or SIMS or as sensitive to trace amounts. A typical AES spectrum taken from a contaminant antimony-doped tin oxide surface is

shown in figure 1 (48). Antimony is often added to tin oxide because it lowers its electrical resistivity by several orders of magnitude or can improve its catalytic properties. The comtamination was present in the various chemicals and apparatus used to prepare the tin oxide film. By using extremely pure chemicals

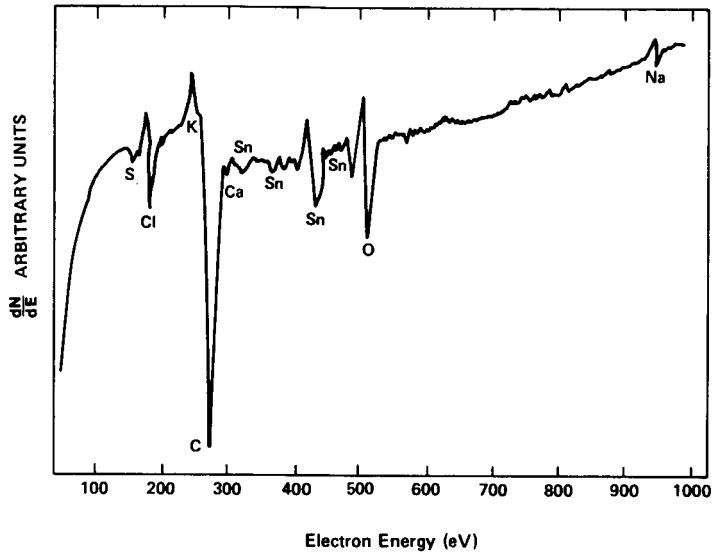

Figure 1. Typical AES spectrum (low energy resolution) taken from a contaminated antimony-doped tin oxide surface. The K and Ca peaks are masked by the large C peak (ref. 48).*

*Reprinted with permission, Elsevier Sequoia.

and meticulously cleaning all apparatus, it is possible to prepare tin oxide surfaces which are only slightly contaminated with a small amount of C. It has been found that the Ca contamination is due to allowing the solutions to sit in glassware, and the amount present depends upon the length of time they remain in the glassware. The oxygen-to-tin ratio in figure 1 is larger than that of an SnO_2-like surface indicating that excess oxygen is present probably as hydroxyl groups, water of hydration or bound to other impurities.

AES is insensitive toward some elements. Examples are Sb and H. Small amounts of Sb are masked by larger Sn features, and H has no distinct AES peaks since it has no core-level electrons. However, both can readily be observed using SIMS. Sb appears in the SIMS negative-ion spectrum as SbO^- (153 and 155 amu) and SbO_2^- (49). Hydrogen influences many m/e peaks in the SIMS positive-ion spectrom (50). Apparently the m/e = 121 peak gives the least ambiguous measure of the amount of H present. It is assigned as 120 SnH^+ and is least affected by scrambling with other tin isotope species. However, it is very difficult to quantify SIMS results since cross sections can vary by orders of magnitude and are not well understood.

Both AES and SIMS are destructive techniques. SIMS alters the surface composition by ion sputtering, and AES alters the surface composition by electron stimulated desorption (EDS). Thus, it is necessary to use very low primary beam doses and to take repeated spectra to be certain that beam damage has not altered the information. Although ESD is a predominant type of damage phenomena in AES, it is now used as a very powerful surface analytical technique (51). Mass analysis, energy analysis, angular distributions and desorption thresholds of the emitted

ions yield important information about binding states of the adsorbed species. Particularly important is the fact the ESD provides an excellent method for studying surface hydrogen since it is a mass spectrometric technique. This point is illustrated in figure 2 (51,52). Figure 2(A) shows the H^+ and O^+ ESD signals

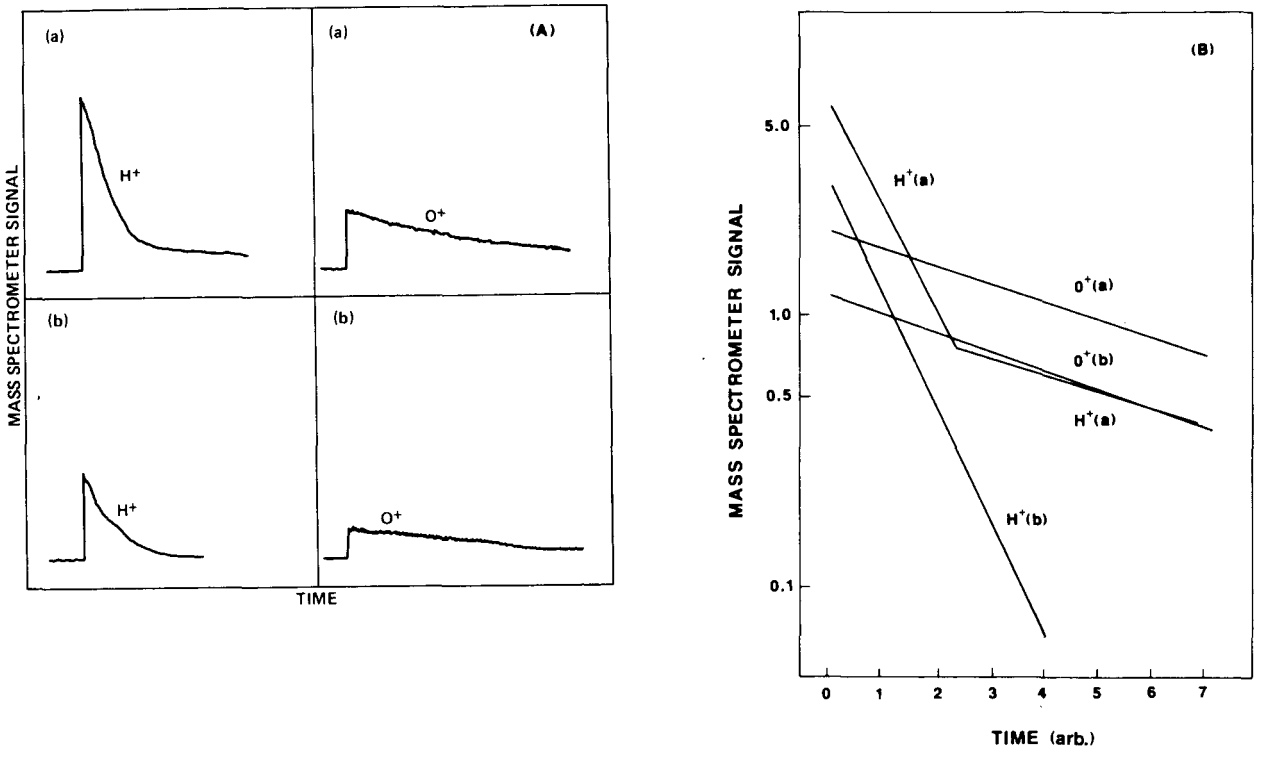

Figure 2. (A) H^+ and O^+ signals as a function of time from a polycrystalline tin oxide surface which had been a: exposed to a 10 M NaOH solution for 30 minutes at 90°C and b: exposed only to atmospheric humidity. The heights are arbitrary but scaled relatively to each other. Both treatments resulted in surface hydroxylation but to different extents. (B) Plots of ln i^+ vs time for the spectra shown in (A). Two adsorbed states of hydrogen appear for the caustic-treated sample whereas only one appears for the air-exposed sample.

as a function of time from (a) a polycrystalline tin oxide surface which had been exposed to a 10 M NaOH solution for 30 minutes at 90°C and (b) a polycrystalline tin oxide surface exposed only to atmospheric humidity. Both surfaces are hydroxylated, but the hydroxyl group concentration is considerably greater for the caustic-treated surface. Plots of ln i^+ versus time of the spectra shown in figure 2(A) show that two adsorbed states of hydrogen are present on the caustic-treated surface whereas only one appears for the air-exposed sample. The presence of multiple binding states of H on a caustic-treated sample has been verified recently using energy analysis of the describing H^+ ions (ESDIED).

ELS is another technique which is extremely useful in characterizing tin oxide surfaces particularly when combined with a valence-band photoemission technique. The difficulty in using ELS lies in interpreting the complex spectra. However, interpretation of the spectra as a mixture of surface plasmons, bulk plasmons and optically allowed interband and intraband transitions yields a satis-

factory understanding of the spectral features (52,53). In order to make an appropriate interpretation, electronic-structure information is required from filled-energy level experiments such as ESCA or VPS, unfilled-energy level experiments such as inverse photoemission spectroscopy (IPS), Bremstrallung spectroscopy or constant initial state UPS, and theory (54-59). After construction of the complete electronic structural diagram from high lying core levels to about 50 eV above the Fermi level for both SnO and SnO_2, it is possible to assign ELS features as plasmons and electronic transitions using dipole selection rules. A typical set of ELS spectra taken from a vacuum-annealed tin oxide surface are shown in figure 3. The spectra shown were taken using electron beam energies from 200 to

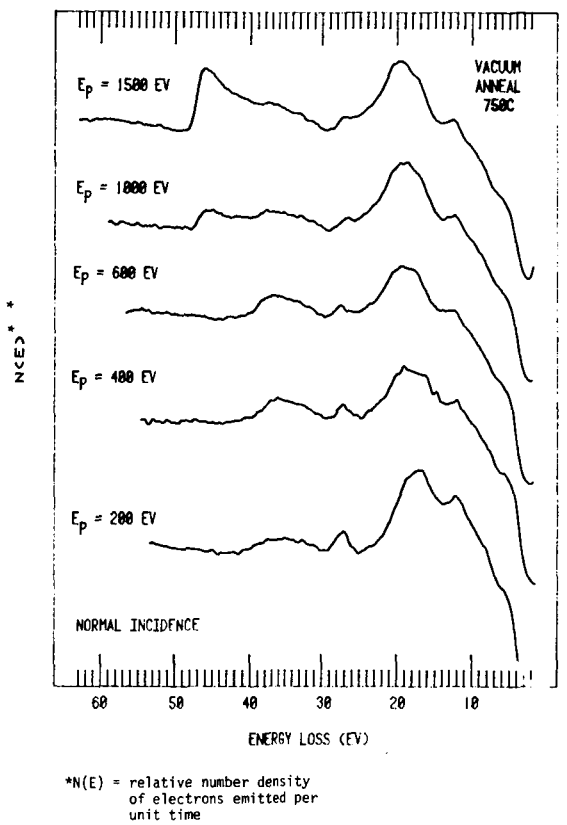

Figure 3. Variation in the N(E) ELS spectrum with primary beam energy E_p. The sets of spectra are essentially a depth profile of the annealed material. Assignment of the features is given in ref. 53.

1500 eV. Increasing the primary beam energy results in a less surface sensitive spectrum. The 1500 eV spectrum is characteristic of bulk SnO_2 while the 200 eV spectrum is more SnO like. The small peak at 27 eV is only dipole allowed for SnO. Note that its contribution decreases as the primary beam energy increases.

Valence-band features are also sensitive to SnO, SnO_2 defects and hydroxyl groups. This is illustrated in figures 4 and 5. Figure 4(A) shows the valence band after annealing the tin oxide at 600°C. This spectrum is characteristic of

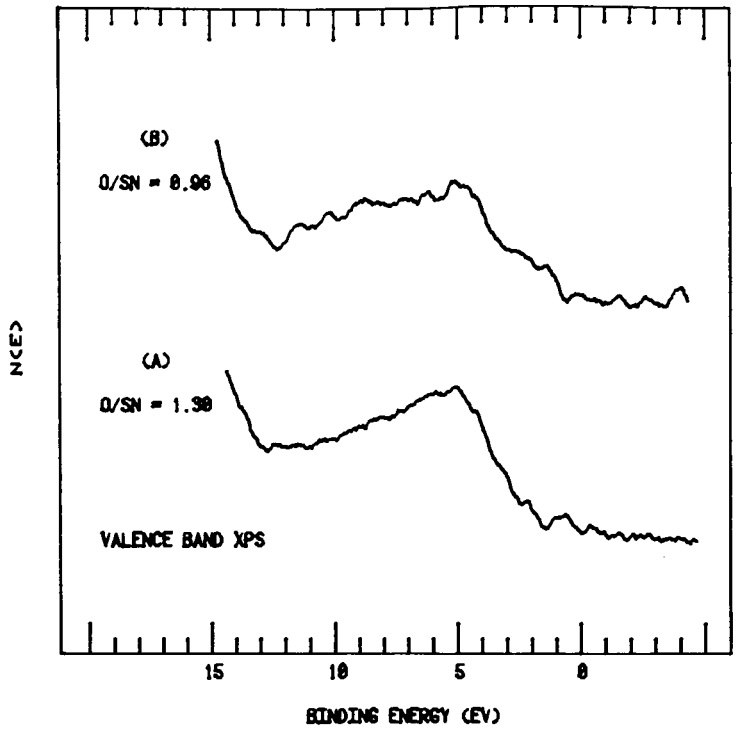

Figure 4. Valence-band ESCA spectra taken after (A) annealing at 600°C and (B) after bombardment with 2 keV argon ions.

bulk SnO_2. Spectrum (B) was taken after sputtering the surface with 2 keV argon ions. A broad defect structure is observed in the bandgap and SnO features are apparent below the Fermi level. Annealing in oxygen converts the valence-band spectrum back to that shown in (A), and corresponding changes appear in the ELS spectra. Figure 5 shows the valence-band spectrum of a hydroxylated tin oxide surface in (A). The large feature at about 10 eV is due to emission from hydroxyl groups. Annealing at 500°C greatly reduces the size of this peak (spectrum (B)), and annealing at 600°C completely eliminates it leaving an SnO_2 spectrum (spectrum (C)). This behavior is consistent with the bulk dehydration study of Giesekke et al. (47). A distinct peak due to hydroxyl groups also appears in ELS spectra (60).

III. PREPARATION AND CHARACTERIZATION OF PLATINIZED TIN OXIDE

Due to the importance of platinized tin oxide and the unique properties of tin oxide, numerous methods of producing these surfaces have been developed. Katayama (61,62) has discussed the preparation and ESCA characterization of platinized tin oxide electrodes. In these studies ethanol solutions containing $SnCl_4$, $SbCl_3$ and H_2PtCl_6 were sprayed onto glass substrates held at 550°C. It is also possible to form a tin oxide layer first by hydrolysis of a tin chloride solution in hydrochloric acid and then deposit the Pt (63). The Pt can be deposited using

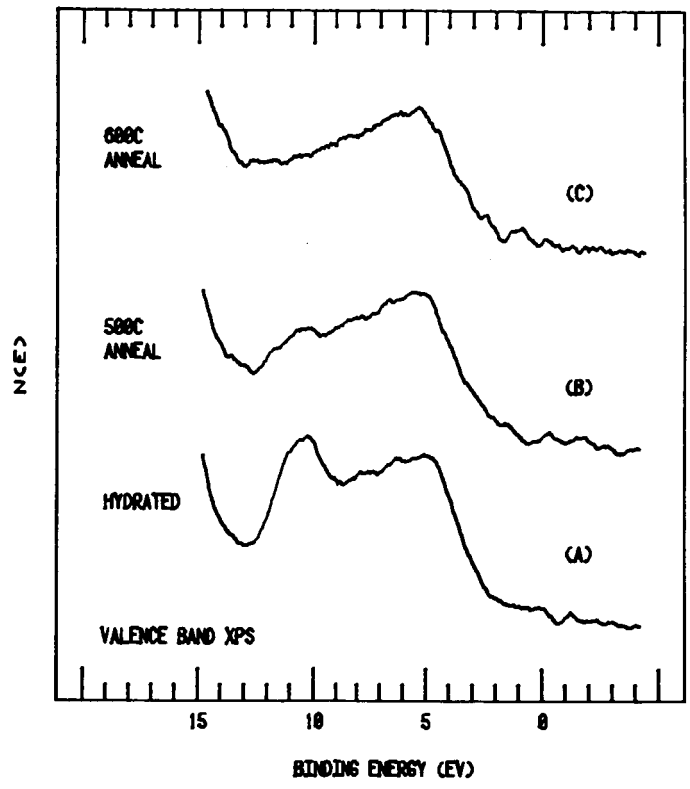

Figure 5. Valence-band XPS spectra taken from a tin oxide surface after (A) hydroxylation by exposure to atmospheric humidity, (B) annealing at 500°C in vacuum for 45 minutes and (C) annealing in vacuum at 600°C for 30 minutes.

one of several different methods including (1) impregnation (chemisorption of a Pt-containing species), (2) an electrochemical deposition, (3) spray hydrolysis, (4) deposition from a molten salt mixture or (5) thermal decomposition of a platinum-containing organic compound such as platinum acetyl acetonate. Watanabe et al. (64) have discussed the pretreatment and chemisorption variables which yield Pt loadings of 0.2 to 1 ug/cm^2 and high dispersions (> 0.9). As described in an earlier study (63), an alkaline pretreatment consisting of immersing the tin oxide in 10M NaOH at 90°C was found to important. A platinizing solution consisting of 1000 ppm Pt (IV), 0.135M $NaHPO_4$ and 0.5M NaCl was found to be most effective in the platinization process. Rutherford back-scattering was used to determine the total amount of Pt present (65), and electrochemical reduction of H^+ was used to determine the concentration of surface Pt atoms. Impregnation of Pt and Sn onto an alumina surface from an acetone solution containing $SnCl_4$ and H_2PtCl_6-$6H_2O$ has been used by Davis (66) and Hoflund et al. (67).

There are two different ways of depositing Pt electrochemically. The first is to simply use cathodic plating conditions from a Pt salt-containing electrolyte

(63). The second is to select an appropriate chemisorption reaction and to influence this reaction using anodic potentials. This process has been examined thoroughly for the case of electrochemisorption of hexahydroxyplatinate onto tin oxide over a potential range of 0.0 to 1.0V versus SCE (68). Figure 6 shows the

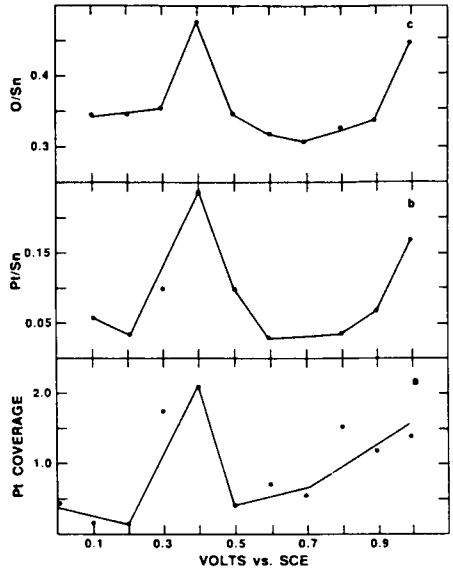

Figure 6. Amount of Pt deposited from a solution containing 0.01 M KOH, 2.56 x 10^{-3}M $Na_2Pt(OH)_6$,and 1.0M $NaClO_4$. Curve a shows the results of the electro-chemical determination. Curve b shows the results of an ESCA determination, and curve c shows the O-to-Sn ratio determined from corrected O 1s and Sn 3d peak area.

amount of Pt deposited as a function of potential. A large maximum occurs at a potential of 0.4V versus SCE which is believed to be due to the formation of active surface intermediates. An ESCA analysis of the deposited Pt also shows that its chemical state varies in a similar way as the amount. This dependence is shown in figure 7 which is a plot of the ESCA Pt 4f binding energy versus potential. Larger values suggest a more oxidized form of the Pt, and again a maximum is observed at about 0.4 eV.

The chemical state of the Pt in Pt/Sn is an important topic which has been considered in several studies (61-63,67-77). Most of these studies rely upon the use of ESCA or Mössbauer for chemical state determination. An ESCA study by Cox et al. (69) of Pt chemisorbed on polycrystalline tin oxide shows that it is possible to alter the chemical state of Pt by various oxidative and reductive treatments. This is illustrated in figure 8 for a lightly loaded sample. Heating the as-prepared sample (A) at 600°C in 11 Torr of O_2 for 30 minutes produces a mixture of PtO and PtO_2 (B) while annealing in hydrogen (C) or vacuum (D) reduces the Pt to mostly metallic form. Related results from a thin film of Pt/SnO_x deposited on alumina are shown in figure 9 (67). In this case the samples were heated in air at 450°C (a) and under 1 atm of H_2 at 500°C (b). Similar chemical state changes are observed in this figure. Furthermore, it appears that exposure to air does not oxidize Pt to metallic form. Since the Pt/SnO_x system is stable at 800°C in vacuum, the bonds between the Pt and substrate must be strong chemical

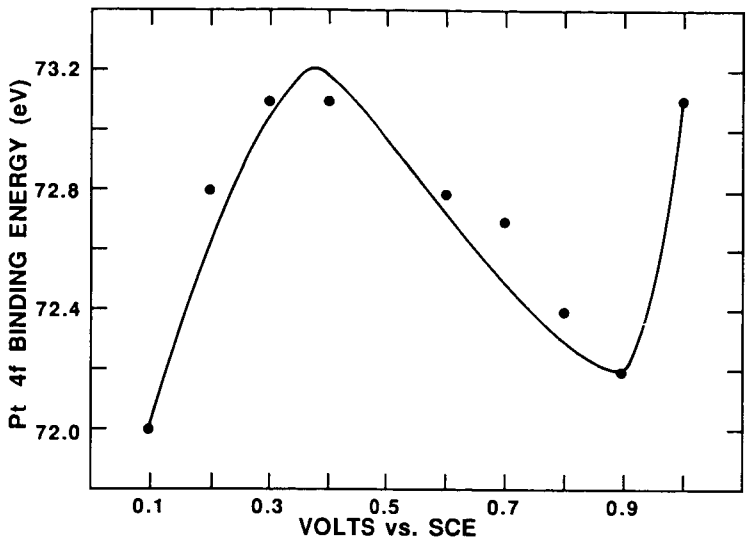

Figure 7. Average binding energies of the low binding energy ESCA Pt 4f peaks as a function of deposition potential.

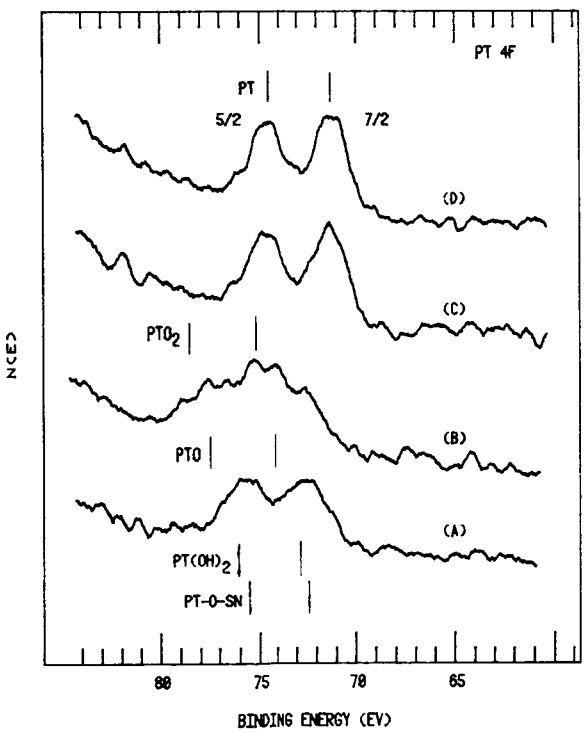

Figure 8. Pt 4f XPS spectra of a sample prepared by platinum chemisorption obtained (A) immediately after pumpdown, (B) after high-temperature oxidation, (C) after high-temperature reduction, and (D) after a high-temperature anneal in vacuo.

bonds. These ESCA studies all suggest that Pt-O-Sn bonds anchor the Pt to the substrate. They also suggest that a crude measure of the dispersion can be obtained from the binding energy of the metallic Pt 4f peaks (see figure 9b). In

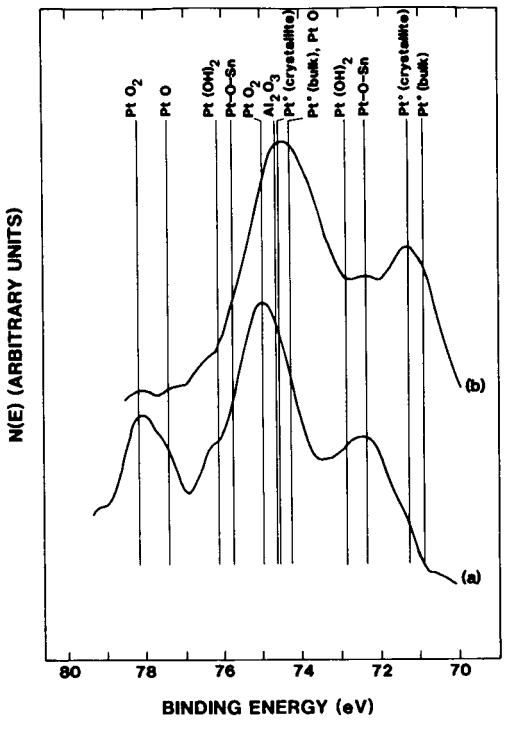

Figure 9. High resolution ESCA spectra of the Pt 4f peaks of an oxidized sample (curve a) and a reduced sample (curve b).

these studies small amounts of Cl were present on the surface which may have facilitated the changes between oxidation states. Similar experiments on Cl-free surfaces have not yet been performed.

Much controversy still exists in the literature concerning the nature of the Pt/Sn interaction. Several studies (70-72) suggest that a Pt/Sn alloy is present. However, two facts suggest that this may not be the case. The first is that studies of Pt/Sn alloys (78-80) generally show that they are poor catalysts and that their performance deteriorates with increasing surface tin concentration. The second is that other studies show that metallic tin is not present even after reduction (73-77). Clearly, more effort will be required to understand the actual situation and resolve the various controversies. However, studies of the two stable Pt/Sn alloys PtSn and Pt_3Sn (81-85) should prove useful in understanding Pt/Sn catalytic systems.

REFERENCES

1. R.A. Powell, Appl. Surface Sci. 2(1979)397.
2. M.E. Woods and B.J. Hopkins, J. Phys. C 18(1985)3255.
3. A.W.C. Lin, N.R. Armstrong and T. Kuwana, Anal. Chem. 49(1977)1228.
4. P. Sen, M.S. Hegde and C.N.R. Rao, Appl. Surface Sci. 10(1982)63.
5. R.A. Powell and W.E. Spicer, Surface Sci. 55(1976)681.
6. C.L. Lau and G.K. Wertheim, J. Vac. Sci. Technol. 15(1978)622.
7. A.J. Bevolo, J.D. Verhoeven and M. Noack, J. Vac. Sci. Technol. 20(1982)943.
8. M. Nagasaka, H. Fuse and T. Yamashina, Thin Solid Films 29(1975)L29.
9. D. Elliot, D.L. Zellmer and H.A. Laitinen, J. Electrochem. Soc. 117(1970)1343.
10. H.A. Laitinen and T.M. Hseu, Anal. Chem. 51(1979)1550.
11. H. Kim and H.A. Laitinen, J. Amer. Cer. Soc. 58(1975)23.
12. K. Din, R.C. Owen and M.A. Fox, J. Phys. Chem. 85(1981)1679.
13. H.A. Laitinen, Denki Kagaku 44(1976)626.
14. H.A. Laitinen, C.A. Vincent and T.M. Bednarski, J. Electrochem. Soc. 115(1968)1024.
15. A. Franz, G. Kent and R.L. Anderson, J. Electron. Mater. 6(1977)107.
16. G.K. Bhagavat and K.B. Sundaram, Thin Solid Films 63(1979)197.
17. A.C. Chang, IEEE Trans. Electron Devices ED-26(1979)1864.
18. H. Pink, L. Treitinger and L. Vite, Jpn. J. Appl. Phys. 19(1980)513.
19. H. Ogawa, A. Abe, M. Nishikawa and S. Hayakawa, J. Electrochem. Soc. 128(1981)2020.
20. J.L. Vossen, RCA Rev. 32(1971)289.
21. R.N. Ghoshtagore, J. Electrochem. Soc. 125(1978)110.
22. Y. Bondeville, F. Figueras, M. Forissier, J-L Portefaix and J.C. Vedrine, J. Cat. 58(1979)52.
23. H.J. Herniman, D.R. Pyke and R. Roid, J. Cat. 58(1979)68.
24. B. Hori, N. Takezawa and H. Kobayashi, J. Cat. 80(1983)437.

25. F. Solymosi and J. Kiss, J. Cat. 54(1978)42.

26. F. Solymosi and J. Kiss, J. Cat. 41(1976)202.

27. M. Stoh, H. Hattori and K, Tanabe, J. Cat. 43(1976)192.

28. M.J. Fuller and M.E. Warwick, J. Cat. 42(1976)418.

29. M.J. Fuller and M.E. Warwick, J. Cat. 29(1973)441.

30. F. Sala and F. Trifiro, J. Cat. 34(1974)68.

31. F. Sala and F. Trifiro, J. Cat. 41(1976)1.

32. F. Sala and F. Trfiro, J. Cat. 34(1974)68.

33. F. Trifiro, P.L. Villa and I. Pasquon, La Chimica e L'Industria 52(1970)857.

34. F. Trifiro and I. Pasquon, La Chemica e L'Industria 52(1970)228.

35. G. Centi and F. Trifiro, App. Cat. 12(1984)1.

36. F. Solymosi and J. Kiss, J.C.S. Chem. Comm. (1974)509.

37. V. Fattore, Z.A. Fuhrman, G. Manara and B. Notari, J. Cat. 37(1975)215.

38. H. Kim and H.A. Laitinen, J. Electrochem. Soc. 122(1975)53.

39. H. Yoneyama and H.A. Laitinen, J. Electroanal. Chem. 79(1977)129.

40. H. Yoneyama and H.A. Laitinen, J. Electroanal. Chem. 75(1977)647.

41. H.A. Laitinen and J.M. Conley, Anal. Chem. 48(1976)1224.

42. I. Uchida, K. Niki and H.A. Laitinen, J. Electrochem. Soc. 125(1978)1760.

43. H.A. Laitinen and N.H. Watkins, J. Electrochem. Soc. 123(1976)804.

44. D.G. Davis and R.W. Murray, Anal. Chem. 49(1977)194.

45. T. Takei and H.A. Laitinen, Surf. Tech. 18(1983)123.

46. T. Takei and H.A. Laitinen, Surf. Tech. 18(1983)117.

47. E.W. Giesekke, H.A. Gutowsky, P. Kirkov and H.A. Laitinen, Inorg. Chem. 6(1967)1294.

48. G.B. Hoflund, D.F. Cox, G.L. Woodson and H.A. Laitinen, Thin Solid Films 78(1981)357.

49. G.B. Hoflund, P.H. Holloway and W.H. Hocking in Secondary Ion Mass Spectrometry SIMS IV edited by A. Benninghoven, J. Okano, R. Shimizu and H.W. Werner, Springer-Verlag, Berlin 36(1984)231.

50. D.F. Cox, G.B. Hoflund and W.H. Hocking, Appl. Surface Sci. 26(1986)239.

51. G.B. Hoflund, SEM Journal IV(19851391.

52. G.B. Hoflund, D.F. Cox, T. Ohuchi, P.H. Holloway and H.A. Laitinen, Appl. Surface Sci. 14(1982-83)281.

53. D.F. Cox and G.B. Hoflund, Surface Sci. 151(1985)202.

54. S. Munnix and M. Schmeits, Sol. St. Commun. 43(1982)867.

55. F. Arlinghaus, J. Phys. Chem. Sol. 35(1974)931.

56. J.G. Gay, W.A. Albers, Jr., and F.J. Arlinghaus, J. Phys. Chem. Sol. 29(1968)1449.

57. S. Munnix and M. Schmeits, Surface Sci. 126(1983)20.

58. S. Munnix and M. Schmeits, Phys. Rev. B 27(1983)7624.

59. J. Robertson, Phys. Rev. B 30(1984)3520.

60. D.F. Cox, G.B. Hoflund and H.A. Laitinen, Appl. Surface Sci. 20(1984)30.

61. A. Katayama, Chem. Lett. (1978)1263.

62. A. Katayama, J. Phys. Chem. 84(1980)376.

63. G.B. Hoflund, D.F. Cox and H.A. Laitinen, Thin Solid Films 83(1981)261.

64. M. Watanabe, S. Venkatesan and H.A. Laitinen, J. Electrochem. Soc. 130(1983)59.

65. J. Rosenfarb, H.A. Laitinen, J.T. Sanders and H.A. Van Rinsvelt, Anal. Chim. Acta 108(1979)119.

66. B.H. Davis, J. Cat. 46(1977)348.

67. G.B. Hoflund, D.A. Asbury and R.E. Gilbert, Thin Solid Films 129(1985)139.

68. H.A. Laitinen, J.R. Waggoner, C.Y. Chan, P. Kirszensztejn, D.A. Asbury and G.B. Hoflund, J. Electrochem. Soc. 133(1986)1568.

69. D.F. Cox, G.B. Hoflund and H.A. Laitinen, Langmuir 1(1985)269.

70. H. Lieske and J. Volter, J. Cat. 90(1984)96.

71. F.M. Dautzenberg, J.N. Helle, P. Biloen and W.M.H. Sachtler, J. Cat. 63(1980)119.

72. R. Bacaud, P. Bussiere and F. Figueras, J. Cat. 69(1981)399.

73. A.C. Muller, P.A. Engelhard and J.E. Weisang, J. Cat. 56(1979)65.

74. R. Burch, J. Cat. 71(1981)348.

75. R. Burch and L.C. Garla, J. Cat. 71(1981)360.

76. S.R. Adkins and B.H. Davis, J. Cat. 89(1984)371.

77. B.A. Sexton, A.E. Hughes and K. Foger, J. Cat. 88(1984)466.

78. K.J. Cathro, J. Electrochem. Technol. 5(1967)441.

79. Z. Karpinski and J.K.A. Clarke, J. Chem. Soc. Faraday Trans. I 71(1975)893.

80. R. Bouwman, L.H. Toneman and A.A. Holsher, Surface Sci. 35(1973)8.

81. G.B. Hoflund, D.A. Asbury, P. Kirszensztejn and H.A. Laitinen, Surface Sci. 161(1985)L583.

82. G.B. Hoflund, D.A. Asbury, P. Kirszensztejn and H.A. Laitinen, Surface and Interface Analysis 9(1986)00.

83. G.B. Hoflund and D.A. Asbury, Langmuir 00(1987)00.

84. R. Bouwman and P. Biloen, Anal. Chem. 46(1974)136.

85. R. Bouwman and P. Biloen, Surface Sci. 41(1974)348.

RARE ISOTOPE STUDIES INVOLVING CATALYTIC OXIDATION OF CO OVER PLATINUM-TIN OXIDE

Billy T. Upchurch
Science and Technology Corporation
Hampton, Virginia

George M. Wood, Jr., Robert V. Hess, and Ronald F. Hoyt
NASA Langley Research Center
Hampton, Virginia

SUMMARY

In this report results of studies utilizing normal and rare oxygen isotopes in the catalytic oxidation of carbon monoxide over a platinum-tin oxide catalyst substrate are presented. Chemisorption of labeled carbon monoxide on the catalyst followed by thermal desorption yielded a carbon dioxide product with an oxygen-18 composition consistent with the formation of a carbonate-like intermediate in the chemisorption process. The efficacy of a method developed for the oxygen-18 labeling of the platinum-tin oxide catalyst surface for use in closed cycle pulsed rare isotope carbon dioxide lasers is demonstrated for the equivalent of 10^6 pulses at 10 pulses per second.

INTRODUCTION

A primary problem limiting the use of pulsed CO_2 lasers for applications involving atmospheric transmission is due to the attenuation of the intensity of the laser frequency via absorption by the atmospheric carbon dioxide present at the level of about 330 ppm concentration. As this is almost exclusively the common isotope $^{12}C^{16}O_2$, the use of the rare isotope CO_2, where the carbon and the oxygen are in the forms of carbon-12 and oxygen-18, would enable the laser to pulse at frequencies which would not be absorbed by the atmosphere. These frequency envelopes or "windows" have been determined (refs. 1 and 2). Among the available rare isotope CO_2 compounds, $C^{18}O_2$ not only contains the cheaper of the two oxygen rare isotopes, but it also provides a laser frequency at 9.1 micrometers with improved atmospheric transmission along with the added potential for an enhanced aerosol scattering coefficient (ref. 3). Other lasing frequencies are available for other possible applications.

Rare isotope $C^{18}O_2$ laser operation has been carried out at 300°C with a Pt/Al_2O_3 catalyst at Los Alamos National Laboratory (ref. 4). In these studies, while the alumina was considered an inert substrate and not a participant in the catalytic recombination of $C^{18}O$ and $^{18}O_2$ to form CO_2, special attention and care were necessary to reduce the exchange or scrambling of the normal isotope oxygen in $Al_2{}^{16}O_3$ with the $^{18}O_2$ and the $C^{18}O$ dissociation products of the laser medium. A platinum-tin oxide catalyst has been shown to operate with a respectable recombinative efficiency at considerably lower temperatures than the Los Alamos study of platinum on alumina (ref. 5).

The primary goals of this effort were to measure isotopic exchange between rare-isotope laser gases (CO_2, CO, O_2) and common isotope Pt/SnO_2 catalyst material

and to develop techniques to maximize isotopic integrity of rare isotope laser gases to maintain laser power at the desired frequency. A further goal was to utilize these rare isotope gases to determine mechanistic details of CO oxidation on the Pt/SnO_2 catalyst.

Experiments described in this paper demonstrate that, while oxygen exchange between the gaseous oxygen and carbon monoxide species and the Pt/SnO_2 substrate does indeed occur at low reaction temperatures, the isotopic scrambling may be eliminated by an inexpensive isotope exchange surface labeling technique developed at Langley Research Center (ref. 6).

EXPERIMENTAL

The experimental apparatus for isotope measurements consisted of a test gas cylinder connected through a gas drying chamber, flow controller, and a temperature controlled catalyst reactor chamber to a mass spectrometer gas sampling inlet. The drying chamber was charged with anhydrous magnesium perchlorate. A Hastings mass flow controller was placed upstream from the catalyst chamber. Excess gas flow not passing into the mass spectrometer was diverted through a Hastings mass flow meter to the outside atmosphere. The mass spectrometer was a DuPont CEC Model 21-104 magnetic sector unit. The catalyst reactor chamber was built from components and maintained temperature control within $0.5^{\circ}C$. The catalyst of $1\%Pt/SnO_2$ was obtained from Englehard Industries. All catalyst charges were placed in the chamber enclosed within a 6.35 mm internal diameter by approximately 40 cm quartz tube. The catalyst was held in place by quartz wool plugs on each end of the charge. All rare isotope gas compositions were obtained from Cambridge Isotope Laboratories with stated purities of better than 98 atom percent and were analyzed mass spectrometrically in our laboratory prior to use. All other gases were from Scott Specialty gases. Chemisorption measurements were carried out using a Shimadzu thermal conductivity detector gas chromatograph. All test gas flow rates were 5 standard cubic centimeters per minute. All CO concentrations were 2 percent by volume in neon. All O_2 concentrations were 1 percent by volume in neon. All stoichiometric mixtures of CO and O_2 were 2 percent and 1 percent, respectively, with a 2 percent neon spike and the balance helium. Hydrogen was 7.5 percent by volume in helium.

RESULTS AND DISCUSSION

During carbon monoxide chemisorption studies, it was found that some CO chemisorbed onto the Pt/SnO_2 catalyst at room temperature while some CO simultaneously oxidized and evolved as CO_2 with the subsequent reduction of the catalyst surface by removal of some oxide. A room temperature CO chemisorption titration of a 1.0 gram sample of 1% Pt/SnO_2 catalyst was found to bind 42 microliters of CO. Thermal desorption yielded 42 microliters of CO_2 as measured mass spectrometrically. Another sample after CO chemisorption followed by chemical displacement by gaseous hydrogen chloride evolved CO_2 as detected with the mass spectrometer. Subsequently, chemisorption of $C^{18}O$ upon a normal isotope Pt/SnO_2 catalyst substrate followed by thermal desorption of CO_2 yielded an approximately 4:4:1 ratio of $C^{16}O_2:C^{16}O^{18}O:C^{18}O_2$ as would be expected from a carbonate species thus lending further support for the existence of such an intermediate species in the recombinative redox mechanism.

Since our primary goal was to develop a catalytic regeneration system for the operation of a rare isotope closed cycle pulsed CO_2 laser system, isotope exchange studies were subsequently carried out to thoroughly investigate the Pt/SnO_2 catalyst system with regard to isotopic interactions with all laser gas species as shown in table 1.

As is noted in table I, $C^{18}O$ was found to readily extract oxygen-16 from the unlabeled Pt/SnO_2 at temperatures from room temperature upwards. Thus, the isotopically unlabeled catalyst cannot be used for regeneration of the dissociation products which would be encountered in a closed cycle rare isotope CO_2 laser. Rows 2, 3, and 4 in table I show that there was no exchange or scrambling reaction observed between $^{18}O_2$ (alone or in combination with $^{16}O_2$) and the Pt/SnO_2 catalyst substrate until temperatures substantially greater than the expected operating temperatures of the laser catalyst bed were attained.

When a stoichiometric mixture of the oxygen-18 labeled carbon monoxide and oxygen was passed over the normal isotope Pt/SnO_2 catalyst at 100°C, 85 percent and 15 percent $C^{18}O_2$ and $C^{16}O^{18}O$, respectively, were initially formed (row 5, table I). These yields gradually changed to 90 percent and 10 percent after 8 hours or more of operation. Evidently, there are two possible recombinative mechanisms occurring, one of which is perhaps at the surface, and one which is interactive with the SnO_2 surface. In addition, the SnO_2 surface must slowly become isotopically labeled with oxygen-18 via the interactive exchange mechanism. Complete surface labeling by this technique would require an inordinately long time for sufficient isotope labeling to be attained even if diffusion from the bulk were inoperative.

With the foregoing data in hand, it was decided that an attempt would be made to label the surface of the $Pt/Sn^{16}O_2$ catalyst with oxygen-18 by first chemically reducing the SnO_2 surface to elemental tin followed by reoxidation of the tin surface to $Sn^{18}O_2$ with $^{18}O_2$. Should all of the active normal-isotope oxygen at the surface be exchanged in this way, then the catalyst would be suitable for use in a rare isotope closed cycle CO_2 laser if diffusion of the bulk matrix oxygen-16 to the surface does not occur.

The chemical reduction of the Pt/SnO_2 catalyst was accomplished by exposing it to a flowing stream of 7.5 percent H_2 in helium at 225°C. The active surface oxygen removal was judged complete after the mass spectrometrically monitored H_2O concentration in the stream had dropped to the instrument background level. The reduced substrate surface was then reoxidized at 225°C with a gas stream containing 1% $^{18}O_2$ until the $^{18}O_2$ concentration exiting the catalyst chamber had attained and remained at the 1 percent concentration level for at least one hour as measured on the mass spectrometer. The temperature was then reduced to ambient under neon flow. The preceding isotope exchange labeling of the metal oxide catalyst was accomplished in about 5 hours and is partly the basis for our patent application (ref. 6).

The 1% $Pt/Sn^{18}O_2$ surface labeled catalyst was then evaluated under conditions listed in row 6 of table I and was found to maintain the isotopic integrity of the rare isotope gas composition for a period of 30 hours of operation before shutting down the reactor voluntarily. The subsurface normal oxygen-16 isotope in the bulk of the catalyst material obviously does not diffuse to the surface at or below the test temperature of 100°C. While the efficacy of the surface labeled catalyst has been demonstrated during continuous operation for 30 hours at the elevated

temperature, as well as other periods at lower temperatures, longer term evaluative tests are needed and will be performed during 1987.

CONCLUDING REMARKS

To summarize our accomplishments and ongoing efforts involving oxygen isotope labels we have demonstrated supportive evidence for the existence of a carbonate-like intermediate species involving the catalyst and chemisorbed CO for the redox mechanism. We have discovered an economical method for preparing a catalyst for use in a closed cycle rare isotope pulsed carbon dioxide laser and have demonstrated its efficacy in our surrogate test facility over test periods which would be comparable with 10^6 pulses at 10 pps. However, studies of longer duration are needed and the ultimate test should, of course, be carried out in a rare isotope pulsed carbon dioxide laser. We are also currently considering developing our own normal and rare isotope Pt/SnO_2 catalyst coatings on high surface-area-to-weight ratio inert support spheres.

REFERENCES

1. Freed, C.; Ross, C.; and O'Donnell, R. G., J. Mol. Spec., 49, 439-453 (1974).

2. Freed, L. E.; Freed, C.; and O'Donnell, R. G., IEEE J. Quant. Elect., QE-18, 1229-1239, (1982).

3. Hess, R. V.; Brockman, B.; Schryer, D. R.; Miller, I. M.; Bair, C. H.; Sidney, B. D.; Wood, G. M.; Upchurch, B. T.; and Brown, K. G., NASA TM-86415, 1985.

4. Sorem, M. S. and Faulkner, A., Rev. Sci. Instrum., 52, 1193-1196 (1981).

5. Brown, K. G.; Sidney, B. D.; Schryer, D. R.; Upchurch, B. T.; Miller, I. M.; Wood, G. M.; Hess, R. V.; Burney, L. G.; Paulin, P. A.; Hoyt, R. F.; and Schryer, J.: Laser Radar Technology and Applications, SPIE Proceedings, 663, 136-144 (1986).

6. NASA Langley Research Center Case No. LAR 13542-1-SB, U. S. Patent Application No. 847,304, June 1986.

TABLE I.- OXYGEN ISOTOPE LABEL STUDIES

Reactants	Catalyst	T, °C	Product Yields
$C^{18}O$	$Pt/Sn^{16}O_2$	24-150	$C^{16}O^{18}O$
$^{18}O_2$	$Pt/Sn^{16}O_2$	25-225	No Reaction
$^{18}O_2 + {}^{16}O_2$	$Pt/Sn^{16}O_2$	25-225	No Reaction
$^{18}O_2 + {}^{16}O_2$	$Pt/Sn^{16}O_2$	> 350	$^{16}O^{18}O$
$C^{18}O + 1/2\,{}^{18}O_2$	$Pt/Sn^{16}O_2$	100	85-90% $C^{18}O_2$
			15-10% $C^{16}O^{18}O$
$C^{18}O + 1/2\,{}^{18}O_2$	$Pt/Sn^{18}O_2$	100	$C^{18}O_2$

STUDIES OF CO OXIDATION ON Pt/SnO_2 CATALYST IN A SURROGATE CO_2 LASER FACILITY

Carmen E. Batten, Irvin M. Miller, and Patricia A. Paulin
NASA Langley Research Center
Hampton, Virginia

Jacqueline Schryer
Old Dominion University
Norfolk, Virginia

SUMMARY

Samples of 1% Pt/SnO_2 catalyst were exposed to a stoichiometric gas mixture of 1% CO and 1/2% O_2 in helium over a range of flowrates from 5 to 15 sccm and temperatures from 338° to 394° Kelvin. Reaction rate constants for the catalytic oxidation of carbon monoxide and their temperature dependence were determined and compared with previous literature values.

INTRODUCTION

Space-born, high-energy, pulsed laser systems are valuable for improved world-wide weather forecasting and for the more efficient operation of aircraft (ref. 1). They can measure wind velocity, temperature, and humidity at various levels in the atmosphere (refs. 1 and 2). They are also useful for measuring atmospheric pollutants, such as NH_3 and HCℓ (ref. 3). In this regard, the CO_2 TEA laser is of particular interest because of its high power, and, when used with rare isotope CO_2, such as $C^{18}O_2$, its capability of improved atmospheric transmission (ref. 4).

For satellite applications the CO_2 laser must be operated closed-cycle to conserve gas, especially if rare isotope CO_2 is used. However, the laser discharge causes a dissociation of CO_2 into CO and O_2; in a short time period (10 to 20 minutes) a build-up of a small concentration of O_2 occurs. This causes a rapid power loss, ending in erratic behavior (ref. 4). To correct this problem, an efficient, low temperature catalyst is needed to recombine CO and O_2 to maintain a constant, high power level for long time periods (a year or more). For efficient laser operation, it should have high activity between 25 and 100°C at low concentrations of O_2 ($< 1/2$ mol %).

Stark and Harris (ref. 5) formulated Pd/SnO_2 and Pt/SnO_2 catalysts that were found useful for the catalytic oxidation of CO. They observed a first order rate law for the conversion of O_2 and CO that fitted their data well; that is,

$$-\ln (p/Po) = A\ wt/V$$

where p is the partial pressure of oxygen at time t (sec), P_o is the initial oxygen partial pressure, w is the catalyst mass(g), V is the volume of the test gas vessel (ℓ), and A is the volumetric pumping speed for the removal of O_2 ($\ell\ s^{-1} g^{-1}$). A was treated like a reaction rate constant in an Arrhenius equation; that is,

$$A = B \exp (-E/RT)$$

$$\text{or } -\ln A = -\ln B + E/RT$$

where B is the pre-exponential ($\ell\ s^{-1} g^{-1}$), E is the activation energy, kJ mol^{-1}, R is the gas constant 8.31×10^3 kJ mol^{-1} $°K^{-1}$, and T is absolute temperature, °K. They found an E of 40 kJ mol^{-1} for the Pd/SnO_2 catalyst and 41 kJ mol^{-1} for Pt/SnO_2 catalyst.

Miller et al. (ref. 6) also observed a first order rate law for the conversion of CO and O_2 in a stoichiometric mixture of $1\%CO + \frac{1}{2}\%O_2$ in He flowing through a $1\%Pt/SnO_2$ catalyst bed, or

$$-\ln (p/P_o) = k\,\tau$$

where k is the reaction rate constant (sec^{-1}) and τ is the contact time (sec) of the flowing gas in the catalyst bed. Then, using the Arrhenius equation

$$k = B \exp (-E/RT)$$

$$\text{or } -\ln k = -\ln B + E/RT$$

where B is the pre-exponential term (sec^{-1}) they found an E of 24 kJ mol^{-1} (ref. 7). That investigation was carried out at temperatures between 25 and 75°C. Data at higher temperatures were not useful because catalyst activity and sample size (~1g) resulted in O_2 conversion approaching 100 percent.

The purpose of the current study was to extend the temperature range by using a smaller sample size and to study the effect of varying the gas flowrate and catalyst temperature on the conversion efficiency of 1% Pt/SnO_2 catalyst which had been preconditioned more rigorously than that cited in reference 6.

In the previous study, the pretreatment conditions were very moderate compared to more rigorous pretreatment procedures developed subsequently in our laboratory. Specifically, in the previous study, one hour pretreatment with helium at 225°C was used, whereas more recent studies have shown that extending the pretreatment time to about 20 hours at the same temperature improved the stability of the catalytic reaction. Therefore, it was felt necessary to re-evaluate the catalyst under the more rigorous pretreatment conditions over a wider temperature range. Consequently, experiments were conducted to determine the activation energy and reaction rate constant of the catalytic oxidation of carbon monoxide and compare them with those obtained from the previous study. Additionally, since the catalyst is being evaluated for space applications, the weight of the catalyst is an important consideration. Therefore, we designed our tests so as to obtain the efficiency of the catalyst per unit weight of catalyst in order to determine the minimum amount of catalyst required for maximum efficiency under various conditions of temperature and gas flowrates.

EXPERIMENTAL MATERIALS AND METHOD

The catalyst is a powder consisting of one percent platinum on tin oxide (w/w) which was prepared commercially by the method of Croft and Fuller (ref. 8). By that method, it was calcined at 450°C for five hours, then reduced with a mixture of 30 percent carbon monoxide in argon for two hours at 150°C. The catalyst parameters are shown in figure 1.

A weighed amount of catalyst was loaded into a plug-flow reactor which consists of a 6.8 mm I.D. quartz tube with stainless steel fittings at each end. The sample was held in place by quartz wool plugs as shown in figure 2. The loaded reactor was placed in a controlled temperature oven with stainless steel connections to the reactant gas mixture at the inlet and to the gas chromatograph at the outlet. A schematic of the entire surrogate laser facility is shown in figure 3.

As indicated in figure 1, the catalyst was pretreated for a period of 20 hours by passing high purity helium which has been dried with magnesium perchlorate and heating the reactor tube at 225°C, then cooled to room temperature under helium flow before starting the tests. The reactant stoichiometric gas mixture was first directed through a by pass line outside the oven to the gas chromatograph to measure the concentration of CO and O_2 at the inlet of the reactor. The test gas mixture contained 1% CO, 0.5% O_2, 2% Ne in helium. The neon served as an internal standard. This mixture was also passed through magnesium perchlorate to remove any water present.

The reactor was heated to the test temperature and the test gas mixture was passed through the catalyst bed at the selected flowrate. The product gases were sampled with a computer-actuated valve in the gas chromatograph which was programmed to sample consecutively for the first hour of testing and then at 90 minute intervals for the remainder of the test period. As indicated in figure 1, the chromatograph uses a coaxial column that has silica gel in one and molecular sieve in the other operated at 80°C. The coaxial column was used to separate the product components and a thermal conductivity detector was used for their measurement. The computer calculated the outlet/inlet ratios and printed the percent yield of CO_2, percent loss of O_2 and percent loss of CO for each sampling sequence. The reaction rate constant of CO and O_2 at the catalyst surface for the reaction

$$CO + 1/2\ O_2 \xrightarrow[1\%Pt/SnO_2]{\Delta} CO_2$$

was determined by plotting the negative natural logarithm of the ratio of the partial pressure of oxygen in the product gas to that of the reactant gas at the inlet as a function of residence time. By using a plot of the logarithm of the reaction rate constant versus reciprocal absolute temperature, the activation energy and pre-exponential values were determined.

TESTS

Two series of tests were conducted as outlined in figure 4. During the first series, the temperature and gas flowrate were held constant at 100°C and 10 sccm, respectively, while samples of different weight were tested. This enabled the determination of the amount of catalyst that was required for complete conversion, or 100 percent CO_2 yield, and to select the size sample for the next series of tests.

For the second series of tests samples of catalyst weighing 0.15 gram (so as to remain below 100 percent conversion) were exposed to the tests gas flowing at 5, 10, or 15 sccm while the temperature was ramped up or down from 55°C to 120°C. Fresh catalyst samples were used for each flowrate condition, each pretreated with helium prior to testing. While data were collected from the beginning of the test, only the data that were obtained after the reaction reached steady state conditions were used for the analysis, usually betwen 1000 and 4400 minutes.

RESULTS

The results of the first series of tests are shown in figure 5. The CO_2 conversion efficiency increased linearly with increase in catalyst sample mass and approached 100 percent with a catalyst mass of approximately 0.17 gram under constant temperature and flowrate. Based on these results, a catalyst sample of 0.15 gram was selected for the next series of tests so as to vary the flowrate and temperature without reaching the 100 percent CO_2 conversion.

The decay of oxygen in the product gas as a function of temperature for 3 different constant flowrate conditions of 5, 10 and 15 sccm is shown in figure 6. On increasing the temperature and returning to the initial temperature condition, no significant hysteresis was found within experimental error.

The reaction rate constants for the various temperature levels are shown in figure 7. The data suggest a first order reaction, which is consistent with the data obtained by Stark and Harris (ref. 5) and Miller et al. (ref. 6). The dependence of the rate constants on temperature is shown in figure 8. A correlation coefficient of .9972 was obtained. Calculations from this graph yielded an activation energy, $E = 55$ kJ mol^{-1} and a pre-exponential, $B = 7.5 \times 10^{7} sec^{-1}$.

DISCUSSION

In order to compare the data in the literature with that in the current study, it is necessary to convert all the data to the same basis, that is, the data need to be normalized. The key parameter that needs to be normalized is the pre-exponential factor B, in the Arrhenius equation:

$$k = B \exp(-E/RT)$$

where k = the reaction rate constant, sec^{-1}
B = pre exponential factor, sec^{-1}
E = activation energy, kJ mol^{-1}
R = Universal Gas Constant, kJ mol^{-1} $°K^{-1}$
T = Absolute temperature °K

By normalizing B, k is also normalized. The value of k found in the present study, as well as that found by Miller et al. is given in the dimension of sec^{-1}, whereas a similar parameter reported by Stark and Harris, which they call A, the pumping speed, is given in the dimension $\ell\ gm^{-1}\ sec^{-1}$.

A reaction rate constant that would be common to all three sets of data is k', in the dimension $sec^{-1}\ gm^{-1}$. To convert the B and k values in the present study, as well as those in the study by Miller et al, requires division of B and k, by the sample weight used, w, in gms, or $k' = k/w\ sec^{-1}\ gm^{-1}$ and $B' = B/w\ sec^{-1}\ gm^{-1}$. The value of w in the current study is 0.15 grams and the value of w reported by Miller et al. is 0.925 grams.

To convert the pumping speed, A, reported by Stark and Harris to k', it is necessary to divide their A value by the volume of the test gas vessel, V, which is 1.2 ℓ, or

$$k' = \frac{A}{V} \text{ gm}^{-1} \text{ sec}^{-1}$$

The pre-exponential, B', was calculated from the Arrhenius equation using their reported activation energy of 41.4 kJ mol^{-1} and several k', T values. The average B' value was 1609 sec^{-1} gm^{-1}.

However, Stark and Harris used a 1.3% Pt loading on SnO_2, whereas Batten and Miller et al. used a 1% Pt loading on SnO_2. To make the k' values of Stark and Harris comparable, it was assumed that catalyst activity was proportional to platinum loading. Therefore, the B' value of 1609 was divided by 1.3 to obtain an adjusted B' value of 1238 sec^{-1} gm^{-1}. The values of B' and E in the Arrhenius equation used to calculate the K' values for all three studies are as follows:

Reference	Pre-exponential B', sec^{-1} gm^{-1}	Activation Energy E, kJ mol^{-1}	Temperature Range, °C
Current Study	5×10^8	55.0	65-121
Miller et al.	1690	24.0	25-75
Stark and Harris	1238	41.4	21-60

Values of k' versus $^1/T$ are plotted in figure 9 for all three studies. Note that the k' values of this study are about an order of magnitude greater than those of Miller et al. Even though aliquots of the same catalyst were used in both studies, in Miller et al. an aliquot was taken from the top end of the initial sample shortly after receipt from the manufacturer. In three years, this sample was drawn down for other studies, so that aliquots taken for the current study represent portions taken from the bottom end of the sample. When there is a mixture of particles of the same density but of different size, the smaller particles will settle to the bottom of the mixture. Therefore, aliquots of the sample used in the present study will probably have a particle size distribution with a smaller mean particle size than in the earlier study. A smaller mean particle size may be associated with a higher surface area and higher Pt loading and may result in higher k' values. Another reason for the higher k' values in the current study is, probably, the more rigorous pretreatment given the catalyst compared to that in the other study. In the other study, the catalyst was pretreated with flowing He at 225°C for one hour. In the present study the catalyst was pretreated with He at 225°C for 20 hours. Previous studies had shown that this extended pretreatment time increased catalyst activity. The effect of catalyst aging during the three year time interval between the two studies is unknown.

Also, in figure 9, the k' values of Stark and Harris are several orders of magnitude below those of the present study. There may be several reasons for these low k' values. The catalyst granules were spread thinly over an area of about 15 cm^2 at the base of the laser envelope. Although no mention was made of gas circulation in the envelope, even if there were good circulation, contact of the gas mixture with the granules would not be as effective as if the granules were in a bed through which the gas mixture flowed. In this case, mass transfer would be limited mostly to diffusional processes rather than by momentum transfer. Furthermore, no mention was made of any preconditioning of the catalyst as was done in the other two studies. Preconditioning has been shown to have a very beneficial effect on catalyst activity. Finally, Stark and Harris used a gas mixture of 31% CO_2, 16% N_2, 43% He, 7% CO and 3% O_2. The concentration levels of CO and O_2 in their study are considerably higher than in the current and the previous study where gas mixtures of

1% CO and $\frac{1}{2}$ % O_2 in He were used. The effect of higher concentrations of CO and O_2 on the activity of the Pt/SnO_2 catalyst is unknown and would have to be determined by kinetic studies.

REFERENCES

1. Anon., "Space-Born Lidar Systems Aim to Improve Weather Forecasting," Research and Development, January 1985, 50-51.

2. Gage, K. S. and Balsey, B. B.: "Advances in Remote Sensing of the Atmosphere," Reviews of Geophysics and Space Physics, 21 (1983), 958-959.

3. Killinger, D. K., Menyuk, N., and Mooradian, A.: "Laser Remote Sensing of Atmospheric Pollutants," MIT Lincoln Laboratory, Final Report to the Air Force Engineering and Services Center, September 30, 1984.

4. Hess, R. V., Brockman, P., Schryer, D. R., Miller, I. M., Blair, C. H., Sidney, B. D., Wood, G. M., Upchurch, B. T., and Brown, K. G.: "Technology Assessment of High Pulse Energy CO_2 Lasers for Remote Sensing from Satellites," NASA TM 86415, April 1985.

5. Stark, D. S., and Harris, M. R.: "Catalyzed Recombination of CO and O_2 in Sealed CO_2 TEA Laser Gases at Temperatures Down to -27°C," J. Phys. E., 16, 1983, 492-496.

6. Miller, I. M., Schryer, D. R., Hess, R. V., Wood, G. M., Jr., Upchurch, B. T., and Brown, K. G.: "The Catalytic Oxidation of CO for Sealed CO_2 Laser Applications," Paper presented at the American Chemical Society National Meeting, Chicago, IL, September 9-13, 1985.

7. Brown, K. G., Sidney, B. D., Schryer, D. R., Upchurch, B. T., Miller, I. M., Wood, G. M., Hess, R. V., Batten, C., Burney, L. G., Paulin, P. A., and Hoyt, R.: "Catalytic Recombination of Dissociation Products with Pt/SnO_2 for Rare and Common Isotope Long-Life, Closed-Cycle CO_2 Lasers," presented at the S.P.I.E. Conference, Quebec City, Canada, June 4, 1986.

8. Croft, G. and Fuller, M. J.: "Water-Promoted Oxidation of Carbon Monoxide Over Tin (IV) Oxide-Supported Palladium," Nature, 269, 1977, 585-586.

A. Catalyst - 1% Pt/SnO_2 in plug-flow reactor

Parameters:

- Average particle size - 1 μm
- Bulk density - 1.934 g/cm^3
- SnO_2 density - 7.0 g/cm^3
- BET area - 6.9 m^2/g
- Specific void volume:

$$V_0' = \left(\frac{1}{1.934} - \frac{1}{7.0}\right) = .374\ cm^3/g$$

Pretreatment:

- 20 hrs at 225°C with helium gas

B. Test gas

Stoichiometric mixture:

- 1% CO, 1/2% O_2, 2% Ne, in He

C. Analytical method

Gas chromatography:

- Column type - coaxial column silica gel/molecular sieve
- Column temperature - 80°C
- Column flowrate - 40 Sccm

Figure 1. Experimental materials and method.

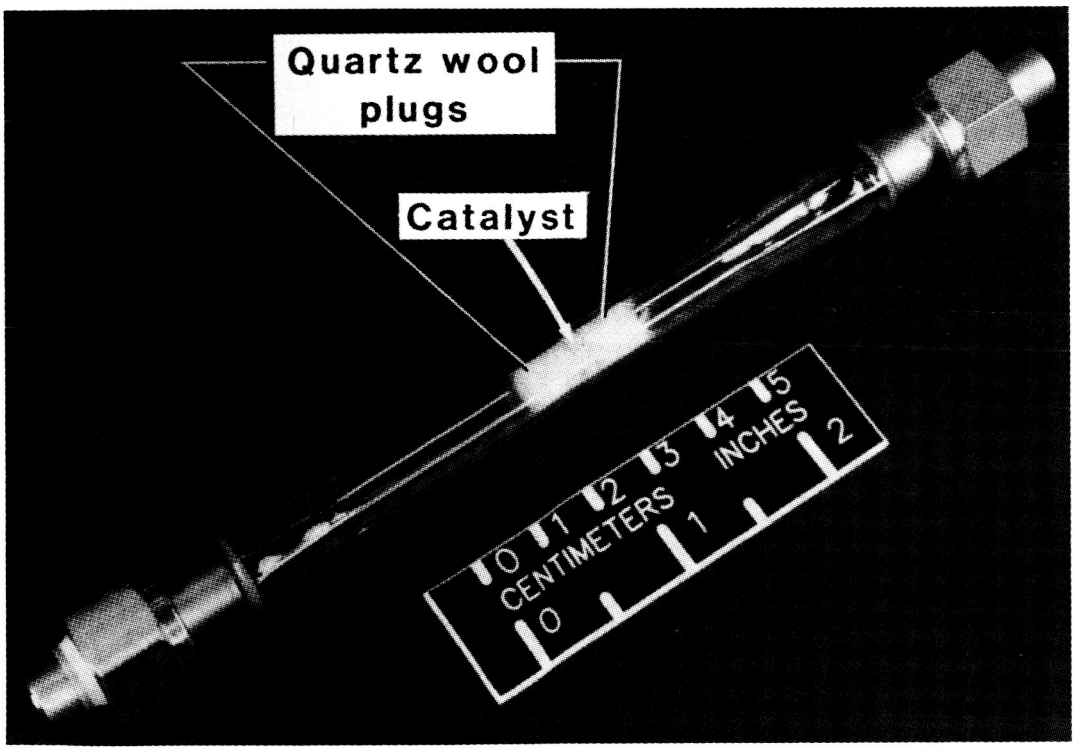

Figure 2. Catalyst reactor.

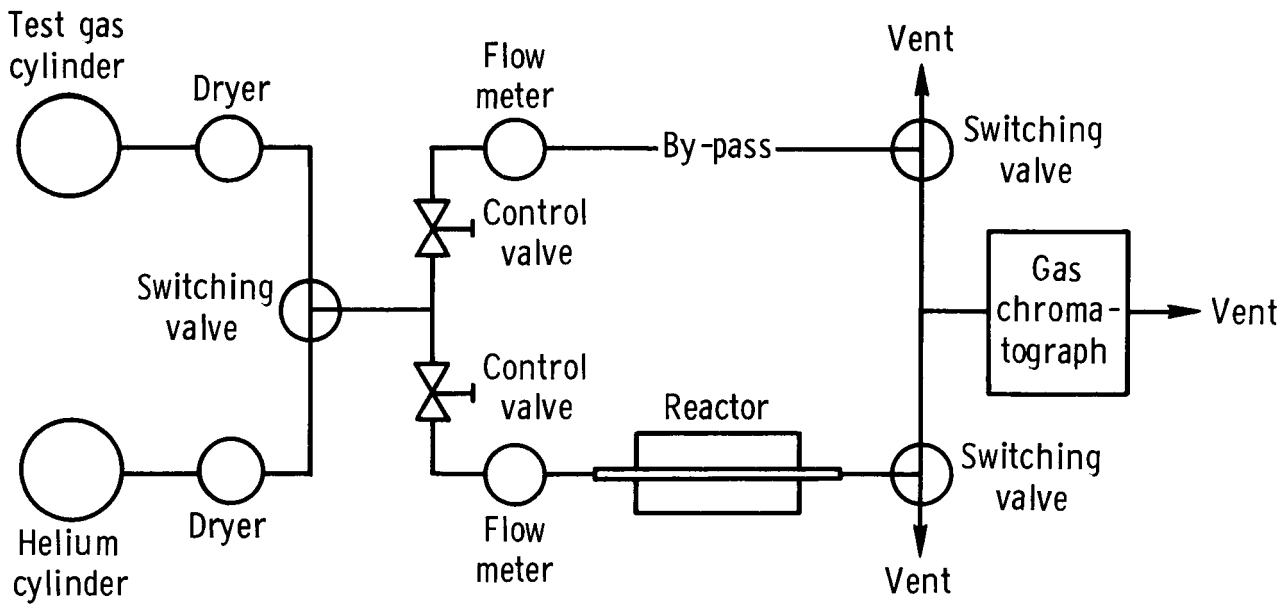

Figure 3. Schematic of surrogate laser facility.

$$CO + 1/2\ O_2 \xrightarrow[1\%\ Pt/SnO_2]{\Delta} CO_2$$

- Test 1 - Constant temperature - 100°C
  Constant flowrate - 10 Sccm
  Varying catalyst mass - 0.06 - 0.24q
- Test 2 - Constant catalyst mass - 0.15q
  Test gas flowrates - 5, 10, 15 Sccm
  Reactor temperatures - 55°C - 120°C

Data obtained	Data calculated
% yield CO_2	Reaction rate constants (sec^{-1})
% loss O_2	Activation energy - (kJ mol^{-1})
% loss CO	Pre-exponential (sec^{-1})

Figure 4. Reaction rate measurements.

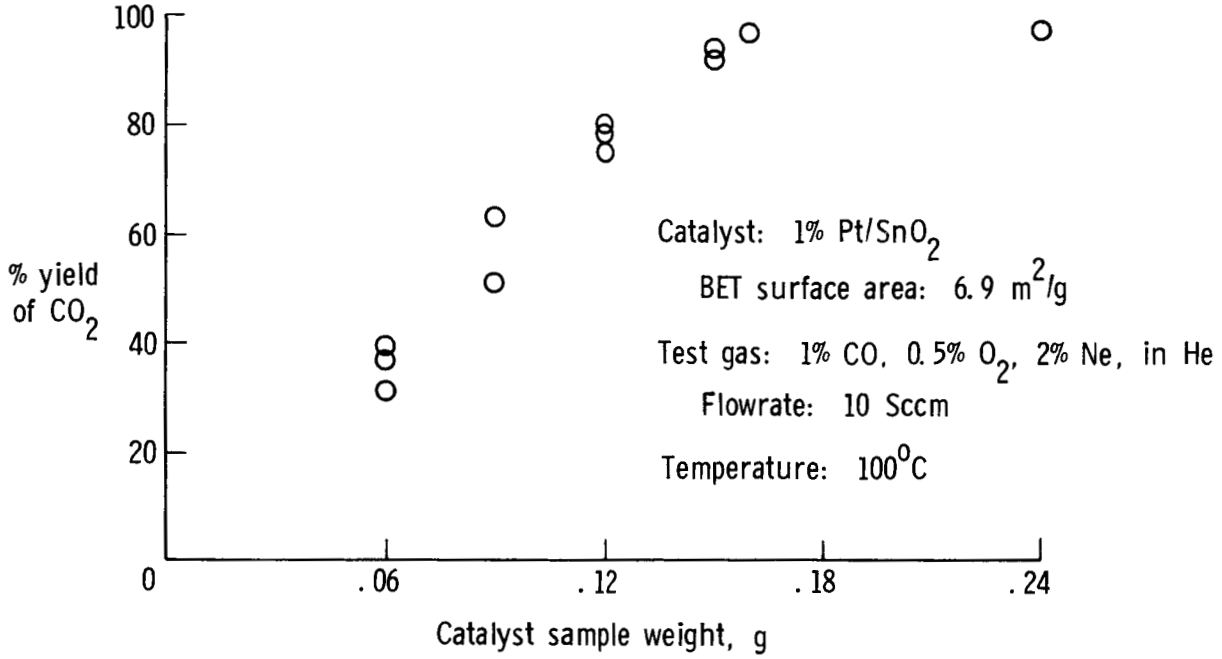

Figure 5. Conversion efficiency of catalyst versus sample weight.

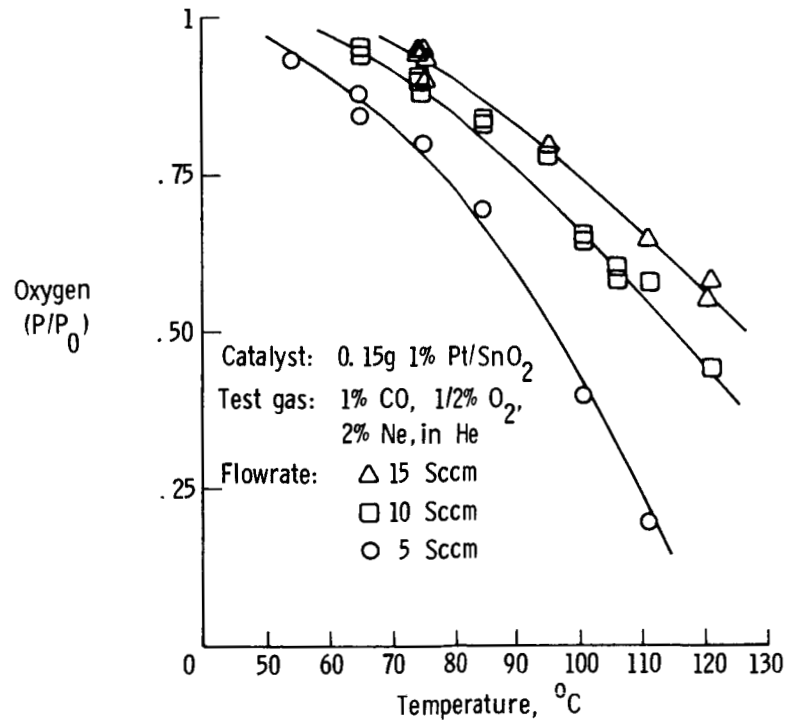

Figure 6. Reaction rates for constant reactant concentrations.

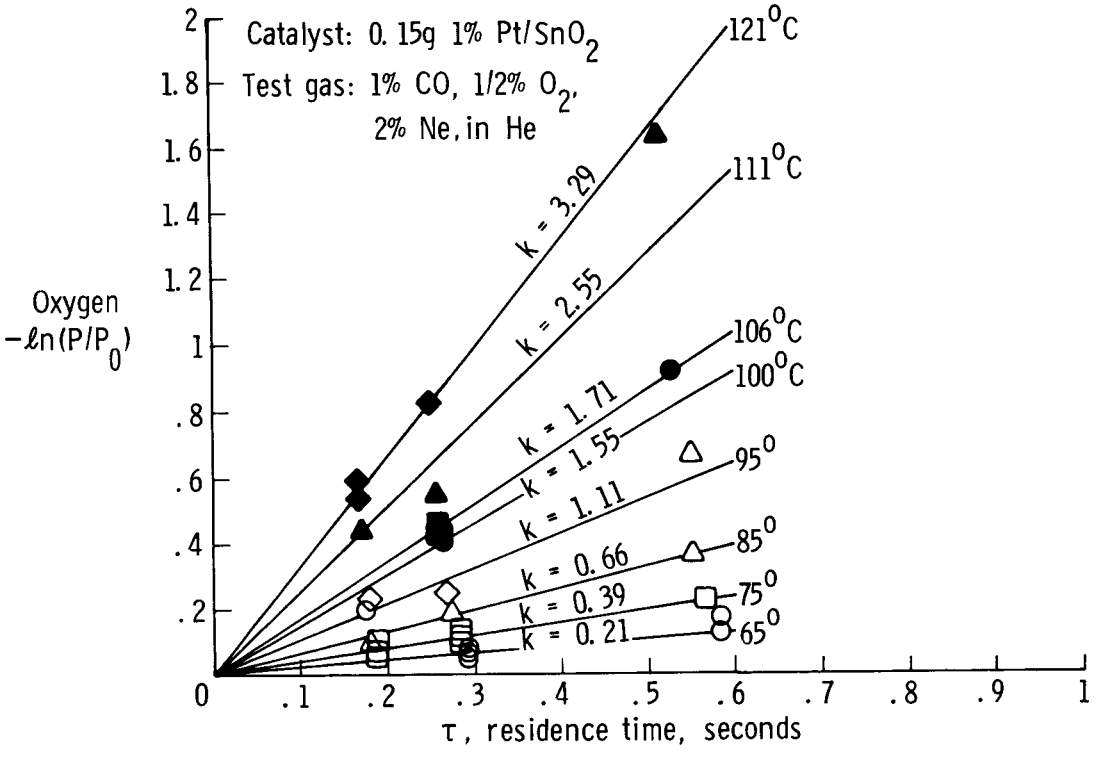

Figure 7. Reaction rate constants, k.

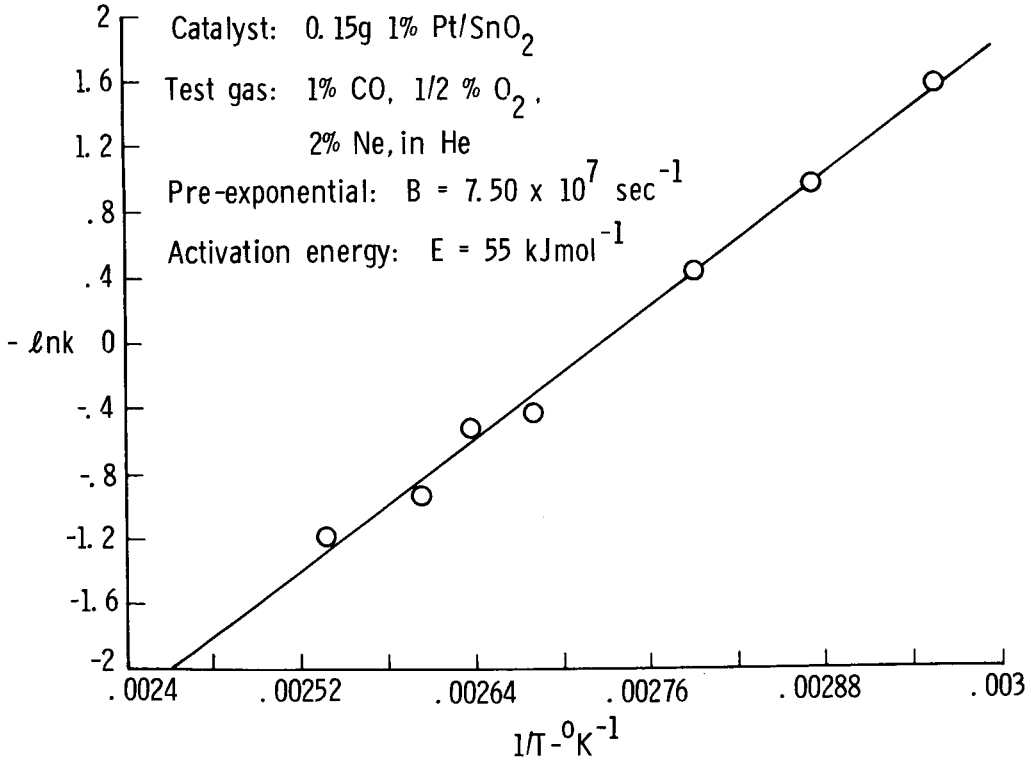

Figure 8. Arrhenius plot.

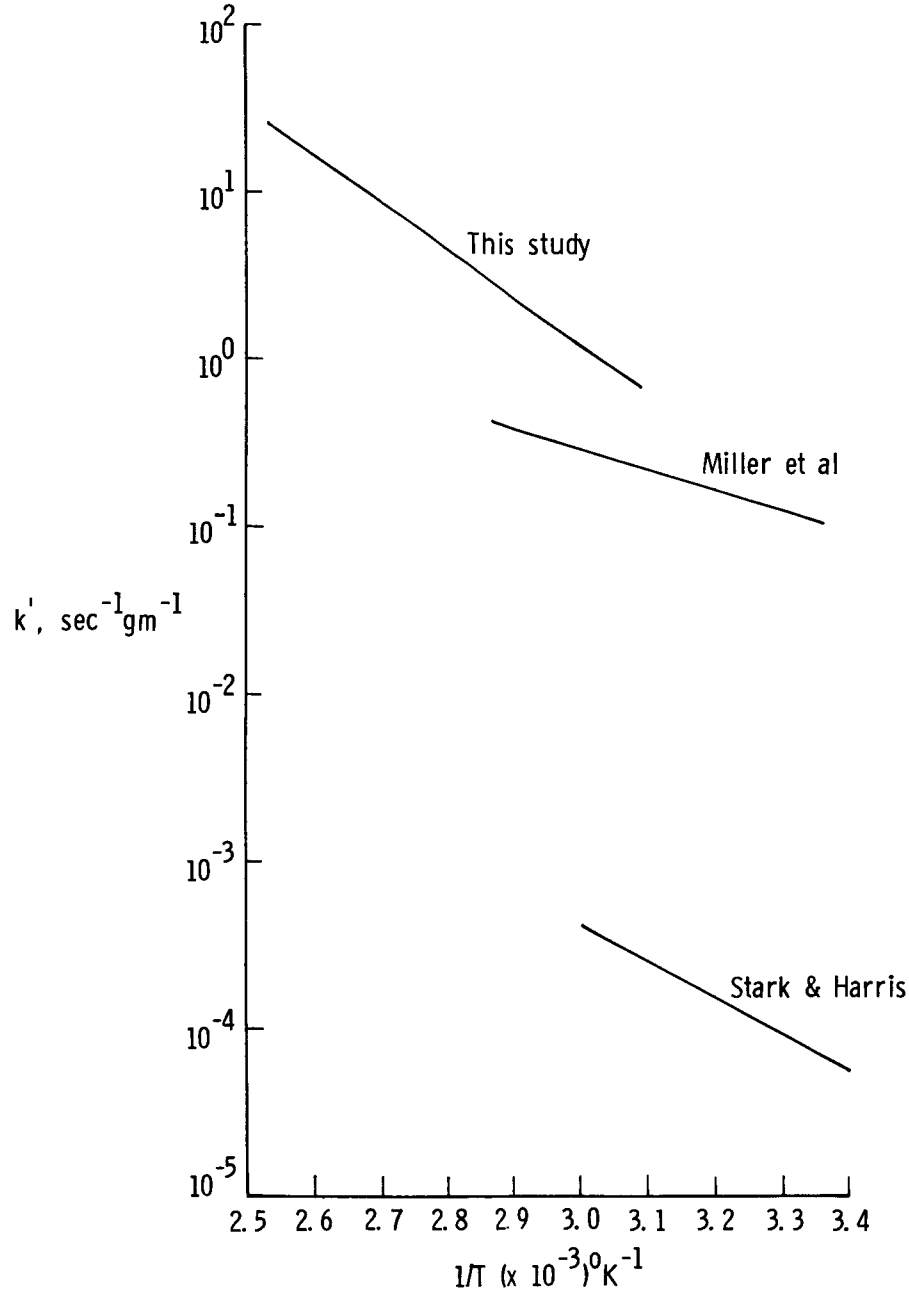

Figure 9. Plots of the Arrhenius equation for CO oxidation on Pt/SnO_2 catalysts.

N87-20540

STUDIES OF LONG-LIFE PULSED CO_2 LASER WITH Pt/SnO_2 CATALYST

Barry D. Sidney
Langley Research Center
Hampton, Virginia

SUMMARY

Closed-cycle CO_2 laser testing with and without a catalyst and with and without CO addition indicate that a catalyst is necessary for long-term operation. Initial results indicate that CO addition with a catalyst may prove optimal, but a precise gas mix has not been determined as yet. A long-term run of 10^6 pulses using 1.3% added CO and a 2% Pt on SnO_2 catalyst yields an efficiency of about 95% of open-cycle steady-state power. A simple mathematical analysis yields results which may be sufficient for determining optimum running conditions. Future plans call for testing various catalysts in the laser and longer tests, 10^7 pulses. A Gas Chromatograph will be installed to measure gas species concentration and the analysis will be slightly modified to include neglected but possibly important parameters.

INTRODUCTION

Langley Research Center is actively engaged in the study of catalytic recombination of CO_2 dissociation products in pulsed, high-energy CO_2 lasers. This paper will present some results of that study, but will primarily concentrate on those aspects of laser operation which precede introduction of the catalyst. We will examine the effect which gas flow rates, laser pulse rates, and variable gas composition (e.g., adding CO to the gas mix) have on the laser output. We will then examine the implications which these variables have on the dissociation and recombination in the laser with attendant implications for use of catalysts.

PROCEDURE

Fig. 1 was presented in the survey paper of Schryer et al. (ref. 1) and, for convenience, is presented again here. It is a plot of laser output power versus time for 10^6 pulses. The laser used is a Lumonics model 820 TEA laser. For this experiment we ran at 30KV discharge voltage, 10 p.p.s., with a gas mix 16% CO_2, 8% N_2, 1.3% CO, and the balance He. As the figure shows, the laser performed at an efficiency of $\approx$ 95% of initial power when operated closed cycle with a 2% platinum on tin oxide catalyst. However, the term "initial power" in the preceding sentence needs explanation to fully understand what happens before the catalyst is introduced into the flow cycle.

Figure 2 shows the exact sequence of events - the laser is operated initially open-cycle with an initial pulse energy of 0.8 joules/pulse. After approximately 30 minutes the gas mixture in the laser has achieved a steady-state with the pulse energy now about 0.7 J/pulse. At this time, the flow is switched to closed-cycle

through the catalyst and after a few minutes of operation the steady-state condition of figure 1 is achieved at approximately 95% of the value of steady-state open-cycle energy.

Since the drop in pulse energy from initial power-on to open-cycle steady-state value is larger than that from open-cycle steady-state to the catalyst-flow, closed-cycle value, we feel it important to analyze this time period and examine the specific events occurring in an attempt to understand and possibly to lessen this initial energy loss. To accomplish this goal, I have performed a mathematical analysis which, although extremely simple, seems to give reasonable results. The unknowns in the equations are determined from actual operating conditions and the equations are then applied to more complicated operating situations to determine their accuracy and usefulness.

We consider a carbon conservation analysis involving the two reactions illustrated in the first line of Fig. 3. A given flow of CO_2 is introduced into the laser where there is some dissociation of CO_2 governed by the rate constant K_D, some recombination of CO and O_2 governed by the rate constant K_R, and an output flow of CO_2 and CO. Referring to Fig. 3, carbon conservation is then written both for time-rate-of-change and steady-state with dissociation (CO production) and recombination (CO_2 production) described on lines 2, 3, and 4. Dissociation is assumed to occur primarily by impact of electrons with CO_2 molecules in the active discharge volume of the laser, V_A, only during the time the discharge is on, T_{on}. Recombination is assumed to occur by collision of a CO molecule, an oxygen atom and a third body, M, at any time in the total laser volume, V_L. (It is assumed that $[O]$ can be related to $[CO]$ by some proportionality constant.) The resultant equation

$$[\dot{CO}_2] = [\dot{CO}_2]_{in} - [\dot{CO}_2]_{out} - K_D'[CO_2] + K_R'([N]-[CO_2])^2$$

represents a closed-form solution which has considerable appeal since one can see what is going on in the laser gas more readily than with a more complicated solution involving more variables. Determination of

$$K_D' = K_D\,[e]\,(V_A/V_L)(T_{on}/T_{off}) \text{ and}$$
$$K_R' = K_R\,([O]/[CO])[M]$$

can now be accomplished by experimental procedures.

The experimental results used for determination of K_D' and K_R' are shown in Figs. 4 and 5. Fig. 4 is a plot of pulse energy as a function of time for open-cycle operation for two different flow rates ($F = [CO_2]_{in}$). For each flow rate, the laser is operated until a steady state is reached or $[\dot{CO}_2] = 0$. Everything in the above equation (1) is known except K_D' and K_R'. N is the Loschmidt number and $[\dot{CO}_2]_{out} = [\dot{CO}_2]_{in}\,([CO_2]/N)$. Therefore, for the two flow rates, K_D' and K_R' can be determined. A second experiment using closed-cycle operation while varying the pulse rate is shown in Fig. 5. For this condition, $[\dot{CO}_2]_{in} = [\dot{CO}_2]_{out} = 0$, and, from the data of Fig. 5, the assumption is made that $[\dot{CO}_2] =$ constant. The assumption is also made that $[CO_2]/[CO_2]_{initial} =$ $Power/Power_{initial}$. Other values used were

$$[e] = 10^{13}, \quad V_A/V_L = 1/100,$$

T_{on}/T_{off} is pulse width times pulse rate (where the pulse width is estimated to be 200 nanoseconds which is not the laser pulse width but rather an estimate of the time width of the electric discharge pulse when the electrons are active), and $[O]/[CO]$ was estimated to be 10^{-3} since published values indicate that $[O] + [O] + [M]$ is about three orders of magnitude faster than $[O] + [CO] + [M]$.

The numerical results obtained from this analysis were $K_D' = 2.5 \times 10^{-3}$/sec or $K_D = 10^{-8}$ cm^3/sec and $K_R' = 8 \times 10^{-20}$ cm^3/sec or $K_R = 3 \times 10^{-36}$ cm^6/sec.

The quality of the foregoing analysis can be judged by comparison of the obtained values of K_D and K_R to published values. The published value of K_D is one or two times 10^{-9} for a temperature of 300K. Since K_D for this experiment is for a significantly higher discharge temperature, one expects a larger value of K_D so that a value of 10^{-8} is probably not far out of line. (There are other ways to obtain K_D for higher temperatures which will be explored in the future.) The situation for K_R is more susceptible to comparison since the published value is for 300K, and the actual recombination in the laser also takes place at this temperature. Accordingly, the obtained value of 3×10^{-36} compares favorably with the published value of two or three times 10^{-36}.

The usefulness of the analysis can be judged by the ability to predict the operating characteristics of the laser for those conditions when various percentages of CO are added to the gas mix (CO is added at the expense of He; CO_2 and N_2 are held constant). Fig. 6 shows power (t)/power (t=0) as a function of time for CO addition of 0, 1.3, 5.2, 10, and 15 percent. Initial power tends to decrease as CO is added - the initial power for the case of 15% added CO is anomalous probably due to the increased voltage (32KV) required to operate the laser for this condition (the other cases were operated at 30KV).

For increasing CO percentage, the operating lifetime is extended, but only for the 15% case is a steady-state achieved (the 10% case was terminated at 130 minutes due to some arcing in the discharge). The data of Fig. 6 are not presented here as representing a new result since gas addition measurements such as these have been carried out for several years. They are presented only as a device for comparing the data to the analysis presented earlier, which comparison is shown in Fig. 7. A slight modification to the equation allows for input flow of CO and the results for the 1.3, 10, and 15% cases are shown as solid lines in Fig. 7. The comparison of analysis with experiment is acceptable, the predicted slope for high percentage CO addition is somewhat faster than the measured slope, but predicted steady state values are close to the measured values. The results are surprisingly good considering the simplicity of the analysis.

CONCLUDING REMARKS

Obviously, several simple refinements could be accomplished to increase the quality of the analysis and its comparison to measurements and these will be done in the near future. First and foremost will be the introduction of a Gas Chromatograph to measure species concentration as a function of time. Measurement of gas temperature and the introduction of a gain term in the equations should also improve the analysis. Closed-cycle CO_2 laser testing with and without a catalyst, and with and without CO addition, indicates that a catalyst is necessary for

long-term operation. Initial results indicate that CO addition with a catalyst may prove optimal, but a precise gas mix has not been determined as yet. A long-term run of 10^6 pulses using 1.3% added CO and a 2% Pt on SnO_2 catalyst yields an efficiency of about 95% of open-cycle steady-state power. A simple mathematical analysis yields results which may be sufficient for determining optimum running conditions. Future plans call for testing various catalysts in the laser, and longer tests, 10^7 pulses. A GC will be installed to measure gas species concentration and the analysis will be slightly modified to include neglected but possibly important parameters.

REFERENCE

1. Schryer, David R., Sidney, Barry D., Miller, Irvin M., Hess, Robert V., Wood, George M., Batten, Carmen E., Burney, Lewis G., Hoyt, Ronald F., Paulin, Patricia A., Brown, Kenneth G., Schryer, Jacqueline, and Upchurch, Billy T.: NASA-LaRC Research on Catalysts for Long-Life Closed-Cycle CO_2 Lasers, NASA CP-2456, 1987.

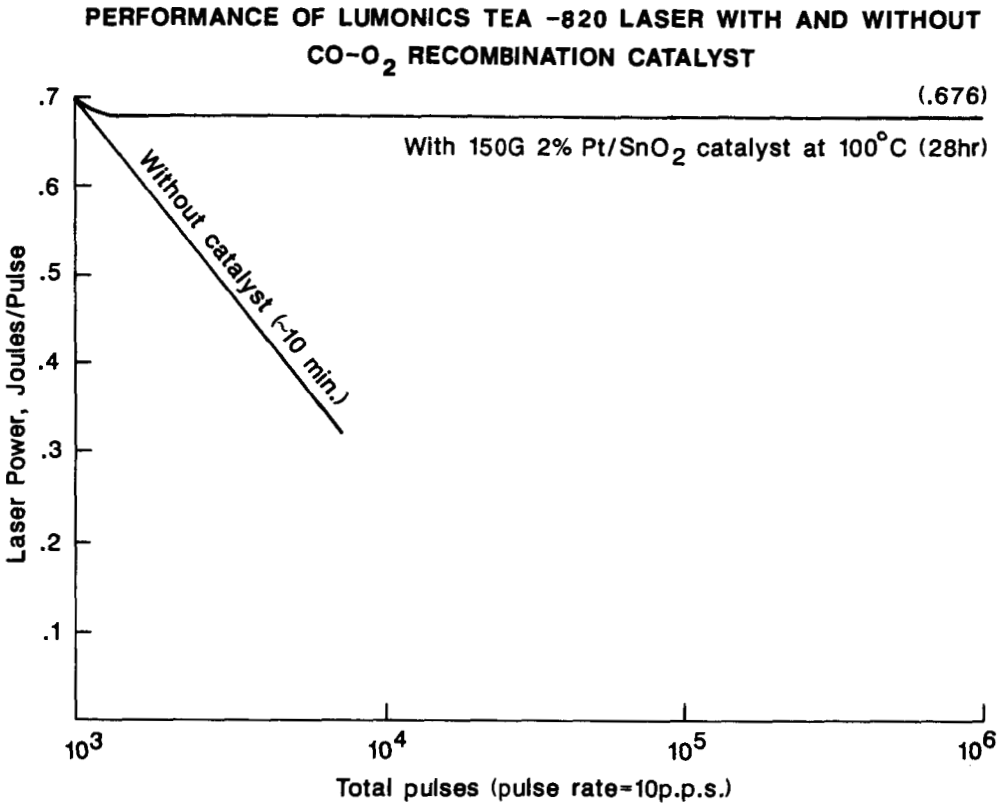

Figure 1

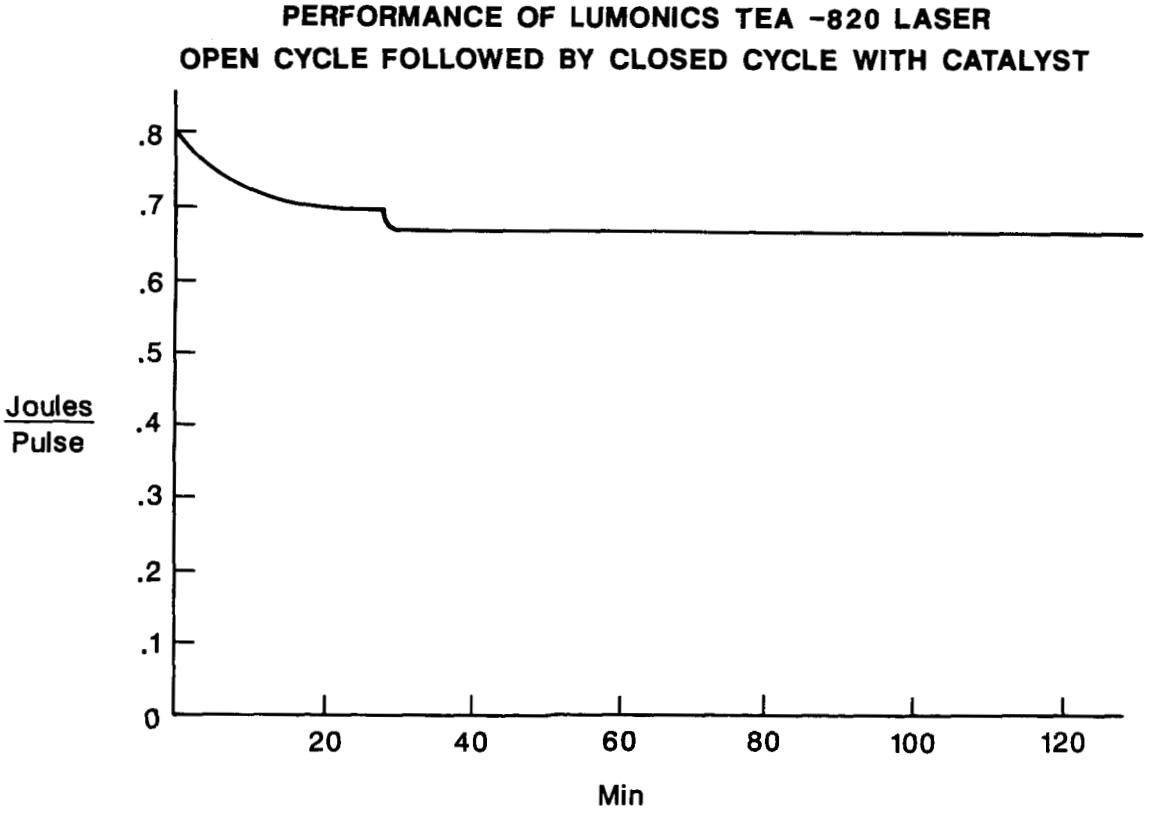

Figure 2

ANALYSIS

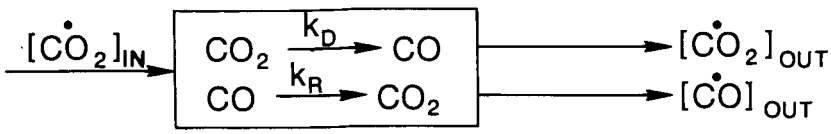

Carbon conservation: $[\dot{C}O_2] = [\dot{C}O_2]_{IN} - [\dot{C}O_2]_{OUT} - [\dot{C}O]_p + [\dot{C}O_2]_p$

$[CO_2] + [CO] = [N]$

Dissociation: $[\dot{C}O]_p = k_D [CO_2] [e] \frac{V_A}{V_L} \frac{T_{ON}}{T_{OFF}} = k_D' [CO_2]$

Recombination: $[\dot{C}O_2]_p = k_R [CO] [O] [M] = k_R' [CO]^2$

$$[\dot{C}O_2] = [\dot{C}O_2]_{IN} - [\dot{C}O_2]_{OUT} - k_D' [CO_2] + k_R' \left([N] - [CO_2]\right)^2$$

Figure 3

OPEN-CYCLE

LASER ENERGY/PULSE VS TIME

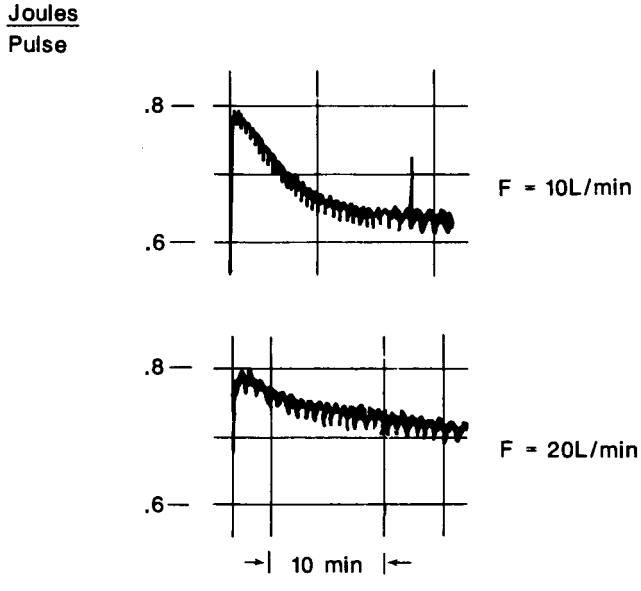

Figure 4

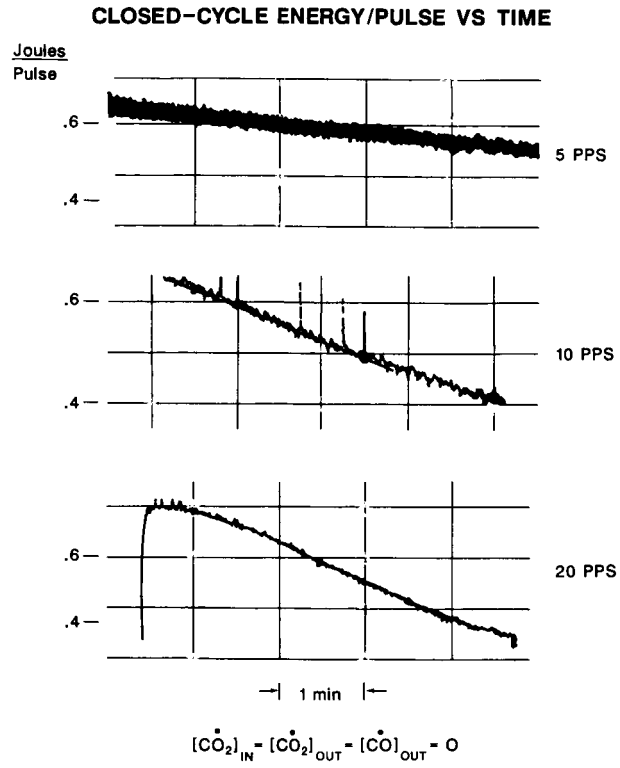

Figure 5

VARIATION OF AVERAGE POWER WITH TIME AS A FUNCTION OF INITIAL CO CONCENTRATION

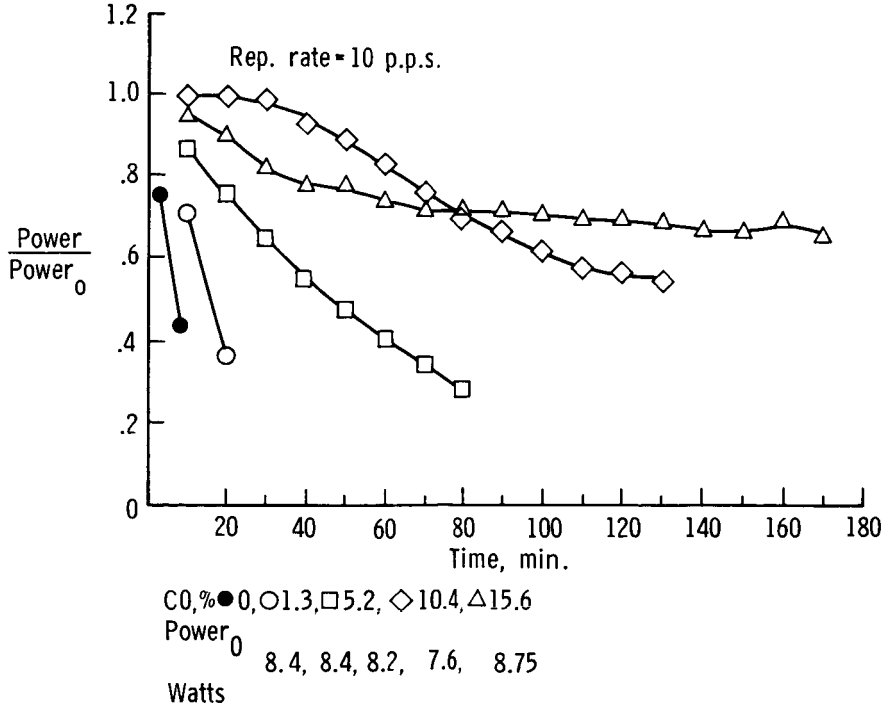

Figure 6

VARIATION OF AVERAGE POWER WITH TIME AS A FUNCTION OF INITIAL CO CONCENTRATION

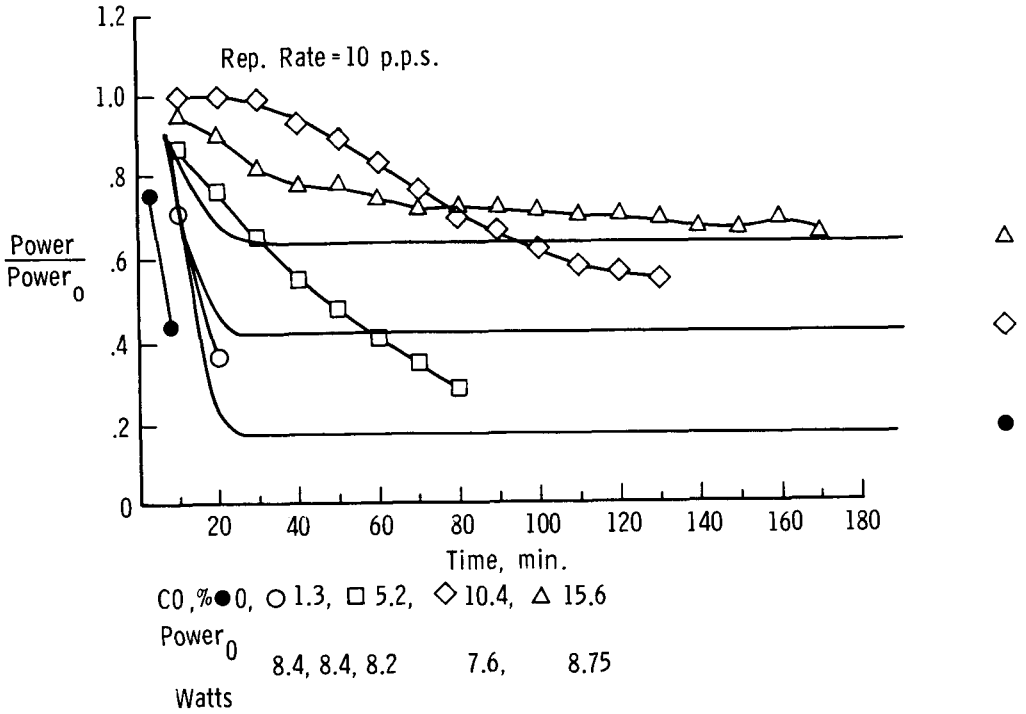

Figure 7

N87-20541

CHARACTERIZATION OF Pt/SnO_2 CATALYSTS FOR CO OXIDATION

K. G. Brown and J. Schryer
Old Dominion University
Norfolk, Virginia

D. R. Schryer, B. T. Upchurch,* G. M. Wood, I. M. Miller,
B. D. Sidney, C. E. Batten, and P. A. Paulin
NASA Langley Research Center
Hampton, Virginia

SUMMARY

We present in this report the results of surface characterization of 2% and 1% (w/w) Pt on SnO_2 catalysts which are being used in promoting the oxidation of CO in pulsed CO_2 lasers. The N_2 adsorption BET surface area for both catalysts is 6.9 m^2/g. The CO chemisorbed area at 313K is 0.17 m^2/g and 0.062 m^2/g for the 2% and 1% catalysts respectively. Monitoring the reaction between CO and O_2 by the same technique, at the same temperature yields a turn-over frequency (TOF) for the 2% catalyst of 2.7×10^2 molecules of CO_2/site/s and for the 1% catalyst a value of 1.2×10^2. The ratio of the TOFs for the two catalysts is 2.2 which is approximately the ratio of the Pt loading.

INTRODUCTION

The determination of the mechanism for the catalytic oxidation of CO requires the measurement of the number of CO molecules that are capable of being adsorbed by the catalyst. Initial attempts to measure the amount of CO adsorbed upon the oxide-supported Pt catalyst utilized the pulse technique first described in references 1-4. However, the initial measurements proved to be quite unreliable since the catalyst was capable of being reduced by the CO even at the moderate temperature (313K) where the measurement was performed. The detector was not able to discern between reactant CO and product CO_2 making it impossible to determine the amount of CO adsorbed. Any attempt to pursue these measurements at the higher temperatures where the catalyst would be expected to operate would also be fruitless.

The pulse technique was then modified to include, following the procedure described in reference 5 (developed to study the methanation of CO), a packed column after the catalyst to allow for the separation and analysis of the reactants and products. The amount of product produced and the amount of material left upon the surface could, then, be determined. This report is a summary of these measurements for the two catalysts currently being employed at NASA-Langley for the catalytic oxidation of CO, 1%$Pt-SnO_2$ and 2%$Pt-SnO_2$.

*Science and Technology Corp., Hampton, VA.

EXPERIMENTAL

The experimental apparatus consists of a Shimadzu gas chromatograph with a "CTR" column obtained from Alltech which enables the quantitative separation of CO and CO_2. The catalyst is placed on a frit located prior to the column in the same containment area as the column. Approximately 0.1g of catalyst can be placed upon the frit. The exact weight for each catalyst sample is determined with an analytical balance having an accuracy of 0.1 mg. The catalyst and column are under He flow at all times with a flow rate of 40 sccm and a temperature of 313K. The detector is a thermal conductivity detector whose response for each gas is calibrated using standards of known concentration with Ne added as an internal standard. For CO adsorption the test gas is 5%CO in He obtained from Scott Specialty Gases. The injections onto the catalyst are performed using the 1 mL sample injection loop of the Gas Chromatograph. Each injection contained 2.05×10^{-6} moles of CO. We also performed chemisorption studies with gas mixtures that contained 1%CO and 0.5% O_2 in He. The injection size was also 1 mL corresponding to 4.09×10^{-7} moles of CO and 2.05×10^{-7} moles of O_2 at each injection. The 1%- and 2%-Pt/SnO_2 catalysts were obtained from Englehard Industries as a catalog item. The method of synthesis is regarded as proprietary information. The Pt loading is a weight percent given by the manufacturer with no further attempt made to determine the precise Pt loading of the catalyst. Due to the current limitations of the experimental design, which placed the catalyst and the column in the same GC oven, the catalyst was not pretreated. All of the data reported herein is, then, for the catalyst on an as received basis.

The surface area of each catalyst was determined by the Brunauer-Emmett-Teller (BET) method using a commercial instrument manufactured by Quantachrome corporation. The catalyst was placed in a glass u-tube and immersed in liquid N_2. The total amount of N_2 gas absorbed at different partial pressures of N_2 in He was determined and the surface area was calculated. For both the 1%Pt/SnO_2 and the 2%Pt/SnO_2 catalysts the determined surface area, by N_2 adsorption was $6.9 m^2/g$.

RESULTS AND DISCUSSION

The progress of the adsorption experiment with injections of 5% CO in He for both catalysts is summarized in figure 1. For both catalysts there is an initial production of CO_2 indicating that the surface is not in an entirely reduced state. The CO_2 production decreases rapidly reaching a low level after a few injections. The CO signal rapidly increases approaching the level that is observed with no catalyst present in the system. The injections were routinely performed at constant time intervals of 13 min. However, there were some breaks in the data since the

entire series of injections were done manually. The longest break in the data was for approximately 1.5 hrs. When the experiment was resumed, at the 20th injection for the 2% Pt-SnO_2 catalyst, the CO_2 production was found to have increased markedly with a concomitant decrease in the amount of CO detected. It would appear as if the surface of the catalyst had reoxidized during this period of time since the resultant behavior resembled that of the fresh catalyst. However, the catalyst was kept under a constant flow of pure Helium during the entire break period making reoxidation of the surface an unlikely event. Rather some sort of relaxation of the surface seems to have occurred producing surface sites that are capable of being reduced by the CO. This phenomenon of surface recovery is even more pronounced when the stoichiometric reaction mixture is run by the pulse technique as will be discussed below.

During the entire time period covered by the injections a small but significant amount of the injected CO is not detected as either CO or CO_2. It is assumed that the difference between the total number of moles of CO injected and that which appears at the detector as either CO or CO_2 is the number of moles of CO that is physisorbed or chemisorbed by the catalyst for each injection. The total number of moles of CO adsorbed can be expressed as a fraction of the total number of moles of Pt present in the catalyst, a quantity often referred to as the dispersion of the catalyst, in order to compare catalysts of differing amounts of added metal. The variation of the dispersion as the number of injections is increased is shown in figure 2. As might be expected the 1% Pt-SnO_2 catalyst levels off at a considerably lower value than that of the 2% Pt-SnO_2 catalyst. Indeed, the dispersion for the 2% catalyst has not leveled after 58 injections while the 1% catalyst appears to have leveled after thirty two injections. The dispersion is quite low for both catalysts attaining values of 1.2×10^{-2} and 1.8×10^{-2} for the 1% and the 2% catalysts respectively. If we assume that the adsorption is a monolayer and each CO is bound by one Pt atom then the amount of Pt at the surface that is capable of acting as an adsorption site for CO is only slightly greater than 1% of the total Pt present in both catalysts. The implication is that there is not a great deal of Pt present at the surface in either catalyst. The latter statement has been confirmed by recent ESCA measurements of this catalyst (G. Hoflund, University of Florida, private communication). If we further assume that the cross-sectional area of an adsorbed CO is 1.63×10^{-19} m^2 (6) then the amount of surface area covered by the CO is 0.17 m^2/g and 0.062 m^2/g for the 2% and the 1% catalysts respectively. For the 2% catalyst the CO coverage is 2.5% of the N_2 BET surface area, for the 1% catalyst the percentage of BET area covered is 0.9%.

The progress of the catalyzed reaction between oxygen and carbon monoxide

$$2CO + O_2 \longrightarrow CO_2$$

may also be followed by the pulse technique. The results expressed in terms of percent loss of both O_2 and CO and the percent yield of CO_2 are shown in figure 3 for both the 1% and the 2% catalysts. Both catalysts are quite active initially with 2% catalyst removing approximately 90% of the CO and and yielding almost 78% of the possible CO_2. The activity of both catalysts declines rather rapidly tending to level off after 5 - 10 injections of the stoichiometric reaction mixture with neither catalyst exhibiting the pronounced minimum that is evidenced in the long term, continuous flow studies performed upon these catalysts at higher temperature range of 328 to 373K. Comparison of the yields after thirty injections shows that the 2% catalyst is approximately four times as efficient in terms of CO_2 yield as the 1% catalyst although the trend in yield for both catalysts is downward.

If we compare the amount of CO adsorbed on the Pt surface for both catalysts we observe a reversal of form when oxygen is present in the system. As is shown in figure 4 there is now more CO per mole of Pt adsorbed on the catalyst for the 1% catalyst than for the 2% catalyst. The difference is significant. In the case of the 2% catalyst the dispersion is approximately the same as that when the CO is added alone. For the 1% catalyst the dispersion is approximately ten times that which was determined when the CO was present in the gas mixture without oxygen.

An alternative way of comparing the two catalysts, which differ, chemically, only by the amount of Pt load, is to ratio the number of moles of product per second to the number of active sites available for reactant absorption. This ratio is referred to in the literature as the turn-over frequency (TOF) an effective normalization of catalyst reaction rate by a number which is characteristic of the catalyst surface. If we assume that the residence time is as calculated in reference 7 the TOF is 2.7×10^2 molecules of CO_2/site/sec for the 2% catalyst and 1.2×10^2 molecules of CO_2/site/sec for the 1% catalyst. The ratio of the TOF for the 2% catalyst to that of the 1% catalyst is 2.2, approximately equal to the Pt loading ratio. The maximum TOF is considerably lower than that reported in the literature on other oxide-supported catalysts. However, the temperature usually studied is 373K rather than the 313K performed here. If, as a rough approximation, we assume that the reaction rate doubles for every 10K rise in temperature the TOF at 373 for the 2% catalyst is 17.1×10^3 molecules of CO_2/site/sec. This latter number compares quite favorably to the TOFs reported for Ru/SiO_2, Rh/SiO_2 and the $RU-Rh/SiO_2$ reported in the literature at 373K with stoichiometric gas mixtures (8).

REFERENCES

1. Gruber, H. L., J. Phys. Chem. 66, 48 (1962).

2. Gruber, H. L., Anal. Chem. 34, 1828 (1962).

3. Hausen, A. and Gruber, H. L., J. Catal. 20, 97 (1971).

4. Roca, F. F., DeMourgues, L. and Trambouze, Y., J. Gas Chromatogr. 6, 161 (1968).

5. Freel, J., J. Catal. 25, 139 (1972).

6. Orr, C. and Dallavalle, J. M., in Fine Particle Measurements: Size, Surface and Pore Volume, 1st ed., The Macmillan Co., New York, (1959).

7. Miller, I. M., Wood, G. M., Schryer, D. R., Hess, R. V., Upchurch, B. T., Brown, K. G. and Sidney, B. D., NASA TM 86421 (1985).

8. McClory, M. M., and Gonzalea, R. D., J. Phys. Chem. 90, 628 (1986).

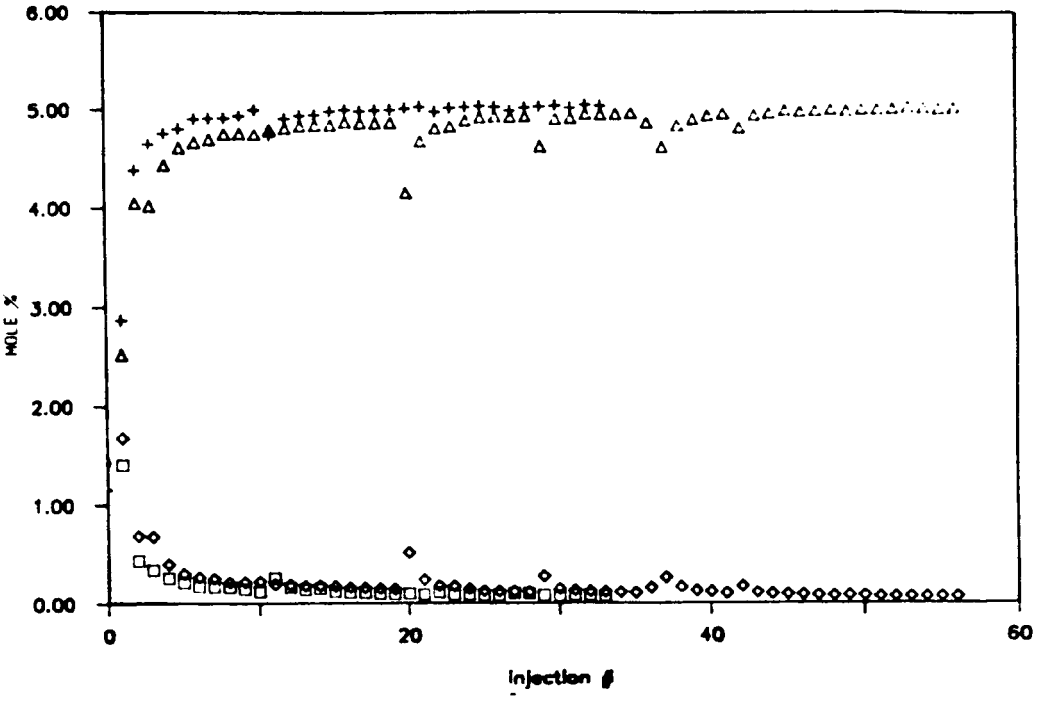

Figure 1: Fraction of Carbon Dioxide produced (lower) or Carbon Monoxide remaining (upper) for injections of 5% CO in Helium. + , □ 1% Pt/SnO_2, ◇ , △ 2% Pt/SnO_2

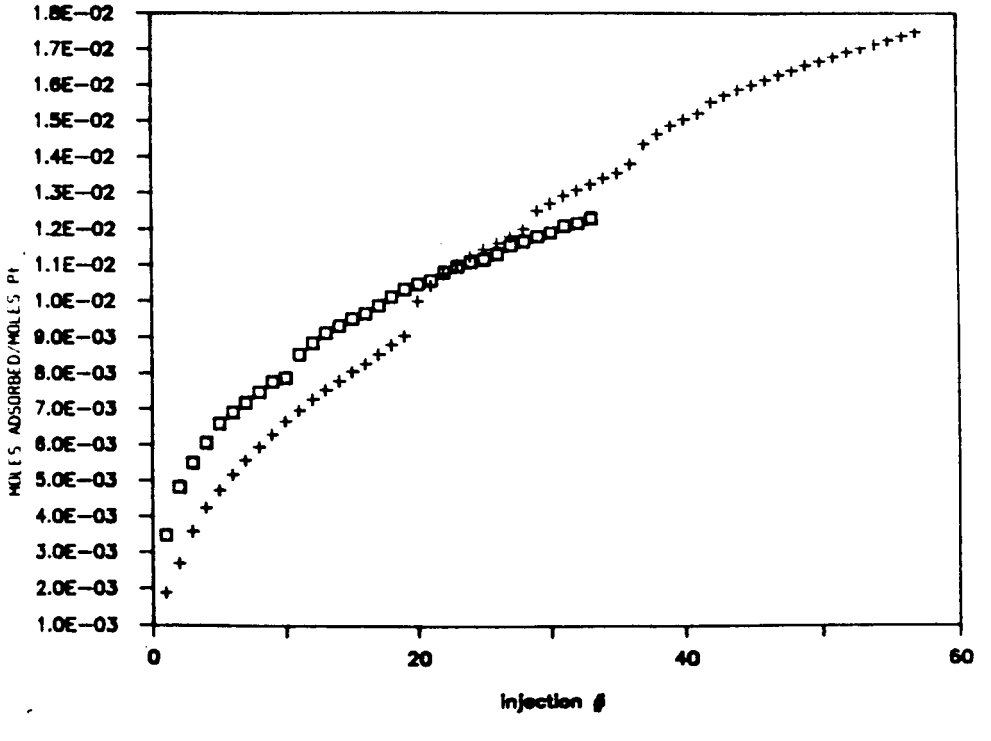

Figure 2: Dispersion as a function of injection for □ 1% Pt/SnO_2 and + 2% $PtSnO_2$

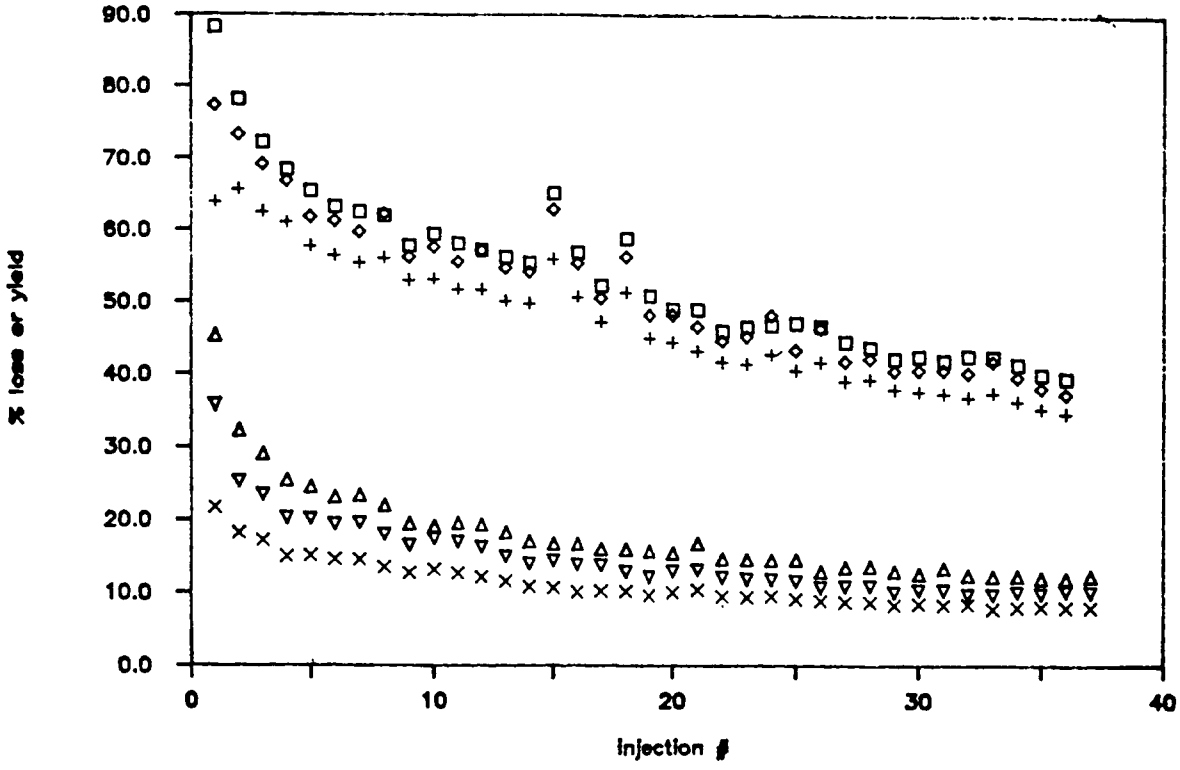

Figure 3: Chemisorption results for the injection of 1%CO, 0.5% O_2 in Helium upon 2% Pt/SnO_2(upper) and 1% Pt/SnO_2. □ , △ loss of CO +,x loss of O ,◇, △ yield of CO_2.

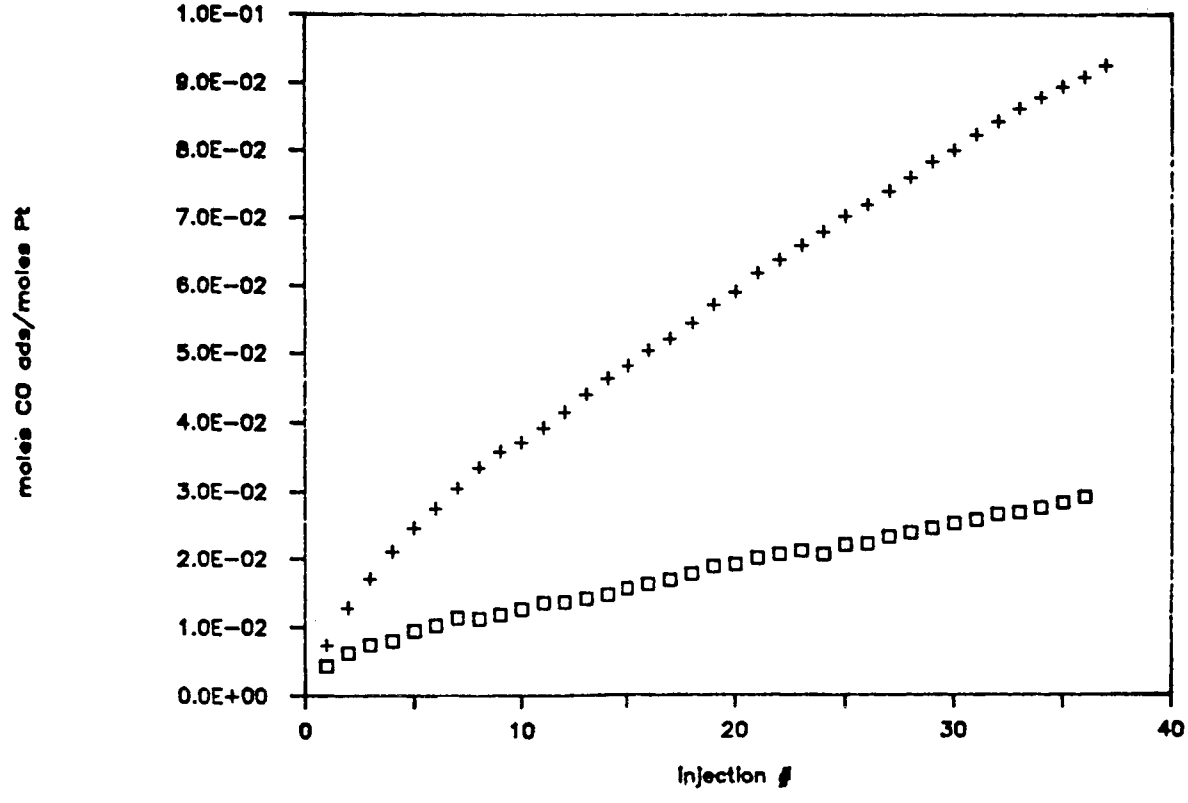

Figure 4: Total CO adsorbed per mole of Pt after each injection of the stoichiometric gas mixture. □ 2% Pt/SnO_2 + 1% Pt/SnO_2.

AN OVERVIEW OF DREV'S ACTIVITIES ON PULSED CO_2 LASER TRANSMITTERS: FREQUENCY STABILITY AND LIFETIME ASPECTS

James Cruickshank, Paul Pace, and Pierre Mathieu
Defence Research Establishment
Valcartier, Canada

SUMMARY

After introducing the desired features in a transmitter for laser radar applications, the output characteristics of several configurations of frequency-stable TEA-CO_2 lasers are reviewed. Based on work carried out at the Defence Research Establishment Valcartier (DREV), output pulses are examined from short cavity lasers, CW-TEA hybrid lasers, and amplifiers for low power pulses. It is concluded that the technique of injecting a low-power laser beam into a TEA laser resonator with Gaussian reflectivity mirrors should be investigated because it appears well adapted to producing high energy, single mode, low chirp pulses. Finally, a brief report on tests carried out on catalysts composed of stannic oxide and noble metals demonstrates the potential of these catalysts, operating at close to room temperature, to provide complete closed-cycle laser operation.

INTRODUCTION

This overview summarizes several investigations and developments carried out at DREV on pulsed CO_2 laser radar transmitters intended for use in coherent detection laser radar systems. With these systems the functions of ranging, velocity measurement and angle tracking are being investigated on hard targets such as airplanes, helicopters and missiles. Many of the pulsed atmospheric sensing lidars, planned or being developed throughout the world for land or space operation, require a transmitter with essentially the same performance characteristics as those sought for our hard-target laser radars.

The output and lifetime characteristics desired in a transmitter will now be discussed, taking into consideration the variety of applications being considered. For the types of targets and ranges involved, pulse repetition rates of up to 100 Hz and pulse energies of approximately 1 J are of the greatest interest. Output pulse lengths varying from 50 ns to 2 μs are suitable for our applications. The longer pulses are more appropriate for measuring velocity from the Doppler frequency shifts, the shorter pulses for precise range measurements. With a monostatic laser radar configuration, a pulse with a short tail (e.g. $\leq$ 2 μs) is preferable for making measurements at close ranges (e.g. $\leq$ 1 km) because of the backscatter generated on the optical components by the outgoing transmitter pulse. Especially for transmitters with the longer output pulses, our objective is to maintain both the pulse to pulse and intrapulse frequency instability to $\leq$ 1 MHz. More precisely, the frequency chirp rate should be low enough that it is the pulse envelope shape and not the total frequency chirp which determines, at low signal-to-noise ratios, the velocity resolution limit. Also, a laser pulse with a short tail generates less total frequency chirp for a given chirp rate. Finally, to be practical the ideal transmitter should

have a closed-cycle gas recirculation system, or have a very low gas consumption. This paper will review some of DREV's activities on closed-cycle, frequency stable, CO_2 laser transmitters.

THE IMPORTANCE OF FREQUENCY STABILITY

Most of DREV's recent experience with pulsed coherent laser radars has been acquired from the Infrared Ranging and Tracking System (IRATS) (ref. 1). The transmitter for this system was a CW-TEA hybrid laser operating at the 10.6-μm wavelength. With this particular transmitter configuration, laboratory measurements indicated that the frequency of the output pulse swept over 8 MHz between the 1-μs and 4-μs points of the pulse. To a Doppler frequency processing unit, this frequency chirp in the return signal appears as a target velocity which varies from 0 m/s to 45 m/s over a distance of 450 m. For the case of a single pulse return, determining the target's range and velocity is relatively straightforward provided the characteristics of the transmitted pulse are known. The signal processing problem becomes much more serious with multiple target returns or the returns from a distributed target such as the atmosphere. In conclusion, for our planned applications, the use of a transmitter with low frequency chirp would undoubtedly facilitate Doppler frequency processing.

FREQUENCY STABLE LASER SOURCES

Over the past years numerous methods have been investigated for generating a single longitudinal mode (SLM) in a TEA-CO_2 laser cavity. As could be expected, the configurations suited to SLM operation were not always well adapted to high energy pulses, high frequency stability or low-divergence transverse modes. This paper will review work at DREV on short-resonator lasers, hybrid lasers and the amplification of low power pulses.

Short, Stable Resonator Laser

Short cavity lasers were first investigated at DREV using a miniature TEA-CO_2 laser which had an 18-cm-long stable resonator, a 1 cm × 1 cm × 10 cm discharge volume, a 7.5-mm diameter iris to limit the oscillation to the fundamental transverse mode, and a piezoelectric transducer to tune the cavity length (ref. 2). At a gas pressure of 400 torr and the properly tuned cavity length, SLM operation was achieved. The 15-mJ output pulse had a 45-ns spike and a 2-μs tail. When the pulse was mixed with the output of a CW laser and heterodyne detected on a HgCdTe photodiode, it was determined that the laser pulse had a chirp rate of 1.7 MHz/μs^2. This TEA laser was also studied when frequency stabilized from pulse to pulse with a feedback loop to apply corrections to the cavity length. For this stabilization, the frequency of each heterodyne detected pulse, measured with a gated counter, was used to produce an error signal to correct the length of the cavity for the next laser pulse. It was found that the long-term frequency drift in the output pulses was eliminated and the measured beat frequency from pulse to pulse had a standard deviation of 500 kHz.

With this type of laser, the limited dimensions of the discharge volume are a major obstacle to producing high energy pulses. With an increased discharge length SLM operation is no longer possible, and with a greater discharge cross section it is not practical to maintain the fundamental transverse mode output.

In summary, this short stable resonator laser produced short frequency stable pulses, which had significant chirp, a low output energy, and a pulse to pulse frequency instability of 500 kHz.

Short Cassegrain Resonator with Gaussian Reflectivity Mirrors

To overcome the drawbacks of the standard short cavity lasers, DREV has supported investigations on the use of Gaussian reflectivity mirrors in a Cassegrain resonator to produce a fundamental mode of large cross sectional area (ref. 3). A Gaussian reflectivity mirror is a mirror whose reflectivity varies as a Gaussian function across the diameter of the mirror. For the investigation the test laser with a 50-cm long optical cavity had a 2 cm × 2 cm × 30 cm TE-CO_2 gain module at a gas pressure of 375 torr. The Cassegrain resonator configuration using Gaussian reflectivity mirrors had a magnification of 1.2. For comparison purposes, this laser was also modified and studied with a conventional "hard" mirror Cassegrain configuration and a stable resonator. It was found that in a full-angle beam divergence of 1.3 mrad (i.e. 2.44 λ/d with d = 2 cm), the encircled energy in the far field was, as a ratio to the 175 mJ total energy, 0.7 for Cassegrain Gaussian mirrors, 0.3 for the Cassegrain hard mirrors, and 0.03 for the stable resonator. With proper tuning of the cavity length, the 70-ns output pulse from the Gaussian mirror did not show the mode-beating which was present with the two other tested resonator configurations. The lack of mode-beating indicated that with the Gaussian mirrors the problem of transverse mode selection in unstable resonators had been overcome and that single longitudinal mode operation had been achieved. By beating the pulse from the Gaussian mirror laser with the output from a CW laser, the chirp rate in the pulse was measured at 60 kHz/μs^2.

The significantly lower chirp measured with the Gaussian mirror laser is the result of having a large laser mode diameter (ref. 4). Also, the large mode diameters which are possible with this unstable mode configuration can produce relatively high output energies with short cavity lengths and relatively low power densities on the laser mirrors.

It can be concluded from this work that a laser having a short Cassegrain resonator with Gaussian reflectivity mirrors can produce short, frequency stable pulses, with low chirp and interesting output energies. Although not measured, a pulse to pulse frequency instability of 500 kHz would be expected. This laser configuration can produce an output with almost all the desired characteristics except for the pulse length which is rather short for many applications involving velocity measurements.

Hybrid CW-TEA Laser

Two experimental laser radar systems developed a DREV (refs. 1 and 5) have used a hybrid laser transmitter because of this transmitter's relative simplicity and output pulse length which is suited to Doppler frequency measurements over a period of $\geq$ 1 μsec. The laser transmitter for IRATS (ref. 6) had a 1 cm × 1 cm × 30 cm TEA discharge section and a 50-cm-long low-pressure CW tube which were mounted in a

130-cm-long resonator. An iris (≈ 0.9 cm) was required inside the cavity to limit operation to the fundamental transverse mode. The output pulse energy was 80 mJ at a 100 Hz pulse repetition rate.

This laser was frequency stabilized in the following manner. The length of the laser resonator was modulated with a voltage applied to a piezoelectric transducer, the output from the CW-CO_2 laser section was mixed with a local oscillator laser on a high-speed detector, and the resulting swept IF frequency was sent to a frequency selector. When the frequency selector detected the desired IF frequency, the TEA-CO_2 laser discharge was triggered and the resulting high power laser pulse was emitted at close to the same IF frequency. Most of the energy in this long-tailed pulse is present in the first 2 μs. The intrapulse chirp was measured at 0.89 MHz/μs^2. With the above stabilization technique the pulse-to-pulse frequency difference between the transmitter and the local oscillator had a standard deviation of 50 kHz. Without the cavity length modulation and the feedback loop in operation the pulse-to-pulse frequency instability was 500 kHz.

In conclusion, we have found that the hybrid CW-TEA laser can produce long, frequency stable pulses which have relatively high-frequency chirp, energies of a few hundred millijoules, and high pulse to pulse stability. It was also found that, because of the time it takes for the gain of the CW tube to re-establish after each TEA-CO_2 pulse, the maximum pulse repetition rate achievable with this type of laser is about 300 Hz. Although this laser configuration has many merits, it does have relatively high chirp and a limited output energy because of the restrictions on the beam cross-sectional area.

Pulse Amplification

Pulse amplification has been investigated (ref. 7) by passing the output of a miniature TEA laser (a short cavity stable resonator configuration) through a three pass TEA amplifier arranged in an off-axis Cassegrain configuration. For the laboratory mesurements each TEA laser pulse was heterodyne detected and recorded both before and after amplification. By comparing the unamplified and amplified pulses it was concluded, to a first approximation, that neither the average pulse frequency nor the intrapulse frequency characteristics have been significantly altered by amplification. However, it was noted that the amplitude of the pulse tail had been decreased upon amplification. The pulse energies were about 1 J at the output of our amplifier.

Our work has shown that pulse amplification can produce frequency stable pulses of > 1 J/pulse. The amplified pulse has appreciably unaltered frequency characteristics but its length is reduced. This investigation was not extended to studying the effects, on the pulse length reduction, of varying the delay between the amplifier's excitation current and its injected signal, or of changing the pulse shape of the amplifier's excitation current.

CATALYSTS IN TEA-CO_2 LASERS

About 10 years ago DREV supported the industrial development of a 300-Hz TEA-CO_2 laser which used a hot platinum catalyst to reduce gas consumption. Although this type of catalyst was very effective, unacceptable amounts of power were required

to heat the catalyst and then cool the laser gas after it had been in contact with the hot catalyst. More recently, catalysts consisting of stannic oxide and noble metals have been prepared (ref. 8) and tested in our laboratories.

The activity of the different SnO_2 catalysts was compared by introducing 30 torr of CO and 15 torr of O_2 into a 1-liter test cell containing a given amount of the catalyst under test. The rate of the reaction $2CO + O_2 \rightarrow 2CO_2$ was monitored with measurements of both the gas pressure and the infrared absorption of CO_2 at 15.9 μm.

In our evaluation it was found that a 2% Pt - SnO_2 catalyst was efficient but that up to 2 or 3 times greater activity could be obtained with 2% bimetal or trimetal catalysts (e.g. Pt-Pd, Pt-Rh, Pt-Pd-Rh).

With the catalyst powder contained in the hollow centers of sintered stainless-steel filter elements, the evaluation was extended to actual tests in a miniature TEA-CO_2 laser. With no forced gas circulation in the laser it was found that 5 gms of catalyst were required to maintain the laser's output energy at 90% of its original value at a pulse repetition rate of 1 Hz. No testing of the catalyst has yet been carried out in a high-repetition-rate laser with forced gas flow.

DISCUSSION

This paper has reviewed some of DREV's work on closed-cycle, frequency-stable TEA-CO_2 lasers. It has been shown that each laser configuration has certain advantages and limitations. To develop a frequency stable transmitter having output energies of > 1 J/pulse, a low-frequency chirp rate, and a long output pulse, it is believed that a technique consisting of injecting a low-power laser beam (ref. 9) into a Cassegrain resonator with Gaussian reflectivity mirrors should be investigated. The injection technique could produce single-longitudinal-mode pulses of 1-μs to 2-μs duration and the Gaussian reflectivity mirrors would eliminate unwanted transverse modes. The large discharge cross section used in the unstable resonator configuration would yield the high energy pulses with low frequency chirp. Also, the cavity mirrors are subjected to lower energy densities.

Closed cycle gas operation using acceptable quantities of a SnO_2 catalyst was first reported for a 100-Hz pulse repetition rate laser in 1983 (ref. 10). With the present effort at several laboratories, it is expected that the addition of catalysts to TEA-CO_2 lasers will become standard technology in all but experimental lasers.

REFERENCES

1. Cruickshank, J.M.; Bonnier, D.; Pace, P.; Larochelle, V.; and Henshall, H: Field Measurements with a Coherent Transversely Excited Atmospheric CO_2 Laser Radar. SPIE, Vol. 415, Coherent Infrared Radar Systems and Applications II, 1983.

2. Pace, P,; and Lacombe, M.: Frequency Characteristics of a Miniature Transversely Excited CO_2 Laser. Can. J. Phys., Vol. 57, pp. 1350-1355 (1979).

3. Lavigne, P.; Parent, A.; Pascale, D.; and McCarthy, N.: A Compact Wide-Aperture Single Mode TE-CO_2 Laser with a Low Chirp Rate. IEEE J. Quantum Electronics, Vol. QE-22, No. 12, pp. 2200-2203, 1986.

4. Willets, D.V.; and Harris, M.R.: Scaling Laws for the Intrapulse Frequency Stability of an Injection Mode Selected TEA-CO_2 Laser. IEEE J. Quantum Electronics, Vol. QE-19, pp. 810-814, 1983.

5. Cruickshank, J.M.: Transversely Excited Atmospheric CO_2 Laser Radar with Heterodyne Detection. Applied Optics, Vol. 18, p. 290, Feb. 1, 1979.

6. Pace, P.; and Cruickshank, J.: Frequency-Stabilized Hybrid CO_2 Laser. SPIE, Vol. 300, CO_2 Laser Devices and Applications, 1980.

7. Pace, P.; Cruickshank, J.; and Otis, G.: Frequency-Stabilized Transversely Excited Atmospheric (TEA) CO_2 Lasers for Coherent Infrared Radar Systems. SPIE, Vol. 300, Physics and Technology of Coherent Infrared Radar, 1981.

8. Mathieu, P.: Method for Producing a Catalyst for Oxidizing Carbon Monoxide. U.S. Patent No. 4,490,482, Dec. 25, 1984.

9. Lachambre, J.-L.; Lavigne, P.; Otis, G.; and Noel, M.: Injection Locking and Mode Selection in TEA-CO_2 Laser Oscillators. IEEE J. Quantum Electronics, Vol. QE-12, pp. 756-764, 1976.

10. Stark, D.S.; Crocker, A.; and Steward, G.J.: A Sealed 100-Hz CO_2 TEA Laser Using High CO_2 Concentrations and Ambient-Temperature Catalysts. J. Phys. E. Sci. Instrum., Vol. 16, 1983.

RECOMMENDATIONS OF THE CATALYSIS PANEL

Richard D. Gonzalez

Department of Chemical Engineering
University of Illinois at Chicago
Chicago, Illinois

The panel reviewed the requirements which need to be met in order to design an effective low temperature catalyst for CO oxidation in a closed loop recycle pulsed laser system. The following criteria should be met:

1.) A high, low temperature CO oxidation activity is essential. A schematic of a proposed closed loop laser-reactor system is shown in figure 1. The catalyst should be capable of reoxidizing the CO and O_2 formed as a result of a pulse rate of between 1 and 100 pulses/sec. It is important that the concentration c_0 of O_2 at the inlet to the laser be kept as low as possible, preferably this oxygen concentration should not exceed 0.5 %. Higher inlet concentrations of oxygen will cause laser damage.
2.) The lifetime of the catalyst should be such that it can effectively convert the CO and oxygen generated as a result of 10^9 pulses. At a pulse rate of 100 pulses/sec, this means that the catalyst should operate effectively for a period of about 3 years.
3.) The catalyst should be such that the isotopic integrity of the CO_2 in the laser be maintained. Because labeled oxygen is needed in the CO_2 laser, it is, therefore, essential that it should not exchange oxygen with the material used to support the active catalyst.
4.) Laminar flow through the catalyst bed should be maintained if at all possible.
5.) The use of Nickel in the construction of the laser should be kept to a minimum in order to prevent the formation of $Ni(CO)_4$. Not only is $Ni(CO)_4$ highly toxic, but it may also reduce the activity of the catalyst by virtue of depositing Ni on the surface. Ni is not a particularly active catalyst for CO oxidation.

CATALYTIC ACTIVITY

The catalytic activity for a series of silica supported noble metal catalysts was discussed. This activity sequence is summarized in table 1 [1].* A Pt/SnO_2 catalyst tested at the NASA Research Center is also included for comparison purposes. In view of these results, SnO_2 supported catalysts appear to be about an order of magnitude more active than other supported catalysts and merit further study. A drawback in the use of SnO_2 is that it readily exchanges its oxygen with labelled CO_2 making it unacceptable for pulsed laser applications. Several possibilities were discussed. The preparation of labeled SnO_2 appears to be unacceptable due to its prohibitive cost. However, SnO_2 in which only the surface oxygen has been exchanged appears to be a possibility.

*Table 1 in D. Böcker and R. D. Gonzalez's paper entitled CO Oxidation Studies Over Supported Noble Metal Catalysts and Single Crystals: A Review, NASA CP-2456, 1987, p. 98.

A promoted SnO_2 based catalyst prepared by RSRE appears to be several orders of magnitude more active than those shown in Table 1. Although its exact composition is at present proprietary information, its high CO oxidation activity appears to be related to its very large surface area. For this reason the catalysis panel recommended that methods aimed at increasing catalyst surface areas be studied. The use of monolithic supports as used in the automotive catalyst industry should be tried. Another promising approach would be to use a high area alumina as a support onto which Pt/SnO_2 could be coated. Perhaps only the oxygen which is incorporated into the SnO_2 need be labeled.

A STANDARDIZED METHOD FOR MEASURING REACTION RATES

Because the measurement of reaction rates obtained in different laboratories may depend rather critically on how the catalyst was pretreated, the Catalysis Panel recommended the following standard pretreatment and reaction rate measurement procedure:

1.) Catalyst dispersion measurements should be performed using the dynamic pulse method [2]. Either H_2 or CO chemisorption is recommended.
2.) Catalyst pretreatment prior to the chemisorption measurements should be performed as follows: Treatment in flowing He at 373 K for 20 hours at a flow rate of 50 ml/min; reduction should be performed in flowing hydrogen (7.5 % in He) for 2 hours at 500 K (flow rate 20 ml/min).
3.) The catalytic activity measurements should be performed using a test gas having the following composition: 1 % CO, 0.5 % O_2 in flowing He. The flow rate should be set at 25 ml/min and adjusted as necessary to give an overall CO conversion not to exceed 5 %. The reaction temperature should be set at 348 K. The low conversion of CO is essential in order to insure that the catalyst is acting in a differential mode.

If comparisons of the catalytic activity between laboratories are to meaningful, it is essential that this procedure be followed as closely as possible. In particular, the temperature and the hydrogen flow rate are critical. Higher reduction temperatures and flow rates might possibly lead to changes in catalytic activity due to an excessive reduction of the support. This is critical for catalysts in which SnO_2 is used as a support material.

OTHER AREAS OF FUTURE RESEARCH

1.) Support Effects

A strong research effort aimed at understanding the promotional effects of the support is strongly encouraged. This is particularly pressing for SnO_2 based catalysts. The mechanism by which CO_2 exchanges oxygen with the support should be studied through the use of carefully planned labelling experiments. *In situ* infrared measurements coupled with a mass-spectrometric analysis of the reaction products may lead to a better understanding of the role played by the support during the reaction. Temperature programmed desorption and temperature programmed reaction measurements coupled with *in situ* infrared measurements may also lead to a better understanding of the

reactivity of chemisorbed CO. Support structures which minimize oxygen exchange with the support should be identified. The use of monolithic supports and possibly high surface area silicas or alumina coated with an active Pt/SnO_2 catalyst should be studied.

Noble metal/SnO_2 catalysts other than Pt/SnO_2 should be prepared and tested for their catalytic activity. In particular, SnO_2 supported bimetallic catalysts might prove promising.

2.) The use of promoters

Several promoters, in particular MgO, should be studied in the formulation and preparation of active CO oxidation catalysts. The British group at RSRE has already made impressive strides in this direction. Perhaps surface science studies performed on single crystal planes using promoters at well defined crystallographic locations may yield important information regarding the specific action of promoters.

3.) Oscillatory and transient behavior

The occurrence of self sustained oscillations is always a possibility when studying CO oxidation. However, the panel did not expect oscillatory behavior under the conditions applicable to pulsed laser operation. The question of transient behavior under pulsed operation was briefly discussed by the panel. Because of the relatively high pulsing rate (100 pulses/sec), the panel concluded that the closed cycle reaction loop essentially operates under steady-state reaction conditions. However, those effects may require further study.

4.) Catalyst Regeneration

Catalyst reactivation may be possible using an auxiliary external flow system capable of pumping oxygen over the catalyst at high temperatures in order to burn off contaminants which may have been deposited as a result of normal operation. It is essential that the catalyst be isolated from the laser system during the regeneration of the catalyst.

5.) Gas phase compositions

The possibility of operating the pulsed laser recycle system under CO rich conditions was discussed by the panel. Perhaps other active supported noble metals such as Ru could be used under these CO rich conditions without fear of catalyst deactivation. It was generally agreed that oxygen rich reaction mixtures should be avoided in order to prevent laser damage.

REFERENCES

[1] Kiss, J. T.; Gonzalez, R. D.: *The catalytic oxidation of CO over Rh/SiO_2, Ru/SiO_2, Pd/SiO_2 An in-situ infrared and kinetic study*, Proceedings of the 8th Intern. Congress on Catalysis, Berlin(West), July 2-4th, 1984; **II,** pp. 635-644; Verlag Chemie, Weinheim, Deerfield Beach - Florida.

[2] Sarkany, J.; Gonzalez, R. D: *On the use of the dynamic pulse method to measure metal surface area*, J. Cat. **76,** pp. 75-83, 1982.

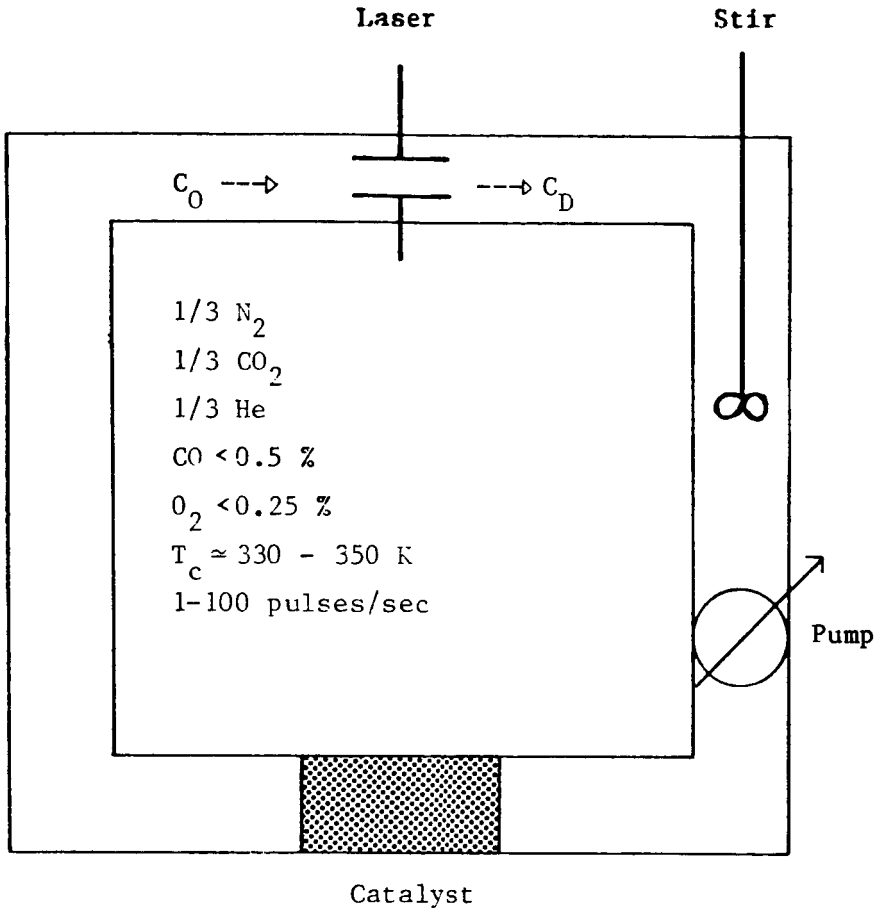

Figure 1: Recycle system for a pulsed CO_2 laser.

SUMMARY AND RECOMMENDATIONS OF FREQUENCY STABILITY PANEL

D. V. Willetts
Royal Signals and Radar Establishment
Malvern, Worcester, United Kingdom

When you're organizing a workshop such as this one, there is always a worry at the back of your mind that things could go horribly wrong, with no comments from the floor or difficulty in getting a discussion going. Certainly, for the Frequency Stability Panel, that didn't happen. There was a vigorous discussion that culminated in a useful workshop session which made real progress. I'd like to thank the people who participated openly in those discussions.

Introduction

We decided to split our discussions into several key areas: (1) resonator configurations (alleviating chirp and getting high-energy good mode quality), and (2) discharge processes (how to get uniform discharges with alleviation of plasma effects and long pulse operation). Both topics are associated with the pulsed oscillator approach. There is an alternative but radically different approach to getting the required long-pulse frequency stable high-energy output which is to use a master oscillator power amplifier (MOPA) configuration (MOPAs are discussed in more detail later). Finally, we wondered whether there were any novel ideas that we wished to encourage, such as matched filtering, which is also discussed in more detail later.

Resonator Configurations

Looking first at the resonator configurations, large mode radii ideally are needed to give a large active volume in a compact size. Large mode radius also greatly ameliorates the laser-induced chirp, and damage resistance is increased by spreading out the intra-cavity energy over a large area. It is also necessary to ensure single-mode operation, good transverse mode discrimination in order to get reasonable far-field beam quality, and single longitudinal mode operation in order to simplify signal processing. Finally, alignment sensitivity is an important engineering design constraint. These are the desirable characteristics of a resonator design.

Stable resonators of some kind, with intra-cavity elements to give a big spot (such as a telescopic resonator), tended not to get discussed as much because there are obvious damage and size problems. Two areas of considerable interest were: (a) resonators containing Gaussian reflectivity mirrors (GRMs), and (b) conventional hard mirror unstable resonators. As we have already heard, work has been done in the United Kingdom and Canada (ref. 1) on resonators containing Gaussian reflectivity mirrors; however, these are preliminary experiments. Comparing what has been obtained so far with ideal objectives, I think all the criteria appear to have been met, with the possible exception of damage resistance, which seems to be the only major problem area of these preliminary experiments.

On the other hand, hard mirror resonators seem to have more problems than resonators containing GRMs. Although these resonators can be made with a large mode radius, single-mode operation is more problematic. My elementary understanding of unstable resonators is that the mode structure is not well understood. Secondly,

transverse mode discrimination seems to be a problem. However, we heard from Bob Menzies that by deliberate misalignment and injection it may be possible to improve transverse mode discrimination. Nevertheless, it does seem that unstable resonators are fairly critical on alignment. In addition, the near-field outputs are rings due to coupling around a hard mirror, and consequently many diffraction lobes appear in the far field. Thus the far-field beam quality is an issue; however, the other objectives of compact size, high energy, and damage resistance seem to have been met.

We feel that more experiments on cavities containing Gaussian reflectivity mirrors are needed. Few experiments have been done compared with the studies on stable resonators and conventional unstable resonators which have a great body of built-up expertise and experience. Also, because it appears that optical damage could be a problem in these GRMs, their damage resistance needs further examination. An alternative fabrication technology could possibly be developed to replace the current germanium wedge technology.

Finally, there was some discussion about the longitudinal mode selection that these resonators demonstrate. Briefly, the resonators give longitudinal mode selection better than would be expected on the basis of their length alone. Perhaps there is something special about these Gaussian resonators that involves their pseudo "ring-like" character (such as spatial hole burning) which results in good mode selectivity. Ideally, the physics of the mode selection process needs to be investigated.

Discharge Technology

In the discharge technology area it is necessary to operate the discharge in a regime in which pumping is efficient and, for the applications we have in mind here, in a way that allows generation of long optical pulses. Taking into account my earlier comments on large mode radius resonators, we also need discharges that can fill a large cross section. In order not to introduce discharge inhomogeneities that can give rise to chirp or readily degrade into an arc, it is required that very uniform discharges are produced over these large cross sections. Long lifetime operation is obviously very desirable.

One very attractive discharge technology would be electron beam sustained operation, which meets practically all of these criteria except one rather important one. First of all, since it is a non-self-sustained mode of operation of the discharge it is possible to separately choose the electron density and the electron energy so you can operate with values of E/N which give optimal efficiency. Secondly, the electrical discharge pulse can be very long; consequently, long optical output pulses can be obtained during which the current remains constant and therefore the plasma effect can be made very small. Furthermore, while there must be some limits to the size of the discharge which can be pumped this way, for the sort of application we have in mind there are no practical restrictions; uniform large volume discharges have been demonstrated routinely and in the UK we've certainly had devices with a 6 in. cross section. In the US we suspect that there are even bigger ones.

In e-beam systems, electrons are injected from a source normally at very low pressure into an atmospheric pressure gas through a window, normally a very thin metal foil. A very large number of pulse operations result in the possibility of foil failure due to main discharge arcs, but this can be ameliorated by correct configuration of the electrode support structure. X-ray shielding may also be an issue;

the gun runs with such a high voltage that quite a lot of X-rays are produced. But it is a very nice way to go if the foil lifetime problems can be overcome.

The other approach is to use a self-sustained discharge. Fairly lengthy discussions took place during the panel session on long pulse generation using this technology, and I think the general feeling was that it isn't really possible to extend the discharge pulse in a self-sustained mode very significantly beyond a few hundred nanoseconds. It will be necessary to tolerate a short discharge but hopefully you can get long pulse duration produced by injection control, attention to the gas mixture, and maybe operating at somewhat reduced pressure. If the mixture is enriched in nitrogen the tail can be enhanced. Injection not only gives transverse mode selection but also can give suppression of the gain switched spike which might make the pulse a more useful shape. There is, however, a residual problem associated with the plasma effects in such discharges. The output pulse almost inevitably seems to come in the decay of the electric discharge pulse so a plasma effect is seen at the beginning of the pulse. Again, a considerable amount of debate took place on this. One option is to try to "chop" very rapidly the tail of the current pulse or to employ transmission line type sources of current to give a sharp current pulse which is cut off before the optical output occurs. A CW injection signal will normally advance the optical pulse into the tail of the current waveform. This could be avoided by injecting a pulsed signal to beat the spontaneous noise just before the gain switched spike is expected to appear. There could be some fairly critical timing requirements on that.

Self-sustained discharges need uniform preionization. A variety of techniques can be used: trigger wires, arc arrays, semi-conductor preionization, corona on dielectrics, X-rays and so on. These methods tend to impact the contamination levels arising in the discharge which interacts with the other panel on lifetime considerations. At present for self-sustained discharges lifetimes of 10^7 pulses are probably almost routine, while 10^9 pulses is a kind of goal which one can see some hope of meeting. In our panel we had a report about a technique in which the proponent claims a predicted lifetime of 10^{12} pulses! Certainly one can imagine ways of getting to the 10^9 pulse lifetime.

MOPAs

Let us now consider a significantly different approach for long-pulse frequency-stable high-energy operation, namely Master-oscillator power amplifier configurations. Two main issues here are high efficiency operation (Can the stored energy be efficiently extracted from the power amplifier?) and the possibility of avoiding pulse distortion phenomena which arise from depletion of the gain in the amplifier by the first part of the pulse to be amplified. Two main ideas were discussed. First, by producing fairly high output energies from a stable oscillator (perhaps using a Gaussian mirror resonator) followed by injection into an amplifier near the saturation energy, it should be possible to get a really efficient overall device. The other idea was to experimentally and theoretically study the compensation effects of laser kinetics on pulse distortion.

Novel Signal Processing Techniques

Finally, let us draw our attention to the most contentious area, namely novel signal processing options. Everybody agrees that for hard targets it is, in

principle, possible to construct a filter matched to the transmitter waveform so that the intrapulse chirp can be disregarded completely. Is this also true of distributed targets, for instance where you are looking at wind velocities from Doppler shifts on aerosols illuminated by long pulse lasers in which returns are obtained from kilometer depths of atmosphere? Personally, I suspect that matched filters still give the same kind of performance that they do for hard targets, but this is by no means an agreed-upon conclusion. We are suggesting that the experts in signal processing should be asked if it is possible to use matched filters in the distributed targets scenario. If so, then clearly it would be advisable to investigate how you actually make an appropriate matched filter for the nonlinear (approximately parabolic) frequency behavior that these lasers exhibit. If you can make these matched filters you will probably have a lot of parallel processors (one for each range bin and velocity channel) and even though each one is not too complex, you will have a lot of electronics. Furthermore, a problem arises that I mentioned at the beginning of my review, namely that with a matched filter it is necessary to have producible performance shot-to-shot (this basically means stability of the laser output energy, which dictates the size of the laser-induced chirp and controls the photon buildup time in the cavity and therefore the size of the plasma effect). To avoid the difficult requirement on output constancy it might be possible to implement an active matched filter scheme in which each time the laser is fired a little of the output is extracted and heterodyned and the actual frequency behavior is put into an array of matched filters which can be altered from pulse to pulse. There were some ideas that acousto-optic opto-electronic techniques, which are currently being developed, could be applicable in this area.

The idea of injection into unstable resonators was an important area to examine and, sadly, Bob Menzies could not be present at our workshop for that part of the discussion. It was proposed that Menzies and a few other people contribute to this subject for this proceedings.

Summary of Suggested Topics for Future Research

1. Resonator Configurations

   1.1 Further experience with cavities using GRMs is needed to establish confidence in this configuration

   1.2 Damage limits of GRMs need to be investigated; alternative fabrication technologies should be studied if necessary

   1.3 Physics of surprisingly good longitudinal mode selection should be investigated

2. Discharge Technology

   2.1 New materials for extended foil lifetime in e-beams should be explored

   2.2 Investigations of effect of pulse injection on pulse shape and plasma chirp should be undertaken

   2.3 Effectiveness of various preionization techniques on large volume coverage and lifetime extension should be determined

2.4 Sympathetic discharge technology should be extended to higher pressures

3. MOPA Systems

3.1 GRM master oscillator should be evaluated at lower pulse energies

3.2 Compensating effects of laser kinetics on pulse distortion (both experimentally and theoretically) should be studied

4. Novel Signal Processing Options

4.1 Theoretical investigation of matched filter use for distributed targets should be performed

4.2 Considering theoretical feasibility, hardware implementation of matched filter approach should be examined

4.3 Advanced technology of active matched filter design should be studied

Reference

1. Laser Radar Technology and Applications. SPIE Proceedings, vol. 663, 1986, pp. 124-131.

CLOSING REMARKS

Richard D. Gonzalez
University of Illinois at Chicago
Chicago, Illinois

Unlike the laser group, the Catalysis Panel had considerable difficulty in attempting to compare catalytic activities obtained in different laboratories. It was immediately apparent that the laser people and those engaged in catalytic research were speaking different languages. Following an hour of discussion we ranked various supported noble metal catalysts as to their activity for CO oxidation activity. The basis for this catalytic activity was expressed in terms of turnover frequencies or molecules of CO_2/site-sec. This catalytic activity is shown in Table I.* From the data given to us by Carmen Batten of NASA Langley for CO oxidation on a commercial Pt/SnO_2 catalyst supplied by Engelhard, we calculated a turnover frequency of 17×10^{-3} molecules/site-sec at 373K. This ranks it with Ru/SiO_2 as being the most active catalyst for CO oxidation. Studies in our research group would also rank bimetallic Ru-Rh/SiO_2 catalysts very highly. This bimetallic catalyst, unlike Ru/SiO_2, is attractive because it does not deactivate.

Professor Vannice calculated a turnover frequency of 540×10^{-3} molecules/site-sec as the lower limit to the catalytic activity of a catalyst prepared by the RSRE group. This turnover frequency was based on the data provided to us by Chris Sampson. However, the chemical formulation of this catalyst is of a privileged nature and may include several promoters. Apparently it has a very large active surface area.

The importance of reporting catalytic activity in terms of turnover frequencies cannot be overstated. However, in order to do this, it is essential to measure metal surface areas through the use of either CO or H_2 chemisorption. The assumption of a well-defined adsorption stoichiometric ratio should yield the total number of metal atoms exposed to the gas phase. The percentage metal dispersion is defined as: metal atoms exposed to the gas phase/total number of metal atoms (100). Normally, dispersions of twenty to thirty percent are acceptable for routine catalytic reactions. However, dispersions of 100% are attainable at low Pt loadings on an alumina support. Other noble metals are more difficult to disperse. However, the ultimate metal dispersion generally depends on who is synthesizing the catalyst and how good he is at preparing it.

In order to make more valid comparisons between laboratories, the Catalysis Panel makes the following recommendations: We suggest that we take a catalyst sample which weighs between 200 and 300 mg. The normal loading for this application should be about 1% metal. The catalyst

*Table I in D. Böcker and R. D. Gonzalez's paper, CO Oxidation Studies Over Supported Noble Metal Catalysts and Single Crystals: A Review, NASA CP-2456, 1987, p. 98.

should be treated in flowing He for 20 hours at a flow rate of 10 ml per min at 373 K. This is essentially a drying period required to remove the moisture from the catalyst. The 20 hours is an arbitrary variable and depends on normal laboratory working schedules. The reduction temperature and hydrogen time on stream is an important variable. It is important because hydrogen will react with SnO_2 to form water. If somebody reduces his catalyst at 723 K, he will obviously have a very different catalyst than somebody who performs the hydrogen reduction at 473 K. For this reason the reduction step requires standardization.

Following some discussion, we settled on 7.5% H_2 in flowing He for two hours at 598 K. The flow rate should be 20 ml/min. Following this pretreatment, we recommend use of either CO or H_2 as adsorbed gases to measure metal dispersions. We recommend use of the dynamic pulse method to measure metal surface areas.

When CO is used to measure metal dispersions on a SnO_2 support, the stoichiometric adsorption ratio may become somewhat elusive due to the reaction between CO and the SnO_2 support to form CO_2. This effect might be minimized by reducing the adsorption temperature to -80 C. The use of H_2 as an adsorbate is desirable in the case of Pt because of the well defined H/Pt(s) stoichiometry of 1. In the case of other noble metals the stoichiometry is more poorly defined. When CO is used to measure Pt surface areas, the dispersion can be normalized to that obtained using hydrogen chemisorption by dividing through by 0.89 for a silica support and 0.7 for alumina. In any case, the errors involved will not be large (10-15%). BET surface areas should be reported whenever possible. Normally they can be obtained from the manufacturer. However, if not available they should be obtained using N_2 adsorption at 77 K.

Carbon dioxide turnover frequencies should be obtained using premixed CO and O_2 (1% CO, 0.5% O_2) in a helium carrier at a flow rate of 25 ml/min. The flow rate should be adjusted to give an overall CO conversion of 5% in order to insure differential flow. The reaction temperature should be set at 348K. We strongly recommend the use of electronic flow controllers in order to insure steady flow rates. The expenditure of $3000-4000 for a set of flow controllers is well worth the investment. The use of rotameters, and poor quality fittings and valves should be avoided. The measurement of activation energies should be obtained by bracketing reaction rates at different temperatures.

Although catalyst activation by hydrogen reduction is strongly recommended, activation using other gases or procedures may result in a more active catalyst. When catalyst activation other than H_2 reduction is used, the procedure should be outlined in detail.

In order to design an effective catalyst for application in pulsed laser systems, the engineering requirements must be known. We know, for example, that the inlet oxygen concentration to the pulsed laser system should be held to less than 0.5%. We need to know the pulsing rate (about 100 pulses/second). The amount of oxygen and CO produced will, of course, depend on the laser geometry, laser power and laser pulse rate. From this knowledge an appropriate required flow rate can be calculated. A circulating pump will be required in order to insure the correct flow

rate over the active catalyst. We will also need to know whether we are operating in a region of turbulent or laminar flow.

We estimate that CO and O_2 flow rates will remain virtually constant throughout the circulation loop and that we will be operating under steady-state rather than transient conditions. From a knowledge of the flow rate reaction rate, reaction temperature, and the particular form of the catalyst bed i.e., porous spheres, monolithic supports or whatever, the amount of catalyst to be charged to the reactor in order to obtain the desired CO conversion can be calculated. A design goal for catalyst durability should be such that it can survive 10^9 - 10^{11} laser pulses. For this reason possible catalyst fouling or poisoning should be studied. It is possible that the transport of materials such as $Ni(CO)_4$ or hydrocarbons from seals from other parts of the system might result in a loss in activity. This deactivation should be kept to a minimum.

CLOSING REMARKS

Richard K. Herz
UCLA
San Diego, CA

I want to briefly review some points, keeping in mind that CO oxidation catalysts exist and do a pretty good job. So it's possible, right now, to design a catalyst laser system that is going to operate. The question is: Is it going to be as small as we want, is it going to operate as long as we want, and are we going to be able to run the catalyst at ambient temperature or do we have to heat the catalyst? So while we can build a laser system with a catalyst today, there is a possibility that we will be able to design a better system in the future. From what we learned about some of the catalysts involved in the system, it seems that the best catalyst will probably be a complex system. It is not going to be simply a metal sitting on an inert support. It may be something like a platinum tin oxide system in which the tin oxide apparently plays an important role in the catalysis. I think that while developing the optimal catalyst in the future, we should keep in mind that we have to address these two functions of the catalysis: the dissociation of oxygen and the adsorption of CO near the active oxygen.

In the precious metal-tin oxide catalyst, we probably have both of these components; however, what the mechanism of this is, we don't know at this stage. There is a lot of research that needs to be done, and the method to determine the mechanism of CO oxidation of this catalyst is to identify how the different sites determine the dissociative absorption of oxygen and the adsorption of CO. In the optimal catalyst the adsorption bond energies of CO and oxygen will be optimally balanced with respect to each other. If you have too weak an absorption, you are not going to have good catalysis; if the catalyst holds the reactant too strongly, you are not going to have good catalysis. You have to have an optimal balance. How then do you perturb adsorption energies? We may be able to use promoters or poisons to modify the activities on different sites. These are areas of research in the future. The best catalyst will not be inhibited by CO_2, will not exchange oxygen with CO, O_2 or CO_2, and will be stable.

Regarding the kinetic studies, a procedure has been outlined for doing some tests under some standard conditions to compare from lab to lab. In addition, I want to remind you that you need to measure the activity of the catalyst in the absence of the concentration gradients, both within the porous catalyst material and also across the catalyst bed. It has been recommended that we use a plug flow reactor with differential conversion. Actually, probably the best reactor for kinetic studies with a solid catalyst is a recycle reactor operated at high recycle ratio. In chemical engineering we call this a CSTR (continuous stirred tank reactor). A recycle reactor is similar to some of the laser systems presented in that there is a continuous feed in and a flow out of the reactor. When you operate at a high recycle ratio (the volume of flow around the loop compared with the volume flowing out of the loop), you reach conditions in which the change in composition across the catalyst is very, very small. So we have differential conversions; that means we have eliminated or almost eliminated concentration gradients across the catalyst, and that it's quite easy to calculate reaction rates. In the case of a recycle reactor operating at a high recycle ratio, the composition of catalyst

is close to being uniform across the outside of the catalyst material such that the rate of reaction is easily determined. The rate is going to simply be equal to the net flow rate through the reactor times the difference in concentration. You'll note that because of the behavior of this recycle reactor at high recycle ratios the gas composition that we're measuring is the outlet concentration coming out of the reactor. Even though we have a very small concentration change across the catalyst bed, we have a very large concentration change between the inlet and outlet of a recycle reactor and this allows very accurate determinations of the reaction rate.

In most applications, we are going to be dealing with stoichiometric ratios of CO and oxygen. We want to determine accurately how the rate of reaction varies as a function of reactant pressure keeping the stoichiometric ratio constant. I think it is also important to perturb the ratio of CO and the oxygen away from the stoichiometric ratio, at least slightly, to see if there is some optimal area of operating conditions slightly off the stoichiometric ratio. It has been suggested that within the silica catalyst it might be advantageous to work with a slight excess of CO in the system. I feel we shouldn't completely rule out the possibility of having an initial oxygen charge to the laser, even though it sounds like you are doing the opposite thing you want. You have to realize that in some catalysts you have a competition between CO and oxygen and you may have CO inhibition. So if you add a little bit of oxygen you might be able to reactively scavenge the first amount of CO forming and convert back to CO_2 and maintain constant oxygen concentration.

With the recycle reactor you can eliminate concentration gradients across the catalyst bed but you have to also realize that there is still the possibility of concentration gradients inside the porous catalyst particles or inside the monolith washcoat. For catalyst comparison and reactor design, we need the rate as a function of reactant concentrations in the absence of concentration gradients. In other words, the rate of reaction has to be specific to a given set of concentrations over the entire catalyst, not just inlet concentration into a bed in which we have a large amount of conversion. We have to make sure we report this within our own laboratories as the rate of reaction per unit active surface area. For a simple monofunctional metal on an inert support, that active surface area determination may be simply determined by measuring the CO adsorption uptake. For some complex catalysts, where you have a reducible oxide and a metal playing a role, it may be much more complicated than simply determining the dispersion of the metal because, with the reducible support playing a role, you have to characterize that also.

CLOSING REMARKS

H. T. W. Price
GEC Avionics, Ltd.
Borehamwood, Herts,
United Kingdom

One of the objectives of the workshop was to consider the feasibility of realizing a sealed-off CO_2 TEA laser with a lifetime of 10^9 pulses. In the workshop sessions, there was considerable discussion of the catalyst, but time did not permit consideration of the laser design perspective. Therefore I would like to consider the objective from this other end of the spectrum, that is, from the laser designer's point of view, and so highlight the sort of problems that we foresee as users of the catalyst.

The first question which we really need to know the answer to is "what sort of laser specification are we dealing with?" There is obviously a significant difference between providing a sealed-off device that produces a few hundred kilowatts output up to 10 hertz, and providing a device with outputs of 10's of joules at 10's of hertz. The specification will dictate just how difficult the problem is going to be in extending the technology from where we are now.

The parameters we need knowledge of are the estimated output power and energy, the repetition rate, and the design lifetime, which would appear to be 10^9 pulses. From the laser output power and energy, modelling can be performed to determine the CO_2 concentration in the laser for the particular type of excitation scheme that is to be used, and we can also determine the active volume. From the active volume and the repetition rate, we can deduce the gas flow requirements, i.e., the gas flow required to maintain arc-free, stable, operation of the laser. The active volume and repetition rate also determine the CO and oxygen formation rate. The design adopted for the excitation scheme (the electrodes and the preionizers), influences the tolerance of the system to oxygen. There will obviously be a major difference in catalyst requirements in a laser that has an oxygen tolerance of perhaps 1 or 2 percent, and one that has an oxygen tolerance of perhaps 0.1 percent.

From this basic laser design information, catalyst requirements can be defined. The gas flow that is needed to maintain the stable discharge is related to the clearing ratio required within the electrode spacing. This in turn is related to the pump energy density of the discharge, as well as the physical dimensions of the discharge volume, but as a rule of thumb we need a clearing ratio of typically three. The gas flow that this implies then impacts on the acceptable impedance of the catalyst. Obviously if the catalyst has a high impedance, this makes it extremely difficult to maintain the desired flow rate. Also, the CO and oxygen formation rates, together with the oxygen tolerance of the laser, define a total catalytic activity required within the device.

To put into context the lifetime of 10^9 pulses, if we assume a repetition rate of say 10 hertz, this equates to operating the laser 24 hours a day, 365 days of the year, for 3 years. Thus a minimum shelf life of 3 years is indicated. This raises the question of the long-term stability of the catalyst, and I don't think anybody has experience with these catalysts in a high repetition rate system for that duration of time, so we clearly don't know what the long-term effects are going to be. We also have to bear in mind of course, the general mechanical design of the

laser, such that we can control the contamination that may arise from leaks or permeation through the envelope.

However, the most critical area will undoubtedly be the laser pulse lifetime. The thought of the laser running continuously at 10 hertz for 3 years is a very daunting prospect, and is a major extrapolation from the 10^7 or several 10^7 pulses achieved at the moment. The active components of the laser will have some finite lifetime, and that lifetime will influence the over-all laser life that is achieved. In addition to which, the erosions that will take place in the violent environment of the laser discharge will also potentially influence the catalyst lifetimes, through contamination of the catalyst surfaces. The electrodes and preionizers will thus have an important influence on catalyst and laser active lifetime. Obviously no laser can operate without quality optics, and a major aspect to be considered over such a 3 year run will be controlling contamination of the surface of the optics. Even in the absence of physical contamination of the optical surfaces, we still need to consider the cumulative damage that can arise on the optic due purely to optical radiation effects. The over-all picture which can be drawn from this is that we who are involved in the laser design need to take steps to minimize the impact of the contamination on both the catalyst and the optics.

Referring to the extrapolation from where we are now to the end goal, it is obviously essential to progress the detailed understanding of the catalyst in terms of the mechanisms involved. However, it is equally important to evaluate these catalysts, not just in a very controlled test situation such as we were discussing yesterday, but, in parallel, in an actual laser, in the real environment in which they have to operate. This is important, not only to see how they perform in that environment but also to progress our knowledge of the other effects which will influence the laser life. I think there is a definite need for this parallel thrust in progressing toward the 10^9 lifetime.

All of the factors mentioned must be addressed - different preionizer geometry, perhaps different electrodes, different techniques to minimize contamination, and cumulative optical damage mechanisms; these all have to progress in parallel. Perhaps another aspect that also needs to be considered in conducting such life tests on lasers is what information can we extract out of those life tests that can be of assistance on the catalyst side? At the moment we measure laser parameters such as power and energy, and we deduce catalyst pumping speeds. Perhaps there are other parameters that we could also be monitoring during these life tests which may assist further the development of the catalyst.

Standard Bibliographic Page

1. Report No.	2. Government Accession No.	3. Recipient's Catalog No.
NASA CP-2456		

4. Title and Subtitle	5. Report Date
Closed-Cycle, Frequency-Stable CO_2 Laser Technology	April 1987
	6. Performing Organization Code 146-74-06-70
7. Author(s) Carmen E. Batten, Irvin M. Miller, George M. Wood, Jr., and David V. Willetts, Editors	8. Performing Organization Report No. L-16271
9. Performing Organization Name and Address NASA Langley Research Center Hampton, VA 23665-5225	10. Work Unit No.
	11. Contract or Grant No.
12. Sponsoring Agency Name and Address National Aeronautics and Space Administration Washington, DC 20546-0001 and Royal Signals and Radar Establishment, Malvern, Worcester, United Kingdom	13. Type of Report and Period Covered Conference Publication
	14. Sponsoring Agency Code

15. Supplementary Notes

Carmen E. Batten, Irvin M. Miller, and George M. Wood, Jr.: Langley Research Center, Hampton, Virginia.
David V. Willetts: Royal Signals and Radar Establishment, Malvern, Worcester, United Kingdom.

16. Abstract

The proceedings of the first workshop on Closed-Cycle, Frequency-Stable CO_2 Laser Technology, which was sponsored by NASA, organized jointly by NASA and The Royal Signals and Radar Establishment, and held at the NASA Langley Research Center, Hampton, Virginia, June 10 to 12, 1986, are presented in this document. The workshop was attended by representatives from government, industry, and academic institutions. The purpose of this workshop was to discuss the rapidly growing area of CO_2 laser technology.

This volume contains documentation of the workshop, including opening addresses, frequency stability and chirp, catalytic oxidation of CO, and panel reports and closing remarks.

17. Key Words (Suggested by Authors(s))	18. Distribution Statement
CO_2 TEA lasers Supported noble metal catalysts Remote sensing CO oxidation	Unclassified - Unlimited Subject Category 36

19. Security Classif.(of this report)	20. Security Classif.(of this page)	21. No. of Pages	22. Price
Unclassified	Unclassified	265	A12

For sale by the National Technical Information Service, Springfield, Virginia 22161

NASA-Langley, 1987